Studies in Systems, Decision and Control 61

Mirza Tariq Hamayun
Christopher Edwards
Halim Alwi

Fault Tolerant Control Schemes Using Integral Sliding Modes

Springer

Studies in Systems, Decision and Control

Volume 61

Series editor

Janusz Kacprzyk, Polish Academy of Sciences, Warsaw, Poland
e-mail: kacprzyk@ibspan.waw.pl

About this Series

The series "Studies in Systems, Decision and Control" (SSDC) covers both new developments and advances, as well as the state of the art, in the various areas of broadly perceived systems, decision making and control- quickly, up to date and with a high quality. The intent is to cover the theory, applications, and perspectives on the state of the art and future developments relevant to systems, decision making, control, complex processes and related areas, as embedded in the fields of engineering, computer science, physics, economics, social and life sciences, as well as the paradigms and methodologies behind them. The series contains monographs, textbooks, lecture notes and edited volumes in systems, decision making and control spanning the areas of Cyber-Physical Systems, Autonomous Systems, Sensor Networks, Control Systems, Energy Systems, Automotive Systems, Biological Systems, Vehicular Networking and Connected Vehicles, Aerospace Systems, Automation, Manufacturing, Smart Grids, Nonlinear Systems, Power Systems, Robotics, Social Systems, Economic Systems and other. Of particular value to both the contributors and the readership are the short publication timeframe and the world-wide distribution and exposure which enable both a wide and rapid dissemination of research output.

More information about this series at http://www.springer.com/series/13304

Mirza Tariq Hamayun · Christopher Edwards
Halim Alwi

Fault Tolerant Control Schemes Using Integral Sliding Modes

Springer

Mirza Tariq Hamayun
Department of Electrical Engineering
COMSATS Institute of Information Technology
Lahore
Pakistan

Halim Alwi
College of Engineering Mathematics and Physical Sciences
University of Exeter
Exeter
UK

Christopher Edwards
College of Engineering Mathematics and Physical Sciences
University of Exeter
Exeter
UK

ISSN 2198-4182 ISSN 2198-4190 (electronic)
Studies in Systems, Decision and Control
ISBN 978-3-319-32236-0 ISBN 978-3-319-32238-4 (eBook)
DOI 10.1007/978-3-319-32238-4

Library of Congress Control Number: 2016936424

Printed on acid-free paper

This Springer imprint is published by Springer Nature
The registered company is Springer International Publishing AG Switzerland

We dedicate this book to
Mirza's parents, wife Attiya Tariq and children Mehreen, Abdur Rafe and Mohib
Chris' parents
Halim's wife Nor Mazuita Noor Azizuddin and son Aydin Yusuf.

Preface

Control is an essential part of many new technology developments, from cell phones to passenger aircraft and from washing machines to oil refineries. The objective of many control applications is to maintain the output (of the process) in the face of unknown disturbances, whilst in others, it is tracking a reference signal and minimising the tracking error, which is important. Ensuring the closed-loop stability of the overall system in the presence of unknown disturbances and in the face of uncertainties which arise as a result of creating an approximate mathematical model used for the controller design is an important part of the control design process. In addition, issues of operating safety, reliability and availability of the system, especially in safety critical plants like aircraft and nuclear reactors, are of great importance. Safety critical systems like aircraft became the basis for the initial research in the field of fault tolerant control systems. Faults or failures in these safety critical systems cannot be totally avoided, however their effects (in terms of human mortality and economic loss) can be mitigated using fault tolerant control schemes. Fault Tolerant Control (FTC) schemes are an important aspect in safety critical systems and seek to maintain overall system stability and acceptable performance in the face of faults and failures within the system. One way to achieve high level of availability is to ensure a suitable level of redundancy in terms of the key actuators and sensors within the system. In emergency situations, this redundancy can be manipulated in a way to achieve fault tolerance. Therefore, increasing demands for safety, reliability and high system performance have motivated the need for fault tolerant control and has stimulated research in this area. For the design of fault tolerant controllers, many different design paradigms have been proposed in the literature. This book will focus on one particular methodology—the so-called integral sliding modes. The objective is to show how the robustness properties of sliding mode control—especially integral sliding modes—can be used within the framework of FTC to provide an increase in the survivability, reliability and stability of safety critical systems.

The book is a mix of theoretical developments and case studies relating to aerospace systems and is organised as follows:

In Chap. 1, the definitions and basic terminologies of FTC and some typical types of faults at the sensor, actuator and component level are defined. In addition, the difference between fault and failure is clearly explained. Different types of fault/failure models used in the literature to design fault tolerant schemes against the actuator faults/failures and component faults are discussed. An introduction to FTC is given together with an introduction to different fault tolerant control methods used in the literature based on passive and active approaches. The terminologies used in the fault detection and isolation framework are defined, and some of the techniques which can be used for FDI are also documented.

In Chap. 2, the concept, properties and design principles of sliding mode control are explained. Different methods which can be used to implement sliding mode controllers in real and practical applications are also given. The concept of integral sliding modes is defined next, with an explanation of how it differs from the classical sliding mode control approach explained earlier in the chapter. A detailed procedure for the design of integral sliding mode control laws together with a special choice of sliding surface which helps to mitigate the effects of unmatched uncertainty is explained. Finally, some motivation for the use of integral sliding modes as a candidate for FTC is discussed.

In Chap. 3, an integral sliding mode FTC scheme is presented, which considers the combination of integral sliding modes and a Control Allocation scheme. The concept of a virtual control is also explained, which is then used by the Control Allocation scheme to achieve the demanded actuator position. The FTC scheme described in this chapter uses the estimated actuator effectiveness level to distribute the control effort among the actuators without changing the underlying ISM controller. A rigorous closed-loop stability analysis is carried out and it is proved that the scheme can handle some level of error in estimating the actuator effectiveness. Furthermore, in order to compute the controller parameters such that the closed-loop stability condition (given in the chapter) is satisfied, an LMI synthesis procedure is described. The resulting fault-tolerant Control Allocation scheme can cope with actuator faults and certain total actuator failures without degrading the desired performance. A benchmark model of a large civil aircraft is used to validate the feasibility of the scheme.

In Chap. 4, a passive FTC scheme is described where the combination of integral sliding mode control with fixed control allocation is considered. The FTC scheme has the capability to deal with actuator faults/failures without any FDI scheme and is suitable for the case where fault information is not available to the controller. A detailed LMI-based procedure is provided to synthesise the controller parameters and a rigorous closed-loop stability analysis is carried out in the presence of unmatched uncertainty for a suitable set of actuator faults/failures.

Chapter 5 focuses on an output feedback integral sliding mode control allocation scheme within the framework of FTC. This chapter relaxes the assumption made in the previous chapters that full state information is available for the controller design. The chapter also builds on the idea that information about actuator faults/failures is not available to the controller. A direct control allocation scheme is employed in this case to distribute the control signal among the actuators. In order

to estimate the plant states, an unknown input observer (UIO) is employed and the necessary conditions for the existence of the UIO are included. A rigorous closed-loop stability analysis is carried out and a stability condition is posed in an LMI framework through which the controller and observer gains are computed. A benchmark model of a large civil aircraft is used to demonstrate the efficacy of the scheme by considering component faults, together with faults or failures in the actuator channels.

In Chap. 6, an integral sliding mode augmentation scheme is considered in order to introduce fault tolerance at an actuator level. The scheme is based on an *a posteri* approach, building on an existing state feedback controller designed using only the primary actuators, without the need to remove or alter existing control loops. The control allocation scheme is developed based on the idea that if the primary actuators are healthy, the secondary actuators should not be activated, and the secondary actuators should only be activated for fault tolerant purposes if the primary actuators are faulty. This FTC approach depends on information about the actuator effectiveness levels, to distribute the control signals among the available actuators in the set. Possible errors in estimating the actuator effectiveness by the FDI scheme are taken into consideration while a closed-loop stability condition is described, which must be satisfied to ensure stability in the case of faults or failures. The efficacy of the scheme is tested by applying it to a nonlinear benchmark model of a large civil aircraft.

In Chap. 7, a nonlinear fault tolerant scheme for the control of longitudinal motion of an aircraft is considered and an integral sliding mode control allocation scheme is combined with a backstepping structure. In fault-free conditions, the closed-loop system is governed by the backstepping controller and the integral sliding mode control allocation scheme only influences the performance if faults/failures occur in the primary control surfaces. In this situation, the allocation scheme redistributes the control signals to the secondary control surfaces and the scheme is able to tolerate total failures in the primary actuator. A backstepping scheme taken from the existing literature is designed for flight path angle tracking (based on the nonlinear equations of motion) and this is used as the underlying baseline controller in nominal conditions.

In Chap. 8, the ideas of integral sliding mode control allocation discussed in Chap. 3 are extended for Linear Parameter Varying (LPV) plants. For the design of the virtual control law, the parameter varying input distribution matrix is factorised into a fixed matrix and a matrix with varying components. In this chapter, a control law is developed which is automatically scheduled with respect to the varying plant operating conditions in order to ensure closed-loop stability for a wider range of operating conditions. The scheme also depends on information about actuator effectiveness levels for control signal distribution. An effective LMI synthesis procedure is described to compute the parameters of the controller and a rigorous closed-loop stability analysis is undertaken, which ensures that certain classes of faults or failures can be dealt with over the entire operating envelope

(with the assumption that the redundancy is available in the system). A benchmark LPV model of the large civil aircraft is used to demonstrate the efficacy of the FTC scheme.

In Chap. 9, the integral sliding mode FTC scheme for LPV plants described in Chap. 8 is implemented in real-time on the SIMONA motion flight simulator at the Delft University of Technology, The Netherlands.

Lahore, Pakistan — Mirza Tariq Hamayun
Exeter, UK — Christopher Edwards
Exeter, UK — Halim Alwi
February 2016

Acknowledgements

The research described in this book was predominantly undertaken during the period of time when the first author was supported as a COMSATS scholar at Leicester University, UK. However, the work has also been influenced by the aerospace benchmark problems, which the other authors have worked on in other EU funded projects over the past ten years.

In particular, we are enormously grateful to Prof. Jan Albert (Bob) Mulder (Control and Simulation Division, Faculty of Aerospace Engineering) and Ir. Olaf Stroosma (International Research Institute for Simulation, Motion and Navigation (SIMONA)) from Delft University of Technology, The Netherlands, for allowing us access to the SIMONA simulator in order to test the LPV controller described in Chap. 9. This work builds on earlier studies under the auspices of the GARTEUR FM-AG16 programme.[1] We would like to thank Ir. Stroosma for sharing with us his technical expertise in terms of interfacing our controller code with the motion simulator and his invaluable help with the implementation process. We would also like to acknowledge the hard work of those involved with the development of the benchmark aircraft model, which was used as a basis for the simulator. This model has evolved over many years in the hands of many people—most recently Hafid Smaili and Jan Breeman of NLR (National Aerospace Laboratory), The Netherlands and Dr. Andres Marcos, now at University of Bristol, UK.

[1]The European Flight Mechanics Action Group FM-AG(16) on Fault Tolerant Control was established in 2004 and concluded in 2008. It represented a collaboration involving thirteen European partners from industry, universities and research establishments under the Group for Aeronautical Research and Technology in Europe (GARTEUR) program.

The authors would like to thank all those who kindly gave their approval to use the pictures and illustrations in this book. The illustrations remain the property of the copyright holders.

Lahore, Pakistan — Mirza Tariq Hamayun
Exeter, UK — Christopher Edwards
Exeter, UK — Halim Alwi
February 2016

Contents

Acronyms

Nomenclature

$\emptyset$	Empty set
α, β, γ	Angle of attack, sideslip and flight path angle (rad)
$\mathbb{C}$	Field of complex numbers
det $(\cdot)$	Determinant of a matrix
$\mathbb{E}(\cdot)$	Mathematical expectation
$\mathbb{R}$	Field of real numbers
$\mathscr{R}(\cdot)$	Range space of a matrix
$\subset$	Subset
diag $(\cdot)$	Diagonal matrix
rank $(\cdot)$	Rank of a matrix
σ	Switching function
$\mathscr{S}$	Sliding surface
$\| \, . \, \|$	Euclidean norm (vectors), induced spectral norm (matrices)
ν	Virtual control input
p, q, r	Roll rate, pitch rate and yaw rate (deg/s)
s	Laplace variable
trace $(\cdot)$	Trace of a square matrix
Var $(\cdot)$	Variance
V_{tas}	True airspeed (m/s)
$\mathscr{W}$	Allowable set of fault or failure
W	Actuator effectiveness matrix
ϕ, θ, ψ	Roll angle, pitch angle and yaw angle (rad)
$\lambda_{min(.)}, \lambda_{max}(.)$	Minimum and maximum eigenvalues
h_e, x_e, y_e	Geometric earth position with respect to the z (altitude), x and y axis (m)

Abbreviations

AFTC	Active Fault Tolerant Control
BRL	Bounded Real Lemma
CA	Control Allocation
CG	Centre of Gravity
DI	Dynamic Inversion
DOF	Degree of Freedom
EPR	Engine Pressure Ratio
FDI	Fault Detection and Isolation
FPA	Flight Path Angle
FTC	Fault Tolerant Control
FTLAB	Flight Lab
GARTEUR	Group for Aeronautical Research and Technology in Europe
GS	Gain Scheduling
ISM	Integral Sliding Modes
ISMC	Integral Sliding Mode Control
IMM	Interacting Multiple Model
LMI	Linear Matrix Inequality
LPV	Linear Parameter Varying
LQR	Linear Quadratic Regulator
LTI	Linear Time Invariant
MMST	Multiple Model Switching and Tuning
MPC	Model Predictive Control
MRAC	Model Reference Adaptive Control
PFTC	Passive Fault Tolerant Control
PIM	Pseudo-Inverse Method
RECOVER	REconfigurable COntrol for Vehicle Emergency Return
SIMONA	SImulation, MOtion and NAvigation
SMC	Sliding Mode Control
STC	Self Tuning Control
UIO	Unknown Input Observer
VSC	Variable Structure Control
VSCS	Variable Structure Control Systems
ail, aol	Inboard and Outboard Left Aileron
air, aor	Inboard and Outboard Right Aileron
s.p.d.	Symmetric Positive Definite
sp	Spoiler

Chapter 1
Fault Tolerant Control

Control is used extensively in industry where it plays an important role in increasing productivity, but it is required to operate safely—especially where interaction with humans takes place. Particularly in safety critical systems like chemical plants, nuclear reactors, aircraft etc., reliability of the system is very important. Broadly speaking, control systems that have such capabilities, are termed Fault Tolerant Control (FTC) systems. In this chapter, different terminologies used in the FTC literature are defined, the concepts of faults and failures are distinguished, and their classification is explained.

1.1 Fault and Failure and Their Classification

The term *fault* will first be defined to avoid any confusion.[1]

Fault: This constitutes an unexpected change in a system parameter from the acceptable/normal condition, which can degrade system performance. It is a fact that a fault can disturb the normal operation of a system from the desired one, but may be tolerable. Faults are usually considered to occur very rarely in the system but cannot be totally prevented. However their consequences can sometimes be mitigated by taking appropriate actions. A FTC system, as the name implies, has the potential to tolerate faults and to maintain the closed-loop performance of the system. A fault is a sudden event, and can occur in any part of the system. Depending upon the location of occurrence, it can be classified as an actuator fault, a sensor fault or a component fault (Fig. 1.1).

Actuator faults: Actuators are the work horses in a control system and represent a linkage/interface between the controller commands and the plant. In Fig. 1.3d, an actuator fault is shown which is termed as a loss of effectiveness, during which

[1]The definition of a *fault* given in this section is in compliance with the definition given in [1].

M.T. Hamayun et al., *Fault Tolerant Control Schemes Using Integral Sliding Modes*, Studies in Systems, Decision and Control 61,
DOI 10.1007/978-3-319-32238-4_1

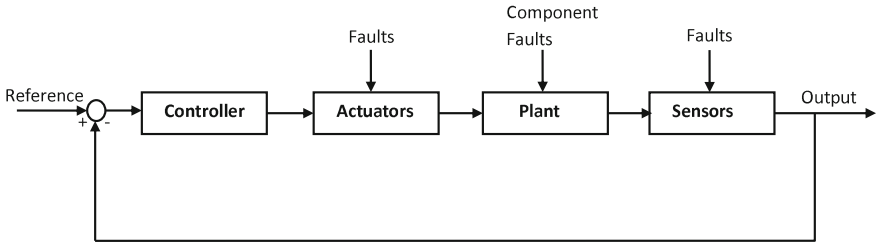

Fig. 1.1 Classification of faults (adapted from [2])

time the actuator works with reduced capability as compared to its normal operating condition (when it is fault-free). This means that in a post fault condition, the actuator will only be partially effective in achieving the required controller demand, which may affect the overall performance of the system. Actuator faults may occur due to, for instance, a drop in voltage supply, increased resistance, hydraulic leakages etc.

Sensor faults: Sensors are used in the control system to measure and convert the physical quantities of interest into a signal (e.g. a tachometer measures the speed of a rotating motor shaft and converts it into a voltage). A fault in the sensor means an incorrect measurement from the sensor, which in turn can result in a continuous constant offset as compared to the true value. Sensor faults can degrade the feedback system performance even in the presence of a well-designed controller. Therefore it is important to detect and isolate sensor faults at an early stage.

Component faults: All faults that do not belong in the category of actuator or sensor faults, can be considered as component faults. A component fault is a very severe type of fault that can occur in the plant components. As a result the input/output dynamical behaviour of the controlled system will be altered. Component faults can in turn result in a change in the physical parameters of the system, and can reduce the overall performance of the system.

Faults can also be classified with respect to their time characteristics i.e. how the fault characteristics change with respect to time. The characteristics of faults can change abruptly, incipiently or intermittently with respect to time as can be seen

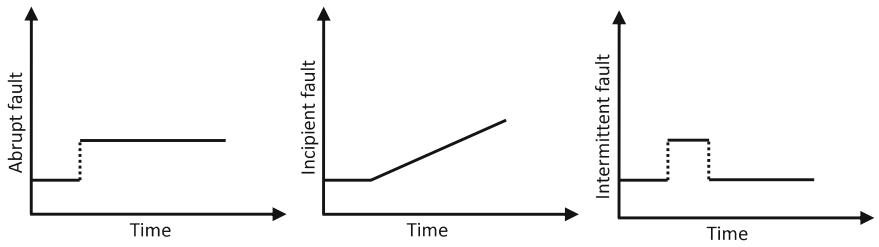

Fig. 1.2 Classification of faults with respect to time (adapted from [2])

in Fig. 1.2. If a fault characteristic changes *abruptly*, it can result in a very severe situation, as the system stability may also be affected. These types of faults often occur due to hardware damage. On the other hand *incipient faults* represent a scenario whereby the fault characteristics change very slowly, due to variations of parameters for instance, and are not severe in nature. However if incipient faults are not attended to promptly, they can result in a severe situation. *Intermittent faults* occur sporadically over time, and can be caused by intermittent contact or damaged wiring in some part of the circuitry.

In the FTC literature, and throughout this book, the notion of faults or failures is frequently used and may cause confusion, therefore the difference between them is clearly outlined in this chapter in order to avoid any ambiguity.

The difference between fault and failure: The term failure is defined in the literature[2] as a permanent interruption or a complete breakdown of a component or system and its complete inability to perform a specific function. A failure is usually a more serious situation than a fault, because the component or system cannot be used any more to perform a task. This means that if a failure occurs in a sensor or in an actuator, a different sensor or actuator is required for the continuation of the process: in other words some sort of reconfiguration mechanism is required in the control system to deal with such a situation, and redundancy must be available. For example, in an aircraft, some very severe types of actuator failure, if not promptly detected, can degrade or even destabilise the overall system. Examples are a jam or lock in place failure, a float failure or a runaway/hardover failure as shown in Fig. 1.3. In a jam failure, the actuator becomes stuck or jams at some (offset) position due to a lack of lubrication for instance, and does not respond even if a control signal is applied to it. In a float failure, the actuator moves freely and does not provide any desired moment. A runaway/hardover failure is a very destructive type of failure and it causes the actuator to move at its maximum rate limit until a saturation limit is reached. This can be caused by a 'wrong signal' being applied to the actuator. In Fig. 1.4, some common types of sensor faults/failures are shown. A sensor in a 'frozen' (failure) situation, provides a constant output value instead of the true value of the physical state. During a loss of accuracy fault, the sensor does not reflect the actual value of the physical state. A specific example is a bias fault which creates a constant offset in the measurement. Finally in a drift fault, the offset in the measurement of an actual physical state increases with time.

In this book, different FTC schemes are described, which have the potential to deal with faults and failures associated with the actuators, provided that redundant actuators are available. Faults at the component level are also considered, but the sensor faults and failures are not within the scope of this book.

[2] See for example [1].

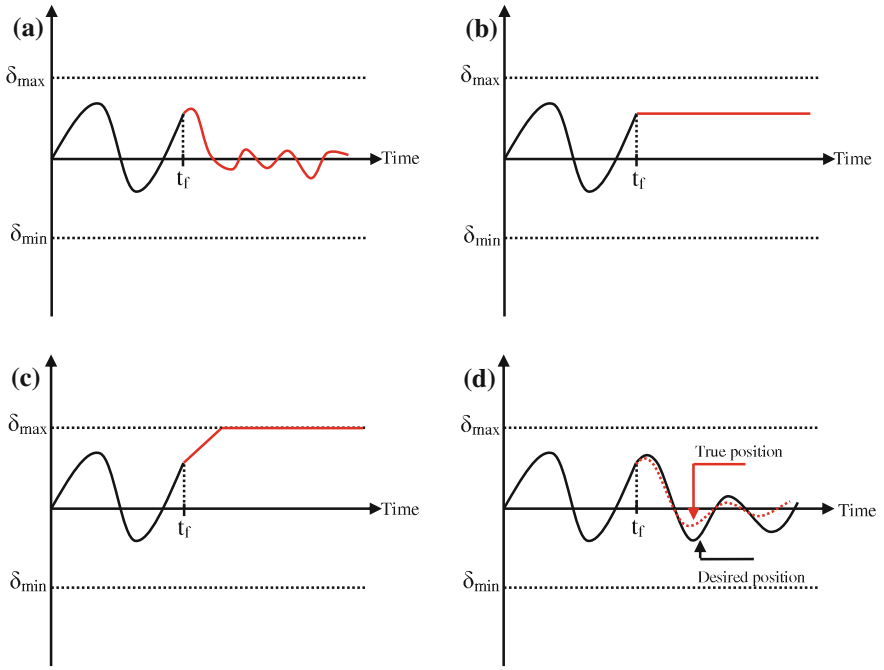

Fig. 1.3 Types of actuator failure (**a**)–(**c**) and actuator fault (**d**) (adapted from [3]). **a** Float failure. **b** Lock in place failure. **c** Hard over failure. **d** Loss of effectiveness

1.1.1 Modeling Faults and Failures

In the literature, different representations have been used to model actuator faults and failures. For example, to model an actuator fault/failure, the state-space model can be written as

$$\dot{x}(t) = Ax(t) + B\Sigma(t)u(t) + B(I - \Sigma(t))\bar{u}(t) \tag{1.1}$$

where $A \in \mathbb{R}^{n\times n}$, $B \in \mathbb{R}^{n\times m}$ and $\Sigma(t) = \text{diag}(\theta_1(t), \ldots, \theta_m(t))$, $\theta_i(t) \in \left[0\ 1\right]$ and $\bar{u}(t)$ is an uncontrollable offset vector. If $\theta_i(t) = 1$, then the ith actuator is functioning normally, whereas if $\theta_i(t) = 0$ then the ith actuator has a failure, i.e. the control action from the failed actuator is equal to $\bar{u}(t)$. Throughout this book, a state-space representation of the plant is considered in order to synthesise the fault tolerant controllers. Mathematically a linear time invariant (LTI) system, subject to actuator faults/failures can be expressed as

$$\dot{x}(t) = Ax(t) + BW(t)u(t) \tag{1.2}$$

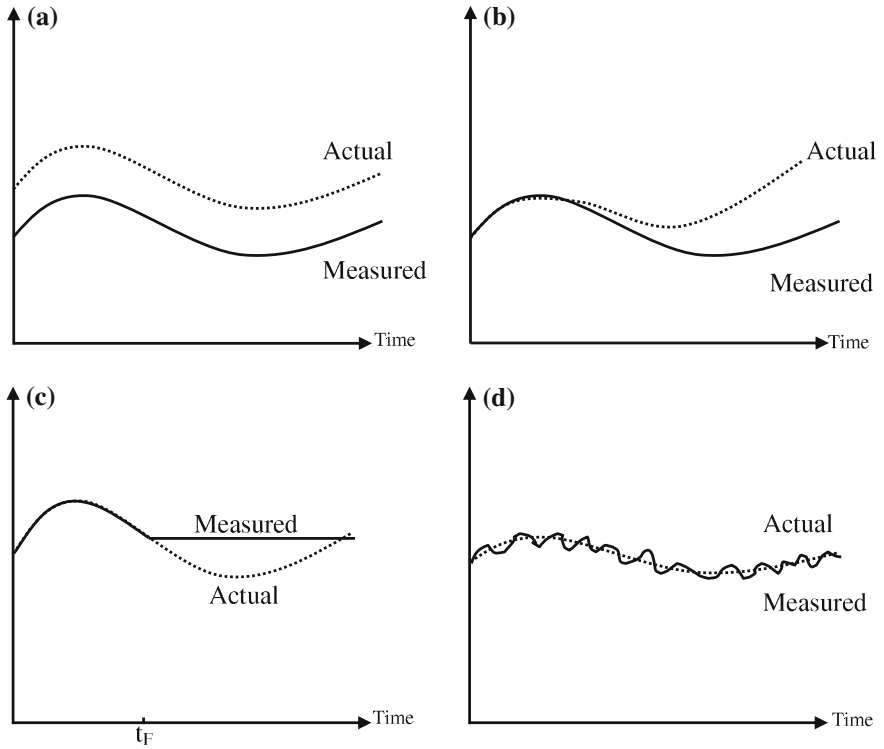

Fig. 1.4 Types of sensor failure (**a**) and sensor faults (**b**)–(**d**) (adapted from [3]). **a** Bias. **b** Drift. **c** Freezing. **d** Loss of accuracy

where $W(t) = \text{diag}(w_1(t), \ldots, w_m(t))$ is a diagonal semi-positive definite weighting matrix. The scalars $w_1(t), \ldots, w_m(t)$ all lie in $\left[\,0\ 1\,\right]$ and model the effectiveness level of the actuators. If $w_i(t) = 1$, it means that the corresponding ith actuator has no fault and is working perfectly, whereas if $1 > w_i(t) > 0$ an actuator fault is present. The situation in which $w_i(t) = 0$, represents a complete loss of effectiveness or failure of a particular actuator. Some common types of actuator fault/failure are shown in Fig. 1.3. The fault and failure representation in (1.2), which is a special case of (1.1) has become the building block for many of the FTC schemes in this book because this representation makes the closed-loop stability analysis tractable, as will be demonstrated in the subsequent chapters. From Eqs. (1.1) and (1.2), it is clear that faults or failures associated with the actuators only affect the input distribution matrix B, whereas a component fault may introduce changes in the system matrix, and can be represented in the following form

$$\dot{x}(t) = (A + \triangle A(t))x(t) + BW(t)u(t) \tag{1.3}$$

where $\triangle A(t)$ represents a change in the system matrix A.

1.2 Fault Detection and Isolation (FDI)

Fault Detection and Isolation (FDI) schemes provide online information about system faults or failures. The fault or failure information provided by the FDI scheme plays an important role in managing any actuator redundancy in an efficient way. On the basis of this information, active FTC methods (as explained in the next section) take appropriate action to mitigate the effects of these faults/failures. One important facet of an FDI scheme is how fast and precisely a fault is detected, isolated and identified, so that prompt action can be taken by the FTC scheme. Generally FDI schemes in the literature are classified into two categories—*model based* and *model free* FDI schemes. Model based schemes utilise (nominal fault-free) mathematical models (analytical redundancy) of the plant for FDI purposes, and can be sub-categorised as residual based FDI schemes or fault estimation based FDI schemes. In residual based FDI schemes, the measurements from the plant sensors are compared with signals from the mathematical model to create residual signals. In the fault-free case, the residuals should vanish or be very close to zero. The increasing size of a residual due to faults or failures can then be used for detection purposes. Residuals are normally used with a threshold level to avoid any false alarms due to disturbances or noise signals. So-called unknown input observer (UIO) based schemes can be used as robust (in the sense of decoupling of disturbance signals) residual generators. The idea behind the UIO scheme is *to decouple the state estimation error from the unknown inputs: in this case the disturbance signals*. Residual based FDI schemes usually provide fault detection capabilities and also the location of the fault. The location of a fault in the system can be inferred by employing a bank of dissimilar residual signals. (One possibility is to make each residual sensitive to a particular fault and insensitive to all the others in order to isolate a particular fault.)

In certain FTC schemes, and more often than not in the ones described in this book, the efficiency level of the actuators (or an estimation of the fault) is also required for FTC purposes. The control effectiveness estimation problem can be posed within an augmented Kalman Filter formulation, where the control effectiveness gains are modelled as augmented states in the linear plant model. Sliding mode approaches have also been proposed (details of which can be found later in Sect. 3.3.1). In certain applications, such as passenger aircraft actuator, effectiveness levels can be obtained by using a measurement of the actual actuator deflection compared to the demand. Such information is typically available in many safety critical systems.[3] This simplifies the problem considerably.

[3] In modern fly-by-wire passenger aircraft [4], sensors measuring the actuator deflections provide this information to local monitoring schemes.

1.3 Fault Tolerant Control Systems

The motivation for the early research in the field of fault tolerant control was in the area of flight control systems to improve the reliability and safety of aircraft. A fault tolerant control system has the capability to maintain some level of acceptable performance, or degrade gracefully subsequent to the occurrence of a fault. From the definitions, it is clear that the main task in achieving fault tolerance is to design a suitable controller which has the ability to maintain overall system stability in fault-free, as well as in situations when a system becomes faulty. Usually to design such a controller, the system should have redundant control effectors, which can be efficiently used and exploited to achieve fault tolerance. In the case of a failure in certain actuators, the control effort can be distributed to healthy actuators to maintain the desired performance or at least some level of acceptable performance. Therefore it is fair to say that redundancy is necessary, or is at least a key ingredient, in achieving fault tolerance. This redundancy can be achieved by the direct replication of the hardware (actuator/sensor) or it can be in the form of dissimilar hardware having similar functionality.

To explain the concept mathematically, consider an over-actuated system with redundancy

$$\dot{x}(t) = Ax(t) + Bu(t) \tag{1.4}$$

where the system matrix $A \in \mathbb{R}^{n\times n}$ and $B \in \mathbb{R}^{n\times m}$. Suppose the input distribution matrix B can be partitioned as $B = \begin{bmatrix} B_p & B_s \end{bmatrix}$ where $B_p \in \mathbb{R}^{n\times l}$ is assumed to be of rank $l < m$ and the pair (A, B_p) is controllable. Provided only l outputs of (1.4) need to be regulated, the channels associated with matrix B_s constitute redundant (secondary) actuators which can be used in the case of faults/failures to the primary one. The ultimate objective of a FTC scheme is to provide a desired level of performance in fault-free as well as in fault/failure situations, provided that redundancy is available in the system. Depending on the way the problem is tackled, FTC systems can be classified as *passive* fault tolerant control (PFTC) systems or *active* fault tolerant control (AFTC) systems. A block diagram representing the classification of FTC methods is shown in Fig. 1.5. However as seen in this book, sometimes this classification is blurred.

1.3.1 Passive Fault Tolerant Control Systems

In PFTC systems the controller is of a fixed structure and is designed off-line.[4] Due to the fact that PFTC systems do not require up-to-date fault information, PFTC methods are computationally more attractive. In passive fault tolerant control schemes, the idea is to design the controller using robust control techniques such that the closed-loop system response is robust against certain classes of uncertainties and presumed

[4]PFTC systems are also called reliable control systems in the literature [5].

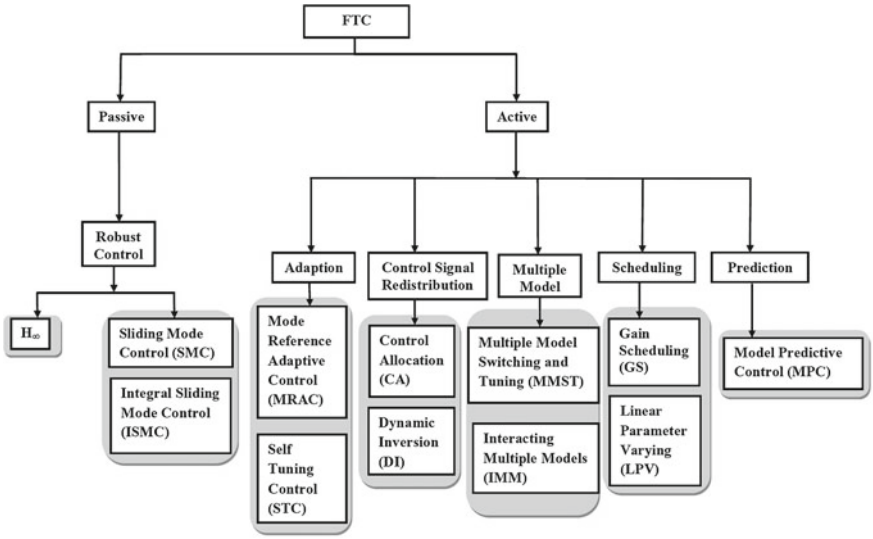

Fig. 1.5 Classification of FTC methods (adapted from [2])

system faults. The $\mathscr{H}_\infty$ methodology is a well-known technique in the field of robust control, and can take into account performance and stability requirements. The idea behind the $\mathscr{H}_\infty$ control methodology is to design a controller which can provide stabilising properties and minimise the effects of uncertainties or disturbances on certain outputs of interest. When designing a robust controller, the worst case performance specifications are taken into account, which may lead to a requirement to sacrifice the nominal performance of the system. Faults usually occur very rarely in the system and so to sacrifice the nominal performance to obtain robustness against a certain class of faults may not be appropriate.

Another robust control methodology is Sliding Mode Control (SMC). This approach underpins the ideas in this book and will be discussed in depth in Chap. 2. SMC schemes have inherent robustness properties against matched uncertainties (i.e. uncertainties which act in the input channels) during a sliding mode. The basic concept is to first design a sliding surface, and then to specify a controller to induce and maintain a sliding motion on the sliding surface. Due to its inherent robustness against matched uncertainties, SMC schemes have *the inherent capability to directly deal with actuator faults—which can be effectively modelled as matched uncertainties*. A shortcoming of SMC schemes is that failures cannot be directly handled, and so some sort of mechanism is required in order to distribute the control effort among the redundant healthy actuators.

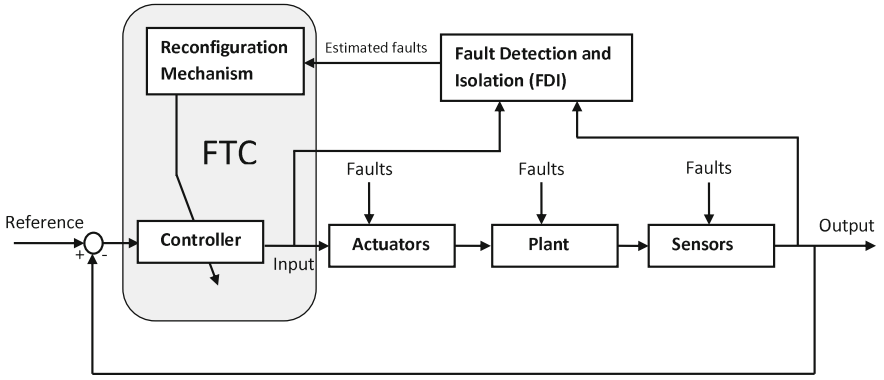

Fig. 1.6 Main structure of AFTC systems (adapted from [2])

1.3.2 Active Fault Tolerant Control Systems

Active fault tolerant control (AFTC) systems on the other hand rely on fault information from the FDI scheme to react appropriately. Specifically AFTC systems, react to faults/failures actively, by reconfiguring control actions so that stability and acceptable performance of the system can be maintained. In certain circumstances, degraded performance may have to be accepted. A typical AFTC system is represented in Fig. 1.6. The structure of an AFTC system is usually more complex compared to PFTC systems, but can deal with a wider class of faults. From Fig. 1.6, it is clear that there are two aspects that distinguish AFTC systems from PFTC systems. The first one is the FDI scheme and the other is the reconfiguration mechanism. The reconfiguration mechanism changes the parameters or structure of the controller, (usually) based on the fault information provided by the FDI unit. It is common practice that FTC and FDI schemes are designed independently. In the literature AFTC methods are further sub-classified as *Projection based* methods, and *online control redesign* methods. In *projection based* methods, one of the pre-computed controllers from a set, which have already been designed off-line for a specific fault scenario, is selected, depending on the fault information provided by the FDI scheme. In *online control redesign* methods, depending on the fault information provided by the FDI scheme, *the new controller is synthesised online*. *Online control redesign* methods are also referred to as *reconfigurable* control or *restructureable* control. In *reconfigurable* control, the controller parameters are computed online depending on the fault information provided by the FDI unit, whereas in *restructureable* control both the structure and controller parameters are computed online.

Many different approaches have been considered for FTC. A summary of these appear in Table 1.1.

Table 1.1 Examples of existing control design methodologies used in FTC (adapted from [5])

Design approaches	References
Adaptive control	[6–9]
Control allocation	[10–22]
Sliding mode control	[15, 19, 23–27]
Dynamic inversion	[28, 29]
Multiple model	[30–35]
Gain scheduling	[36]
Linear parameter varying	[37–41],
Model predictive control	[42–47]
$\mathscr{H}_\infty$ robust control	[8, 48–50]

1.3.3 Control Allocation

As discussed in Sect. 1.3, hardware redundancy provides opportunities that can be exploited when designing fault tolerant controllers. The advantage of the Control Allocation (CA) method is that the underlying control law can be designed separately in order to produce the desired control effort and the CA distributes this virtual effort among the available actuators to achieve the required system performance. To get insight into how the CA method works, consider a linear model of the plant with redundant actuators

$$\dot{x}(t) = Ax(t) + Bu(t) \tag{1.5}$$

where $A \in \mathbb{R}^{n\times n}$, $B \in \mathbb{R}^{n\times m}$. Assume that the control input distribution matrix B can be factorised as

$$B = B_v B_u \tag{1.6}$$

where $B_v \in \mathbb{R}^{n\times l}$ and $B_u \in \mathbb{R}^{l\times m}$, and both matrices have rank $l < m$. Substituting (1.6) into (1.5) yields the new system description

$$\dot{x}(t) = Ax(t) + B_v \underbrace{B_u u(t)}_{v(t)} = Ax(t) + B_v v(t)$$

where

$$v(t) := B_u u(t) \tag{1.7}$$

Usually $v(t) \in \mathbb{R}^l$ is called the virtual control effort. If $u(t)$ is chosen as

$$u(t) = B_u^\dagger v(t) \tag{1.8}$$

where $B_u^\dagger = \Omega B_u^T (B_u \Omega B_u^T)^{-1}$ (i.e. a weighted right pseudo-inverse of B_u) where Ω is any matrix such that $\det(B_u \Omega B_u^T) \neq 0$, then $u(t)$ as defined in (1.8) satisfies

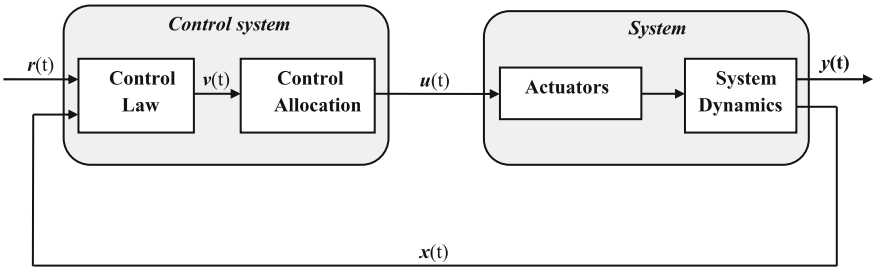

Fig. 1.7 Control Allocation scheme (adapted from [51])

the constraint in (1.7). In order to redistribute the control signals in the case of faults or failures, different researchers utilise the design freedom in the pseudo-inverse matrix $B_u^{\dagger}$ in different ways. The structure of the CA scheme is shown in Fig. 1.7, which demonstrates that the CA element is not part of the virtual control law $\nu(t)$. The virtual control effort $\nu(t)$ produced by the controller is directly translated into actuator deflections by the CA module.

1.4 Summary

In this chapter a brief introduction to FTC and some common terminologies that are used in the FTC literature have been defined. Typical faults or failures associated with the actuators and sensors were also explained. Redundancy, which is a key criterion in FTC has been identified and defined. Methods which have been used to design fault tolerant controllers using active and passive approaches were also discussed and in particular control allocation has been introduced as a means of managing actuator redundancy. The remainder of the book discusses how sliding mode methods, specifically integral sliding mode schemes, can be combined with CA to create practical FTC schemes, which can cope with faults and certain classes of total failure (in actuators).

1.5 Notes and References

The motivation for the early research in the field of fault tolerant control was in the area of flight control systems, to improve the reliability and safety of aircraft [5, 52]. In the area of FDI and FTC many books have been written: for example [3, 12, 53–55]. A classic early book on FDI is [56]. A key reference for (robust) model based FDI schemes is [57]. This provides a detailed account of unknown input observers, eigenstructure and $\mathscr{H}_\infty$ methods. In [3], the authors describe fault reconstruction and fault tolerant control schemes to deal with sensor and actuator faults/failures using

SMC schemes for aerospace applications. Reference [12] describes advanced FDI and FTC methods for linear and nonlinear small UAVs models. To model actuator faults and failures, other FTC researchers have used different representations to the one considered in this book: see for example [2, 15, 58–61]. The schemes proposed in [62] use a Kalman filter based approach to estimate the actuator efficiency. Model based FDI and FTC methods are described in [54] to deal with actuator and sensor faults. In [55], different kinds of FDI schemes—specifically knowledge based, signal based and process model based methods are described for different kinds of engineering systems. The survey papers, for example [5, 52, 63], and books [3, 64], provide a bibliographical review of different FTC methods. In addition a review of FTC applied to aerospace problems appears in [64]. A comparative study between active and passive FTC approaches is given in [65]. The work in [19, 25–27, 66] shows that if there is enough redundancy in the system, SMC can deal with total actuator failures. A detailed discussion on the requirements and merits of FDI and FTC schemes was documented in [67].

Control Allocation (CA) has attracted the attention of many FTC researchers because of its ability to handle actuator faults or failures without the need to modify the underlying control law [10–13]. The CA method can also deal effectively with actuator constraints. The work in [11, 68] explicitly uses information about the actuator constraints (rate and position) for CA. The work in [16, 17] describes a special structure of CA called daisy chaining. In [69], a modified daisy chaining method is proposed to deal with actuator loss of effectiveness. The benefits of using CA in terms of FTC are exploited in [10, 18] for high performance aircraft. In [70], a comparison between different control allocation methods is made and in [14] optimal control and CA are compared in terms of redistributing a virtual control signal among redundant actuators. In [15, 19] a combination of CA with SMC is considered for FTC.

References

1. Isermann, R., Ballé, P.: Trends in the application of model-based fault detection and diagnosis of technical processes. Control Eng. Pract. **5**(5), 709–719 (1997)
2. Verhaegen, M., Kanev, S., Hallouzi, R., Jones, C., Maciejowski, J., Smail, H.: Fault tolerant flight control - a survey. In Edwards, C., Lombaerts, T., Smaili, H. (eds.) Fault Tolerant Flight Control of LNCIS, vol. 399, pp. 47–89. Springer, Heidelberg (2010)
3. Alwi, H., Edwards, C., Tan, C.P.: Fault Detection and Fault Tolerant Control Using Sliding Modes. Advances in Industrial Control Series. Springer, New York (2011)
4. Brire, D., Traverse, P.: Airbus A320/A330/A340 electrical flight controls: a family of fault-tolerant systems. In: Digest of Papers FTCS-23 The Twenty-Third International Symposium on Fault-Tolerant Computing, pp. 616–623 (1993)
5. Zhang, Y., Jiang, J.: Bibliographical review on reconfigurable fault-tolerant control systems. Annu. Rev. Control **32**, 229–252 (2008)
6. Aström, K.J., Wittenmark, B.: Adaptive Control, 2nd edn. Addison Wesley, Boston (1995)
7. Dumont, G.A., Huzmezan, M.: Concepts, methods and techniques in adaptive control. In: Proceedings of the American Control Conference, pp. 1137–1150 (2002)

8. Magni, J.F., Bennani, S., Terlouw, J.: Robust Flight Control: A Design Challenge. Springer, Heidelberg (1997)
9. Jung, B., Kim, Y., Ha, C.: Fault tolerant flight control system design using a multiple model adaptive controller. Proc. Inst. Mech. Eng. Part G: J. Aerosp. Eng. **223**, 39–50 (2009)
10. Davidson, J.B., Lallman, F.J., Bundick, W.T.: Real-time adaptive control allocation applied to a high performance aircraft. In: 5th SIAM Conference on Control and Its Application, (2001)
11. Bošković, J.D., Mehra, R.K.: Control allocation in over-actuated aircraft under position and rate limiting. In: Proceedings of the American Control Conference, (2002)
12. Ducard, G.: Fault-tolerant Flight Control and Guidance Systems: Practical Methods for Small Unmanned Aerial Vehicles. Advances in Industrial Control Series. Springer, London (2009)
13. Zhang, Y., Suresh, V.S., Jiang, B., Theilliol, D.: Reconfigurable control allocation against aircraft control effector failures. In: Proceedings of the 16th IEEE International Conference on Control Applications, (2007)
14. Härkegård, O., Glad, S.T.: Resolving actuator redundancy - optimal control vs. control allocation. Automatica **41**, 137–144 (2005)
15. Alwi, H., Edwards, C.: Fault tolerant control using sliding modes with on-line control allocation. Automatica **44**, 1859–1866 (2008)
16. Buffington, J.M., Enns, D.F.: Lyapunov stability analysis of daisy chain control allocation. J. Guid. Control Dyn. **19**, 1226–1230 (1996)
17. Oppenheimer, M., Doman, D., Bolender, M.: Control allocation for overactuated systems. In: 14th IEEE Conference on Control and Automation MED 06, pp. 1–6 (2006)
18. Buffington, J.: Tailless aircraft control allocation, In: AIAA Guidance, Navigation and Control, pp. 737–747 (1997)
19. Hess, R.A., Wells, S.R.: Sliding mode control applied to reconfigurable flight control design. J. Guid. Control Dyn. **26**, 452–462 (2003)
20. Khelassi, A., Jiang, J., Theilliol, D., Weber, P., Zhang, Y.M.: Reconfiguration of control inputs for overactuated systems based on actuators health, pp. 13729–13734. 18th IFAC World Congress, Milano (2011)
21. Yan-Ping, F., Yue-Hua, C., Bin, J., Ming-Kai, Y.: Fault tolerant control with on-line control allocation for flexible satellite attitude control system. In: 2nd International Conference on Intelligent Control and Information Processing, pp. 42–46 (2011)
22. Johansen, T., Fossen, T.I.: Control allocation - a survey. Automatica **49**, 1087–1103 (2013)
23. Utkin, V., Guldner, J., Shi, J.: Sliding Mode control in Electromechanical Systems. Taylor and Francis, Abingdon (1999)
24. Edwards, C., Spurgeon, S.K.: Sliding Mode control: Theory and Applications. Taylor and Francis, London (1998)
25. Shtessel, Y., Buffington, J., Banda, S.: Tailless aircraft flight control using multiple time scale re-configurable sliding modes. IEEE Trans. Control Syst. Technol. **10**, 288–296 (2002)
26. Shin, D., Moon, G., Kim, Y.: Design of reconfigurable flight control system using adaptive sliding mode control: actuator fault. Proc. Inst. Mech. Eng. Part G: J. Aerosp. Eng. **219**, 321–328 (2005)
27. Corradini, M.L., Orlando, G., Parlangeli, G.: A fault tolerant sliding mode controller for accommodating actuator failures. In: Proceedings of the 44th IEEE Conference on Decision and Control, (2005)
28. Ito, D., Georgie, J., Vasalek, J., Ward, D.T.: Re-entry vehicle flight controls design guidelines: dynamic inversion. Technical Report 210771, NASA/TP, NASA, (2002)
29. Joosten, D., van den Boom, T., Lombaerts, T.: Fault-tolerant control using dynamic inversion and model-predictive control applied to an aerospace benchmark. In: Proceedings of the 17th World Congress IFAC, Seoul, pp. 12030–12035 (2008)
30. Bošković, J.D., Mehra, R.K.: A multiple model-based reconfigurable flight control system design. In: Proceedings of the 37th IEEE Conference on Decision and Control, pp. 4503–4508. Tampa, Florida (1998)
31. Narendra, K.S., Driollet, O.A., Feiler, M., George, K.: Adaptive control using multiple models, switching and tuning. Int. J. Adapt. Control Signal Process. **17**, 87–102 (2003)

32. Bošković, J.D., Mehra, R.K.: Stable multiple model adaptive flight control for accommodation of a large class of control effector failures. In: Proceedings of the American Control Conference, pp. 1920–1924. San Diego, California (1999)
33. Aravena, J., Zhou, K., Li, X., Chowdhury, F.: Fault tolerant safe flight controller bank. In: Proceedings of the IFAC Symposium SAFEPROCESS, pp. 807–812. Beijing (2006)
34. Kanev, S., Verhaegen, M.: A bank of reconfigurable LQG controllers for linear systems subjected to failures. In: Proceedings of the 39th IEEE Conference on Decision and Control, pp. 3684–3689. Sydney, Australia (2000)
35. Zhang, Y., Jiang, J.: Integrated Active Fault-Tolerant Control using IMM approach. IEEE Trans. Aerosp. Electron. Syst. **37**(4), 1221–1235 (2001)
36. Leith, D.J., Leithead, W.E.: Survey of gain-scheduling analysis and design. international journal of control. Int. J. Control **73**(11), 1001–1025 (2000)
37. Marcos, A., Balas, G.J.: Development of linear-parameter-varying models for aircraft. AIAA J. Guid. Control Dyn. **27**(2), 218–228 (2004)
38. Patton, R.J., Klinkhieo, S.: LPV fault estimation and FTC of a two link manipulator. In: Proceedings of the American control Conference, pp. 4647–4652. Baltimore, MD (2010)
39. Marcos, A., Veenman, J., Scherer, C., Zaiacomo, G., Mostaza, D., Kerr, M., Koroglu, H., Bennani, S.: Application of LPV modeling, design and analysis methods to a re-entry vehicle. In: AIAA GNC/AFM/MST/ASC/ASE Conference, pp. 1–18 (2010)
40. Theilliol, D., Aberkane, S., Sauter, D.: Fault tolerant control design for polytopic LPV systems. Int. J. Appl. Math. Comput. Sci. **17**(1), 27–37 (2007)
41. Montes, S., Puig, V., Witczak, M., Dziekan, L.: Fault tolerant strategy for actuator faults using LPV techniques: application to a two degree of freedom helicopter. J. Appl. Math. Comput. Sci. **22**(1), 161–171 (2012)
42. Mayne, D.Q., Rawlings, J.B., Rao, C.V., Scokaert, P.O.M.: Constrained model predictive control: Stability and optimality. Automatica **36**, 789 (2000)
43. Maciejowski, J.M., Jones, C.N.: MPC fault-tolerant flight control case study: Flight 1862. In: IFAC Symposium SAFEPROCESS, pp. 121–126. Washington DC (2003)
44. Joosten, D.A., Maciejowski, J.M.: MPC design for fault-tolerant flight control purposes based upon an existing output feedback controller. In: Proceedings of the 7th IFAC Symposium on Fault Detection, Supervision and Safety of Technical Processes, pp. 253–258. Barcelona, Spain (2009)
45. Sun, S., Dong, L., An, C., Liu, W.: Fault-tolerant control design for linear systems with input constraints and actuator failures. In: CDC and CCDC Conference, pp. 5278–5283 (2009)
46. Miksch, T., Gambier, A., Badreddin, E.: Real-time implementation of fault-tolerant control using model predictive control. In: 17th IFAC World Congress, pp. 11136–11141. Seoul (2008)
47. Yetendji, A., Seron, M., Dona, J.: Robust MPC multicontroller design for actuator fault tolerance of constrained systems. In: 18th IFAC World Congress, pp. 4678–4683. Milano (2011)
48. Marcos, A., Balas, G.J.: A robust integrated controller/diagnosis aircraft application. Int. J. Robust Nonlinear Control **15**, 531–551 (2005)
49. Wei, X., Verhaegen, M.: LMI solutions to the mixed $H2/\mathscr{H}_\infty$ fault detection observer design for linear parameter-varying systems. Int. J. Adapt. Control Signal Process. **25**(2), 114–136 (2011)
50. Yang, Z., Stoustrup, J.: Robust reconfigurable control for parametric and additive faults with FDI uncertainties. In: Decision and Control 2000. Proceedings of the 39th IEEE Conference, pp. 4132–4137 (2000)
51. Härkegård, O.: Backstepping and control allocation with applications to flight control, PhD thesis, Division of Automatic Control, Department of Electrical Engineering Linköping, University, Sweden (2003)
52. Patton, R.J.: Fault tolerant control systems: the 1997 situation. In: Proceedings of the IFAC symposium SAFEPROCESS'97, pp. 1033–1054 (1997)
53. Blanke, M., Kinnaert, M., Lunze, J., Staroswiecki, M.: Diagnosis and Fault-Tolerant Control, 2nd edn. Springer, Berlin (2006)

54. Noura, H., Theilliol, D., Ponsart, J.C., Chamseddine, A.: Fault tolerant Control systems, design and practical applications. Springer, London (2009)
55. Isermann, R.: Fault diagnosis Applications: Model Based condition monitoring: Actuators, drives, machinery, plants, sensors and fault tolerant systems. Springer, Berlin (2011)
56. Patton, R.J., Frank, P.M., Clark, R.N.: Fault Diagnosis in Dynamic Systems: Theory and Application. Prentice Hall, New York (1989)
57. Chen, J., Patton, R.: Robust model-based fault diagnosis for dynamical systems. Kluwer Academic Publishers, Berlin (1999)
58. Noura, H., Sauter, D., Hamelin, F., Theilliol, D.: Fault-tolerant control in dynamic systems: application to a winding machine. IEEE Control Syst. Mag. **20**(1), 33–49 (2000)
59. Tao, G., Joshi, S.M., Ma, X.: Adaptive state feedback and tracking control of systems with actuator failures. IEEE Trans. Autom. Control **46**(1), 78–95 (2001)
60. Zhang, Y., Jiang, J.: Fault tolerant control system design with explicit consideration of performance degradation. IEEE Trans. Aerosp. Electron. Syst. **39**(3), 838–848 (2003)
61. Jiang, J., Zhang, Y.: Accepting performance degradation in fault-tolerant control system design. IEEE Trans. Control Syst. Technol. **14**(2), 284–292 (2006)
62. Wu, N., Zhang, Y., Zhou, K.: Detection, estimation, and accommodation of loss of control effectiveness. Int. J. Adapt. Control Signal Process. **14**(7), 775–795 (2000)
63. Jiang, J.: Fault-tolerant control systems - an introductory overview. Autom. SINCA **31**(1), 161–174 (2005)
64. Edwards, C., Lombaerts, T., Smaili, H.: Fault Tolerant Flight Control: A Benchmark Challenge, vol. 399, Springer, Heidelberg (2010)
65. Jiang, J., Yu, X.: Fault tolerant control systems: a comparative study between active and passive approaches. Annu. Rev. Control **36**(1), 60–72 (2012)
66. Alwi, H., Edwards, C.: Fault tolerant control of a civil aircraft using a sliding mode based scheme. 44th IEEE Conference on Decision and Control. and the European Control Conference, pp. 1011–1016. Seville, Spain (2005)
67. Zhang, Y., Jiang, J.: Issues on integration of fault diagnosis and reconfigurable control in active fault-tolerant control systems. In: Proceedings of the IFAC Symposium SAFEPROCESS, pp. 1437–1448. Beijing, China (2006)
68. Durham, W.C.: Constrained control allocation. J. Guid. Control Dyn. **16**(4), 717–725 (1993)
69. Kim, J., Yang, I., Lee, D.: Accommodation of actuator faults using control allocation with modified daisy chaining. In: 11th International Conference on Control, Automation and Systems, pp. 717–720, Korea (2011)
70. Page, A., Steinberg, M.: Closed-loop comparison of control allocation methods. In: Proceedings of the AIAA Guidance, Navigation and Control Conference, pp. 1760–1770 (2000)

Chapter 2
Integral Sliding Mode Control

Variable Structure Control Systems (VSCS) are a class of systems where the control law, as a function of the system state, is deliberately changed (from one structure to another) according to some predefined rules: for example a relay system. During a sliding mode the closed-loop system response is constrained to evolve along a sliding surface in the state-space to an equilibrium point. In sliding mode schemes, a switching function typically dictates which structure of control law is to be used at a particular time instant, depending on the position of the state from the sliding surface. The set of points for which the switching function is zero is called the sliding surface. SMC has now become an established tool to design controllers for uncertain systems, and provides robustness properties against matched uncertainties i.e. uncertainties that affect the plant dynamics acting in the input channels. However this robustness against external disturbances and parameter variations matched to the control can only be achieved after the occurrence of the sliding mode. Before the occurrence of the sliding mode i.e. during the so-called reaching phase, the system is affected by external disturbances—even matched ones. In order to eliminate the reaching phase and to ensure robustness throughout the entire closed-loop system response (i.e. to enforce a sliding mode for all time) the idea of Integral Sliding Modes (ISM) was proposed. In this chapter a step-by-step design procedure is described for the synthesis of sliding mode controllers; then these ideas are extended to integral sliding modes in order to ensure robustness throughout the entire system response. Necessary conditions for the existence of sliding modes are also given. The properties of the system while in the sliding mode are also explained, and are examined through simulations.

2.1 Introduction

SMC is a useful robust technique to handle sudden and large changes in the system dynamics and has been applied to many areas—for example motor control, aircraft and spacecraft control, process control and power systems. The realisation of a sliding

M.T. Hamayun et al., *Fault Tolerant Control Schemes Using Integral Sliding Modes*, Studies in Systems, Decision and Control 61,
DOI 10.1007/978-3-319-32238-4_2

mode controller comprises two steps. The first step is to design a sliding (switching) surface on which the sliding motion will take place. The second step is to design a control law, which depends on the choice of switching function and forces the system state trajectories to reach and slide on the surface. An important condition in the sliding mode literature is the reachability condition, which guarantees the existence of the sliding mode. Once sliding is achieved and maintained, robustness against matched uncertainties is guaranteed. Details of the design procedures are given in the next sections.

2.2 Problem Statement and Equivalent Control

In order to explain the design procedure for a system where *full state information* is available, consider an uncertain linear time invariant (LTI) system of the form

$$\dot{x}(t) = Ax(t) + Bu(t) + M\xi(t, x) \tag{2.1}$$

where $A \in \mathbb{R}^{n\times n}$, $B \in \mathbb{R}^{n\times m}$.

Assumption 2.1 It is assumed that the matrix B has full rank i.e. $\text{rank}(B) = m$, where $1 \leq m < n$ and the pair (A, B) is controllable.

Assumption 2.2 The matrix $M \in \mathbb{R}^{n\times l}$ is assumed to be known and lies in the range space of the input distribution matrix B i.e. $\mathscr{R}(M) \subset \mathscr{R}(B)$, therefore it is possible to write $M = BD$ for some $D \in \mathbb{R}^{m\times l}$.

The function $\xi(t, x)$ represents an external disturbance or models uncertainty which is unknown but has a known upper bound for all x and t. Therefore the uncertain system in (2.1) can be rewritten as

$$\dot{x} = Ax(t) + Bu(t) + BD\xi(t, x) \tag{2.2}$$

Uncertainty of the form in (2.2), acting in the channel of the input distribution matrix, is referred to as matched uncertainty. As a first step, define a sliding surface as

$$\mathscr{S} = \{x \in \mathbb{R}^n \quad : \quad \sigma(t) = 0\} \tag{2.3}$$

where $\sigma(t)$ is a linear switching function defined as

$$\sigma(t) = Gx(t) \tag{2.4}$$

where $G \in \mathbb{R}^{m\times n}$ is a design matrix and is of full rank. Furthermore by design it is assumed that the square matrix GB is nonsingular i.e. $\det(GB) \neq 0$. It is important that the sliding motion on the sliding surface should be stable and robust against the

uncertainty $\xi(t, x)$. Therefore in order to analyse the sliding motion associated with the sliding surface in (2.3), consider the time derivative of (2.4) given by

$$\dot{\sigma}(t) = G\dot{x}(t) \tag{2.5}$$

Substituting the open-loop system equations from (2.2) into (2.5) gives

$$\dot{\sigma}(t) = G\left(Ax(t) + Bu(t) + BD\xi(t, x)\right) \tag{2.6}$$

It is assumed that the system states are forced to reach the sliding surface at time t_s say, so that for all $t \geq t_s$ an ideal sliding motion can be obtained i.e.

$$\sigma(t) = \dot{\sigma}(t) = 0 \quad \text{for all } t \geq t_s$$

The control signal $u(t)$ such that the time derivative $\dot{\sigma}(t)$ along the state trajectories is equal to zero can be obtained by equating Eq. (2.6) to zero which yields

$$u_{eq}(t) = -(GB)^{-1}\left(GAx(t) + GBD\xi(t, x)\right) \quad \text{for } t \geq t_s \tag{2.7}$$

where the square matrix GB is nonsingular by design. The expression $u_{eq}(t)$ in (2.7) is termed the equivalent control and can be thought of as the average value which the control signal must take to maintain the sliding motion on the sliding surface. However, it is not the control law that is applied to the system to induce the sliding mode. In order to obtain an expression for the sliding motion (i.e. the motion while the system is in the sliding mode), substituting the value of $u_{eq}(t)$ from (2.7) into (2.2), yields

$$\begin{aligned}\dot{x}(t) &= Ax(t) + B\left(-(GB)^{-1}(GAx(t) + GBD\xi(t, x))\right) + BD\xi(t, x) \\ &= \underbrace{(I_n - B(GB)^{-1}G)}_{\Gamma} Ax(t) + (I_n - B(GB)^{-1}G)BD\xi(t, x)\end{aligned} \tag{2.8}$$

Note that the projection operator Γ has the property that

$$\Gamma B = 0 \tag{2.9}$$

As a result, Eq. (2.8) reduces to

$$\dot{x}(t) = \Gamma Ax(t) \quad \text{for } t \geq t_s \tag{2.10}$$

From (2.10), it is clear that the effect of the uncertainty $\xi(t, x)$ during the sliding mode is completely rejected i.e. the reduced order system motion is insensitive to matched uncertainties. Also the stability of the sliding motion depends on the choice of sliding surface, i.e. the choice of switching matrix G.

2.2.1 Sliding Mode Control Laws

The second step is to design a control law such that the sliding motion on the surface $\mathscr{S}$ is guaranteed in finite time. A sliding mode controller for a system of the form in (2.1) typically consists of two parts; a linear part and a nonlinear part so that

$$u(t) = u_l(t) + u_n(t) \tag{2.11}$$

where the nonlinear part contains a discontinuous component and is responsible for inducing a sliding motion on $\mathscr{S}$, whereas the linear part, which is normally the nominal equivalent control, is responsible for helping to maintain sliding. Specifically

$$u(t) = -(GB)^{-1}GAx(t) - \rho(t,x)(GB)^{-1}\frac{\sigma(t)}{\|\sigma(t)\|} \quad \text{for } \sigma(t) \neq 0 \tag{2.12}$$

where $\frac{\sigma(t)}{\|\sigma(t)\|}$ is the unit vector component and $\rho(t,x)$ is a scalar gain chosen large enough (i.e. greater than the size of the uncertainty present in the system) to enforce the sliding motion.

Remark 2.1. For single input systems, the sliding mode controller in (2.12) becomes

$$u(t) = -(GB)^{-1}GAx(t) - \rho(t,x)(GB)^{-1}\text{sign}(\sigma(t)) \quad \text{for } \sigma(t) \neq 0 \tag{2.13}$$

where sign(.) is the signum function and has the property that $\sigma\,\text{sign}(\sigma) = |\sigma|$.

2.3 Reachability Problem

In the sliding mode literature the controller $u(t)$ is designed so that the so-called reachability condition is satisfied, which is a sufficient condition to ensure that at each time instant, the system state trajectories will converge towards the sliding surface. Mathematically this can be expressed for the case of single input systems as

$$\lim_{\sigma(t)\to 0+} \dot{\sigma}(t) < 0 \qquad \lim_{\sigma(t)\to 0-} \dot{\sigma}(t) > 0 \tag{2.14}$$

or in a compact form as

$$\sigma(t)\dot{\sigma}(t) < 0 \tag{2.15}$$

near the sliding surface $\sigma(t) = 0$. A stronger condition which ensures an ideal sliding motion in finite time, even in the presence of external disturbances or uncertainty, is given by

$$\sigma(t)\dot{\sigma}(t) \leq -\eta|\sigma(t)| \tag{2.16}$$

where η represents a positive design scalar. The expression in (2.16) is often called the η-reachability condition.

For multi-input systems, a natural multivariable version of the reachability condition in (2.16) is

$$\sigma^T(t)\dot{\sigma}(t) \leq -\eta\|\sigma(t)\| \tag{2.17}$$

This is a sufficient condition to show that the sliding surface $\mathscr{S}$ is attractive.

In order to demonstrate that the controller designed in (2.12) satisfies the η-reachability condition (2.17), substituting the value of (2.12) into (2.6) gives

$$\begin{aligned}\dot{\sigma}(t) &= GAx(t) + GB\left(-(GB)^{-1}GAx(t) - \rho(t,x)(GB)^{-1}\frac{\sigma(t)}{\|\sigma(t)\|}\right) + GBD\xi(t,x)\\ &= -\rho(t,x)\frac{\sigma(t)}{\|\sigma(t)\|} + GBD\xi(t,x)\end{aligned} \tag{2.18}$$

Pre-multiplying both sides of (2.18) by $\sigma^T(t)$ yields

$$\sigma^T(t)\dot{\sigma}(t) = -\rho(t,x)\frac{\sigma^T(t)\sigma(t)}{\|\sigma(t)\|} + \sigma^T(t)GBD\xi(t,x) \tag{2.19}$$

and using the property that $\sigma^T\sigma = \|\sigma\|^2$, Eq. (2.19) becomes

$$\begin{aligned}\sigma^T(t)\dot{\sigma}(t) &= -\rho(t,x)\|\sigma(t)\| + \sigma^T(t)GBD\xi(t,x)\\ &\leq \|\sigma(t)\|(-\rho(t,x) + \|GBD\xi(t,x)\|)\end{aligned} \tag{2.20}$$

For any particular choice of scalar gain $\rho(t,x)$ such that

$$\rho(t,x) \geq \|GBD\xi(t,x)\| + \eta \tag{2.21}$$

where η is a positive scalar, the inequality in (2.20) becomes

$$\sigma^T(t)\dot{\sigma}(t) \leq -\eta\|\sigma(t)\| \tag{2.22}$$

From (2.22), it is clear that the η-reachability condition is satisfied, which ensures the existence of an ideal sliding motion on the sliding surface $\mathscr{S}$.

2.4 A Simple Simulation Example

In this section, the design procedure for the typical sliding mode controller discussed in the previous sections is applied to a simulation example, to offer insight into the design procedure.

2.4.1 Spring Mass Damper System

A simple example of a spring-mass-damper system (SMDS), driven by a force $u(t)$, is considered here as shown in Fig. 2.1. It is assumed that at $t = 0$ the mass m is pulled down from the equilibrium position, such that $y(0) = 0.1\,\text{m}$ and $\dot{y}(0) = 0.05\,\text{m/s}$. The dynamical equation of the mechanical system (Fig. 2.1) can be written as

$$m\ddot{y}(t) + c\dot{y}(t) + ky(t) = u(t) \tag{2.23}$$

where k is the spring constant, c is the viscous-friction coefficient and m is the mass. A disturbance signal $a\sin(y)$ is added to the control input channel to demonstrate the invariance against a disturbance while in the sliding mode. The values of these constants are chosen as $m = 1\,\text{kg}$, $c = 3\,\text{N}\cdot\text{s/m}$, $k = 2\,\text{N/m}$ and $a = 0.1$. In order to write the differential equation in (2.23) in state-space form, define the state variables as $x_1(t) = y(t)$ and $x_2(t) = \dot{y}(t)$, which represent the position and velocity of the mass m. Equation (2.23) can be written in terms of the state variables as

$$\dot{x}_1(t) = \dot{y}(t) = x_2(t) \tag{2.24}$$

$$\dot{x}_2(t) = \ddot{y}(t) = -\frac{k}{m}x_1(t) - \frac{c}{m}x_2(t) + \frac{1}{m}(u(t) + a\sin(x_1(t))) \tag{2.25}$$

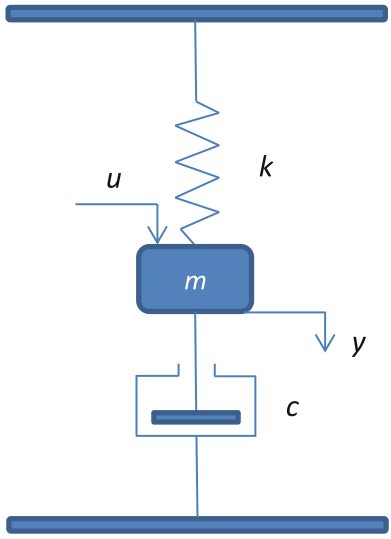

Fig. 2.1 Spring mass damper system

By substituting values for the spring constant k, viscous friction coefficient c, and mass m;

$$\begin{bmatrix} \dot{x}_1(t) \\ \dot{x}_2(t) \end{bmatrix} = \underbrace{\begin{bmatrix} 0 & 1 \\ -2 & -3 \end{bmatrix}}_{A} \begin{bmatrix} x_1(t) \\ x_2(t) \end{bmatrix} + \underbrace{\begin{bmatrix} 0 \\ 1 \end{bmatrix}}_{B} (u(t) + 0.1 \sin(x_1(t))) \tag{2.26}$$

2.4.2 Simulation Objective and SMC Design

In the simulation it is assumed that at $t = 0$ the mass m is pulled down from the equilibrium position such that $y(0) = 0.1$ m and $\dot{y}(0) = 0.05$ m/s. The objective here is to design a sliding mode controller to bring the system back to the equilibrium position from the initial conditions without overshooting in terms of displacement, and with a settling time of not more than 6 s.

The first step is to design a sliding surface. The switching function in (2.4) can be written in terms of the states $x_1(t)$ and $x_2(t)$ as

$$\sigma(t) = \begin{bmatrix} G_1 & G_2 \end{bmatrix} \begin{bmatrix} x_1(t) \\ x_2(t) \end{bmatrix} = G_1 x_1(t) + G_2 x_2(t) \tag{2.27}$$

where $G_1 \in \mathbb{R}$ and $G_2 \in \mathbb{R}$. Here it is assumed $G_2 \neq 0$. While sliding, the switching function $\sigma(t) = 0$, and Eq. (2.27) can be written as

$$x_2(t) = -G_2^{-1} G_1 x_1(t) \tag{2.28}$$

It is clear from (2.28) that once x_1(t) is known, the state $x_2(t)$ can be easily determined, therefore substituting the value of (2.28) into (2.24), the sliding motion is given by

$$\dot{x}_1(t) = -G_2^{-1} G_1 x_1(t) \tag{2.29}$$

From (2.29) it is clear that during sliding the system behaves as a reduced order system. Choosing the value of $G_2 = 1$, the switching matrix G takes the form

$$G = \begin{bmatrix} G_1 & 1 \end{bmatrix}$$

In this example the value of $G_1 = 0.9$ is chosen. Using the fact that $GB = 1$, the sliding mode control law defined in (2.13) becomes

$$u(t) = \begin{bmatrix} 2 & 2.1 \end{bmatrix} x(t) - \rho(t, x) \operatorname{sign}(\sigma(t)) \tag{2.30}$$

Finally in order to verify that the control law $u(t)$ in (2.30) satisfies the reachability condition (2.16), by substituting (2.30) and (2.26) into the time derivative of (2.27):

$$\begin{aligned}\dot{\sigma}(t) &= G_1\dot{x}_1(t) + G_2\dot{x}_2(t) \\ &= -\rho(t,x)\text{sign}(\sigma(t)) + 0.1\sin(x_1(t))\end{aligned} \tag{2.31}$$

Multiplying (2.31) with $\sigma(t)$ and choosing $\rho(t,x) \geq |0.1\sin(x_1(t))| + \eta = 0.1 + \eta$, it is clear the reachability condition in (2.16) has been established and

$$\sigma(t)\dot{\sigma}(t) \leq -\eta|\sigma(t)| \tag{2.32}$$

which ensures the existence of an ideal sliding mode.

2.4.3 Simulation Results

The sliding mode controller in (2.30) based on the nominal system (2.26) is now tested in simulation using the MATLAB/SIMULINK environment. In the simulations, the value of $\rho(t,x)$ is selected as $\rho(t,x) = 0.15$. From Fig. 2.2 it is clear that the disturbance has no effect on the system performance, which means that the design requirements of the displacement reaching the equilibrium position with no overshoot

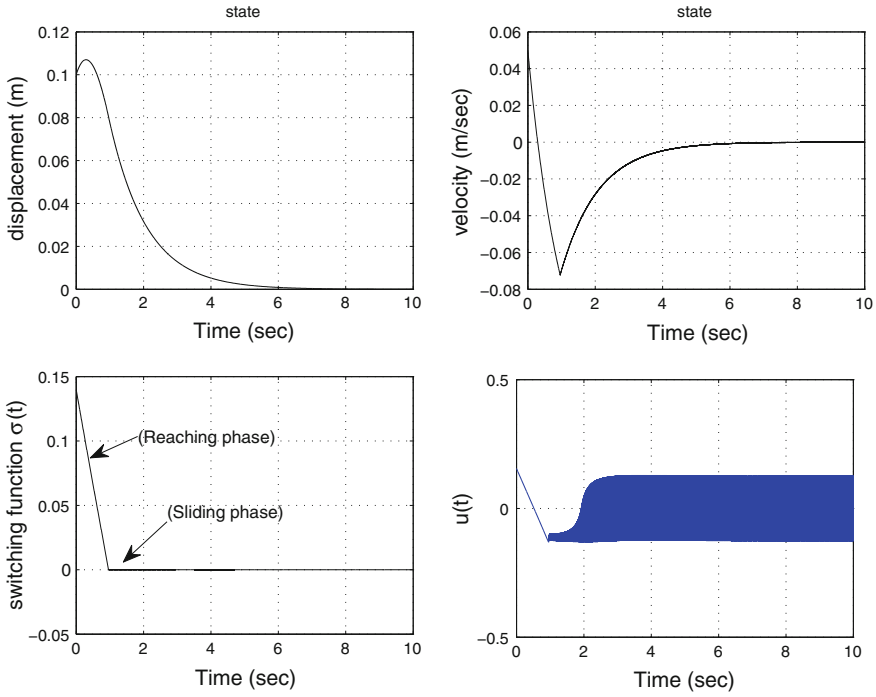

Fig. 2.2 Simulation results for the SMDS with disturbance

and within 6 s is met. The switching function plot in Fig. 2.2 shows that the sliding surface is attained in 1 s, i.e. the sliding motion starts after $t \geq 1$ s. However the discontinuous control signal exhibits high frequency switching which is undesired in most systems due to high wear on moving mechanical components.

2.5 Practical Sliding Mode Control Law

The discontinuity associated with the nonlinear discontinuous part of the control law in (2.12) is the main hurdle in a practical implementation—especially in mechanical systems. Traditionally this has been circumvented by "smoothing" the discontinuity. After doing this the state trajectories no longer slide on the sliding surface, and instead they evolve in the vicinity of the sliding surface: this is termed as pseudo-sliding. However this means total invariance against matched uncertainties is not guaranteed. Nevertheless a good (point-wise) approximation of the discontinuous control term ensures a certain level of robustness against matched uncertainties still remains.[1] One possibility is to use a sigmoidal approximation, where the unit vector term in (2.12) is replaced by

$$u_n(t) = -\rho(t,x)(GB)^{-1}\frac{\sigma(t)}{||\sigma(t)|| + \delta} \tag{2.33}$$

where δ is a small positive design scalar. In this book the sigmoidal approximation given in (2.33), as shown in Fig. 2.3, is used. Here, the value of δ is chosen as $\delta = 0.0001$, and the control law in (2.30) becomes

$$u(t) = \begin{bmatrix} 2 & 2.1 \end{bmatrix} x(t) - 0.15\frac{\sigma(t)}{|\sigma(t)| + 0.0001}$$

From Fig. 2.4, it is clear that the chattering or high frequency switching of the control signal has been removed. Due to this approximation, the sliding motion will be in the vicinity of the sliding surface and will be termed pseudo-sliding instead of ideal sliding. The design requirements however are still met in the presence of the external disturbance as can be seen in Fig. 2.4.

[1] An alternative approach to smoothing the discontinuity which leads to chattering is to use a higher order sliding mode control approach [2]. Now the sliding motion takes place on the constraint set $\sigma = \dot{\sigma} = \cdots = \sigma^{r-1} = 0$ and is called an rth order sliding mode. Furthermore if it is possible to steer σ to zero using the discontinuous control based on $\dot{u}(t)$, then the actual control signal $u(t)$ will be continuous and the unwanted chattering effects can be alleviated [3].

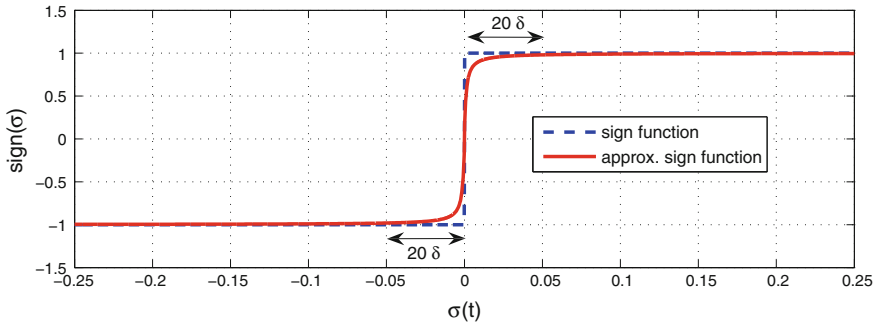

Fig. 2.3 An approximation of the sign function [1]

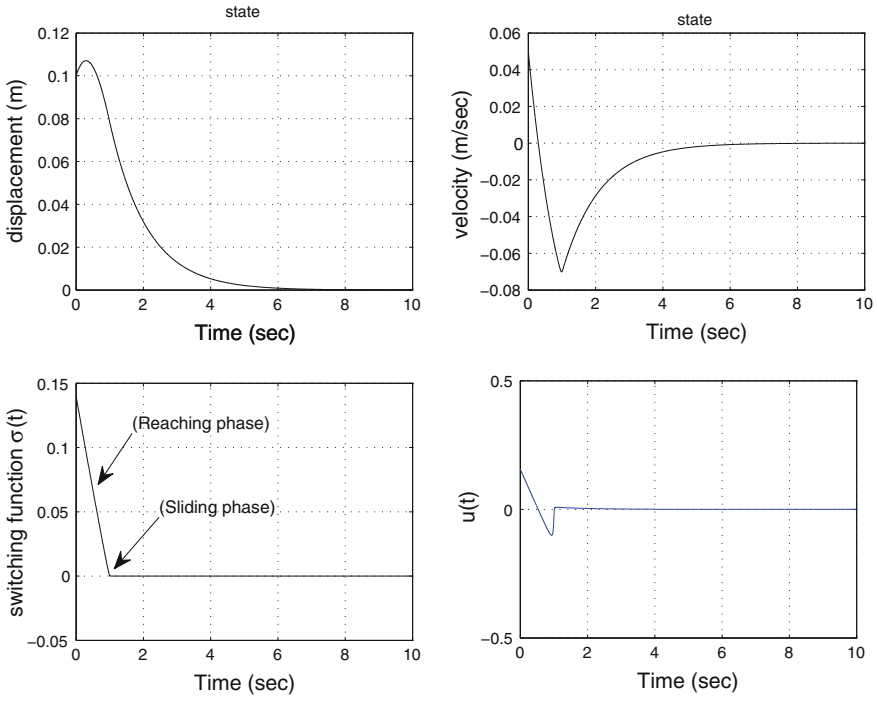

Fig. 2.4 Simulation results for the SMDS with modified control law

2.6 Properties of the Sliding Mode

The properties of conventional (1st order) siding modes are summarised below:

- during a sliding mode, the order of the sliding motion is $n - m$, where n and m represent the number of states and the number of inputs respectively;

- the stability of the closed-loop sliding motion depends only on these $n - m$ non-negative eigenvalues;
- the performance of the closed-loop sliding motion depends on the choice of sliding surface;
- during sliding, the sliding motion is invariant to matched uncertainties;

It should be noted that the robustness to uncertainty is only achieved once sliding takes place. In the sequel, Integral Sliding Mode Control (ISMC) schemes are discussed which eliminate the reaching phase associated with the classical SMC approach discussed in the previous sections, and induce a sliding mode for the entire closed-loop system response.

2.7 Integral Sliding Mode Control (ISMC)

The basic idea of ISMC was initially proposed to enforce a sliding mode from the beginning of the system response, which means a controller based on ISMC ideas can provide compensation to matched uncertainties throughout the entire system response. In this section, a step-by-step design procedure for Integral Sliding Mode (ISM) controllers is explained, and the special features associated with ISMC design are discussed. Again in this section, it is assumed that state information is available for the controller design.

2.7.1 Introduction

In ISMC, it is assumed that there exists a nominal plant, for which a properly designed state feedback controller has already been designed to ensure asymptotic stability of the closed-loop system, and to satisfy predefined performance specifications. A discontinuous controller is 'added' to the nominal state feedback controller to ensure the nominal performance is maintained, and the system is insensitive to external disturbances (faults/failures from a FTC perspective). This design philosophy provides the opportunity to retro-fit an ISM to the existing baseline controller to compensate for the matched uncertainties and external disturbances throughout the system response. As demonstrated in this chapter, when using sliding mode based schemes, the system state trajectories are insensitive to matched uncertainties while in the sliding mode. However no discussion has been made regarding unmatched uncertainties i.e. uncertainties which are not in the range space of the input distribution matrix. This will be addressed in the remainder of the chapter.

2.7.2 Problem Statement and ISM Controller Design

To explain the design procedure, consider an uncertain LTI system of the form

$$\dot{x}(t) = Ax(t) + Bu(t) + M\xi(t, x) + f_u(t, x) \tag{2.34}$$

subject to Assumptions 2.1 and 2.2, where $\xi(t, x)$ is a bounded unknown disturbance and the matrix M satisfies the matching condition and can be written as $M = BD$, for some $D \in \mathbb{R}^{m\times l}$.

Assumption 2.3 The function $f_u(t, x)$ represents unmatched uncertainty i.e. it does not lie within the range space of matrix B, but is assumed to be bounded with known upper bound.

The nominal linear system associated with Eq. (2.34) can be written as

$$\dot{x}(t) = Ax(t) + Bu_o(t) \tag{2.35}$$

where $u_o(t)$ is a nominal control law which can be designed by any suitable state feedback paradigm to achieve desired nominal performance. Since it is assumed that the pair (A, B) is controllable, then there exists a state feedback controller of the form

$$u_o(t) = -Fx(t) \tag{2.36}$$

where $F \in \mathbb{R}^{m\times n}$ is a state feedback gain to be designed, so that the state trajectories of the nominal system (2.35), say $x_o(t)$, are stable and meet the performance specifications. The matrix F can be designed using any state feedback design approach. The objective is to design a control law $u(t)$, such that the state trajectories $x(t)$ of (2.34), while in the sliding mode satisfy the condition $x(t) \equiv x_o(t)$ for all time if $f_u(.) = 0$, starting from the initial time instant i.e. when $x(0) \equiv x_o(0)$. To achieve $x(0) \equiv x_o(0)$ the order of the sliding dynamics should be the same as the nominal system.

2.7.3 Design Principles

Define a control law $u(t)$ of the form

$$u(t) = u_o(t) + u_n(t) \tag{2.37}$$

where $u_o(t)$ is the nominal controller and $u_n(t)$ is a nonlinear injection to induce a sliding mode. Then using (2.37), (2.34) can be written as

$$\dot{x}(t) = Ax(t) + Bu_o(t) + Bu_n(t) + BD\xi(t, x) + f_u(t, x) \tag{2.38}$$

where $u_o(t)$ is the state feedback controller defined in (2.36), and where $u_n(t)$ is chosen to reject the disturbance term $\xi(t,x)$ while in the sliding mode. Here the switching function is defined as

$$\sigma(t) = Gx(t) + z(t) \tag{2.39}$$

where $G \in \mathbb{R}^{m\times n}$ is design freedom and $z(t)$ is to be specified. Since the matrix B is of full rank, the switching matrix G can be chosen so that the matrix GB is nonsingular i.e. $\det(GB) \neq 0$. During sliding $\sigma(t) = \dot{\sigma}(t) = 0$ and therefore

$$\dot{\sigma}(t) = G\dot{x}(t) + \dot{z}(t) = 0 \tag{2.40}$$

In order to ensure that the equivalent control term associated with $u_n(t)$ rejects the effect of the matched disturbance term $\xi(t,x)$ (in the case when $f_u(t,x) = 0$), so that the condition $x(t) \equiv x_o(t)$ is satisfied for all $t > 0$, substituting the value of (2.38) into (2.40) gives:

$$\dot{\sigma}(t) = G\left(Ax(t) + Bu_o(t) + Bu_n(t) + BD\xi(t,x)\right) + \dot{z}(t) = 0 \tag{2.41}$$

During sliding it is expected that $u_{n_{eq}}(t) = -D\xi(t,x)$, i.e. it should compensate for the uncertainty, then selecting

$$\dot{z}(t) = -G(Ax(t) + Bu_o(t)), \quad z(0) = -Gx(0) \tag{2.42}$$

ensures

$$\dot{\sigma}(t) = GBu_n(t) + GBD\xi(t,x) \tag{2.43}$$

and so during sliding $u_{n_{eq}}(t) = -D\xi(t,x)$. Substituting the value of $u_{n_{eq}}(t)$ into (2.38) means the integral sliding mode is governed by

$$\dot{x}(t) = Ax(t) + Bu_o(t) \tag{2.44}$$

which confirms that the condition $x(t) \equiv x_o(t)$ is satisfied if $f_u(t,x) = 0$ and $x(0) = x_o(0)$. In the case when $f_u(t,x) \neq 0$ in (2.38), the equivalent control obtained from (2.41) can be written as

$$\begin{aligned} u_{n_{eq}}(t) &= -(GB)^{-1}GBD\xi(t,x) - (GB)^{-1}Gf_u(t,x) \\ &= -D\xi(t,x) - (GB)^{-1}Gf_u(t,x) \end{aligned} \tag{2.45}$$

Substituting the value of equivalent control $u_{n_{eq}}(t)$ from (2.45) into (2.38) and simplifying, the expression for the integral sliding mode dynamics can be written as

$$\dot{x}(t) = Ax(t) + Bu_o(t) + \underbrace{(I - B(GB)^{-1}G)}_{\Gamma} f_u(t,x) \tag{2.46}$$

From Eq. (2.46), it is clear that the effect of the matched uncertainty has been completely rejected while in the sliding mode. However the matrix Γ in (2.46) can amplify the effect of unmatched uncertainty $f_u(t, x)$. Therefore the objective in the next section is to design the integral sliding surface design parameter G to avoid any amplification of the unmatched uncertainty.

2.7.4 Integral Switching Surface

Using Eqs. (2.39) and (2.42), an integral switching function which eliminates the reaching phase is

$$\sigma(t) = Gx(t) - Gx(0) - G\int_0^t (Ax(\tau) + Bu_o(\tau))\, d(\tau) \tag{2.47}$$

The term $-Gx(0)$ ensures that $\sigma(0) = 0$, so the reaching phase is eliminated. The sliding mode will exist from time $t = 0$ and the system will be robust throughout the entire closed-loop system response against matched uncertainties.

From the previous analysis, it is clear that in the case of only matched uncertainty, then any choice of G which ensures GB is invertible is sufficient for the ISM design, but for unmatched uncertainty, a specific choice of G is needed. Here it will be argued that

$$G = B^+ = (B^T B)^{-1} B^T \tag{2.48}$$

is an appropriate choice. Note G in (2.48) is the Moore–Penrose left pseudo-inverse of the input distribution matrix B. The particular choice of G in (2.48) brings two advantages:

1. the modulation gain associated with $u_n(t)$ in (2.37) is minimised which means the amplitude of the chattering can be reduced;
2. it avoids amplifying the effect of the unmatched disturbance.

This choice of G also has the simplifying property that

$$GB = \underbrace{(B^T B)^{-1} B^T}_{G} B = I_m$$

and ensures that the square matrix GB is nonsingular. With the choice of G in (2.48), the projection operator Γ in (2.46) becomes

$$\Gamma = I_n - B(B^T B)^{-1} B^T \tag{2.49}$$

Notice that the projection operator Γ in (2.49) is symmetric and idempotent i.e. $\Gamma^2 = \Gamma$. The properties of symmetry and idempotency imply that $\|\Gamma\| = 1$, which means that the effect of f_u is not amplified since $\|\Gamma f_u\| \leq \|f_u\|$. In fact, it can be

proved that $\|I - B(GB)^{-1}G\| \geq 1$ for any G, and so the choice of G in (2.48) is an optimal one in the sense of non-amplification of the unmatched uncertainty.

2.7.5 Integral Sliding Mode Control Laws

An integral sliding mode controller will now be designed based on the nominal system in (2.35). The control law has a structure given by

$$u(t) = u_o(t) + u_n(t) \tag{2.50}$$

where $u_o(t)$ is the linear part of the controller, and $u_n(t)$ is the discontinuous part to enforce a sliding mode along the sliding surface in (2.47). One choice of $u(t)$ is

$$u(t) = -Fx(t) - \rho(t,x)(GB)^{-1}\frac{\sigma(t)}{\|\sigma(t)\|} \quad \text{for } \sigma(t) \neq 0 \tag{2.51}$$

where F is the state feedback controller which is responsible for the performance of the nominal system and $\rho(t,x)$ is the modulation gain to enforce the sliding mode—whose precise value is given in the next subsection.

2.7.6 The Reachability Condition

To justify that the controller designed in (2.51) satisfies the η-reachability condition (2.22), which is a sufficient condition to ensure the existence of an ideal sliding motion, it can be shown from (2.34) and (2.36) that

$$\dot{\sigma}(t) = G\left(Ax(t) + Bu(t) + BD\xi(t,x) + f_u(t,x)\right) - GAx(t) + GBFx(t)$$

then substituting from (2.51), and after some simplification

$$\begin{aligned}\dot{\sigma}(t) &= GAx(t) + GB(-Fx(t) + u_n(t)) + GBD\xi(\cdot) + Gf_u(\cdot) - GAx(t) + GBFx(t)\\ &= -\rho(t,x)\frac{\sigma(t)}{\|\sigma(t)\|} + GBD\xi(t,x) + Gf_u(t,x)\end{aligned} \tag{2.52}$$

Then

$$\begin{aligned}\sigma^T(t)\dot{\sigma}(t) &= -\rho(t,x)\|\sigma(t)\| + \sigma^T(t)D\xi(t,x) + \sigma^T(t)Gf_u(t,x)\\ &\leq \|\sigma(t)\|(-\rho(t,x) + \|D\xi(t,x)\| + \|Gf_u(t,x)\|)\end{aligned} \tag{2.53}$$

where the fact that $GB = I_m$, has been used. In order to enforce a sliding mode the value of the modulation gain $\rho(t,x)$ should be greater than any disturbance or uncertainty in the system, and therefore for any choice of $\rho(t,x)$ which satisfies

$$\rho(t,x) \geq \|D\|\|\xi(t,x)\| + \|G\|\|f_u(t,x)\| + \eta \tag{2.54}$$

where η is some positive scalar, the η-reachability condition

$$\sigma^T(t)\dot{\sigma}(t) \leq -\eta||\sigma(t)|| \tag{2.55}$$

is satisfied.

Remark 2.2. Inequality (2.55) can also be interpreted from a Lyapunov perspective. Define $V(t) = \frac{1}{2}\sigma^T(t)\sigma(t)$, then $\dot{V}(t) = \sigma^T(t)\dot{\sigma}(t)$ and from the inequalities in (2.53)–(2.55) it follows

$$\dot{V}(t) \leq -\eta||\sigma(t)|| = -\eta\sqrt{2V(t)} \tag{2.56}$$

Integrating both sides of (2.56) yields

$$\sqrt{2V(t)} - \sqrt{2V(0)} \leq -\eta t$$

which implies $V(t) \equiv 0$ in less than $\frac{\eta}{\sqrt{2V(0)}}$ units of time.

2.7.7 Properties of Integral Sliding Mode

The properties of integral sliding modes can be summarised as follows:

- there is no reaching phase and a sliding mode is enforced throughout the entire system response;
- during sliding, the order of the motion is the same as the original system;
- by a suitable choice of sliding surface, the effect of unmatched uncertainty can be ameliorated;
- during the sliding mode, the system motion is invariant to matched uncertainties;
- the ISM approach has the ability to be retro-fitted to an existing feedback controller;

2.7.8 Simulation Example

Here in this section, to make a direct comparison, the simulation scenario of the spring-mass-damper system from Sect. 2.4 will be simulated. Recall the system was represented as

$$\begin{bmatrix} \dot{x}_1(t) \\ \dot{x}_2(t) \end{bmatrix} = \underbrace{\begin{bmatrix} 0 & 1 \\ -2 & -3 \end{bmatrix}}_{A} \begin{bmatrix} x_1(t) \\ x_2(t) \end{bmatrix} + \underbrace{\begin{bmatrix} 0 \\ 1 \end{bmatrix}}_{B} (u(t) + 0.1\sin(x_1(t)))$$

The objective is to design an ISM controller to bring the system back to the equilibrium position from the initial conditions without overshooting in terms of displacement, and with a settling time not more than 6 s. The integral switching function from Eq. (2.47) is

$$\sigma(t) = Gx(t) - Gx(0) - G\int_0^t (A - BF)\, x(\tau) d(\tau)$$

where the value of G is chosen as in (2.48), and here is equal to

$$G = (B^T B)^{-1} B^T = \begin{bmatrix} 0 & 1 \end{bmatrix} \tag{2.57}$$

The gain F in this example has been designed using the linear quadratic regulator (LQR) method,[2] and aims to regulate the system states to the origin by minimising the cost function

$$J = \int_0^\infty (x(t)^T Q x(t) + u_o(t)^T R u_o(t)) dt \tag{2.58}$$

where Q is a symmetric positive definite ($s.p.d.$) matrix and R is a positive scalar. These matrices penalise the magnitude of the control signal $u_o(t)$ and the deviation of the system states from the origin. Here the values of Q and R are chosen as $Q = \text{diag}(1, 0.5)$ and $R = 1$, which results in the matrix

$$F = \begin{bmatrix} 0.2361 & 0.1579 \end{bmatrix}$$

The ISM control law is

$$u(t) = -Fx(t) - \rho \text{sign}(\sigma(t)) \quad \text{for } \sigma(t) \neq 0 \tag{2.59}$$

since the choice of G in (2.57) makes $GB = 1$. Here ρ is a fixed scalar satisfying $\rho = 0.1 + \eta$ where $\eta > 0$. It is easy to check that the control law $u(t)$ satisfies the reachability condition $\sigma(t)\dot{\sigma}(t) \leq -\eta|\sigma(t)|$. Here the sigmoidal approximation given in (2.33) and shown in Fig. 2.3 is used, and therefore the ISM control law in (2.59) is modified to become

$$u(t) = -Fx(t) - \rho \frac{\sigma(t)}{|\sigma(t)| + \delta} \tag{2.60}$$

where the value of the small positive scalar δ is chosen as $\delta = 0.0001$, to eliminate chattering. The control law $u(t)$, after substituting for the value of F, can be written as

[2] This is a well-known 'classical' state-space technique: for details see for example [4].

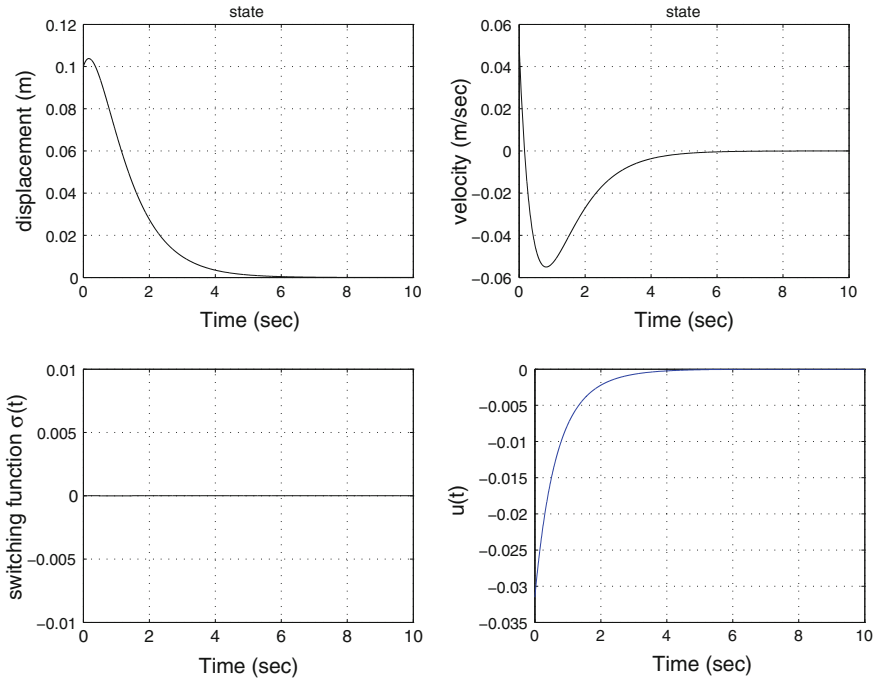

Fig. 2.5 Simulation results for the SMDS nominally (with ISMC)

$$u(t) = -0.2361x_1(t) - 0.2361x_2(t) - \rho\frac{\sigma(t)}{|\sigma(t)| + \delta}$$

The displacement plots in Figs. 2.5 and 2.6 show that the design requirements are met both nominally (without any disturbance) and in the presence of a disturbance term. From Fig. 2.6, it is clear that the effect of the disturbance $0.1\sin(x_1(t))$ has been completely rejected. From the switching function plots in Figs. 2.5 and 2.6, it is clear there is no reaching phase i.e. the sliding mode starts from time $t = 0$.

2.8 Sliding Modes as a Candidate for FTC

Sliding mode based control schemes are a strong candidate for fault tolerant control because of their inherent robustness to matched uncertainties. As argued in Sect. 1.3.1, actuator faults can be effectively modelled as matched uncertainties and therefore sliding mode based control schemes have an inherent capability to directly deal with actuator faults. However actuator failures cannot be handled directly by sliding modes schemes because the complete loss of effectiveness in a channel destroys

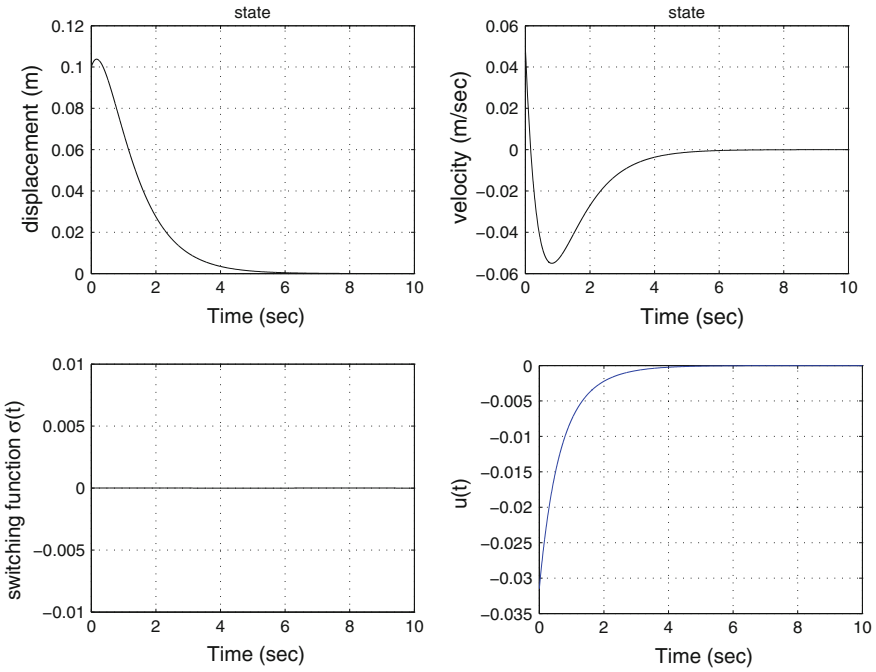

Fig. 2.6 Simulation results for the SMDS with disturbance (with ISMC)

the regularity of the sliding mode, and a unique equivalent control signal can no longer be determined.

In the subsequent chapters, Control Allocation (as discussed in Sect. 1.3.3) is considered as a potential candidate to be combined with ISM control to deal with actuator faults or failures due to its ability to effectively manage the actuator redundancy and to redistribute the control signals to the healthy actuators in the case of an actuator failure. The use of integral sliding modes ensures robustness for all time by eliminating the reaching phase associated with 'classical' SMC based methods. Furthermore integral sliding modes have the capacity to be retro-fitted to the existing controller design to introduce fault tolerance without changing or altering the existing control loops, which is advantageous from an industrial perspective.

2.9 Notes and References

The term sliding mode was first used in the literature in the context of relay systems [5]. Sliding mode control (SMC) is a particular class of variable structure control systems (VSCS) [6]. VSCS evolved from work in Russia in the early 1960s and spread around the world in the late 1970s after the publication of the survey paper by

Utkin [7]. SMC design paradigms [1, 2, 5] have become mature techniques for the control of uncertain systems and provide effective solutions against matched uncertainties; however to provide compensation against matched uncertainties throughout the entire system response, the idea of integral sliding mode control was initially proposed in [5, 8–10]. In [11–13], integral sliding mode control ideas were used for uncertain systems considering both matched and unmatched uncertainties and demonstrated that the system dynamics while on the sliding surface meet the performance specifications in the presence of matched uncertainties. In [13], it was first demonstrated that the effect of mismatched uncertainties can be minimised by the suitable choice of an integral sliding surface (the specific choice of G is given in Sect. 2.7.4). Details of the integral sliding mode approach in the context of robust LQ output control (but not in the context of FTC) can be found in [14]. Different methods have been used in the literature to smooth the transition near the sliding surface to remove chattering—see for example Chap. 3 in [1, 15]. An alternative approach to smoothing the discontinuous switching control law (which leads to chattering) is to use a higher order sliding mode control approach [3]. Many researchers have identified SMC as a potential candidate for FTC, see for example [16–20]. Researchers in [21] have focused on fault reconstruction and fault tolerant control schemes for aerospace applications using traditional SMC approaches. In [16, 17], it was argued that SMC could deal with significant and sudden changes in the system dynamics due to actuator faults and has the capability to become an alternative to reconfigurable control systems. In [18], a 'hedging' based SMC design is used to reduce the effect of neglected parasitic dynamics in a longitudinal control system for an aircraft. In [16, 19] the authors have demonstrated the combination of SMC with control allocation for FTC purposes. Recently in [22], a continuous integral sliding mode FTC scheme was proposed using a higher order sliding mode observer by incorporating fixed control allocation.

References

1. Edwards, C., Spurgeon, S.K.: Sliding Mode Control, Theory and Applications. Taylor and Francis, London (1998)
2. Shtessel, Y., Edwards, C., Fridman, L., Levant, A.: Sliding Mode Control and Observation. Birkhauser, New York (2013)
3. Bartolini, G., Ferrara, A., Usai, E.: Chattering avoidance by second order sliding mode control. IEEE Trans. Autom. Control **43**(2), 241–246 (1998)
4. Anderson, B.D.O., Moore, J.B.: Optimal Control: Linear Quadratic Methods. Prentice Hall International Edition, Upper Saddle River (1989)
5. Utkin, V., Guldner, J., Shi, J.: Sliding Mode Control in Electromechanical Systems. Taylor and Francis, London (1999)
6. Utkin, V.: Sliding mode control. In: Sabanovic, A., Fridman, L.M., Spurgeon, S.K. (eds.) Variable Structure Systems: From Principles to Implementation. IEE Control Series 66, pp. 3–17. IEE, London (2004)
7. Utkin, V.: Variable structure systems with sliding mode. IEEE Trans. Autom. Control **22**(2), 212–222 (1977)

8. Matthews, G.P., DeCarlo, R.A.: Decentralized tracking for a class of interconnected nonlinear systems using variable structure control. Automatica **24**(2), 187–193 (1988)
9. Utkin, V., Shi, J.: Integral sliding mode in systems operating under uncertainty conditions. In: Proceedings of the 35th IEEE Conference on Decision and Control (1996)
10. Wang, J., Lee, T., Juang, Y.: New methods to design an integral variable structure controller. IEEE Trans. Autom. Control **41**(1), 140–143 (1996)
11. Cao, W., Xu, J.: Nonlinear integral type sliding surface for both matched and unmatched uncertain systems. IEEE Trans. Autom. Control **49**(8), 1355–1360 (2004)
12. Xu, J., Pan, Y., Lee, T.: Analysis and design of integral sliding mode control based on Lyapunov's direct method. In: Proceedings of the American Control Conference (2003)
13. Castanos, F., Fridman, L.: Analysis and design of integral sliding manifolds for systems with unmatched perturbations. IEEE Trans. Autom. Control **51**(5), 853–858 (2006)
14. Fridman, L., Poznyak, A., Bejarano, F.J.: Robust LQ Output Control: Integral Sliding Mode Approach. Springer, Heidelberg (2013)
15. Burton, J.A., Zinober, A.S.: Continuous approximation of variable structure control. Int. J. Syst. Sci. **17**(6), 875–885 (1986)
16. Wells, S.R., Hess, R.A.: Multi-input/multi-output sliding mode control for a tailless fighter aircraft. J. Guid., Control, Dyn. **26**(3), 463–473 (2003)
17. Hess, R.A., Wells, S.R.: Sliding mode control applied to reconfigurable flight control design. J. Guid., Control Dyn. **26**, 452–462 (2003)
18. Vetter, T.K., Wells, S.R., Hess, R.A.: Designing for damage-robust flight control design using sliding mode techniques. Proc. Inst. Mech. Eng., Part G: J. Aerosp. Eng. **217**, 245–261 (2003)
19. Shtessel, Y., Buffington, J., Banda, S.: Tailless aircraft flight control using multiple time scale re-configurable sliding modes. IEEE Trans. Control Syst. Technol. **10**, 288–296 (2002)
20. Shin, D., Moon, G., Kim, Y.: Design of reconfigurable flight control system using adaptive sliding mode control: actuator fault. Proc. Inst. Mech. Eng., Part G: J. Aerosp. Eng. **219**, 321–328 (2005)
21. Alwi, H., Edwards, C., Tan, C.P.: Fault Detection and Fault Tolerant Control Using Sliding Modes. Advances in Industrial Control Series. Springer, Heidelberg (2011)
22. Ríos, H., Kamal, S., Fridman, L.M., Zolghadri, A.: Fault tolerant control allocation via continuous integral sliding-modes: a HOSM-observer approach. Automatica **51**, 318–325 (2014)

Chapter 3
Design and Analysis of an Integral Sliding Mode Fault Tolerant Control Scheme

One of the important elements necessary for achieving FTC, is the availability of redundant actuators. This provides increased freedom in terms of controller design to mitigate the effects of faults and failures. Although these 'redundant' actuators are often designed for different purposes, in the event of an emergency (such as faults or failures to the primary actuators), they can be used to retain satisfactory performance. This chapter is concerned with the development of fault tolerant controllers for a class of linear systems with redundant actuators. This redundancy will be exploited to achieve tolerance to a specified class of faults/failures, which includes the possibility of total failure to certain primary actuators. Furthermore the precise class of total actuator failure which can be accommodated is identified. The idea is to design an ISM controller based on a 'virtual' system. The associated virtual control signal is then translated into actual control surface deflections using CA. This distinctive design strategy is beneficial since only one controller is designed to cover a wide range of fault/failure cases, while the CA redistributes the signals to the available 'healthy' actuators. The scheme uses the measured or estimated effectiveness level of the actuators to redistribute the control effort during faults/failures to maintain close to nominal closed-loop performance without reconfiguring the controller. The relative error in the estimation of the actuator effectiveness gains is also taken into consideration. The stability test in this chapter allows an effective *synthesis procedure* to be employed using Linear Matrix Inequality (LMI) optimisation to compute the parameters involved in the control law. The effectiveness of the scheme against faults or failures is tested in simulation based on a large transport aircraft model.

3.1 System Description and Problem Formulation

In this chapter an LTI system with actuator faults or failures is modelled as

$$\dot{x}(t) = Ax(t) + BW(t)u(t) \tag{3.1}$$

M.T. Hamayun et al., *Fault Tolerant Control Schemes Using Integral Sliding Modes*, Studies in Systems, Decision and Control 61,
DOI 10.1007/978-3-319-32238-4_3

where $A \in \mathbb{R}^{n\times n}$, $B \in \mathbb{R}^{n\times m}$, and

$$W(t) = \text{diag}(w_1(t), \ldots, w_m(t)) \tag{3.2}$$

is a diagonal semi-positive definite matrix.

Assumption 3.1 The pair (A, B) is assumed to be controllable.

The time varying scalars $w_1(t), \ldots, w_m(t)$ model the effectiveness level of the actuators. As discussed in Sect. 1.1.1, if $w_i(t) = 1$, it means that the ith actuator has no fault (i.e. a 100 % healthy actuator) and is working perfectly, whereas if $1 > w_i(t) > 0$, an actuator fault is present i.e. the actuator functions with reduced capability. If $w_i(t) = 0$, actuator i has completely failed and the control input component u_i has no effect on the system dynamics. The matrix $W(t)$ will be termed the efficiency matrix indicating the health level of each actuator. Associate with (3.1) a set of controlled outputs

$$y_c(t) = Cx(t) \tag{3.3}$$

where $C \in \mathbb{R}^{l\times n}$ and $l < m$. The variables $y_c(t)$ are required to respond to desired (external) commands. In terms of 'controlling' these outputs it follows that only l independent actuators are required to produce the required closed-loop performance. The remaining $m-l$ actuators constitute redundancy and can be exploited to achieve fault tolerance. In this chapter an estimate of the actuator efficiency

$$\widehat{W}(t) = \text{diag}(\hat{w}_1(t), \ldots, \hat{w}_m(t)) \tag{3.4}$$

where the scalars $0 \leq \hat{w}_i(t) \leq 1$, will be used explicitly in the control law. One way to obtain an estimate of the actuator efficiency is by using a measurement of the actual actuator deflection compared to the demand. Such information is typically available in many safety critical systems e.g. passenger aircraft.[1] In other situations $\widehat{W}(t)$ would need to be provided by an FDI scheme. It is important to note that whatever method is employed, the estimate $\widehat{W}(t)$ will not be perfect and there will be a difference between the actual efficiency matrix $W(t)$, and its estimate $\widehat{W}(t)$:

Assumption 3.2 It is assumed

$$W(t) = (I - \triangle(t))\widehat{W}(t) \tag{3.5}$$

where the 'uncertainty'

$$\triangle(t) = \text{diag}(\delta_1(t), \ldots, \delta_m(t)) \tag{3.6}$$

represents the estimation error. The unknown scalars $\delta_1(t), \ldots, \delta_m(t)$ model the level of imperfection in the fault estimation.

[1] See for example [1].

The effect of this imperfection will be analysed later. In this chapter a virtual control concept for resolving actuator redundancy will be employed. In Sect. 1.3.3 the input distribution matrix B was factorised into two matrices (i.e. $B = B_v B_u$, where $B_v \in \mathbb{R}^{n\times k}$ and $B_u \in \mathbb{R}^{k\times m}$ and both have rank $k < m$). This factorisation is only possible if $\text{rank}(B) = k < m$. In many actuator redundant systems, this condition is not satisfied. However re-ordering of the states is possible, and the input distribution matrix B can be partitioned as:

$$B = \begin{bmatrix} B_1 \\ B_2 \end{bmatrix} \tag{3.7}$$

where $B_1 \in \mathbb{R}^{(n-l)\times m}$ and $B_2 \in \mathbb{R}^{l\times m}$ is of rank $l < m$. Suppose that by design of the partition in (3.7), the pair (A, B_v) where $B_v = BB_2^T$, is controllable. In aircraft systems for example, the component B_2 is associated with the equations of angular acceleration in pitch, roll and yaw, because *the control objectives in (most) aircraft systems can be obtained by commanding the desired moments*.

Assumption 3.3 It is assumed the partition of matrix B is such that the elements of B_2 have large magnitude compared to $\|B_1\|$, so that the channels associated with B_2 represents the dominant contribution of the control action on the system.

Although this is a restriction, aircraft systems often satisfy such a constraint. By hypothesis $\|B_1\|$ is assumed to be small. To create this separation, a permutation of the states must usually be undertaken. The virtual control input is defined as

$$v(t) := B_2 u(t) \tag{3.8}$$

where $v(t) \in \mathbb{R}^l$ can be interpreted as the total control effort produced by the actuators. Once the partition of B in (3.7) has been achieved, the states can be scaled so that $B_2 B_2^T = I_l$ i.e. $\|B_2\| = 1$. This can be achieved without loss of generality, because $\text{rank}(B_2) = l$. The physical control signal $u(t)$ sent to the actuators can be determined from Eq. (3.8) as

$$u(t) = B_2^\dagger(t) v(t) \tag{3.9}$$

where $B_2^\dagger(t) \in \mathbb{R}^{m\times l}$ is a weighted right pseudo-inverse of the matrix B_2. Thus the matrix $B_2^\dagger(t)$ provides some design freedom and 'distributes' the virtual control signal to the physical actuators via (3.9). Different researchers have utilised the design freedom in the pseudo-inverse matrix in different ways. A generic choice of $B_2^\dagger(t)$ such that $B_2 B_2^\dagger(t) = I_l$ is

$$B_2^\dagger(t) = \widehat{W}(t) B_2^T (B_2 \widehat{W}(t) B_2^T)^{-1} \tag{3.10}$$

assuming $\det(B_2 \widehat{W}(t) B_2^T) \neq 0$.

Remark 3.1 In the special case when there are no faults present in the system i.e. when $\widehat{W}(t) = I_m$, then the weighted right pseudo-inverse matrix $B_2^\dagger(t)$ simplifies to

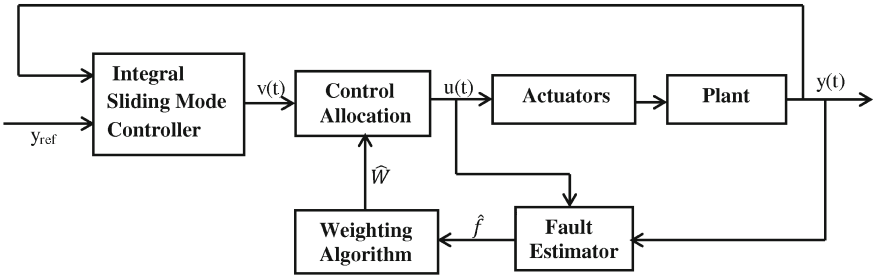

Fig. 3.1 Schematic of the overall control strategy

$B_2^{\dagger}(t) = B_2^T$, using the fact that $B_2 B_2^T = I_l$. This means the physical control law in (3.9) becomes

$$u(t) = B_2^T \nu(t) \tag{3.11}$$

The overall control structure in block diagram form is presented in Fig. 3.1, where the virtual control signal $\nu(t)$ is designed using integral sliding mode control ideas. The virtual control is translated into the actual control signal $u(t)$ by using control allocation based on knowledge of $\widehat{W}(t)$. In order to clarify the set of faults or failures the scheme can tolerate, define the set

$$\mathscr{W} = \{(\hat{w}_1, \ldots, \hat{w}_m) \in \underbrace{[0\ 1] \times \cdots \times [0\ 1]}_{m \text{ times}} : \det(B_2 \widehat{W} B_2^T) \neq 0\} \tag{3.12}$$

Because $l < m$, it is possible that $\det(B_2 \widehat{W}(t) B_2^T) \neq 0$ even if up to $m - l$ of the entries $\hat{w}_i(t) = 0$ in the matrix $\widehat{W}(t)$: in other words, potentially up to $m - l$ actuators can totally fail and yet $\det(B_2 \widehat{W}(t) B_2^T) \neq 0$. However if more than $m - l$ entries are zero, then $\text{rank}(\widehat{W}(t)) < l$ and $\det(B_2 \widehat{W}(t) B_2^T) = 0$. The set $\mathscr{W}$ will be shown to constitute the faults/failures for which closed-loop stability can be maintained.

Substituting (3.9) into (3.1) and using (3.10) results in

$$\dot{x}(t) = Ax(t) + \begin{bmatrix} B_1(I - \triangle(t))\widehat{W}^2(t) B_2^T (B_2 \widehat{W}(t) B_2^T)^{-1} \\ B_2(I - \triangle(t))\widehat{W}^2(t) B_2^T (B_2 \widehat{W}(t) B_2^T)^{-1} \end{bmatrix} \nu(t) \tag{3.13}$$

with

$$\hat{\nu}(t) := (B_2 \widehat{W}^2(t) B_2^T)(B_2 \widehat{W}(t) B_2^T)^{-1} \nu(t) \tag{3.14}$$

and then (3.13) can be written as

$$\dot{x}(t) = Ax(t) + \underbrace{\begin{bmatrix} B_1(I - \triangle(t)) B_2^{+}(t) \\ B_2(I - \triangle(t)) B_2^{+}(t) \end{bmatrix}}_{\widehat{B}(t)} \hat{\nu}(t) \tag{3.15}$$

where

$$B_2^+(t) := \widehat{W}^2(t)B_2^T(B_2\widehat{W}^2(t)B_2^T)^{-1} \tag{3.16}$$

Notice that $B_2^+(t)$ is a weighted right pseudo-inverse of B_2 since $B_2B_2^+(t) = I_l$, for all $\widehat{W}(t) \in \mathscr{W}$. Furthermore when $\widehat{W}(t) = I$, then $B_2^+(t) = B_2^T(B_2B_2^T)^{-1} = B_2^T$.

Remark 3.2 Note that whilst the pseudo-inverse $B_2^\dagger(t)$ defined in (3.10) is used for control allocation, the pseudo-inverse $B_2^+(t)$ defined in (3.16) plays a significant role in the closed-loop analysis which will be demonstrated in the sequel.

For the closed-loop stability analysis, an upper bound on the norm of the weighted pseudo-inverse $B_2^+(t)$ is required. Here results on the boundedness of pseudo-inverses will be exploited[2]: Specifically there exists a scalar γ_o such that

$$\|B_2^+(t)\| = \|\widehat{W}^2(t)B_2^T(B_2\widehat{W}^2(t)B_2^T)^{-1}\| < \gamma_o \tag{3.17}$$

for all $(\hat{w}_1(t), \ldots, \hat{w}_m(t)) \in \mathscr{W}$.

In the case when the estimates of the efficiency matrix are perfect (i.e. $\triangle(t) = 0$), and when there are no faults present (i.e. $\widehat{W}(t) = I$), Eq. (3.15) simplifies to

$$\dot{x}(t) = Ax(t) + \underbrace{\begin{bmatrix} B_1B_2^T \\ I_l \end{bmatrix}}_{B_v} v(t) \tag{3.18}$$

since $B_2^+(t)|_{\widehat{W}(t)=I} = B_2^T$. The nominal fault-free equation (3.18) will be used to *design* the control scheme. During faults or failures the inherent properties of integral sliding modes will be relied upon.

Assumption 3.4 The pair (A, B_v) associated with (3.18) is controllable.

Since the pair (A, B_v) associated with (3.18) is assumed to be controllable, then there exists a state feedback controller $v(t) = -Fx(t)$, so that the nominal system

$$\dot{x}(t) = (A - B_vF)x(t) \tag{3.19}$$

is stable. The state feedback controller F can be designed to achieve optimality against some appropriate criteria. The choice of the matrix F will be discussed in the sequel.

[2]Here the results from Stewart [2] will be exploited: specifically if X is a full column rank matrix and W is a diagonal matrix with positive scalars, then the weighted left pseudo-inverse of X defined by $X^+ = (X^TWX)^{-1}X^TW$ is norm bounded by some number that is independent of W.

3.2 Integral Sliding Mode Controller Design

This section, develops a systematic design procedure for the synthesis of an ISM controller. There are two steps to design an ISM controller, first a sliding surface is designed, and then in the second step, a control law to induce and maintain a sliding motion is created.

3.2.1 Integral-Type Switching Surface Design

The ideas of integral sliding surface control discussed in Chap. 2 will be used here for the system in (3.18) associated with the virtual control input $\nu(t)$. The sliding surface is defined by the set:

$$\mathscr{S} = \{x \in \mathbb{R}^n : \quad \sigma(t) = 0\} \tag{3.20}$$

where the switching function $\sigma(t) \in \mathbb{R}^l$ is defined as

$$\sigma(t) := Gx(t) - Gx(0) - G\int_0^t (A - B_\nu F)\, x(\tau) d\tau \tag{3.21}$$

and $G \in \mathbb{R}^{l\times n}$ is design freedom. At $t = 0$, the switching function $\sigma(0) = 0$, and hence the reaching phase is eliminated. In Chap. 2, it was shown that, in the case of matched uncertainty, the sliding motion associated with (3.21) is always nominally governed by $(A - B_\nu F)$ independent of the choice of G, but the effects of unmatched uncertainty cannot be rejected while in the sliding mode. Here G will be chosen to attempt to ameliorate the effects of unmatched uncertainty as discussed in Chap. 2. In this chapter

$$G := B_2(B^T B)^{-1} B^T \tag{3.22}$$

is suggested. Notice that since by definition $B_\nu = BB_2^T$, this choice of G in (3.22) has the property that

$$GB_\nu = B_2(B^T B)^{-1} B^T BB_2^T = B_2 B_2^T = I_l$$

and so G in (3.22) is a specific choice of left-pseudo-inverse of B_ν.

Remark 3.3 The choice of G in (2.48), is a left-pseudo-inverse of the virtual input matrix B_ν and ensures that while in the sliding mode the impact of unmatched uncertainty will not be amplified. With the choice of G in (3.22) generically $G\widehat{B}(t) = I_l - B_2 \triangle(t) B_2^T$ i.e. a symmetric matrix. The symmetry is important and simplifies much of the subsequent analysis and avoids the introduction of conservatism. Also nominally, when there are no faults and $W(t) = I$, from the special properties of the matrix B_2, it follows that $G\widehat{B}(t)|_{W(t)=I} = B_2 B_2^T = I$. This means,

nominally, G has the 'pseudo-inverse properties' which are optimal from the point of view of minimising the impact of unmatched uncertainties on the closed-loop dynamics.

From (3.21) it is easy to see that

$$\dot{\sigma}(t) = G\dot{x}(t) - GAx(t) + GB_{v}Fx(t) \tag{3.23}$$

Substituting (3.15) in (3.23), and using the fact that $GB_{v} = I$, yields

$$\dot{\sigma}(t) = G\widehat{B}\hat{v}(t) + Fx(t) \tag{3.24}$$

The equivalent control can be obtained by solving for $\hat{v}(t)$ in $\dot{\sigma}(t) = 0$ which yields

$$\hat{v}_{eq}(t) = -(G\widehat{B})^{-1}Fx(t) \tag{3.25}$$

Adding and subtracting $Fx(t)$ in Eq. (3.25) and substituting into (3.15) yields

$$\dot{x}(t) = (A - B_{v}F)x(t) + \left(B_{v} - \widehat{B}(G\widehat{B})^{-1}\right)Fx(t) \tag{3.26}$$

where B_{v} is defined in (3.18) and $\widehat{B}$ is defined in (3.15). Using G as defined in (3.22), further simplifying Eq. (3.26) gives:

$$\dot{x}(t) = (A - B_{v}F)x(t) + \tilde{B}\tilde{\Phi}(t)Fx(t) \tag{3.27}$$

where the time varying uncertain term is

$$\tilde{\Phi}(t) := B_1B_2^T - B_1(I - \triangle(t))B_2^{+}(t)(B_2(I - \triangle(t))B_2^{+}(t))^{-1} \tag{3.28}$$

and

$$\tilde{B} := \begin{bmatrix} I_{n-l} \\ 0 \end{bmatrix} \tag{3.29}$$

Remark 3.4 Notice in the case of perfect knowledge of the actuator efficiency (i.e. $\triangle(t) = 0$), and when there are no faults in the system (i.e. $\widehat{W}(t) = I$), the matrices $\widehat{B}|_{\widehat{W}(t)=I} = B_{v}$ and $B_2^{+}(t)|_{\widehat{W}(t)=I} = B_2^T$. As a consequence $\tilde{\Phi}(t) = 0$ and Eq. (3.27) simplifies to

$$\dot{x}(t) = (A - B_{v}F)x(t) \tag{3.30}$$

which is stable by design of the state feedback gain F. The nominal equation (3.30) constitutes ideal fault-free behavior. In the case, when there is uncertainty in the fault estimation i.e. $\triangle(t) \neq 0$, and during faults or failures i.e. $\widehat{W}(t) \neq I_m$, the uncertain term $\tilde{\Phi}(t) \neq 0$. This will be treated as unmatched uncertainty in the closed-loop stability analysis. Therefore for the generic fault/failure case, *closed-loop stability*

needs to be proven since the closed-loop system equation (3.27) depends on matrices $\widehat{W}(t)$ and $\triangle(t)$.

3.2.2 Closed-Loop Stability Analysis

In the presence of faults/failures, the closed-loop system (assuming a sliding motion is maintained) is governed by

$$\dot{x}(t) = (A - B_v F + \tilde{B}\tilde{\Phi}(t)F)x(t) \tag{3.31}$$

To ensure closed-loop stability in the presence of the unmatched term $\tilde{\Phi}(t)$, the small gain theorem is used. In the subsequent analysis, define a transfer function matrix

$$\tilde{G}(s) = F(sI - \tilde{A})^{-1}\tilde{B} \tag{3.32}$$

where $\tilde{A} := A - B_v F$. By construction, $\tilde{G}(s)$ is stable, and define

$$\gamma_2 = \|\tilde{G}(s)\|_\infty \tag{3.33}$$

Proposition 3.1 *Assume the effectiveness gain estimate $\widehat{W}(t)$ is sufficiently accurate so that the condition $\triangle_{max}\gamma_o < 1$ holds, where γ_o is defined in (3.17) and $\|\triangle(t)\| < \triangle_{max}$ bounds the relative error in the estimation of the effectiveness gains. Then during fault/failure conditions, for any $(\hat{w}_1(t), \ldots, \hat{w}_m(t)) \in \mathscr{W}$, the sliding motion in (3.31) will be stable if:*

$$\frac{\gamma_2\,\gamma_1(1+\gamma_o)}{1-\triangle_{max}\gamma_o} < 1 \tag{3.34}$$

where $\gamma_o > \|B_2^+(t)\|$, $\gamma_1 = \|B_1\|$ and γ_2 is as defined in (3.33).

Proof The system in (3.31), which represents the dynamics of the sliding motion, can be written as

$$\dot{x}(t) = \tilde{A}x(t) + \tilde{B}\tilde{u}(t) \tag{3.35}$$

$$\tilde{y}(t) = Fx(t) \tag{3.36}$$

where

$$\tilde{u}(t) = \tilde{\Phi}(t)\tilde{y}(t) \tag{3.37}$$

In this form, the differential equation in (3.31) may be considered to be the closed-loop dynamics of the negative feedback interconnection of $\tilde{G}(s)$ and the 'feedback gain' in (3.37) as shown in Fig. 3.2.

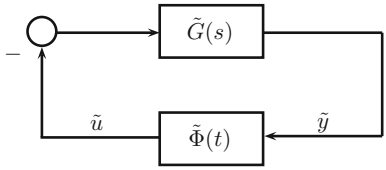

Fig. 3.2 Feedback interconnection of $\tilde{G}(s)$ and $\tilde{\Phi}(t)$

According to the small gain theorem, (see Appendix B.1.2) if

$$\|\tilde{G}(s)\|_\infty \|\tilde{\Phi}(t)\| < 1 \tag{3.38}$$

then (3.31) will be stable. In (3.38), $\|\tilde{G}(s)\|_\infty$ is the $\mathscr{H}_\infty$ norm of the transfer function $\tilde{G}(s)$ (which is equal to the $\mathscr{L}_2$ gain of the system in the time domain) and $\|.\|$ is the induced spectral norm. From (3.28) it is clear that

$$\|\tilde{\Phi}(t)\| \leq \|B_1 B_2\| + \|B_1(I - \triangle(t))B_2^+(t)\| \|(B_2(I - \triangle(t))B_2^+(t))^{-1}\| \tag{3.39}$$

Using the fact that $\|B_2\| = 1$, $B_2 B_2^+(t) = I_l$ and also that for a generic square matrix X, in general $\|(I - X)^{-1}\| \leq (1 - \|X\|)^{-1}$ if $\|X\| < 1$, then

$$\|\tilde{\Phi}(t)\| \leq \|B_1\| + \|B_1\|(1 + \triangle_{max})\|B_2^+(t)\|(I - \|B_2 \triangle(t) B_2^+(t)\|)^{-1} \tag{3.40}$$

This is well-defined since $\|B_2 \triangle(t) B_2^+(t)\| < \triangle_{max}\gamma_o < 1$. Since $\gamma_o > \|B_2^+(t)\|$ and $\gamma_1 = \|B_1\|$, inequality (3.40) becomes

$$\|\tilde{\Phi}(t)\| \leq \frac{\gamma_1(1 + \gamma_o)}{1 - \triangle_{max}\gamma_o} \tag{3.41}$$

Since $\gamma_2 = \|\tilde{G}(s)\|_\infty$, in conjunction with (3.41), it is clear that if inequality (3.34) holds, the small gain condition (3.38) holds, and consequently the system in (3.31) is stable. ■

Remark 3.5 By hypothesis, $\gamma_1 = \|B_1\|$ is assumed to be small. Note that from (3.39) the size $\|B_1\|$ has a significant impact on the norm of the nonlinearity in the small gain feedback loop. If $\|B_1\|$ is small, the gain of the nonlinearity is small, and there is a less stringent requirement on the magnitude of the $\mathscr{H}_\infty$ norm of the linear transfer function matrix. Furthermore, $\|\tilde{\Phi}(t)\| \to 0$ as $\|B_1\| \to 0$ and Proposition 3.1 is trivially satisfied.

Remark 3.6 In the case of exact estimation of the effectiveness matrix $W(t)$, i.e. $\widehat{W}(t) = W(t)$ and $\triangle(t) = 0$, the stability condition (3.34) reduces to

$$\gamma_2\gamma_1(1 + \gamma_o) < 1 \tag{3.42}$$

3.2.3 Integral Sliding Mode Control Laws

Now a sliding mode control law must be designed based on the virtual system (3.15) with respect to $\hat{v}(t)$. The control structure has the form given by:

$$\hat{v}(t) = \hat{v}_l(t) + \hat{v}_n(t) \tag{3.43}$$

where

$$\hat{v}_l(t) := -Fx(t) \tag{3.44}$$

The scaled unit vector

$$\hat{v}_n(t) := \begin{cases} -\rho(t,x)\frac{\sigma(t)}{||\sigma(t)||} & \text{if } \sigma(t) \neq 0 \\ 0 & \text{otherwise} \end{cases} \tag{3.45}$$

where $\rho(t,x)$ is a scalar modulation function to enforce the sliding motion. A suitable choice of $\rho(t,x)$ will be described explicitly in the sequel.

Proposition 3.2 *Suppose that*

$$\|\triangle(t)\| \leq \triangle_{max} < \frac{1}{\gamma_o} \tag{3.46}$$

where γ_o is defined in (3.17). If $\rho(t,x)$ is chosen as

$$\rho(t,x) = \frac{\triangle_{max}\gamma_o\|\hat{v}_l\| + \eta}{1 - \triangle_{max}\gamma_o} \tag{3.47}$$

where η is a positive scalar, then, the control law in (3.43) satisfies the so-called reachability condition and sliding on $\mathscr{S}$ in (3.20) is maintained.

Proof Substituting (3.15) in (3.23) gives

$$\dot{\sigma}(t) = (G\widehat{B})\hat{v}(t) + Fx(t) \tag{3.48}$$

Substituting for $\hat{v}(t)$ from Eqs. (3.43)–(3.45) and then exploiting the fact that $G\widehat{B} = (I - B_2\triangle(t)B_2^+(t))$, gives

$$\dot{\sigma}(t) = -\rho(\cdot)\frac{\sigma(t)}{||\sigma(t)||} + B_2\triangle(t)B_2^+(t)\left(Fx(t) + \rho(\cdot)\frac{\sigma(t)}{||\sigma(t)||}\right) \quad \text{for } \sigma(t) \neq 0 \tag{3.49}$$

Consider as the candidate Lyapunov function

$$V(t) = \frac{1}{2}\sigma^T(t)\sigma(t) \tag{3.50}$$

The time derivative of the Lyapunov function along the trajectories satisfies

$$\dot{V} = -\rho\|\sigma\| + \sigma^T B_2 \triangle(t) B_2^+(t) Fx(t) + \rho\sigma^T (B_2 \triangle(t) B_2^+(t)) \frac{\sigma}{\|\sigma\|} \quad \text{for } \sigma \neq 0$$

and therefore

$$\begin{aligned}\dot{V}(t) &\leq -\rho(\cdot)\|\sigma(t)\| + \|\sigma(t)\|\|B_2\triangle(t)B_2^+(t)\|\|\overbrace{Fx(t)}^{-\hat{v}_l}\| + \rho(\cdot)\|\sigma(t)\|\|B_2\triangle(t)B_2^+(t)\| \\ &\leq -\rho(\cdot)\|\sigma(t)\| + (\rho(\cdot) + \|\hat{v}_l\|)\|\sigma(t)\|\triangle_{max}\gamma_o \\ &\leq -\rho(\cdot)(1 - \triangle_{max}\gamma_o)\|\sigma(t)\| + \|\hat{v}_l\|\|\sigma(t)\|\triangle_{max}\gamma_o \end{aligned} \tag{3.51}$$

Substituting for $\rho(t, x)$ from (3.47) into (3.51) gives $\dot{V}(t) \leq -\eta\|\sigma(t)\| = -\eta\sqrt{2V(t)}$. This implies that the sliding motion is maintained for all time. ■

Finally using Eqs. (3.9), (3.10) and (3.14) it follows that the physical control law is given by

$$u(t) = \widehat{W}(t) B_2^T (B_2 \widehat{W}^2(t) B_2^T)^{-1} \Big(- Fx(t) - \rho(t, x) \frac{\sigma(t)}{||\sigma(t)||} \Big) \quad \text{if } \sigma(t) \neq 0 \tag{3.52}$$

This is the actual control signal which will be sent to the actuators, and depends on the effectiveness levels. The controller in (3.52) can deal with actuator faults and even total actuator failures, provided that $(\hat{w}_1(t), \ldots, \hat{w}_m(t)) \in \mathscr{W}$ and the conditions of Proposition 3.1 are satisfied.

Remark 3.7 In this chapter, actuator position limits are not considered formally in the control design, However the fault estimation scheme would declare it as a fault if an actuator exceeds its position limits. This is because the actual position of the actuator will be different from the expected position based on the commanded control signal. The scheme attempts to reduce the burden on the faulty actuator channels ($\hat{w}_i(t) < 1$) and hence mitigates the effects of actuator saturation, and redistributes the control effort among the redundant actuators.

The results developed in this section can be summarised in the form of the following theorem.

Theorem 3.1 *The system in (3.1) is closed-loop stable for any fault/failure combination belonging to $\mathscr{W}$ in (3.12) under the control law (3.52), if a feedback gain F can be found such that*

$$\frac{\gamma_2\, \gamma_1(1 + \gamma_o)}{1 - \triangle_{max}\gamma_o} < 1$$

where γ_2 is defined in (3.33), $\gamma_1 = \|B_1\|$, γ_o satisfies $\gamma_o \geq \|B_2^+(t)\|$ where $B_2^+(t)$ is defined in (3.16), and $\triangle_{max}$ bounds the relative error in the estimation of the effectiveness gains in (3.5).

3.2.4 Design of the Controller Gains

In this section, it will be demonstrated that the stability test in Proposition 3.1 is amenable to incorporation within a synthesis framework for determining the feedback gain F in (3.19). For the nominal system (3.19), the matrix F must be chosen to stabilise $(A - B_v F)$. Since (A, B_v) is assumed to be controllable, an LQR formulation is adopted to synthesise the control signal $\hat{v}(t)$ to minimise the energy cost function

$$J = \int_0^\infty z^T z \, dt \tag{3.53}$$

where

$$z = \begin{bmatrix} Q_1 & 0 \\ 0 & R_1 \end{bmatrix} \begin{bmatrix} x \\ v \end{bmatrix} \tag{3.54}$$

and Q_1 and R_1 are symmetric positive definite matrices. Details of the LMI formulation are given in Appendix B.2.1, where it is argued the LQR problem can be posed as an LMI optimisation:

Minimise trace(X^{-1}) subject to

$$\begin{bmatrix} AX + XA^T - B_v Y - Y^T B_v^T & (Q_1 X - R_1 Y)^T \\ Q_1 X - R_1 Y & -I \end{bmatrix} < 0 \tag{3.55}$$

$$X > 0 \tag{3.56}$$

where

$$Q_1 = \begin{bmatrix} Q^{\frac{1}{2}} \\ 0_{l \times n} \end{bmatrix} \quad \text{and} \quad R_1 = \begin{bmatrix} 0_{n \times l} \\ R^{\frac{1}{2}} \end{bmatrix} \tag{3.57}$$

In (3.55) the variable $Y := FX$ with $Y \in \mathbb{R}^{l \times n}$ and $X \in \mathbb{R}^{n \times n}$ is the Lyapunov matrix. In this LMI formulation, the decision variables are X and Y.

However in addition, the small gain stability condition (3.34) needs to be satisfied. From the Bounded Real Lemma, the $\mathscr{L}_2$ gain from $\tilde{u}$ to $\tilde{y}$, which in this situation is equal to the $\mathscr{H}_\infty$ norm of its transfer matrix $\tilde{G}(s)$, satisfies $||\tilde{G}(s)||_\infty < \gamma$ if and only if there exist $X > 0$ and $\gamma \geq 0$ such that

$$\begin{bmatrix} AX + XA^T - B_v Y - Y^T B_v^T & \tilde{B} & Y^T \\ \tilde{B}^T & -\gamma^2 I & 0 \\ Y & 0 & -I \end{bmatrix} < 0 \tag{3.58}$$

where $\tilde{B}$ is defined in (3.29). For details of the LMI formulation see Appendix B.2.2. In (3.58) γ is an a-priori fixed scalar gain which may be viewed as a tuning parameter. The decision variables in this LMI formulation are again X and Y. If

$$\gamma < \frac{(1 - \Delta_{max}\gamma_o)}{\gamma_1(1 + \gamma_o)}$$

then the conditions of Theorem 3.1 are satisfied and closed-loop stability for a fault/failure combination belonging to $\mathscr{W}$ is guaranteed.

Since a common Lyapunov matrix is sought in the LMI formulations, the overall optimisation process is:

Minimise trace(Z) subject to (3.55), (3.56) and (3.58) and

$$\begin{bmatrix} -Z & I_n \\ I_n & -X \end{bmatrix} < 0 \tag{3.59}$$

The matrix Z is a slack variable, which using the Schur complement satisfies $Z > X^{-1}$ and therefore trace(Z) $\geq$ trace(X^{-1}). Finally the feedback gain F can be recovered as $F = YX^{-1}$.

3.3 Simulations

In this section control of the lateral axis of a large transport aircraft, discussed in Appendix A.1, will be considered to demonstrate the effectiveness and feasibility of the scheme described in the earlier section. To design the state feedback gain F in (3.44), a linear model has been obtained around an operating condition of straight and level flight at 263,000 kg, 92.6 m/s true airspeed, and at an altitude of 600 m based on 25.6% of maximum thrust and at a 20 deg flap position. The lateral axis states which are considered for the controller design are (ϕ, β, r, p), where ϕ is roll angle (rad), β is sideslip angle (rad), r is yaw rate (rad/s), and p is roll rate (rad/s). The controlled outputs $y_c(t) = Cx(t)$ are (β, ϕ) where

$$C = \begin{bmatrix} 0\,1\,0\,0 \\ 1\,0\,0\,0 \end{bmatrix}$$

It is clear in this example that $l = 2$. For the lateral control, the inboard and outboard ailerons (δ_{air}, δ_{aor}) on the right wing are aggregated to produce one control input. The available control surfaces are $\delta = (\delta_a, \delta_r, \delta_{epr})$, which represent anti-symmetric aileron deflection (rad), rudder deflection (rad) and differential aggregated engine pressure ratios (EPR). Note in this example the number of control inputs $m = 3$, while the number of controlled outputs $l = 2$, and so in theory, only two control inputs would be required to force the controlled outputs to follow a commanded trajectory. Here the fact that three control inputs can be manipulated, indicates the existence of redundancy in the system which can be exploited to achieve fault

tolerance. The ordering of the states ensures $\|B_1\| \ll \|B_2\|$, so that B_2 represents the dominant contribution to the control action as compared to B_1. After scaling the states to ensure $B_2 B_2^T = I_l$ the state-space representation is

$$A = \begin{bmatrix} 0 & 0 & 0.0084 & 0.3334 \\ 0.1055 & -0.0999 & -0.3170 & 0.0538 \\ -0.0059 & 0.5617 & -0.1856 & -0.1796 \\ 0.0008 & -4.8828 & 0.2154 & -1.0789 \end{bmatrix}$$

$$B = \begin{bmatrix} 0 & 0 & 0 \\ 0 & 0.0174 & -0.0010 \\ \hline -0.1459 & -0.7584 & -0.6352 \\ -0.9387 & 0.3089 & -0.1531 \end{bmatrix} \begin{matrix} \} B_1 \\ \\ \} B_2 \end{matrix} \tag{3.60}$$

For tracking the (β, ϕ) commands, integral action is used. To accomplish this, the integral action states $x_r(t)$ satisfying the relation

$$\dot{x}_r(t) = r(t) - Cx(t) \tag{3.61}$$

are introduced, where $r(t)$ is the reference signal to be tracked. By defining $x_a(t) = \text{col}(x_r(t), x(t))$, the system in (3.18) is augmented with the integral action states to become

$$\dot{x}_a(t) = A_a x_a(t) + B_{v_a} v(t) + B_r r(t) \tag{3.62}$$

where

$$A_a = \begin{bmatrix} 0 & -C \\ 0 & A \end{bmatrix} \quad B_{v_a} = \begin{bmatrix} 0 \\ B_v \end{bmatrix} \quad B_v = \begin{bmatrix} B_1 B_2^T \\ I_l \end{bmatrix} \quad B_r = \begin{bmatrix} I_l \\ 0 \end{bmatrix} \tag{3.63}$$

By design the pair (A_a, B_{v_a}) is controllable and a state feedback gain $v(t) = -Fx_a(t)$ is to be designed to stabilise the nominal system in (3.62). The switching function in (3.21) for the augmented system will become

$$\sigma(t) = G_a x_a(t) - G_a x_a(0) - G_a \int_0^t \left((A_a - B_{v_a} F) x_a(\tau) + B_r r(\tau) \right) d\tau \tag{3.64}$$

where $G_a := B_2 (B_a^T B_a)^{-1} B_a^T$, and the augmented input distribution matrices

$$B_a = \begin{bmatrix} B_{1_a} \\ B_2 \end{bmatrix} \quad B_{1_a} = \begin{bmatrix} 0_{l \times m} \\ B_1 \end{bmatrix}$$

In a fault-free scenario, i.e. in normal flight, the primary control surfaces for ϕ and β tracking are the ailerons and rudder respectively; however the engine thrust can be used as redundancy for both surfaces. Based on these assumptions, using a numerical

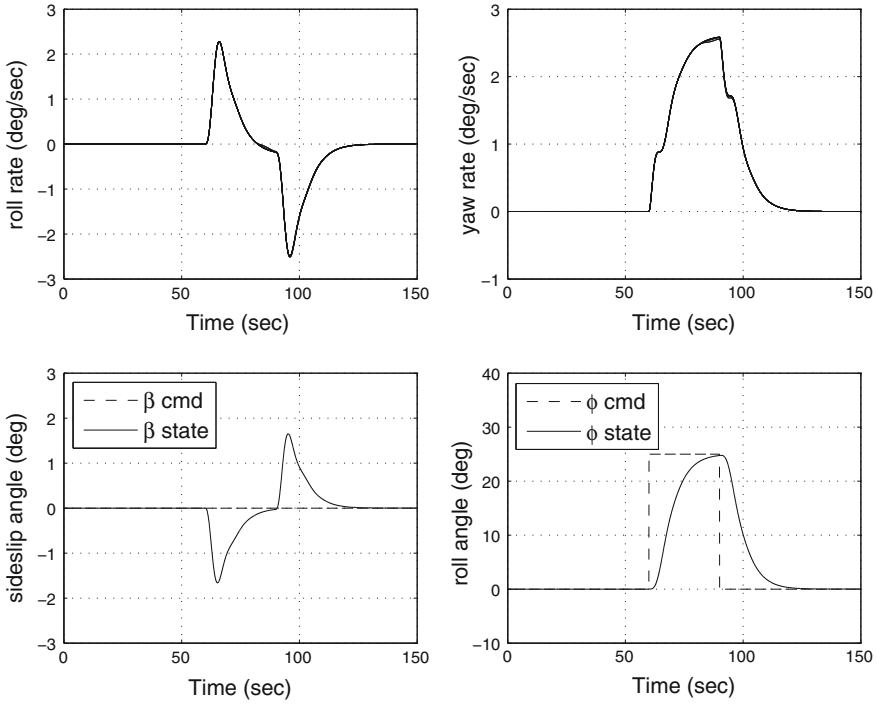

Fig. 3.3 Aileron-fault, loss of effectiveness: plant states

search, a suitable bound for the scalar in (3.17) is $\gamma_o = 3.2020$. Here it can be easily verified that $\gamma_1 = \|B_{1_a}\| = 0.0174$. The nominal state feedback controller gain F associated with Eq. (3.19) for the augmented system has been designed using the LMI approach described in Sect. 3.2.4 and is given by

$$F = \begin{bmatrix} 0.4165 & -0.0839 & 0.2936 & -1.9273 & 0.7983 & -0.1356 \\ -0.5265 & -0.1241 & 1.1878 & -0.6954 & -0.1000 & 0.3879 \end{bmatrix} \tag{3.65}$$

The performance design matrices Q and R in (3.55) have been chosen as

$$Q = \text{diag}(0.95, 0.08, 2, 1, 15, 5) \quad \text{and} \quad R = \text{diag}(10, 2)$$

respectively, where the first two states in Q represent the integral action states. Here $\triangle_{max} = 0.17$ which implies an upper bound on the relative error in $\widehat{W}(t)$ of 17 %. The choice of $\gamma = 8.8$ in LMI (3.58) results in $\gamma_2 = 5.8832$ and it can be verified that

$$\frac{\gamma_2\, \gamma_1(1+\gamma_o)}{1 - \triangle_{max}\gamma_o} = 0.9440 < 1$$

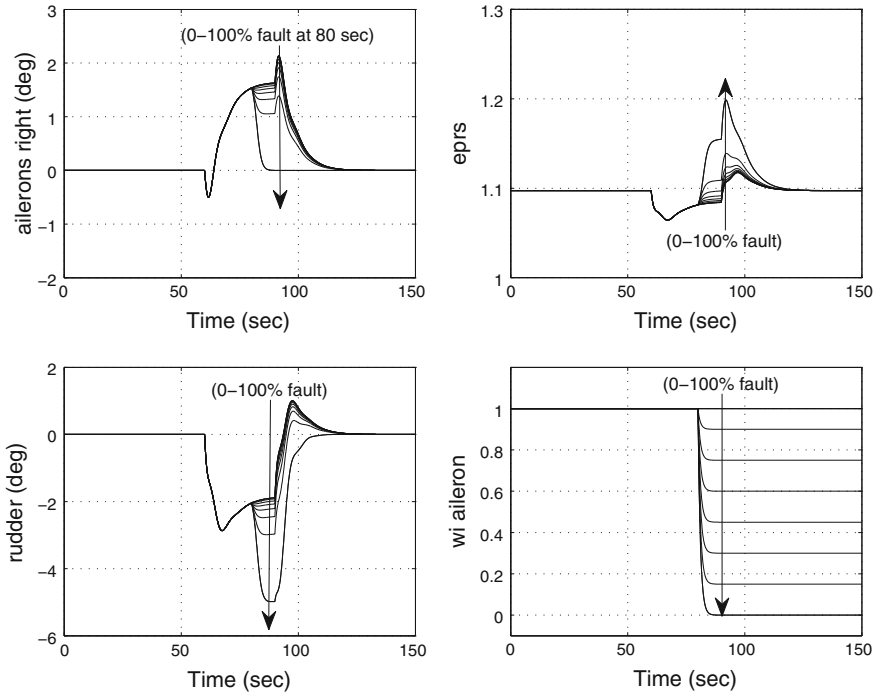

Fig. 3.4 Aileron-fault, loss of effectiveness: actuator deflections

Consequently the conditions of Theorem 3.1 are satisfied and the closed-loop stability of the system for any combination of faults $(\hat{w}_1, \hat{w}_2, \hat{w}_3) \in \mathscr{W}$ is ensured.

3.3.1 Sliding Mode Fault Reconstruction Scheme

The control law $u(t)$ in (3.52) depends on an estimate of the $W(t)$ matrix to distribute the control effort among the actuators. A sliding mode fault reconstruction scheme, can be used to estimate the actuator effectiveness levels. To explain this, without loss of generality, the actuator fault model in (3.1) can be written as

$$\dot{x}(t) = Ax(t) + B \underbrace{(I_m - K(t))}_{W(t)} u(t) \tag{3.66}$$

where it is assumed that the input matrix B is of full column rank. In (3.66) the matrix $K(t) = \text{diag}(k_i(t), \ldots, k_m(t))$ where the scalars $k_i(t) = 1 - w_i(t)$. By writing the

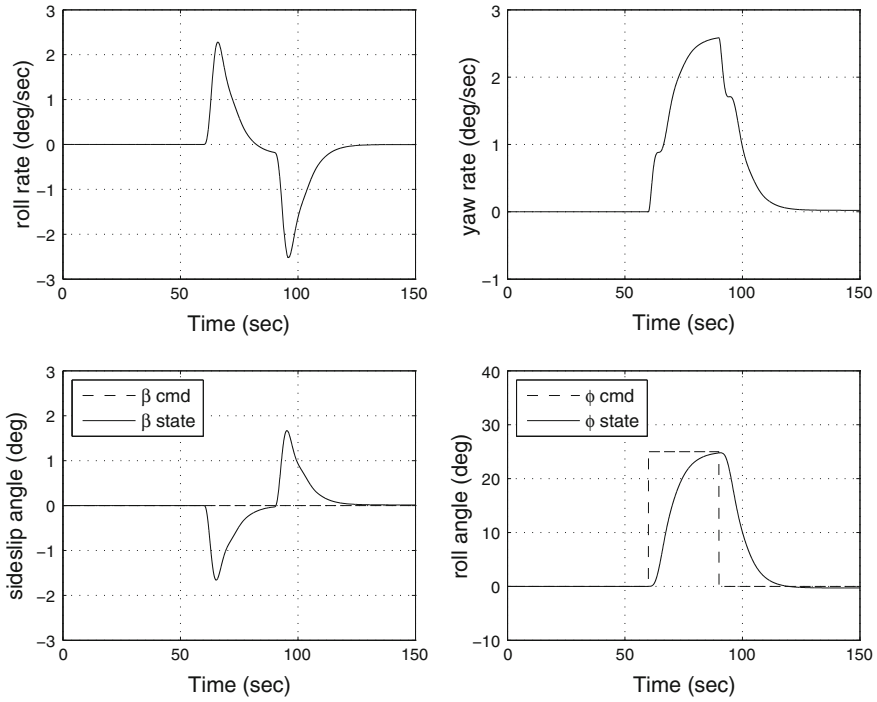

Fig. 3.5 Aileron Jam/Lock in place failure: plant states

term $K(t)u(t)$ in this way, it can be considered as a fault term. To estimate the fault term $K(t)u(t)$ an estimator is given by

$$\dot{z}(t) = Az(t) + Bu(t) + G_n\vartheta(t) \tag{3.67}$$

where G_n is an appropriate gain matrix, $z(t)$ is the estimator state and $\vartheta(t)$ is a discontinuous injection term defined by

$$\vartheta(t) := -\rho_e \frac{e(t)}{\|e(t)\|} \qquad \text{for } e(t) \neq 0 \tag{3.68}$$

where the scalar ρ_e must be chosen such that $\rho_e \geq \|K(t)u(t)\|$. From (3.67) and (3.66) it is clear that the error dynamics $e(t) = x(t) - z(t)$ satisfy

$$\begin{aligned} \dot{e}(t) &= \dot{x}(t) - \dot{z}(t) \\ &= Ae(t) - \vartheta(t) - BK(t)u(t) \end{aligned} \tag{3.69}$$

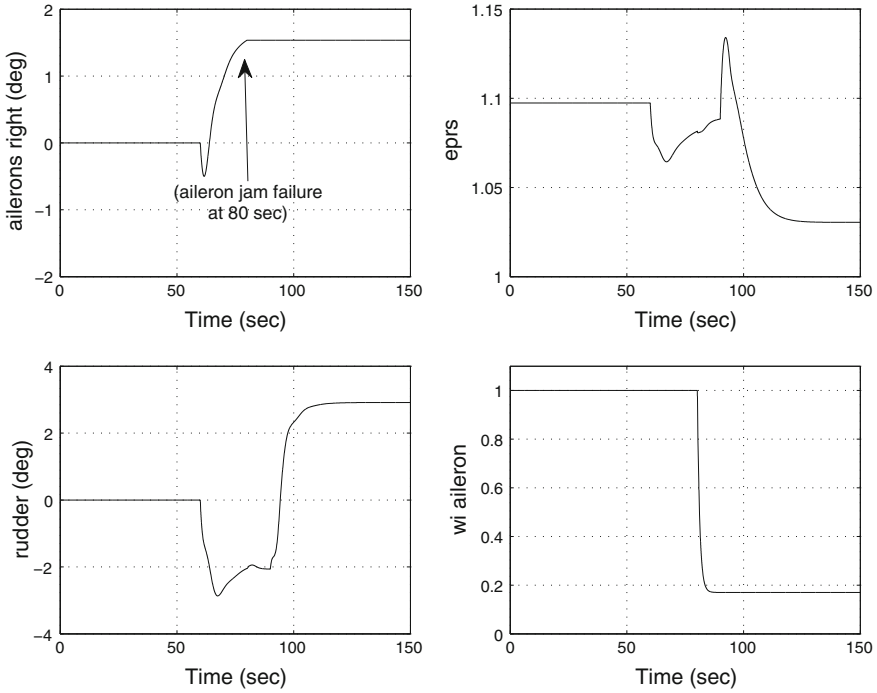

Fig. 3.6 Aileron Jam/Lock in place failure: actuator deflections

A sliding motion on $e(t) = 0$ will be enforced by the discontinuous injection term $\vartheta(t)$. Then during sliding $e(t) = \dot{e}(t) = 0$ and the fault signal $K(t)u(t)$ can be reconstructed from Eq. (3.69) as

$$-K(t)u(t) \approx (B^T B)^{-1} B^T \vartheta_{eq}(t) \tag{3.70}$$

where $\vartheta_{eq}(t)$ is the equivalent injection term necessary to maintain sliding. The injection term is discontinuous and can be approximated to any level of accuracy using the relation

$$\vartheta_\delta(t) := -\rho_e \frac{e(t)}{\|e(t)\| + \delta} \tag{3.71}$$

where δ is a small positive scalar. The scalars $k_i(t)$ can be obtained from (3.70) by introducing a small threshold ε such that if at time t_ε, $|u_i(t)| \leq \varepsilon$, then

$$k_i(t) = \begin{cases} \frac{((B^T B)^{-1} B^T \vartheta_\delta(t))_i}{u_i(t)} & \text{if } |u_i(t)| > \varepsilon \\ k_i(t_\varepsilon) & \text{otherwise} \end{cases} \tag{3.72}$$

A saturation block with limits $\begin{bmatrix} 0 & 1 \end{bmatrix}$ is used before the information is provided to the control allocation unit to keep the estimates within the theoretical limits.

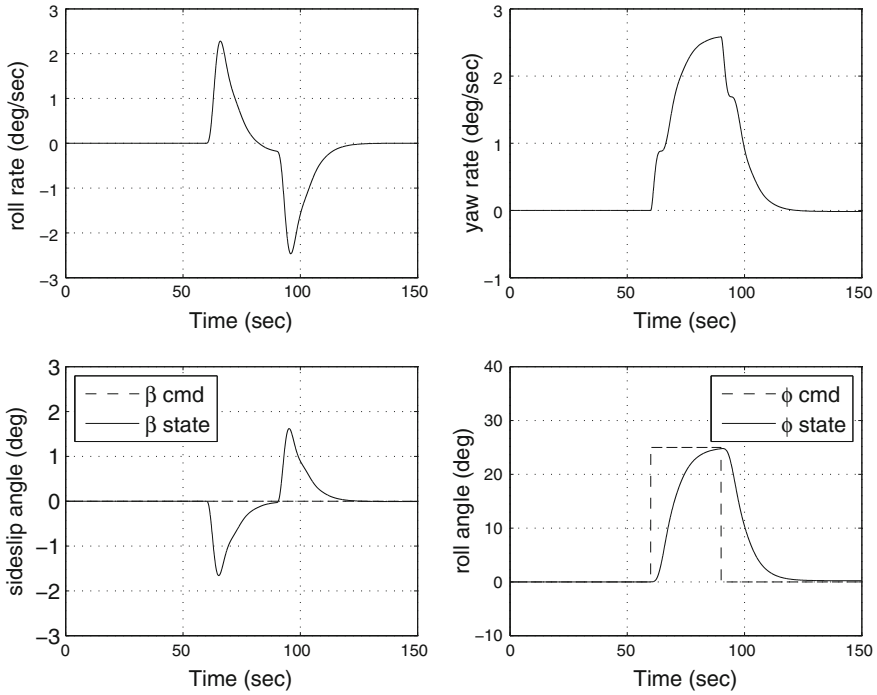

Fig. 3.7 Rudder Jam/Lock in place failure: plant states

3.3.2 Manoeuvre and Fault Scenarios

In the simulations which follow the linear aircraft model undertakes a turning manoeuvre, where the reference command requests a change in ϕ to 25 deg during the period of time 60–90 s. A 0 deg reference command is applied to β throughout. In the simulations, the discontinuity associated with the nonlinear control term in (3.45) is smoothed using the sigmoidal approximation (2.33), discussed in Sect. 2.5, and given by $\frac{\sigma(t)}{||\sigma(t)||+\delta_o}$ where the value of the positive scalar δ_o is chosen to be 0.001. An ideal sliding motion will not be obtained in this situation, and instead a pseudo-sliding will be achieved, where the sliding motion is in the vicinity of the sliding surface $\mathscr{S}$. This boundary layer can be made arbitrarily small by selecting δ_o sufficiently small.

3.3.2.1 Aileron Faults and Lock in Place Failure

In this subsection to test the efficacy of the FTC scheme, aileron faults and failures are considered. Various levels of aileron faults (from 0 to 100 %) are tested, each occurring at 80 s in 15 % increments. In Figs. 3.3 and 3.4, the plant states and actuator deflections are shown during the aileron fault scenario (when the estimation of $W(t)$

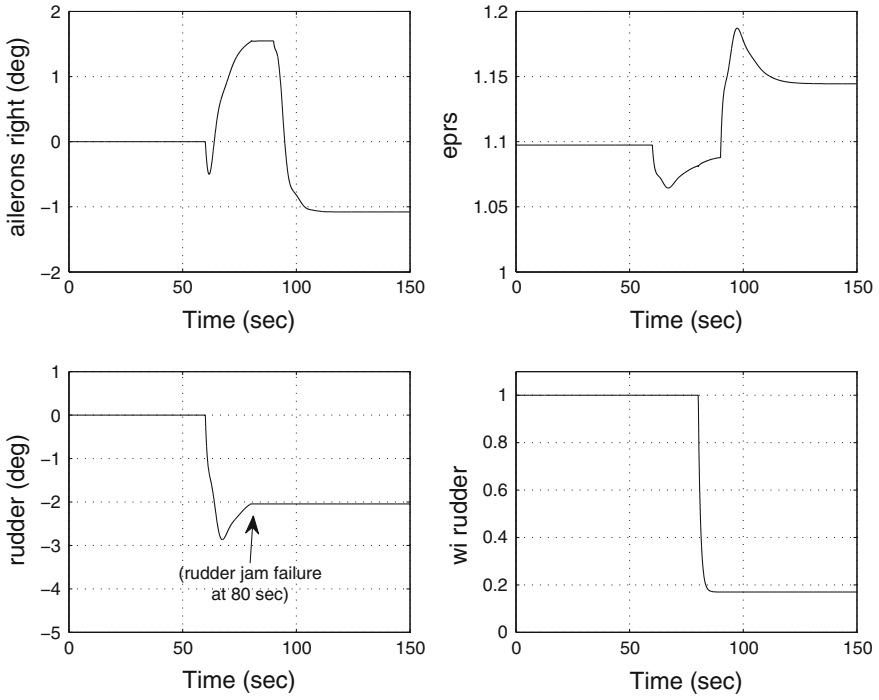

Fig. 3.8 Rudder Jam/Lock in place failure: actuator deflections

Fig. 3.9 Switching function

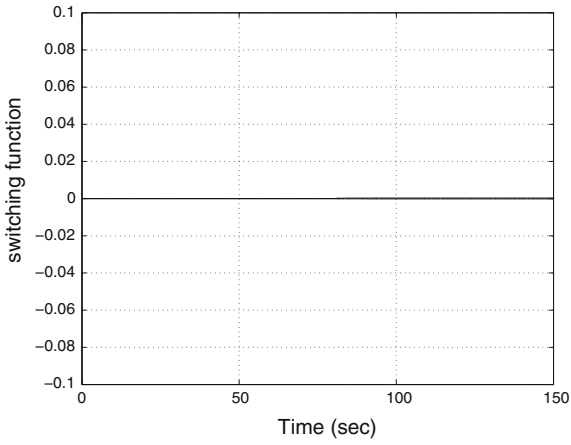

is perfect). It can be seen that the CA scheme systematically redistributes the control signals to the rudder and the engines, while maintaining the same level of tracking performance as in the fault-free condition.

In Figs. 3.5 and 3.6, the aileron undergoes lock in place failure (where the actuator jams at some offset position), which means the effectiveness of the aileron after the failure time (80 s) is 0 %. If the estimate of the actuator effectiveness is perfect then the information provided to the CA unit regarding the actuator effectiveness ($\hat{w}_i(t)$) should be 0 %. But since the estimate $\widehat{W}(t)$ is not perfect, the effect of a 17 % error in the estimate of $W(t)$ can be seen in Fig. 3.6, which is the maximum theoretical percentage error $\triangle_{max}$ which can be tolerated by the scheme without violating the stability conditions of Proposition 3.1. Due to the availability of redundancy in the system, the CA scheme involves the engines more actively to achieve a performance close to the nominal (Fig. 3.5).

3.3.2.2 Rudder Lock in Place Failure

This subsection validates the scheme, by considering a rudder failure scenario. Figures 3.7 and 3.8 show the tracking performance of the states and the control surface deflections, when a rudder jam/lock-in place occurs at 80 s at a position of -2 deg. The estimate of the rudder effectiveness is not perfect and has a 17 % error as can be seen in Fig. 3.8. The FTC scheme redistributes the control effort between the aileron and the engines to cope with the rudder failure, and to maintain the nominal tracking performance (Fig. 3.7). Figure 3.9 shows that sliding is maintained throughout the simulations, even in the presence of actuator faults or failures.

3.4 Summary

An Integral Sliding Mode fault tolerant control scheme has been described. To handle total actuator failures, integral sliding mode ideas have been incorporated into a control allocation framework, which has the capability to redistribute the control effort among the healthy redundant actuators automatically in the case of faults or failures, without reconfiguring the controller. The estimation of the actuator effectiveness levels is a key source of information for the control allocation scheme. A formal stability analysis guarantees closed-loop stability of the system in the face of a class of faults and failures, and for a certain level of mismatch between the actual and the estimated actuator effectiveness levels. The efficacy of the fault tolerant scheme was demonstrated through simulation, based on different fault or failure scenarios in a benchmark civil aircraft.

3.5 Notes and References

The uncertain model used in this chapter represents a LTI system subject to actuator faults/failures and has been used by many other FTC researchers: see for example [3–7]. Other ways of representing fault models used in the literature can be found in [8]. Control allocation provides access to redundant actuators and has the ability to cope with actuator faults/failures without the need to modify the underlying control laws [9–12]. Actuator constraints (rate and position) are explicitly used in [10, 13] for CA. In terms of FTC, the benefits of CA are exploited in [9, 14]. In [15], a modified daisy chaining method, which is a special structure of CA, was proposed to deal with actuator loss of effectiveness. In [16], fault reconstruction and fault tolerant control schemes are described for both sensors and actuators, where a combination of CA with SMC is considered to design fault tolerant controllers for aerospace applications. In [17, 18] researchers have considered the combination of SMC with CA to deal with actuator faults on a tailless fighter aircraft. In [19], SMC is argued to have the potential to become an alternative to reconfigurable control to directly deal with actuator faults, which can be effectively modelled as matched uncertainties.

References

1. Briére, D., Traverse, P.: Airbus A320/A330/A340 electrical flight controls: a family of fault-tolerant systems. In: Digest of Papers FTCS-23 The Twenty-Third International Symposium on Fault-Tolerant Computing, pp. 616–623 (1993)
2. Stewart, G.W.: On scaled projections and pseudoinverses. Linear Algebr. Appl. **112**, 189–193 (1989)
3. Noura, H., Sauter, D., Hamelin, F., Theilliol, D.: Fault-tolerant control in dynamic systems: application to a winding machine. IEEE Control Syst. Mag. **20**(1), 33–49 (2000)
4. Tao, G., Joshi, S.M., Ma, X.: Adaptive state feedback and tracking control of systems with actuator failures. IEEE Trans. Autom. Control **46**(1), 78–95 (2001)
5. Zhang, Y., Jiang, J.: Fault tolerant control system design with explicit consideration of performance degradation. IEEE Trans. Aerosp. Electron. Syst. **39**(3), 838–848 (2003)
6. Jiang, J., Zhang, Y.: Accepting performance degradation in fault-tolerant control system design. IEEE Trans. Control Syst. Technol. **14**(2), 284–292 (2006)
7. Alwi, H., Edwards, C.: Fault tolerant control using sliding modes with on-line control allocation. Automatica **44**, 1859–1866 (2008)
8. Verhaegen, M., Kanev, S., Hallouzi, R., Jones, C., Maciejowski, J., Smail, H.: Fault tolerant flight control - a survey. In: Edwards, C., Lombaerts, T., Smaili, H. (eds.) Fault Tolerant Flight Control. LNCIS, vol. 399, pp. 47–89. Springer, New York (2010)
9. Davidson, J.B., Lallman, F.J., Bundick, W.T.: Real-time adaptive control allocation applied to a high performance aircraft. In: 5th SIAM Conference on Control and Its Application (2001)
10. Bošković, J.D., Mehra, R.K.: Control allocation in over-actuated aircraft under position and rate limiting. In: Proceedings of the American Control Conference (2002)
11. Ducard, G.: Fault-tolerant Flight Control and Guidance Systems: Practical Methods for Small Unmanned Aerial Vehicles. Advances in Industrial Control Series. Springer, New York (2009)
12. Zhang, Y., Suresh, V.S., Jiang, B., Theilliol, D.: Reconfigurable control allocation against aircraft control effector failures. In: Proceedings of the 16th IEEE International Conference on Control Applications (2007)

13. Durham, W.C.: Constrained control allocation. J. Guid. Control Dyn. **16**(4), 717–725 (1993)
14. Buffington, J.: Tailless aircraft control allocation. In: AIAA Guidance, Navigation and Control, pp. 737–747 (1997)
15. Kim, J., Yang, I., Lee, D.: Accommodation of actuator faults using control allocation with modified daisy chaining. In: 11th International Conference on Control, Automation and Systems, pp. 717–720. Korea (2011)
16. Alwi, H., Edwards, C., Tan, C.P.: Fault Detection and Fault Tolerant Control Using Sliding Modes. Advances in Industrial Control Series. Springer, New York (2011)
17. Wells, S.R., Hess, R.A.: Multi-input/multi-output sliding mode control for a tailless fighter aircraft. J. Guid. Control Dyn. **26**(3), 463–473 (2003)
18. Shtessel, Y., Buffington, J., Banda, S.: Tailless aircraft flight control using multiple time scale re-configurable sliding modes. IEEE Trans. Control Syst. Technol. **10**, 288–296 (2002)
19. Hess, R.A., Wells, S.R.: Sliding mode control applied to reconfigurable flight control design. J. Guid. Control Dyn. **26**, 452–462 (2003)

Chapter 4
A Fault Tolerant Direct Control Allocation Scheme with Integral Sliding Modes

The FTC scheme described in this chapter looks at the possibility of introducing fault tolerance without having information about actuator effectiveness levels. Here the idea of *direct control allocation* is incorporated within the ISM/FTC framework. Achieving performance close to the nominal and maintaining overall closed-loop stability in the face of actuator faults/failures and in the presence of aerodynamic disturbances (i.e. wind gusts) and sensor noise is the main objective. An LMI based procedure is described to synthesise the controller parameters, and a rigorous closed-loop stability analysis is carried out in the presence of unmatched uncertainty for a suitable set of actuator faults/failures. The FTC scheme is compared in simulation with the one from Chap. 3 by considering the same manoeuvre on the RECOVER benchmark model in the presence of wind gusts and sensor noise.

4.1 Problem Formulation

In this chapter again consider an over-actuated system with actuator faults or failures modelled as

$$\dot{x}(t) = Ax(t) + BW(t)u(t) + D\xi(t, x) \tag{4.1}$$

where $A \in \mathbb{R}^{n\times n}$ and $B \in \mathbb{R}^{n\times m}$ are the state and input distribution matrices. As before, the term $W(t) = \text{diag}(w_1(t), \ldots, w_m(t))$ is a diagonal semi-positive definite weighting matrix wherein the scalars $w_1(t), \ldots, w_m(t)$ model the individual effectiveness/efficiency levels of the actuators. As in the previous chapter if the diagonal entry $w_i(t) = 1$, this indicates that the corresponding ith actuator is healthy/fault-free, whereas if $1 > w_i(t) > 0$, actuator i is faulty. Finally the value $w_i(t) = 0$ indicates that the corresponding actuator has failed.

Assumption 4.1 It is assumed that the pair (A, B) is controllable and B has full column rank.

M.T. Hamayun et al., *Fault Tolerant Control Schemes Using Integral Sliding Modes*, Studies in Systems, Decision and Control 61,
DOI 10.1007/978-3-319-32238-4_4

Assumption 4.2 In this chapter it is assumed that the actuator effectiveness level (i.e. the matrix $W(t)$) is not available, and neither is an estimate.

In (4.1), the function $\xi(t, x)$ represents uncertainties/nonlinearities in the system.

Assumption 4.3 The structure of the D matrix is assumed to be such that $B^T D = 0$ i.e. D is in the null space of B.

Suppose that the input distribution matrix B in (4.1) has been partitioned as

$$B = \begin{bmatrix} B_1 \\ B_2 \end{bmatrix} \tag{4.2}$$

where $B_1 \in \mathbb{R}^{(n-l)\times m}$ and $B_2 \in \mathbb{R}^{l\times m}$ is of rank $l < m$. It will be demonstrated later in the chapter that the norm of $\|B_1\|$ plays a significant role in the closed-loop stability analysis.

Assumption 4.4 Assume that $\|B_2\| \gg \|B_1\|$, so that B_2 is more dominant in the delivery of the control effort to the system compared to B_1.

As discussed in Chap. 3, a state permutation may be required to achieve the form in (4.2). It is also assumed without loss of generality that the states are scaled to ensure that $B_2 B_2^T = I_l$. This will help simplify the analysis and design process in the sequel. In order to follow a reference demand, a tracking capability is included in the design. For this purpose, the states $x(t)$ in (4.1) are augmented with integral action states $x_r(t)$ creating the vector $x_a(t) = \text{col}(x_r(t), x(t))$, where

$$\dot{x}_r(t) = r(t) - C_c x(t) \tag{4.3}$$

In (4.3) the signal $r(t)$ is the reference command to be tracked, whereas $C_c \in \mathbb{R}^{l\times n}$ is the output distribution matrix which extracts the controlled outputs from the states. The overall augmented system becomes

$$\dot{x}_a(t) = A_a x_a(t) + B_a W(t) u(t) + B_r r(t) + D_a \xi(t, x) \tag{4.4}$$

and the augmented matrices are

$$A_a = \begin{bmatrix} 0 & -C_c \\ 0 & A \end{bmatrix}, \quad B_a = \begin{bmatrix} B_{1_a} \\ B_2 \end{bmatrix}, \quad B_{1_a} = \begin{bmatrix} 0 \\ B_1 \end{bmatrix}, \quad B_r = \begin{bmatrix} I_l \\ 0 \end{bmatrix}, \quad D_a = \begin{bmatrix} 0 \\ D \end{bmatrix} \tag{4.5}$$

Note that by definition, B_a has full column rank (inherited from B).

Assumption 4.5 It is assumed that the function $\xi(t, x)$ satisfies the relationship $\xi(t, x) = \phi(t, x)x(t)$, where $\|\phi(t, x)\|$ is bounded.

In the next section, an integral sliding mode FTC scheme with direct CA will be described for the system in (4.4).

4.2 Integral Sliding Mode FTC Scheme with Direct Control Allocation

In the FTC scheme which will be introduced in this section, the fault information (i.e. the matrix $W(t)$) is not required for the control allocation scheme. The strategy "distributes" control effort among all the actuators and constitutes a passive fault tolerant control scheme. A schematic of the proposed scheme, is shown in Fig. 4.1. In this chapter, a virtual control input, $\nu(t) \in \mathbb{R}^l$, is defined as

$$\nu(t) = B_2 u(t) \tag{4.6}$$

where B_2 is taken from (4.5). Here the physical control law $u(t)$ is chosen as

$$u(t) = B_2^T \nu(t) \tag{4.7}$$

Using the fact that $B_2 B_2^T = I_l$, B_2^T is a right pseudo-inverse of B_2, and hence the choice of control law in (4.7) satisfies (4.6). In the sequel, a framework for the design of the virtual control law $\nu(t)$ will be formulated. Substituting (4.7) into (4.4) yields

$$\dot{x}_a(t) = A_a x_a(t) + \underbrace{\begin{bmatrix} B_{1_a} W(t) B_2^T \\ B_2 W(t) B_2^T \end{bmatrix}}_{B_{w_a}(t)} \nu(t) + B_r r(t) + D_a \xi(.) \tag{4.8}$$

The ISM approach will now be used to design the virtual controller $\nu(t)$ in (4.8), based on the nominal fault-free system (i.e. when $W(t) = I_m$). Then substituting $W(t) = I_m$ into (4.8), yields

$$\dot{x}_a(t) = A_a x_a(t) + \underbrace{\begin{bmatrix} B_{1_a} B_2^T \\ I_l \end{bmatrix}}_{B_{\nu_a}} \nu(t) + B_r r(t) + D_a \xi(.) \tag{4.9}$$

Assumption 4.6 It is assumed that the pair (A_a, B_{ν_a}) is (preferably) controllable but at least stabilisable.

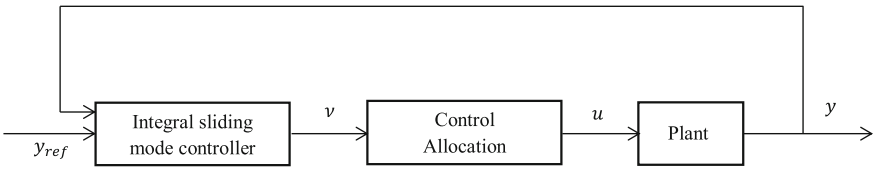

Fig. 4.1 FTC strategy with direct Control Allocation

Note that

$$\|B_{1a}B_2^T\| \leq \|B_{1a}\|\|B_2^T\| \leq \|B_{1a}\| \leq \|B_1\|$$

because $\|B_2^T\| = 1$ (since $B_2B_2^T = I$), and where the last inequality follows from the definition in (4.5). Consequently the control contribution in the first n channels of (4.9) is still small. To design $v(t)$ based on an ISM methodology, an integral switching function which eliminates the reaching phase and which aims to retain the nominal closed-loop performance is defined as

$$\sigma(t) = G_a x_a(t) - G_a x_a(0) - G_a \int_0^t (A_a - B_{v_a}F)x_a(\tau)\, d\tau \tag{4.10}$$

where the matrix $G_a \in \mathbb{R}^{l\times(n+l)}$ is design freedom. In (4.10) the matrix $F \in \mathbb{R}^{l\times(n+l)}$ is a state feedback gain matrix chosen to make the matrix $(A_a - B_{v_a}F)$ Hurwitz. The associated sliding motion occurs on the surface $\mathscr{S} = \{x_a \in \mathbb{R}^{n+l} : \sigma(t) = 0\}$. The choice of G_a suggested in Sect. 3.2.1, will also be employed here:

$$G_a := B_2\left(B_a^TB_a\right)^{-1}B_a^T \tag{4.11}$$

The choice of G_a is a left pseudo-inverse of B_{v_a} i.e. $G_aB_{v_a} = I$. The inverse in (4.11) exists because the control distribution matrix B_a is assumed to be full column rank. The choice of G_a in (4.11) brings some simplifying properties to the closed-loop analysis which are explained later. The sliding motion associated with the surface in (4.10), in the presence of faults or failures, will now be analysed. The time derivative of (4.10) along the trajectories of the differential equation (4.8) is given by

$$\dot{\sigma}_a(t) = G_aB_{w_a}(t)v(t) + G_aB_{v_a}Fx_a(t) \tag{4.12}$$

Note that (4.12) does not depend on the reference signal $r(t)$ because

$$\begin{aligned} G_aB_r &= B_2\left(B_a^TB_a\right)^{-1}B_a^TB_r \\ &= B_2\left(B_a^TB_a\right)^{-1}\begin{bmatrix}0 & B^T\end{bmatrix}\begin{bmatrix}I_l\\0\end{bmatrix} = 0 \end{aligned}$$

Also note that (4.12) is independent of the uncertainty $\xi(t,x)$, because

$$G_aD_a = B_2\left(B_a^TB_a\right)^{-1}\underbrace{B_a^TD_a}_{0} = 0$$

by assumption. In order to obtain an expression for the closed-loop motion during sliding, an equivalent control approach will be adopted. The equivalent control which maintains motion on the surface in (4.10) is obtained by equating $\dot{\sigma}_a(t) = 0$ in (4.12) to obtain

$$v_{eq}(t) = -(G_aB_{w_a}(t))^{-1}G_aB_{v_a}Fx_a(t) \tag{4.13}$$

Note the expression in (4.13) is not the virtual control signal used in (4.7) to obtain the physical control signal, it is purely an abstraction used to obtain an expression for the sliding motion. For the existence of such a control, $G_a B_{w_a}(t)$ needs to be nonsingular, which will be discussed later in (4.15). It is easy to verify that with the choice of G_a in (4.11),

$$G_a B_{w_a}(t) = B_2 \left(B_a^T B_a\right)^{-1} \left(B_a^T B_a\right) W(t) B_2^T = B_2 W(t) B_2^T$$

Therefore, the expression for the equivalent control in (4.13) can be simplified to

$$v_{eq}(t) = -\left(B_2 W(t) B_2^T\right)^{-1} F x_a(t) \tag{4.14}$$

It is assumed that $W(t)$ belongs to the set

$$\mathscr{W} = \{(w_1, \ldots, w_m) : \lambda_{min}\left(B_2 W B_2^T\right) > \lambda_o\} \tag{4.15}$$

where λ_o is a positive design scalar.

Remark 4.1 Because $l < m$, it is possible that $\lambda_{min}(B_2 W(t) B_2^T) > \lambda_o$ even if up to $m - l$ of the entries $w_i(t) = 0$ in the matrix $W(t)$. This means that up to $m - l$ actuators can be subjected to total failure and yet $\lambda_{min}(B_2 W(t) B_2^T) \neq 0$ i.e. matrix is nonsingular. However if more than $m - l$ entries become zero then $\text{rank}(W(t)) < l$ and $\lambda_{min}(B_2 W(t) B_2^T) = 0$. The set $\mathscr{W}$ constitutes the faults or failures which the scheme described in this chapter can cope with. Notice that the fault set in (4.15) is a strict subset of the one in Chap. 3 and so technically the scheme from Chap. 3 can accommodate a wider class of faults.

The dynamics associated with the sliding surface $\mathscr{S}$ can be obtained by substituting the equivalent control from (4.14) into (4.8) gives

$$\dot{x}_a(t) = A_a x_a(t) - B_{w_a}(t)\left(B_2 W(t) B_2^T\right)^{-1} F x_a(t) + B_r r(t) + D_a \xi(t, x) \tag{4.16}$$

Adding and subtracting the term $B_{v_a} F x_a(t)$ to (4.16), and then rearranging, yields the expression

$$\dot{x}_a(t) = (A_a - B_{v_a} F) x_a(t) + B_m(t) F x_a(t) + B_r r(t) + D_a \xi(.) \tag{4.17}$$

where the matrix

$$B_m(t) := \begin{bmatrix} B_{1_a} B_2^T - B_{1_a} W(t) B_2^T (B_2 W(t) B_2^T)^{-1} \\ 0 \end{bmatrix} \tag{4.18}$$

Note that in Eq. (4.17), since $r(t)$ is a bounded signal, the closed-loop stability of the sliding motion only depends on the first two and the last term which can be expressed in the form

$$\dot{x}_a(t) = \underbrace{(A_a - B_{v_a}F)}_{\tilde{A}} x_a(t) + \tilde{B}_a \overbrace{\Delta_{af}(t) \underbrace{F_a x_a(t)}_{\tilde{y}(t)}}^{\tilde{u}(t)} \tag{4.19}$$

where

$$\tilde{B}_a = \begin{bmatrix} \tilde{B} \; D_a \end{bmatrix} \quad \tilde{B} := \begin{bmatrix} I_n \\ 0 \end{bmatrix} \quad \Delta_{af}(t) = \begin{bmatrix} \Delta_f(t) & 0 \\ 0 & \tilde{\phi}(t,x) \end{bmatrix} \quad F_a = \begin{bmatrix} F \\ I \end{bmatrix} \tag{4.20}$$

and $\tilde{\phi}(t,x) = [\,0 \;\; \phi(t,x)\,]$. The uncertain fault/failure dependent term

$$\Delta_f(t) := B_{1_a} B_2^T - B_{1_a} W(t) B_2^T \left(B_2 W(t) B_2^T\right)^{-1} \tag{4.21}$$

Note that since $W(t)$ is unknown, and $\tilde{\phi}(t,x)$ is assumed to be bounded, the expression $\Delta_{af}(t)$ above is treated as uncertainty. To facilitate the closed-loop stability analysis, assume the following hold:

Assumption 4.7 The augmented uncertainty satisfies

$$\|\Delta_{af}(t)\| < \gamma_1 \quad \text{for all } W(t) \in \mathscr{W} \tag{4.22}$$

where γ_1 is a positive scalar.

Such a bound is guaranteed to exist since $\|W(t)\| < 1$ and $\|B_2 W(t) B_2^T\| < \frac{1}{\lambda_o}$. Define

$$\gamma_2 = ||\tilde{G}(s)||_\infty \tag{4.23}$$

where the transfer function matrix

$$\tilde{G}(s) := F_a(sI - \tilde{A})^{-1}\tilde{B}_a \tag{4.24}$$

Note that by design of F, the matrix $\tilde{A} = A_a - B_a F$ is stable, and so the $\mathscr{H}_\infty$ norm of γ_2 is well-defined and finite.

Proposition 4.1 *For any combination of faults or failures belonging to the set $\mathscr{W}$, the sliding motion in (4.19) will be stable if*

$$\gamma_2 \gamma_1 < 1 \tag{4.25}$$

where γ_1 and γ_2 are defined in (4.22) and (4.23) respectively.

Proof The structure of differential equation (4.19) can be considered as the interconnection of the transfer function $\tilde{G}(s)$ (in the feedforward path) with the uncertain term $\Delta_{af}(t)$ (in the feedback loop) of a closed-loop system. Using Eqs. (4.22)–(4.24), from the small gain theorem, if

$$\|\tilde{G}(s)\|_\infty \|\Delta_{af}(t)\| < 1 \tag{4.26}$$

then the closed-loop stability of (4.19) is ensured. The condition in (4.26) is exactly the stability condition in the proposition statement, and the proof is complete. ■

In a sliding mode framework, the control law should be designed to satisfy the so-called reachability condition, which is a sufficient condition to guarantee that sliding will be enforced and maintained.

Proposition 4.2 *The virtual control based on the integral sliding mode control law*

$$\nu(t) = \nu_l(t) + \nu_n(t) \tag{4.27}$$

where

$$\nu_l(t) := -Fx_a(t) \tag{4.28}$$

$$\nu_n(t) := -\rho(t,x)\frac{\sigma_a(t)}{||\sigma_a(t)||} \quad \text{for } \sigma_a(t) \neq 0 \tag{4.29}$$

will maintain sliding during faults or failures belonging to the set $\mathscr{W}$, if the modulation gain $\rho(t,x)$ in (4.29) is selected as

$$\rho(t,x) > \frac{2\|\nu_l(t)\| + \eta}{\lambda_o} \tag{4.30}$$

where η is a positive design scalar.

Proof Substituting (4.27) into (4.12), and using the fact $G_a B_{w_a}(t) = B_2 W(t) B_2^T$ and $G_a B_{\nu_a} = I$, it follows that

$$\begin{aligned}\dot{\sigma}_a(t) &= \left(B_2 W(t) B_2^T\right)(\nu_l(t) + \nu_n(t)) + Fx_a(t) \\ &= \left(B_2 W(t) B_2^T\right)\nu_n(t) + \left(B_2 W(t) B_2^T\right)\nu_l(t) + Fx_a(t)\end{aligned} \tag{4.31}$$

Consider a positive definite Lyapunov candidate function $V(t) = \frac{1}{2}\sigma_a^T(t)\sigma_a(t)$. Taking the time derivative along the system trajectories gives

$$\begin{aligned}\dot{V}(t) &= \sigma_a^T(t)\left(\left(B_2 W(t) B_2^T\right)\nu_n(t) + \left(B_2 W(t) B_2^T\right)\nu_l(t) + Fx_a(t)\right) \\ &\leq -\lambda_{min}\left(B_2 W(t) B_2^T\right)\rho(\cdot)\|\sigma_a(t)\| + \|\sigma_a(t)\|\|B_2 W(t) B_2^T\|\|\nu_l\| + \|\sigma_a(t)\|\|\nu_l\| \\ &\leq -\lambda_o \rho(\cdot)\|\sigma_a(t)\| + \|\sigma_a(t)\|\|\nu_l\| + \|\sigma_a(t)\|\|\nu_l\|\end{aligned} \tag{4.32}$$

since $\|B_2 W(t) B_2^T\| < 1$. By using a value of $\rho(t,x)$ satisfying (4.30), inequality (4.32) can be written as

$$\dot{V}(t) \leq -\eta \|\sigma_a(t)\| = -\eta \sqrt{2V(t)} \tag{4.33}$$

which is equivalent to the η-reachability condition, and the proof is complete. ■

Finally substituting the integral sliding mode control law given in (4.27)–(4.29) into (4.7) gives the physical control law

$$u(t) = -B_2^T \left(F x_a(t) + \rho(t,x) \frac{\sigma_a(t)}{\|\sigma_a(t)\|} \right) \tag{4.34}$$

Remark 4.2 Compared to the control law in (3.52), it is clear that the control law $u(t)$ in (4.34) has no information about the actuator effectiveness matrix $W(t)$ and will distribute the control effort amongst all the actuators.

4.2.1 Design of Feedback Gain F

The feedback gain F associated with the physical control law $u(t)$ in (4.34) can be designed by using the LMI optimisation method from Chap. 3 (which is also explained in this chapter for completeness) such that the small gain stability condition given in Proposition 4.1 is satisfied. A necessary condition is that the matrix $\tilde{A} = A_a - B_a F$ in (4.24) must be stable. The feedback gain F must be designed to meet the nominal performance requirements (when $W = I_m$) whilst also satisfying the stability condition in Proposition 4.1. For the nominal performance specification, as in Chap. 3 an LQR formulation is adopted, which can be posed as an LMI optimisation:
Minimise trace(X^{-1}) subject to

$$\begin{bmatrix} A_a X + X A_a^T - B_{v_a} Y - Y^T B_{v_a}^T & (\hat{Q}X - \hat{R}Y)^T \\ \hat{Q}X - \hat{R}Y & -I \end{bmatrix} < 0 \tag{4.35}$$

$$X > 0 \tag{4.36}$$

where $Y := FX$ and the symmetric matrix $X \in \mathbb{R}^{(n+l)\times(n+l)}$. In (4.35) the matrices

$$\hat{Q} := \begin{bmatrix} Q^{1/2} \\ 0 \end{bmatrix} \quad \text{and} \quad \hat{R} := \begin{bmatrix} 0 \\ R^{1/2} \end{bmatrix} \tag{4.37}$$

To encapsulate the small gain stability condition (4.25), the Bounded Real Lemma is used:

$$\begin{bmatrix} A_a X + X A_a^T - B_{v_a} Y - Y^T B_{v_a}^T & \tilde{B}_a & Y^T \\ \tilde{B}_a^T & -\gamma^2 I & 0 \\ Y & 0 & -I \end{bmatrix} < 0 \tag{4.38}$$

where $\tilde{B}_a$ is defined in (4.20). In (4.38) the scalar gain γ may be viewed as a tuning parameter.
The overall optimisation process is:

Minimise trace(Z) subject to (4.35), (4.36) and (4.38) and

$$\begin{bmatrix} -Z & I_n \\ I_n & -X \end{bmatrix} < 0 \tag{4.39}$$

As argued in Chap. 3 the slack variable Z satisfies $Z > X^{-1}$ and therefore trace$(Z) \geq$ trace(X^{-1}). Finally the feedback gain F can be recovered as $F = YX^{-1}$.

4.3 Simulations

The RECOVER benchmark model of a large passenger aircraft (as described in Appendix A) is used to test the effectiveness of the FTC scheme. This software represents a "real world" model of the large body B747-100/200 aircraft. The feedback gain F, has been designed based on a linearisation of the model around an operating condition of straight and level flight at 263,000 kg, 92.6 m/s true airspeed, and at an altitude of 600 m based on 25.6 % of maximum thrust and at a 20 deg flap position. In the simulations, an up-and-away flight manoeuvre is considered. For longitudinal control, only the states $x = (\theta, \alpha, V_{tas}, q)$ are considered, where θ is the pitch angle (rad), α is the angle of attack (rad), V_{tas} is the true airspeed (m/s), and q is the pitch rate (rad/s). The available longitudinal control surfaces are $\delta_{long} = (\delta_e, \delta_s, \delta_{epr})$ which represent aggregated elevator deflection (rad), horizontal stabiliser deflection (rad), and aggregated longitudinal EPR (i.e. the four engine pressure ratio (EPRs) are added to produce one control input). The state-space model obtained at the operating condition of straight and level flight is

$$A = \begin{bmatrix} 0 & 0 & 0 & 1 \\ 0 & -0.6284 & -0.0021 & 1.0064 \\ -9.8046 & 1.7171 & -0.0166 & 0 \\ 0 & -0.5831 & 0.0004 & -0.5137 \end{bmatrix}$$

$$B = \begin{bmatrix} 0 & 0 & 0 \\ -0.0352 & -0.0819 & -0.0084 \\ \hline 0 & -0.1756 & 5.7072 \\ -0.6228 & -1.3578 & 0.0600 \end{bmatrix}$$

where the input matrix B is partitioned according to (4.2). For the up-and-away manoeuvre it is required to track the flight path angle (FPA) γ (where $\gamma = \theta - \alpha$) and V_{tas}. The controlled output matrix is

$$C_c = \begin{bmatrix} 1 & -1 & 0 & 0 \\ 0 & 0 & 1 & 0 \end{bmatrix}$$

To design the state feedback gain F, the LMI approach given in Sect. 4.2.1 has been used in which the design matrices

$$Q = \text{diag}(0.95, 0.004, 0.01, 2, 0.1, 5) \quad \text{and} \quad R = \text{diag}(4, 8)$$

With the choice $\gamma = 7$ in (4.38), the feedback gain F obtained is

$$F = \begin{bmatrix} -0.1714 & -0.0296 & -0.7450 & -0.8077 & 0.9828 & -0.2921 \\ -0.3226 & 0.0079 & 2.0833 & 1.2277 & -0.1549 & 1.8162 \end{bmatrix} \tag{4.40}$$

In this example the elevator is the primary control surface for FPA tracking while the horizontal stabiliser is used as a redundant control surface. However for V_{tas} tracking, aggregated EPR is the only available actuator (and has no redundancy). Based on the assumption that the engines are fault-free, using a numerical search, a suitable value of scalar in (4.15) is $\lambda_0 = 0.0826$, and a suitable upper bound in Eq. (4.22) is $\gamma_1 = 0.01$. With the feedback gain F given above,it can be verified that $\gamma_2 = 75.3013$ in (4.23), which fulfils the stability requirement of Proposition 4.1.

4.4 Nonlinear Simulation Results

In the simulations, a series of 3 deg FPA pulses together with a change in V_{tas} of 10 m/s are used to increase the altitude and the speed of the aircraft. In the simulations the discontinuity associated with the nonlinear controller term in (4.29) has been smoothed by the sigmoidal approximation $\frac{\sigma_a(t)}{\|\sigma_a(t)\|+\delta}$ where δ is chosen small (here $\delta = 0.05$). (In so doing, a pseudo-sliding motion takes place in which the system trajectories move in the vicinity of the sliding surface.) To enforce sliding during faults/failures belonging to the set $\mathscr{W}$, the design scalars in (4.30) are chosen as $\eta = 1$ and $\lambda_0 = 0.0826$, which satisfy the requirements of Proposition 4.2.

The scheme described in this chapter is also compared in simulation with the FTC scheme in Chap. 3 where the efficacy of both schemes is compared based on the longitudinal dynamics of the RECOVER model. All the simulations in this chapter are obtained in the presence of wind and gust models and sensor noise. The wind model generates wind velocities ($u_{wind} = -11$, $v_{wind} = -12$ and $w_{wind} = 0$) along the positive axis of the earth reference frame, whereas the Dryden spectra[1] is used

[1] See for example [1].

in the gust model. Both the models are embedded in the RECOVER software. The sensor noise which appears in the measured states (θ, α, V_{tas}, q) is based on Gaussian distributions of zero mean and variances $3e^{-8}$, $1e^{-2}$, $3e^{-6}$, $3e^{-8}$ respectively.

In Figs. 4.2 and 4.3, the nominal fault-free performance, using the approach described in this chapter, is shown. The control signals $u(t)$ are also plotted together with the actual actuator deflections for comparison with online CA scheme described in Chap. 3. The tracking performance of the commands γ and V_{tas} is promising. In Figs. 4.5 and 4.7 a fault scenario is demonstrated whereby the elevator's effectiveness decreases from 100 to 40 % during 250–550 s; after that, the elevator completely fails. It is clear from Figs. 4.4 and 4.6 that good tracking performance (close to nominal) is still achieved with both the FTC schemes. For online CA, it is clear from Fig. 4.5 that the scheme in Chap. 3 stops sending control signals to the elevator after it has failed completely at 550 s due to the availability of fault information (the $W(t)$ matrix) in the controller. The scheme described in this chapter distributes control effort amongst all the actuators (Fig. 4.7) despite fault/failure to the elevator, as fault information is not available to the controller. Figures 4.9 and 4.11 present the case when the elevator jams at some offset position for both the online and direct CA schemes. However due to the availability of the redundant control surface (the horizontal stabiliser), both schemes can cope with this failure and still maintain the sliding motion as seen in Figs. 4.8 and 4.10. No apparent degradation in performance is visible which shows the effectiveness of both the schemes, despite the severe failure condition. Based on the comparison between the direct CA with online CA, it can be seen that despite the

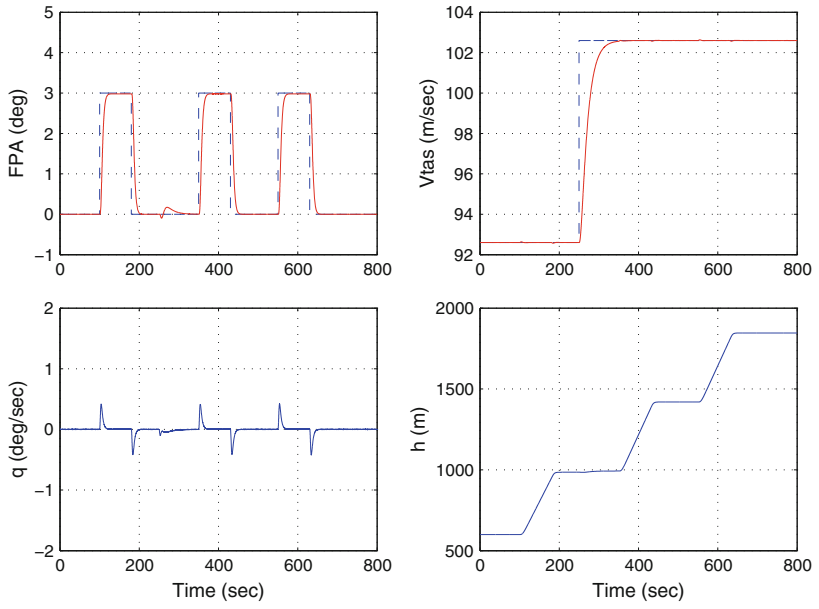

Fig. 4.2 Nominal fault-free performance: system states based on direct control allocation scheme

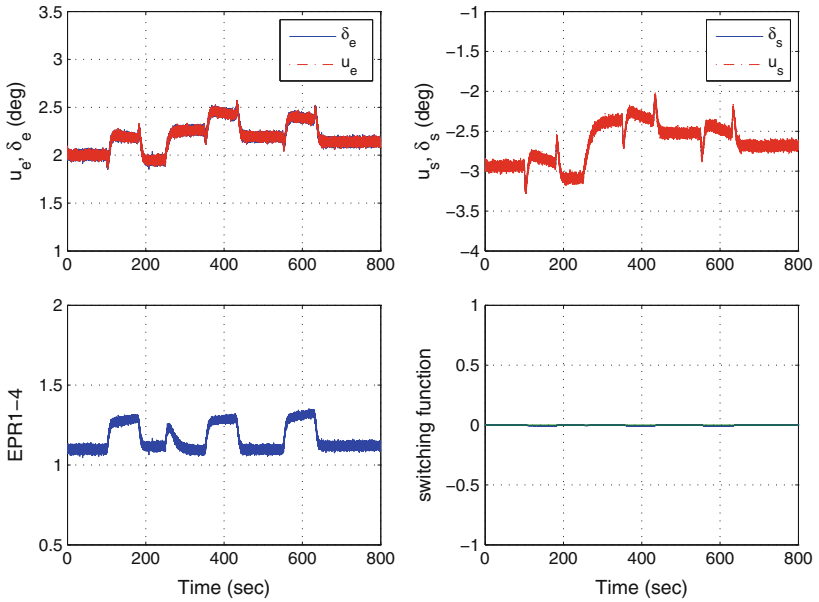

Fig. 4.3 Nominal fault-free performance: actuators deflections based on direct control allocation scheme

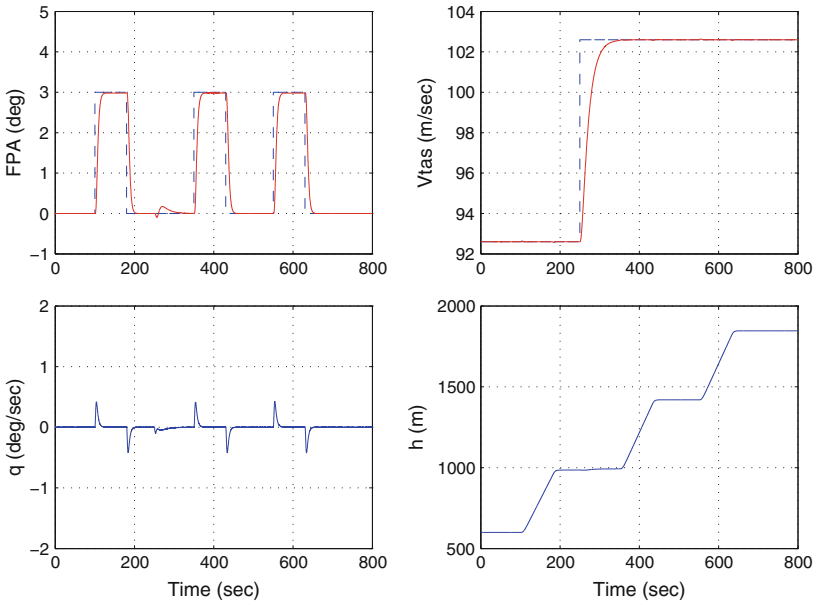

Fig. 4.4 Elevator with partial to complete failure: system states based on online control allocation scheme

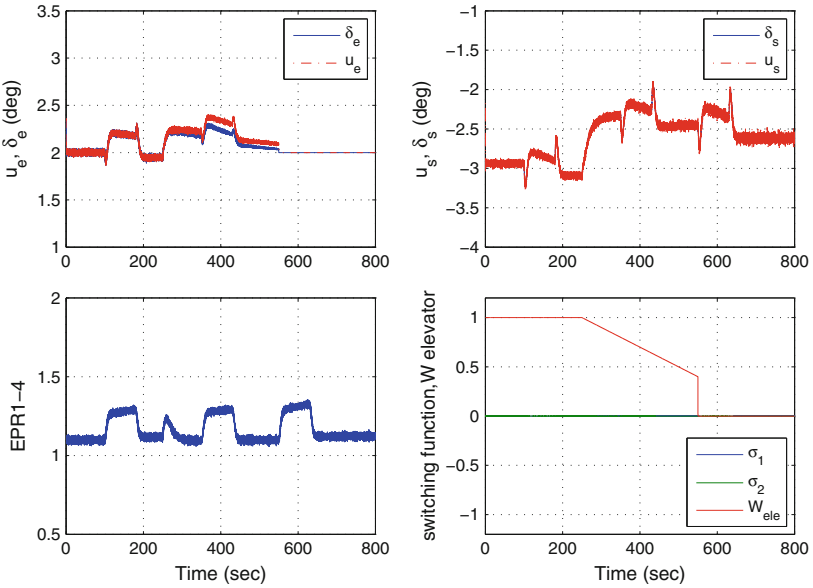

Fig. 4.5 Elevator with partial to complete failure: actuator deflections based on online control allocation scheme

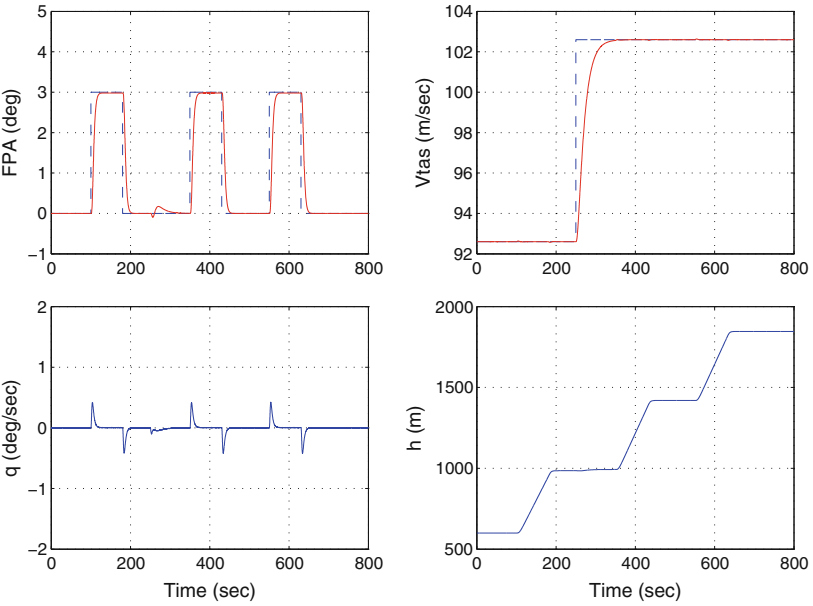

Fig. 4.6 Elevator with partial to complete failure: system states based on direct control allocation scheme

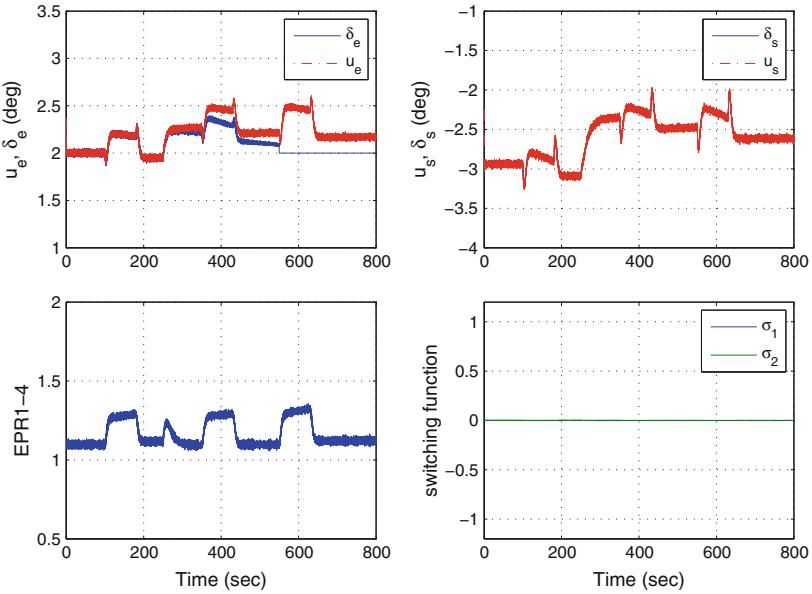

Fig. 4.7 Elevator with partial to complete failure: actuators deflections based on direct control allocation scheme

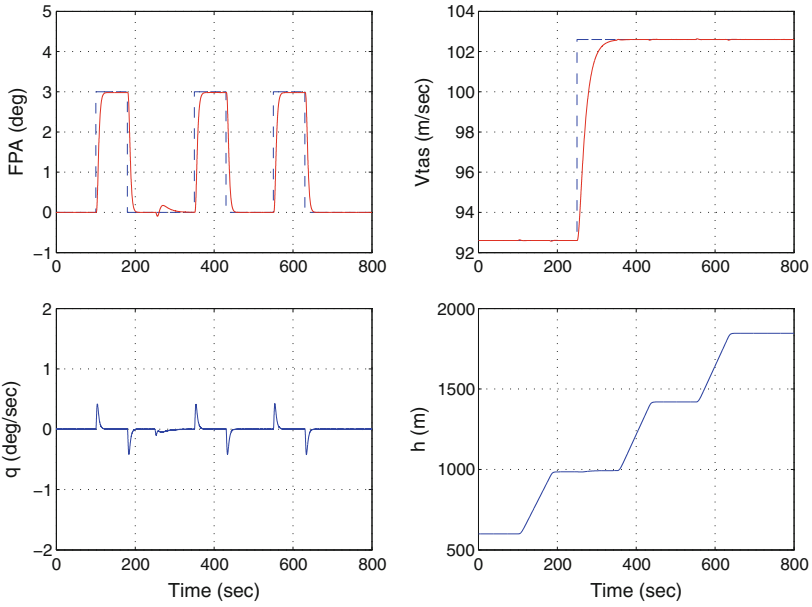

Fig. 4.8 Elevator jam: system states based on online control allocation scheme

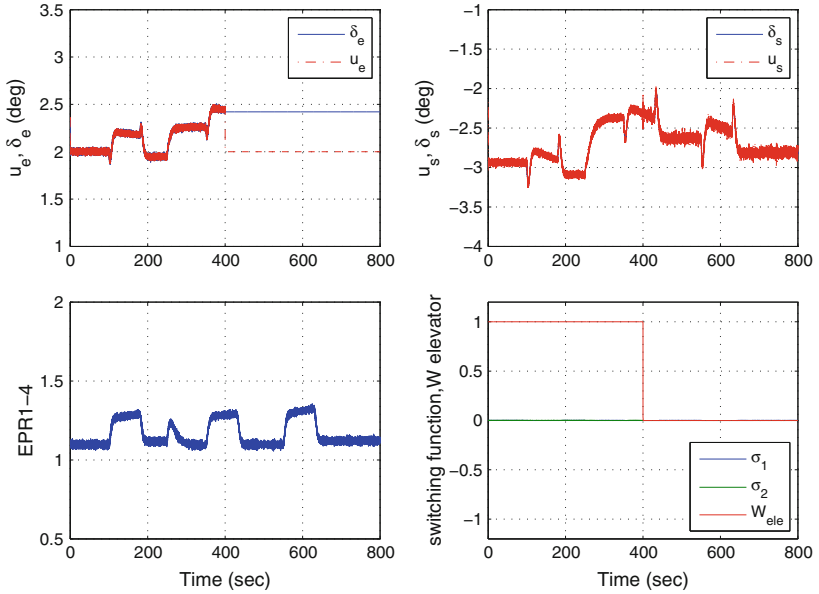

Fig. 4.9 Elevator jam: actuators deflections based on online control allocation scheme

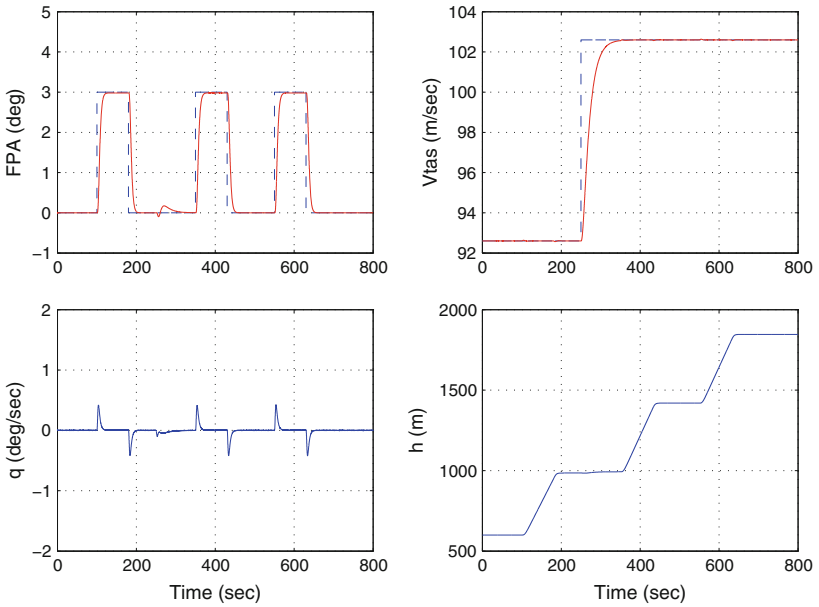

Fig. 4.10 Elevator jam: system states based on direct control allocation scheme

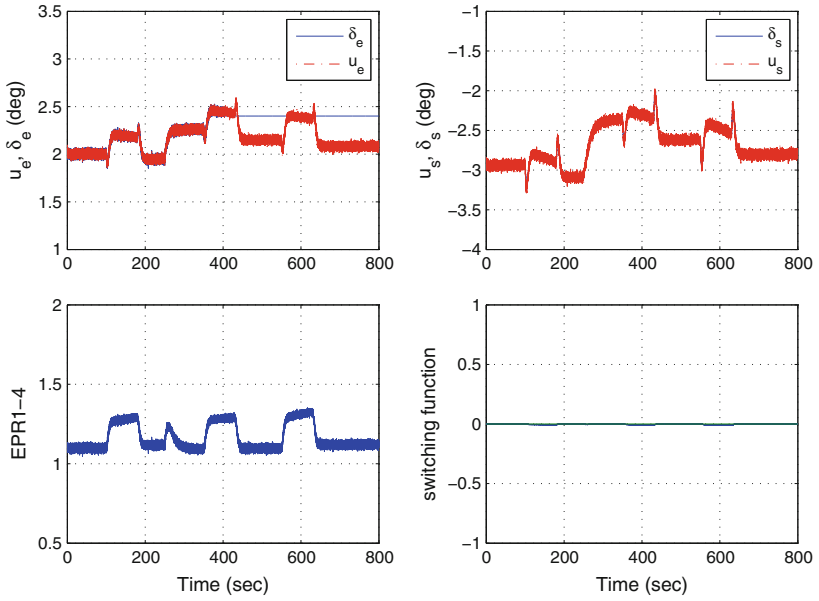

Fig. 4.11 Elevator jam: actuators deflections based on direct control allocation scheme

absence of FDI information (matrix $W(t)$), the results for the direct CA scheme in this chapter are comparable to the online CA scheme in Chap. 3. The only limitation of not knowing the actuator effectiveness level (matrix $W(t)$) as compared to Chap. 3, is that, theoretically, a slightly more limited set of faults/failures given in (4.15) must be assumed.

4.5 Summary

In this chapter, a passive FTC scheme has been described which has the potential to provide fault tolerance against actuator faults/failures without requiring any information from an FDI scheme. The inclusion of direct control allocation allows a single controller to deal with a range of actuator faults/failures without any fault information. The direct control allocation structure maintains an acceptable level of closed-loop performance both nominally and in fault/failure situations by distributing the control effort computed by virtual control law amongst the actuators. A rigorous closed-loop stability analysis has been carried out in the presence of unmatched uncertainty and demonstrates the class of faults/failures which can be dealt with without any performance degradation. A range of actuator fault/failure scenarios are considered in simulation, in the presence of wind, gusts and sensor noise, for validation purposes, on the RECOVER benchmark model. The results obtained show the efficacy

of the scheme. The controller was also compared in simulation with the FTC scheme described in Chap. 3, which does require fault information. Comparable results have been achieved.

4.6 Notes and References

RECOVER is an established FDI/FTC benchmark developed during GARTEUR FM-AG16 [1]. An overview of different approaches employed within the GARTEUR FM-AG16 project are described in [1]. These include indirect adaptive schemes, $\mathscr{H}_\infty$ and μ-synthesis methods, sliding mode schemes, MRAC, predictive subspace methods, MPC and control allocation. Many of the schemes in [1] require FDI information. One exception is the SMC/CA work described in [2]. To deal with actuator faults/failures in over actuated systems, the most commonly employed strategy is to distribute the control effort generated by the virtual controller equally amongst the actuators [3, 4].

References

1. Edwards, C., Lombaerts, T., Smaili, H.: Fault Tolerant Flight Control: A Benchmark Challenge, vol. 399. Springer, Berlin (2010)
2. Alwi, H., Edwards, C., Stroosma, O., Mulder, J.A.: Evaluation of a sliding mode fault-tolerant controller for the EL AL incident. AIAA J. Guid. Control Dyn. **33**(3), 677–694 (2010)
3. Shtessel, Y., Buffington, J., Banda, S.: Tailless aircraft flight control using multiple time scale re-configurable sliding modes. IEEE Trans. Control Syst. Technol. **10**, 288–296 (2002)
4. Wells, S.R., Hess, R.A.: Multi-input/multi-output sliding mode control for a tailless fighter aircraft. J. Guid. Control Dyn. **26**(3), 463–473 (2003)

Chapter 5
An Output Integral Sliding Mode FTC Scheme Using Control Allocation

In this chapter a fault tolerant control scheme is described for systems where only output information is available. The assumption made in the earlier chapters was that the state information is known and available for the controller design. In this chapter, it is assumed only measured outputs are available and knowledge of the actuator faults or failures is not available from an FDI scheme. A full order linear unknown input observer (UIO) is employed to estimate the system states used in the underlying virtual controller. No attempt is made to estimate the actuator faults or failures (using an FDI scheme), instead, the robustness properties of the UIO coupled with the ISM components are relied upon. A fixed control allocation scheme (which does not require actuator effectiveness levels $W(t)$) is used to translate the virtual control signals into physical actuator demands. An LMI procedure is used to synthesise the observer gains and the controller parameters, and a rigorous closed-loop stability analysis is carried out to ensure the stability of the sliding motion in the face of actuator faults and certain failures, provided that redundancy is available in the system. A civil aircraft benchmark model is used to investigate the feasibility of the scheme.

5.1 Problem Formulation

Consider a system with actuator faults or failures, and component faults written as

$$\dot{x}(t) = (A + A^{\delta}(t))x(t) + Bu(t) - BK(t)u(t) \tag{5.1}$$

$$y(t) = Cx(t) \tag{5.2}$$

where $A \in \mathbb{R}^{n\times n}$ is the state matrix, $A^{\delta}(t)$ is parametric uncertainty in the system matrix arising from imprecisely known parameters and possible faults at a component level, $B \in \mathbb{R}^{n\times m}$ is the input distribution matrix and $C \in \mathbb{R}^{p\times n}$ is the

M.T. Hamayun et al., *Fault Tolerant Control Schemes Using Integral Sliding Modes*, Studies in Systems, Decision and Control 61,
DOI 10.1007/978-3-319-32238-4_5

output distribution matrix where $p \geq m$. The diagonal weighting matrix $K(t) = \text{diag}(k_1(t), \ldots, k_m(t))$, where the scalars $k_1(t), \ldots, k_m(t)$, model the effectiveness level of the actuators. If $k_i(t) = 0$, the corresponding ith actuator is fault-free and is working perfectly, whereas if $1 > k_i(t) > 0$, an actuator fault is present. The value $k_i(t) = 1$ indicates the ith actuator has completely failed.

Remark 5.1 The description of the actuator faults or failures in (5.1) looks different from the early chapters, but in structure it is the same because the actuator effectiveness matrix $W(t)$ can be defined as $W(t) := I_m - K(t)$. Note that the matrix $K(t)$ in (5.1) is assumed to be unknown.

Here it is assumed that the outputs to be controlled are given by $y_c(t) = C_c x(t)$ where $C_c \in \mathbb{R}^{l \times n}$, where $l < m$. It follows that there is redundancy in the system in terms of the number of control inputs. This will be exploited to achieve fault tolerance. To resolve the actuator redundancy, (by permuting the states if necessary) it is assumed the matrix B can be partitioned as

$$B = \begin{bmatrix} B_1 \\ B_2 \end{bmatrix} \tag{5.3}$$

where $B_1 \in \mathbb{R}^{(n-l)\times m}$ and $B_2 \in \mathbb{R}^{l \times m}$ is of rank $l < m$. By appropriate scaling of the last l states, without loss of generality, $B_2 B_2^T = I_l$.

Assumption 5.1 Assume that $\|B_1\| \ll \|B_2\| = 1$, so that B_2 reflects that the dominant control action contribution on the system acting in the lower l channels.

Using (5.3), the system in (5.1) can be written as

$$\dot{x}(t) = (A + A^{\delta}(t))x(t) + \begin{bmatrix} B_1 \\ B_2 \end{bmatrix} \underbrace{(I - K(t))}_{W(t)} u(t) \tag{5.4}$$

By definition $W(t)$ is diagonal and its diagonal elements $w_i(t)$ satisfy $0 \leq w_i(t) \leq 1$. The objective of this chapter is to develop a control scheme, based on only output measurements, which can maintain closed-loop stability in the face of a class of actuator faults and failures. The physical control law $u(t)$ is realised by a so-called 'fixed' control allocation scheme of the form

$$u(t) = B_2^T \nu(t) \tag{5.5}$$

where $\nu(t) \in \mathbb{R}^l$ is the 'virtual control' effort produced by the control law, which will be described explicitly in the sequel. In Eq. (5.5) the fact that $B_2 B_2^T = I_l$ is exploited.

Remark 5.2 The control allocation structure in (5.5) is similar to the one employed in Chap. 4. The fixed CA/ISM scheme developed in this chapter will be independent of $W(t)$ and will not require an FDI scheme.

By using (5.5), Eq. (5.4) can be written as

$$\dot{x}(t) = (A + A^{\delta}(t))x(t) + \underbrace{\begin{bmatrix} B_1 W(t) B_2^T \\ B_2 W(t) B_2^T \end{bmatrix}}_{B_w(t)} \nu(t) \tag{5.6}$$

In the nominal case, when there is no fault ($W(t) = I_m$ and $A^{\delta}(t) = 0$), Eq. (5.6) simplifies to

$$\dot{x}(t) = Ax(t) + \underbrace{\begin{bmatrix} B_1 B_2^T \\ I_l \end{bmatrix}}_{B_\nu} \nu(t) \tag{5.7}$$

because $B_2 B_2^T = I_l$ by design.

Assumption 5.2 Here it is assumed that the pair (A, B_ν) is controllable.

5.2 ISM Controller Design

In this section the integral sliding mode strategy will be adopted for synthesising the virtual control signal $\nu(t)$. The virtual control signal $\nu(t)$ will use estimated states $\hat{x}(t)$, obtained from an observer, so that only outputs need to be measured. Consider a switching function of the form

$$\sigma(t) = Gy(t) - Gy(0) + \int_0^t F\hat{x}(\tau)d\tau \tag{5.8}$$

where $G \in \mathbb{R}^{l \times p}$ and $F \in \mathbb{R}^{l \times n}$ are design matrices selected to specify nominal closed-loop performance and $\hat{x}(t)$ represents an estimate of $x(t)$. In order to create the state estimate $\hat{x}(t)$, a full-order unknown input observer (UIO) is used. The term $BK(t)u(t)$ in (5.1) is treated as an unknown input since by assumption $K(t)$ is unknown. Consequently the distribution matrix associated with the unknown input signal to be rejected is chosen as B. Necessary and sufficient conditions for a linear UIO to exist for the system in (5.1) and (5.2), to provide insensitivity with respect to the term $BK(t)u(t)$, are

Assumption 5.3 $\text{rank}(CB) = m$ and the triple (A, B, C) is minimum phase

Consider a full-order observer of the form:

$$\dot{z}(t) = A_0 z(t) + TBu(t) + Ly(t) \tag{5.9}$$

$$\hat{x}(t) = z(t) + Hy(t) \tag{5.10}$$

where $\hat{x}(t)$ is the estimated state, and A_0, T, L and H are design matrices of appropriate dimension chosen in order to decouple the unknown inputs. The ultimate objective

of an UIO is to make the error signal $e(t) = x(t) - \hat{x}(t)$ converge to zero, despite the presence of the unknown input $K(t)u(t)$ so that the estimated states converge to the true states asymptotically. In particular, the matrix $H \in \mathbb{R}^{n\times p}$ must be chosen so that

$$\underbrace{(I - HC)}_{T} B = 0 \tag{5.11}$$

because B is the unknown-input-direction in this case. Assumption 5.3 is sufficient to solve (5.11) and $H := B((CB)^T CB)^{-1}(CB)^T$ is an appropriate choice. After computing H, the matrix

$$A_0 := \underbrace{A - HCA}_{A_h} - L_1 C \tag{5.12}$$

can be defined, where $L_1 \in \mathbb{R}^{n\times p}$ is design freedom which is exploited to make A_0 Hurwitz. Finally

$$L_2 := A_0 H \tag{5.13}$$

and the gain $L := L_1 + L_2$. If $e(t) = x(t) - \hat{x}(t)$, using the plant equation in (5.1) and the UIO equations in (5.9) and (5.10), the error dynamics can be written as

$$\begin{aligned}\dot{e}(t) &= Ax(t) + A^{\delta}(t)x(t) + Bu(t) - BK(t)u(t) - A_0 z(t) - TBu(t) - Ly(t)\\ &\quad -HC(Ax(t) + A^{\delta}(t)x(t) + Bu(t) - BK(t)u(t))\\ &= (I - HC)Ax(t) + (I - HC)A^{\delta}(t)x(t) + (I - HC)Bu(t) - (I - HC)BK(t)u(t)\\ &\quad -A_0 z(t) - TBu(t) - Ly(t)\end{aligned} \tag{5.14}$$

where it can be seen that with the choice of $H := B((CB)^T CB)^{-1}(CB)^T$ and using Eq. (5.11) the error dynamics can be made invariant to the unknown input $BK(t)u(t)$. Furthermore using Eqs. (5.10), (5.13) together with the relationship $L = L_1 + L_2$, the error dynamics in (5.14) can be further simplified to yield

$$\begin{aligned}\dot{e}(t) &= TAx(t) + TA^{\delta}(t)x(t) - A_0(\hat{x}(t) - Hy(t)) - L_1 y(t) - L_2 y(t)\\ &= TAx(t) + TA^{\delta}(t)x(t) - A_0\hat{x}(t) - L_1 Cx(t)\\ &= \underbrace{(TA - L_1 C)}_{A_0} x(t) + TA^{\delta}(t)x(t) - A_0\hat{x}(t)\\ &= A_0 e(t) + TA^{\delta}(t)x(t)\end{aligned} \tag{5.15}$$

Choose

$$G := B_2 \left((CB)^T CB\right)^{-1} (CB)^T \tag{5.16}$$

where the existence of the inverse is guaranteed by Assumption 5.3. As a result of this choice of G, $GCB_w(t) = B_2 W(t) B_2^T$ which is symmetric. This symmetry is important and simplifies much of the subsequent analysis. Also nominally, when there are no faults and $W(t) = I$, from the special properties of the matrix B_2, it follows that

$$GCB_w(t)|_{W=I} = B_2 B_2^T = I$$

This means, nominally, G has the pseudo-inverse properties which, as explained in Chap. 2, are optimal from the point of view of minimising the impact of unmatched uncertainties on the closed-loop dynamics. The derivative of $\sigma(t)$ in Eq. (5.8) is

$$\dot{\sigma}(t) = G\dot{y}(t) + F\hat{x}(t) \tag{5.17}$$

then substituting from Eq. (5.6), and equating $\dot{\sigma}(t) = 0$, yields an expression for the equivalent control of the form

$$v_{eq}(t) = -(GCB_w(t))^{-1}\left(F\hat{x}(t) + GC(A + A^{\delta}(t))x(t)\right) \tag{5.18}$$

under the assumption that $\det(GCB_w(t)) \neq 0$. With the choice of G in (5.16) the matrix $GCB_w(t) = B_2 W(t) B_2^T$, and (5.18) becomes

$$v_{eq}(t) = -\left(B_2 W(t) B_2^T\right)^{-1}\left(F\hat{x}(t) + GC(A + A^{\delta}(t))x(t)\right) \tag{5.19}$$

Substituting (5.19) into (5.6), the sliding mode dynamics are given by

$$\dot{x}(t) = (A + A^{\delta}(t))x(t) - B_m(t)\left(F\hat{x}(t) + GC(A + A^{\delta}(t))x(t)\right) \tag{5.20}$$

where

$$B_m(t) := \begin{bmatrix} B_1 W(t) B_2^T (B_2 W(t) B_2^T)^{-1} \\ I_l \end{bmatrix}$$

Adding and subtracting the term $B_v\left(F\hat{x}(t) + GC(A + A^{\delta}(t))x(t)\right)$ to the right hand side of (5.20) and exploiting the fact that $e(t) := x(t) - \hat{x}(t)$, the sliding mode dynamics in (5.20) can be written as

$$\begin{aligned}
\dot{x}(t) &= (A + A^{\delta}(t))x(t) - B_v\left(F\hat{x}(t) + GC(A + A^{\delta}(t))x(t)\right) \\
&\quad + (B_v - B_m(t))\left(F\hat{x}(t) + GC(A + A^{\delta}(t))x(t)\right) \\
&= (A - B_v F - B_v GCA)x(t) + A^{\delta}(t)x(t) + B_v Fe(t) - B_v GCA^{\delta}(t)x(t) \\
&\quad + \widetilde{B}\Phi(t)\left(Fx(t) - Fe(t) + GC(A + A^{\delta}(t))x(t)\right) \\
&= (A - B_v F - B_v GCA)x(t) + (I - B_v GC)A^{\delta}(t)x(t) + B_v Fe(t) \\
&\quad + \widetilde{B}\Phi(t)(GCA + F)x(t) - \widetilde{B}\Phi(t)Fe(t) + \widetilde{B}\Phi(t)GCA^{\delta}(t)x(t)
\end{aligned} \tag{5.21}$$

where

$$\widetilde{B} := \begin{bmatrix} I_{n-l} \\ 0 \end{bmatrix} \tag{5.22}$$

and

$$\Phi(t) = B_1 B_2^T - \underbrace{B_1 W(t) B_2^T \left(B_2 W(t) B_2^T\right)^{-1}}_{\psi(t)} \tag{5.23}$$

Combining Eqs. (5.15) and (5.21), the closed-loop system dynamics can be written as

$$\begin{aligned}\begin{bmatrix}\dot{e}(t)\\ \dot{x}(t)\end{bmatrix} &= \begin{bmatrix}A_0 & 0\\ B_v F & A - B_v F - B_v GCA\end{bmatrix}\begin{bmatrix}e(t)\\ x(t)\end{bmatrix} + B_a \Delta(t) C_a \begin{bmatrix}e(t)\\ x(t)\end{bmatrix}\\ &= \underbrace{\begin{bmatrix}A_0 & 0\\ B_v F & A_c - B_v F\end{bmatrix}}_{A_a}\underbrace{\begin{bmatrix}e(t)\\ x(t)\end{bmatrix}}_{x_a} + B_a \Delta(t) C_a \begin{bmatrix}e(t)\\ x(t)\end{bmatrix}\end{aligned} \tag{5.24}$$

where

$$A_c := (I - B_v GC)A \tag{5.25}$$

$$B_a := \begin{bmatrix}(I - HC) & 0 & 0\\ (I - B_v GC) & \widetilde{B} & \widetilde{B}\end{bmatrix} \tag{5.26}$$

$$C_a := \begin{bmatrix}0 & I\\ -F & GCA + F\\ 0 & I\end{bmatrix} \tag{5.27}$$

and the uncertainty term $\Delta(t)$ is

$$\Delta(t) := \begin{bmatrix}A^{\delta}(t) & 0 & 0\\ 0 & \Phi(t) & 0\\ 0 & 0 & \Phi(t) GCA^{\delta}(t)\end{bmatrix} \tag{5.28}$$

Define

$$\underbrace{\begin{bmatrix}e(t)\\ \hat{x}(t)\end{bmatrix}}_{\hat{x}_a} = \underbrace{\begin{bmatrix}I & 0\\ -I & I\end{bmatrix}}_{\widetilde{T}}\begin{bmatrix}e(t)\\ x(t)\end{bmatrix} \tag{5.29}$$

then in the new $(e, \hat{x})$ coordinates, Eq. (5.24) can be written as

$$\dot{\hat{x}}_a(t) = \widetilde{A}_a \hat{x}_a(t) + \widetilde{B}_a \Delta(t) \widetilde{C}_a \hat{x}_a(t) \tag{5.30}$$

where

$$\widetilde{A}_a := \widetilde{T}A_a\widetilde{T}^{-1} = \begin{bmatrix} A_0 & 0 \\ A_c - A_0 & A_c - B_vF \end{bmatrix} \tag{5.31}$$

$$\widetilde{B}_a := \widetilde{T}B_a = \begin{bmatrix} (I - HC) & 0 & 0 \\ HC - B_vGC & \widetilde{B} & \widetilde{B} \end{bmatrix} \tag{5.32}$$

$$\widetilde{C}_a := C_a\widetilde{T}^{-1} = \begin{bmatrix} I & I \\ GCA & GCA + F \\ I & I \end{bmatrix} \tag{5.33}$$

Now in order to demonstrate that the term $\Phi(t)$ in (5.23) is bounded, note that $\Phi(t) = B_1B_2^T - \psi(t)$ and $\psi(t) = B_1B_2^\dagger(t)$ where $B_2^\dagger(t)$ is a right pseudo-inverse of B_2. Then, by using arguments similar to those as given in Chap. 3, there exists a scalar γ_0 such that

$$\|B_2^\dagger(t)\| := \|W(t)B_2^T\left(B_2W(t)B_2^T\right)^{-1}\| < \gamma_0 \tag{5.34}$$

for all combinations of $(w_1(t), \ldots, w_m(t))$ such that $\det(B_2W(t)B_2^T) \neq 0$. Therefore $\|\psi(t)\| \leq \gamma_1\gamma_0$ and hence

$$\|\Phi(t)\| \leq \gamma_1(1 + \gamma_0) \tag{5.35}$$

where $\gamma_1 = \|B_1\|$. As in earlier chapters γ_1 is assumed to be small.

Assumption 5.4 Assume that the uncertainty $A^\delta(t)$ in the system matrix A is bounded.

Therefore in (5.28) since $\Phi(t)$ is bounded, it follows

$$\|\Delta(t)\| < \gamma_a \tag{5.36}$$

for some positive scalar γ_a.

5.2.1 Closed-Loop Stability Analysis

In the nominal case, (i.e. when $W(t) = I$, $A^\delta(t) = 0$ and $\Delta(t) = 0$), Eq. (5.30) simplifies to $\dot{\hat{x}}_a(t) = \widetilde{A}_a\hat{x}_a(t)$. From (5.31) it is clear the eigenvalues of $\widetilde{A}_a$ are given by the union of the eigenvalues of A_0 and $A_c - B_vF$. Both these matrices can be made Hurwitz by choice of the design freedom matrices L_1 from (5.12) and F respectively. Consequently, by design, $\widetilde{A}_a$ can be made Hurwitz, and hence nominally the closed-loop system is stable. However for the fault/failure cases, stability needs to be proven. Define

$$\gamma_2 = \|\widetilde{G}_a(s)\|_\infty \tag{5.37}$$

where

$$\widetilde{G}_a(s) := \widetilde{C}_a(sI - \widetilde{A}_a)^{-1}\widetilde{B}_a \tag{5.38}$$

Proposition 5.1 *In fault or failure conditions, for any* $(w_1(t), \ldots, w_m(t))$ *such that* $\det(B_2 W(t) B_2^T) \neq 0$*, the closed-loop system in (5.30) is stable if:*

$$\gamma_2 \gamma_a < 1 \tag{5.39}$$

Proof In order to establish closed-loop stability, the system defined in (5.30) can be written as

$$\dot{\hat{x}}_a(t) = \widetilde{A}_a \hat{x}_a(t) + \widetilde{B}_a \widetilde{u}_a(t) \tag{5.40}$$

$$\widetilde{y}_a(t) = \widetilde{C}_a \hat{x}_a(t) \tag{5.41}$$

where $\widetilde{u}_a(t) := \Delta(t)\widetilde{y}_a(t)$. In this form, Eq. (5.30) is the feedback interconnection of the known linear system $\widetilde{G}_a(s)$, and the bounded uncertain gain $\Delta(t)$. According to the small gain theorem (Appendix B.1.2), the feedback interconnection of $\widetilde{G}_a(s)$ and $\Delta(t)$ will be stable if (5.39) is satisfied. ■

Remark 5.3 By hypothesis, $\gamma_1 = \|B_1\|$ is assumed to be small. Basically the size of $\|B_1\|$ has a significant impact on the norm of the nonlinearity in the small gain feedback loop, and so if $\|B_1\|$ is small, the gain of the nonlinearity is small, and there is a less stringent requirement on the magnitude of the $\mathscr{H}_\infty$ norm of the linear part. Furthermore if $A^\delta(t) = 0$, then $\|\Delta(t)\| \to 0$ as $\|B_1\| \to 0$ and Proposition 5.1 is trivially satisfied.

5.2.2 LMI Synthesis

In this section the observer gain L_1 and the controller gain F are synthesised, so that the stability condition in (5.39) is satisfied. For the triple $(\widetilde{A}_a, \widetilde{B}_a, \widetilde{C}_a)$, from the Bounded Real Lemma, $\|\widetilde{G}_a(s)\|_\infty < \gamma_2$ if and only if there exists a s.p.d. matrix $X \in \mathbb{R}^{2n \times 2n}$ such that

$$\begin{bmatrix} \widetilde{A}_a X + X\widetilde{A}_a^T & \widetilde{B}_a & X\widetilde{C}_a^T \\ \widetilde{B}_a^T & -\gamma_2^2 I & 0 \\ \widetilde{C}_a X & 0 & -I \end{bmatrix} < 0 \tag{5.42}$$

Here it is assumed that $X = \mathrm{diag}(X_1, X_2)$ where the two sub-blocks $X_1, X_2 \in \mathbb{R}^{n \times n}$ are s.p.d. With this assumption

$$\widetilde{C}_a X = \begin{bmatrix} X_1 & X_2 \\ GCAX_1 & GCAX_2 + Y \\ X_1 & X_2 \end{bmatrix} \tag{5.43}$$

where $Y := FX_2$. The top left sub-block in (5.42) is

$$\widetilde{A}_a X + X\widetilde{A}_a^T = \begin{bmatrix} A_0X_1 + X_1A_0^T & X_1A_c^T - X_1A_0^T \\ A_cX_1 - A_0X_1 & A_cX_2 + X_2A_c^T - B_vY - Y^TB_v^T \end{bmatrix} \tag{5.44}$$

Also write $A_0 = A_h - L_1C$ where A_h is defined in (5.12). To create a convex representation, define the observer gain as

$$L_1 := \beta BE \tag{5.45}$$

where β is a positive scalar and $E \in \mathbb{R}^{m\times p}$ is chosen so that (A_h, B, EC) is minimum phase and $\det(ECB) \neq 0$. This is possible if (A, B, C) is minimum phase [1] (Assumption 5.3). Then it can be argued[1] that it is possible to find an s.p.d. matrix P which has a structure $P = N^T\mathrm{diag}(P_1, P_2)N$ such that $PB = (EC)^T$, where $N \in \mathbb{R}^{n\times n}$ is invertible (and depends on E) and the s.p.d. matrices $P_1 \in \mathbb{R}^{(n-m)\times(n-m)}$, $P_2 \in \mathbb{R}^{m\times m}$. Define $X_{11} = P_1^{-1}$ and $X_{12} = P_2^{-1}$. It follows that $L_1C = \beta BEC = \beta BB^TP$ and so if

$$X_1 := P^{-1} = N^{-1}\mathrm{diag}(X_{11}, X_{12})(N^{-1})^T > 0 \tag{5.46}$$

then $L_1CX_1 = \beta BB^T$ and $A_0X_1 = A_hX_1 - \beta BB^T$. It follows that the matrix inequality in (5.42) is affine with respect to the decision variables $X_{11}, X_{12}, X_2, \beta, Y$ and so the synthesis problem is convex. For the nominal system in (5.7), (i.e. when $W(t) = I$ and $A^\delta(t) = 0$), the matrix F must stabilise $(A - B_vF)$. Since (A, B_v) is assumed to be controllable (Assumption 5.2), an LQR formulation will be adopted where F is selected to minimise

$$J = \int_0^\infty (x^TQx + v^TRv)dt$$

where Q and R are symmetric positive definite design matrices. This problem can be posed as an LMI optimisation:
Minimise $\mathrm{trace}(X_2^{-1})$ subject to

$$\begin{bmatrix} AX_2 + X_2A^T - B_vY - Y^TB_v^T & (Q_1X_2 - R_1Y)^T \\ Q_1X_2 - R_1Y & -I \end{bmatrix} < 0 \tag{5.47}$$

where

$$Q_1 = \begin{bmatrix} Q^{\frac{1}{2}} \\ 0_{l\times n} \end{bmatrix} \quad \text{and} \quad R_1 = \begin{bmatrix} 0_{n\times l} \\ R^{\frac{1}{2}} \end{bmatrix} \tag{5.48}$$

For a given $\mathscr{L}_2$-gain γ_2, the overall optimisation problem, posed in convex form becomes:

[1] For details see [1].

Minimise trace(Z) with respect to $X_{11}, X_{12}, X_2, \beta, Y$ subject to (5.42), (5.47), (5.46) and (5.49) and

$$\begin{bmatrix} -Z & I_n \\ I_n & -X_2 \end{bmatrix} < 0 \tag{5.49}$$

The s.p.d. matrix Z is a slack variable which from (5.49) satisfies $Z > X_2^{-1}$ and therefore trace$(Z) \geq$ trace(X_2^{-1}). Finally the controller and observer gains can be recovered as $F = YX_2^{-1}$ and $L_1 = \beta BE$.

5.2.3 ISM Control Laws

A control law will be defined to ensure sliding is maintained from $t = 0$. Define the virtual control law in (5.7) as

$$\nu(t) = \nu_l(t) + \nu_n(t) \tag{5.50}$$

where the linear part, responsible for the nominal performance of the system is

$$\nu_l(t) = -F\hat{x}(t) - GCA\hat{x}(t) \tag{5.51}$$

and the nonlinear part is defined as

$$\nu_n(t) = -\rho(t)\frac{\sigma(t)}{\|\sigma(t)\|} \quad \text{for } \sigma(t) \neq 0 \tag{5.52}$$

where $\rho(t)$ is the modulation gain and is defined in Proposition 5.2.

Also define a time varying scalar $\varepsilon(t)$ as the solution to

$$\dot{\varepsilon}(t) = -m_0\varepsilon(t) + m_1\|\hat{x}(t)\| \tag{5.53}$$

where m_0 and m_1 are positive scalars to be defined in the sequel. Let $V_0 = e^T P_0 e$ where P_0 is the s.p.d. matrix obtained from solving

$$P_0A_0 + {A_0}^T P_0 = -I \tag{5.54}$$

Further suppose that $\|A^\delta(t)\|$ is sufficiently small so that P_0 also satisfies

$$2\|P_0\|\|(I - HC)A^\delta(t)\| < 1 - \mu_o \tag{5.55}$$

where $\mu_o > 0$. Then the following Proposition can be proved:

Proposition 5.2 *Define the modulation gain from (5.52) as*

$$\rho(t) = \frac{\|GCA^{\delta}(t)\|\|\hat{x}(t)\| + \|\nu_l\| + \varepsilon(t)(\|GCA\| + \|GCA^{\delta}(t)\|)/p_0 + \eta}{(1-\lambda_0)} \tag{5.56}$$

where $p_0 = \sqrt{\lambda_{min}(P_0)}$ *and* η *is a positive design scalar. Also assume that the fault* $(k_1(t), \ldots, k_m(t))$ *belongs to*

$$\mathscr{D} = \left\{(k_1, \ldots, k_m) : \lambda_{max}\left(B_2 K B_2^T\right) < \lambda_0 < 1\right\}$$

Also assume that by choice of $\hat{x}(0)$ *and* $\varepsilon(0)$ *the state estimation error at* $t = 0$*, written* $e(0)$*, satisfies* $\sqrt{e(0)^T P_0 e(0)} < \varepsilon(0)$*. Then the integral sliding mode control law defined in (5.51) and (5.52), guarantees that the system trajectories remain on the sliding surface.*

Proof Equation (5.15) can be written as

$$\dot{e}(t) = (A_0 + (I - HC)A^{\delta}(t))e(t) + (I - HC)A^{\delta}(t)\hat{x}(t) \tag{5.57}$$

then the derivative of the positive definite function $V_0 = e^T P_0 e$ is given by

$$\begin{aligned}\dot{V}_0 &= e\left(P_0 A_0 + A_0^T P_0\right)e^T + 2e^T P_0 (I - HC)A^{\delta}(t)e + 2e^T P_0 (I - HC)A^{\delta}(t)\hat{x} \\ &\leq -\|e\|^2 + 2\|e\|^2\|P_0\|\|(I - HC)A^{\delta}(t)\| + 2\|e\|\|P_0\|\|(I - HC)A^{\delta}(t)\|\|\hat{x}\|\end{aligned}$$

and therefore since by assumption $2\|P_0\|\|(I - HC)A^{\delta}(t)\| < 1 - \mu_o$ where $\mu_o > 0$ it follows

$$\dot{V}_0 \leq -\mu_0\|e\|^2 + (1-\mu_0)\|\hat{x}\|\|e\| \leq -\frac{\mu_0}{\lambda_{max}(P_0)}V_0 + \frac{1-\mu_0}{\sqrt{\lambda_{max}(P_0)}}\|\hat{x}\|\sqrt{V_0} \tag{5.58}$$

Define $\widetilde{V} = \sqrt{V_0}$, then (5.58) implies

$$\dot{\widetilde{V}}(t) \leq -\frac{\mu_0}{2\lambda_{max}(P_0)}\widetilde{V}(t) + \frac{1-\mu_0}{2\sqrt{\lambda_{max}(P_0)}}\|\hat{x}(t)\| \tag{5.59}$$

which for notational convenience can also be written as

$$\dot{\widetilde{V}}(t) \leq -m_0\widetilde{V}(t) + m_1\|\hat{x}(t)\| \tag{5.60}$$

where the positive scalars m_0, and m_1 are appropriately defined. Comparing (5.60) and (5.53) if $\varepsilon(0) > \tilde{V}(0)$, then it can be shown that $\varepsilon(t) > \tilde{V}(t)$ for all $t \geq 0$ and consequently

$$\varepsilon(t) \geq \sqrt{\lambda_{min}(P_0)}\|e(t)\| \quad \text{for} \quad t \geq 0 \tag{5.61}$$

Now it will be shown that the control law defined in (5.50) satisfies the standard reachability condition. Using the relationship $K(t) = I - W(t)$, Eq. (5.17) can be written as

$$\begin{aligned}\dot{\sigma}(t) &= GC(A + A^{\delta}(t))x(t) + \left(B_2 W(t) B_2^T\right)\nu(t) + F\hat{x}(t) \\ &= GC(A + A^{\delta}(t))x(t) + \nu(t) - \left(I - B_2 W(t) B_2^T\right)\nu(t) + F\hat{x}(t) \\ &= GC(A + A^{\delta}(t))x(t) + \nu(t) - \left(B_2(I - W(t))B_2^T\right)\nu(t) + F\hat{x}(t) \\ &= GC(A + A^{\delta}(t))x(t) + \nu(t) - B_2 K(t) B_2^T \nu(t) + F\hat{x}(t) \end{aligned} \tag{5.62}$$

Substituting the control law (5.50)–(5.52), into Eq. (5.62) and exploiting the fact that $e(t) = x(t) - \hat{x}(t)$ yields

$$\dot{\sigma}(t) = GCA^{\delta}(t)\hat{x}(t) + GCA^{\delta}(t)e(t) + GCAe(t) - \left(B_2 K(t) B_2^T\right)(\nu_l + \nu_n) + \nu_n \tag{5.63}$$

Now consider the derivative of the candidate Lyapunov function $V(t) = \frac{1}{2}\sigma^T(t)\sigma(t)$. From (5.63) the time derivative

$$\begin{aligned}\dot{V}(t) \leq & \|\sigma(t)\|\Big(\|GCA^{\delta}(t)\|\|\hat{x}(t)\| + (\|GCA^{\delta}(t)\| + \|GCA\|)\|e(t)\| \\ & + \|B_2 K(t) B_2^T\|\|\nu_l(t)\| - \rho(\cdot)\left(1 - \|B_2 K(t) B_2^T\|\right)\Big) \\ \leq & \|\sigma(t)\|\Big(\|GCA^{\delta}(t)\|\|\hat{x}(t)\| + (\|GCA^{\delta}(t)\| + \|GCA\|)\|e(t)\| \\ & + \|B_2 K(t) B_2^T\|\|\nu_l\| - \rho(\cdot)(1 - \lambda_0)\Big) \end{aligned} \tag{5.64}$$

for a fault set $(k_1(t), \ldots k_m(t)) \in \mathscr{D}$. Then from the definition of $\rho(t)$ in (5.56) and using the fact that $\varepsilon(t)$ satisfies $\varepsilon(t) \geq \sqrt{\lambda_{min}(P_0)}\|e(t)\|$ for all t, inequality (5.64) can be written as

$$\dot{V}(t) \leq -\eta\|\sigma(t)\| = -\eta\sqrt{2V(t)} \tag{5.65}$$

which is a standard reachability condition and sufficient to guarantee that a sliding motion is maintained for all subsequent time. ■

Finally the physical control law $u(t)$ is obtained by substituting (5.50)–(5.52) into (5.5) to obtain

$$u(t) = B_2^T\left(-F\hat{x}(t) - GCA\hat{x}(t) - \rho(t)\frac{\sigma(t)}{\|\sigma(t)\|}\right) \quad \text{for } \sigma(t) \neq 0 \tag{5.66}$$

5.3 Simulations

The civil aircraft benchmark model discussed in Appendix A.1 will be used to demonstrate the effectiveness and fault tolerant nature of the scheme. The simulation scenario which is considered in this section is that the aircraft undergoes an actuator

fault or failure during a climb from straight and level flight. This scenario can be realised by tracking a suitable flight path angle (FPA) while keeping the speed at a fixed level. To design the linear component of the controller in (5.51), the flight operating condition considered here is the same as in Chap. 3. The linearised state-space model obtained at straight and level flight is

$$A_p = \begin{bmatrix} -0.5137 & 0.0004 & -0.5831 & 0 \\ 0 & -0.0166 & 1.7171 & -9.8046 \\ 1.0064 & -0.0021 & -0.6284 & 0 \\ 1 & 0 & 0 & 0 \end{bmatrix}$$

$$B_p = \begin{bmatrix} -0.6228 & -1.3578 & 0.0599 \\ 0 & -0.1756 & 5.7071 \\ -0.0352 & -0.0819 & -0.0085 \\ 0 & 0 & 0 \end{bmatrix}$$

The system states are $x(t) = (q, V_{tas}, \alpha, \theta)$ where q is the pitch rate (rad/s), V_{tas} is the true airspeed (m/s), α is the angle of attack (rad) and θ is the pitch angle (rad). In the simulations, only measured system outputs

$$y = \underbrace{\begin{bmatrix} 1 & 0 & 0 & 0 \\ 0 & 1 & 0 & 0 \\ 0 & 0 & 0 & 1 \end{bmatrix}}_{C_p} \begin{bmatrix} q \\ V_{tas} \\ \alpha \\ \theta \end{bmatrix}$$

are available for use in the control law. The control surfaces are $\delta_{long} = (\delta_e, \delta_s, \delta_{epr})$ which represent elevator deflection (rad), horizontal stabiliser deflection (rad) and aggregated longitudinal EPR (i.e. the four individual engine pressure ratios (EPRs) aggregated to produce one control input). In the simulations a series of 3 deg flight path angle (FPA) commands are given to increase the altitude of the aircraft, while the true airspeed V_{tas} is held constant by using a separate inner-loop Proportional Integral (PI) controller which creates an auto-throttle manipulating EPR. Throughout the simulations *it is assumed that the engines are fault-free*. By splitting the input distribution matrix into matrices which are associated with (δ_e, δ_s) and δ_{epr}, the linear model can be written as

$$\dot{x}_p(t) = A_p x(t) + B_s u_1(t) + B_e \delta_{epr}(t) \tag{5.67}$$

$$y(t) = C_p x(t) \tag{5.68}$$

where $u_1(t) = (\delta_e, \delta_s)$ and matrices $B_s \in \mathbb{R}^{4\times 2}$ and $B_e \in \mathbb{R}^{4\times 1}$. Define a new state associated with the PI controller for V_{tas} as

$$\dot{x}_r(t) = r_{V_{tas}}(t) - C_1 x_p(t) \tag{5.69}$$

where $r_{V_{tas}}(t)$ is the reference signal for V_{tas} tracking and $C_1 = \begin{bmatrix} 0 & 1 & 0 & 0 \end{bmatrix}$. The inner-loop PI control is given by

$$\delta_{epr} = K_{pi_p}(r_{V_{tas}}(t) - C_1 x(t)) + K_{pi_i} x_r(t)$$

where the PI gains are chosen as $K_{pi_p} = 0.6$, and $K_{pi_i} = 0.9$. Now augmenting the plant in (5.67) with $x_r(t)$ yields

$$\begin{bmatrix} \dot{x}_r(t) \\ \dot{x}_p(t) \end{bmatrix} = \underbrace{\begin{bmatrix} 0 & -C_1 \\ B_e K_{pi_i} & (A_p - B_e K_{pi_p} C_1) \end{bmatrix}}_{A} \underbrace{\begin{bmatrix} x_r(t) \\ x_p(t) \end{bmatrix}}_{x(t)} + \underbrace{\begin{bmatrix} 0 \\ B_s \end{bmatrix}}_{B} u_1(t) + \underbrace{\begin{bmatrix} I \\ B_e K_{pi_p} \end{bmatrix}}_{B_r} r_{V_{tas}}(t) \tag{5.70}$$

It is assumed that $x_r(t)$ is available for the controller design, and $y = Cx(t)$ where $C = \text{diag}(1, C_p)$. In order to introduce steady state tracking for the controlled output $y_c(t)$, a feedforward term $L_r r_{FPA}(t)$ is introduced where

$$L_r := (C_c(A - B_v F - B_v GCA)^{-1} B_v)^{-1} \tag{5.71}$$

and the exogenous constant signal r_{FPA} is the reference to be tracked by the FPA. Since $(A - B_v F - B_v GCA)$ is Hurwitz, $\det(A - B_v F - B_v GCA) \neq 0$ and consequently the inverse in (5.71) is well-defined. In the absence of faults and uncertainty it is easy to see the linear control law

$$u(t) = -F\hat{x}(t) + L_r r_{FPA} - GCA\hat{x}(t)$$

ensures that at steady state $y_c(t) = r_{FPA}(t)$. To accommodate this tracking requirement, the control law in (5.66) must be changed to

$$u(t) = B_2^T \left(-F\hat{x}(t) + L_r r_{FPA}(t) - GCA\hat{x}(t) - \rho(t) \frac{\sigma(t)}{\|\sigma(t)\|} \right) \quad \text{for } \sigma(t) \neq 0 \tag{5.72}$$

and

$$\sigma(t) = Gy(t) - Gy(0) + \int_0^t (F\hat{x}(\tau) - L_r r_{FPA}(\tau)) d\tau \tag{5.73}$$

A fault tolerant control law will now be designed based on the system in (5.70) governed by the triple (A, B, C) using only the elevator and stabiliser as inputs. A further scaling of B is required to ensure that $B_2 B_2^T = I_l$ (where in this example $l = 1$). It can be verified that $\text{rank}(CB) = \text{rank}(B) = 2$, and therefore Assumption 5.3 holds. In this aircraft system (A, B, C) has one stable invariant zero. Since the objective is to track a FPA command, the controlled output is $y_c(t) = C_c x(t)$, where $C_c = \begin{bmatrix} 0 & 0 & 0 & -1 & 1 \end{bmatrix}$. The gain G in Eq. (5.16) is

$$G = \begin{bmatrix} 0 & 0.6694 & 0 & 0 \end{bmatrix}$$

In addition to actuator faults or failures, to introduce potential faults which cause changes to the aerodynamics of the aircraft, a 10 % change in the aerodynamic coefficients (due to airframe damage) is considered in the simulation, specifically:

$$A^{\delta} = \begin{bmatrix} 0 & 0 & 0 & 0 & 0 \\ 0 & 0.0514 & 0 & 0.0583 & 0 \\ 0 & 0 & 0.0017 & 0 & 0 \\ 0 & 0.1006 & 0 & 0.0628 & 0 \\ 0 & 0 & 0 & 0 & 0 \end{bmatrix}$$

Choosing

$$E = \begin{bmatrix} -12.4139 & -1.6056 & 12.4139 & -1.6056 \\ 5.6942 & 0 & -5.6942 & 0 \end{bmatrix}$$

gives $ECB = I$, and makes (A_h, B, EC) minimum phase with stable zeros at

$$(-1.0000, -0.6451, -1.0000)$$

The corresponding value of the observer gain L_1 is

$$BE = \begin{bmatrix} 0 & 0 & 0 & 0 \\ 0 & 1 & 0 & 1 \\ -1 & 0 & 1 & 0 \\ -0.0290 & 0.0566 & 0.0290 & 0.0566 \\ 0 & 0 & 0 & 0 \end{bmatrix}$$

and $A_0 = (A_h - \beta BEC)$ is then stable for any $\beta > 0$. Choosing

$$Q = \text{diag}(0.02, 0.5, 0.2, 0.1, 10)$$

and $R = 1$ in (5.47) the feedback gain matrix F, obtained by solving the LMIs (5.42), (5.47), (5.49) is given by

$$F = \begin{bmatrix} -0.8142 & 9.9401 & -2.2095 & -0.3356 & 8.8802 \end{bmatrix}$$

In the simulations, it is assumed that the engines are fault-free. Based on this assumption, using a numerical search, it can be verified using (5.28) that the value of γ_a in (5.36) is $\gamma_a = 0.1597$. To satisfy the closed-loop stability condition in (5.39), the value of γ_2 must satisfy $\gamma_2 < \frac{1}{0.1597} = 6.2621$. This has been satisfied through the designed parameters L_1 and F.

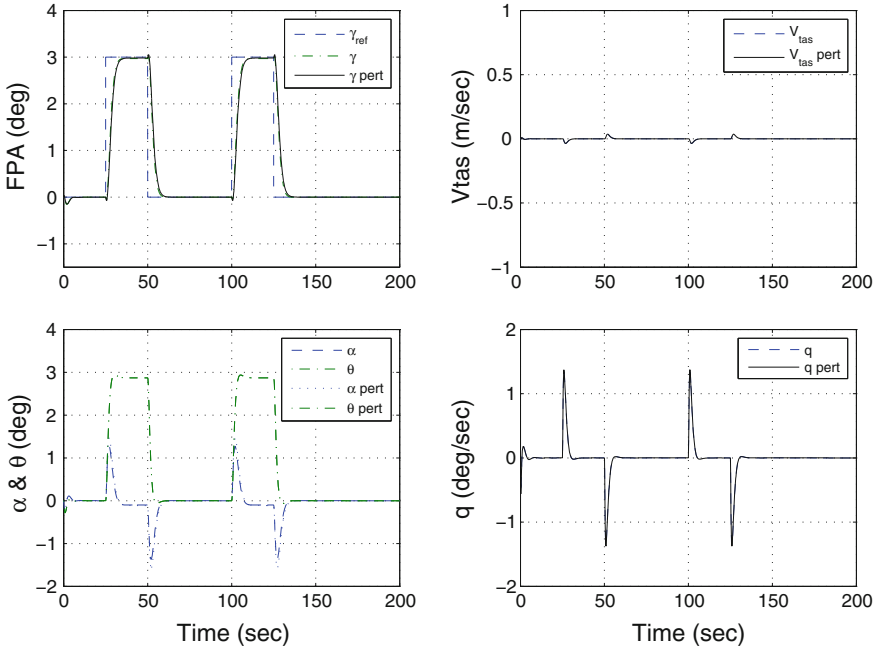

Fig. 5.1 No fault versus perturbation in *A* matrix states

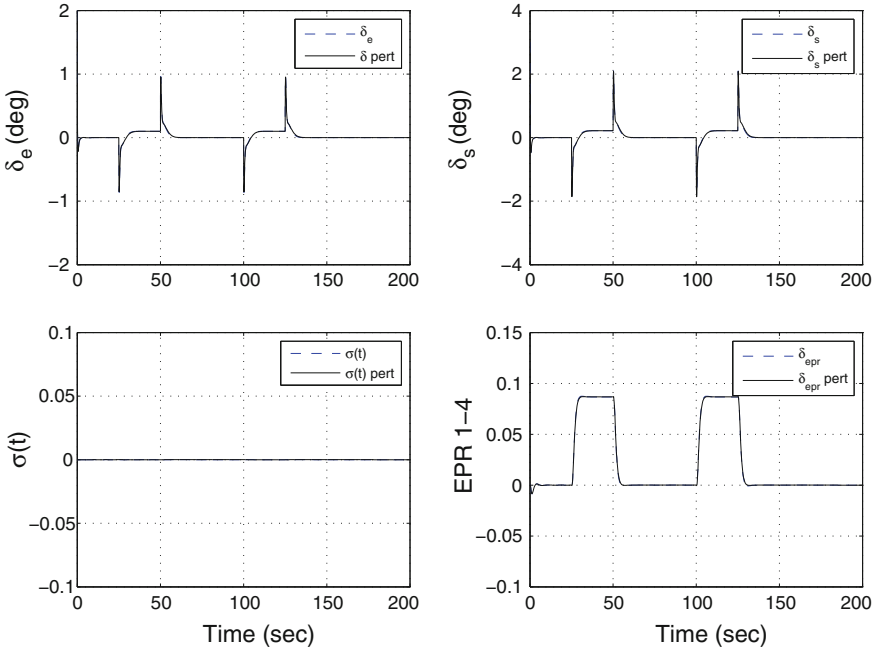

Fig. 5.2 No fault versus perturbation in *A* matrix surface deflections

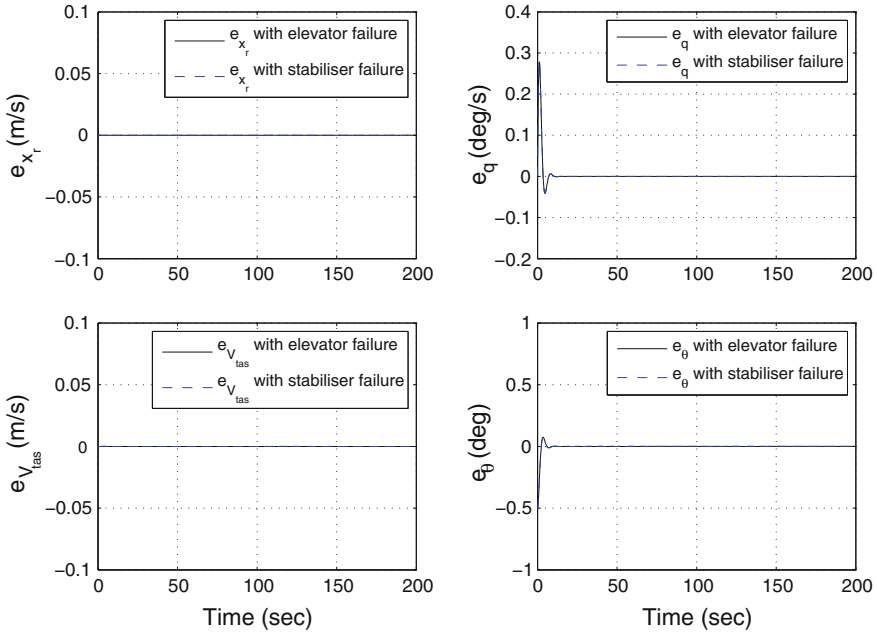

Fig. 5.3 State estimation error signals (elevator jam and stabiliser runaway)

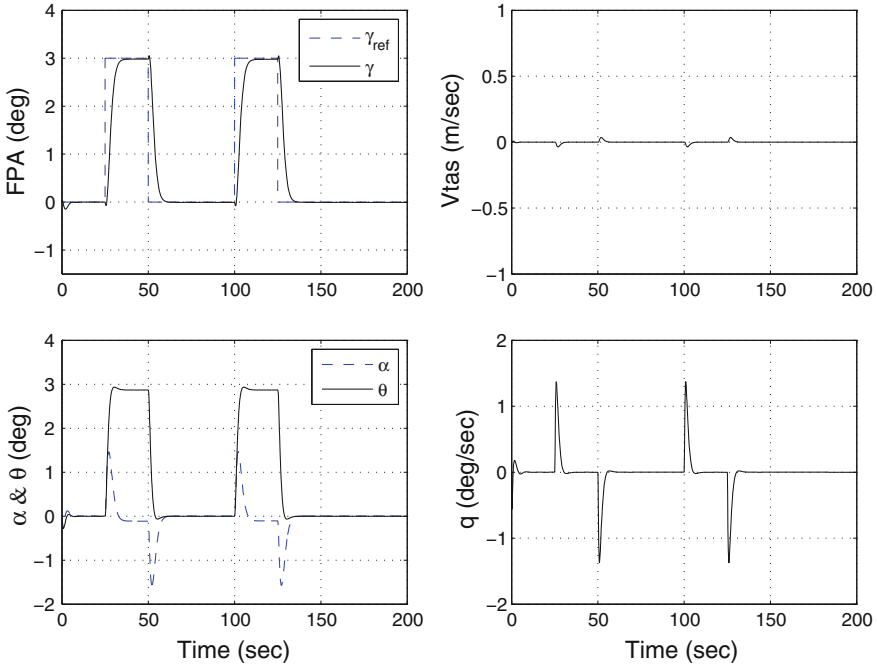

Fig. 5.4 Elevator Lock in place/jam failure states

5.3.1 Simulation Results

In this section the performance of the benchmark civil aircraft model is demonstrated by considering potential failures in the actuators. In the simulations, the discontinuity associated with the control signal in (5.52), is smoothed using the sigmoidal approximation $\frac{\sigma(t)}{\|\sigma(t)\|+\delta(t)}$, where the value of the positive scalar δ is chosen as $\delta = 0.01$. The value of the modulation gain is chosen here as $\rho(t) = 2$. In the simulations the aircraft undergoes a series of 3 deg FPA commands issued in two intervals between 25–50 s and between 100–125 s in order to increase the altitude of the aircraft, while the true airspeed V_{tas} is kept constant as shown in Fig. 5.1. The initial conditions for the plant and observer are taken as $x_0 = (0, 0, 0, 0)$ and $x_{0_{obs}} = (0, 0, 0, 0, 0.5(\pi/180))$ respectively.

5.3.1.1 Nominal Versus Perturbed System Matrix

In Figs. 5.1 and 5.2 good tracking performance of the commanded signals is achieved (nominally when $A^{\delta} = 0$) and also when perturbing the system matrix with A^{δ} representing a 10 % change in the aerodynamic coefficients (due to possible airframe

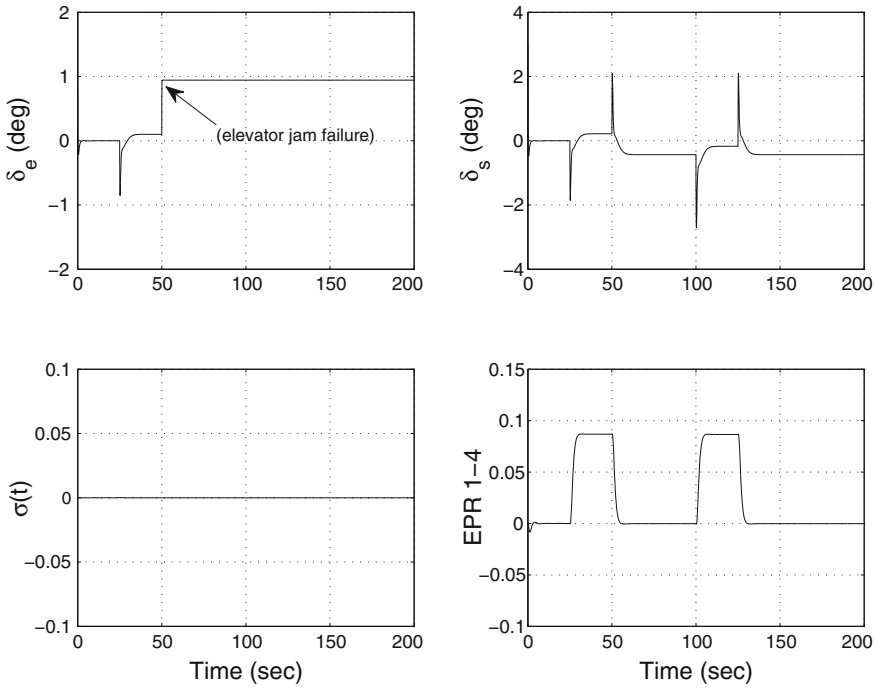

Fig. 5.5 Elevator Lock in place/jam failure surface deflections

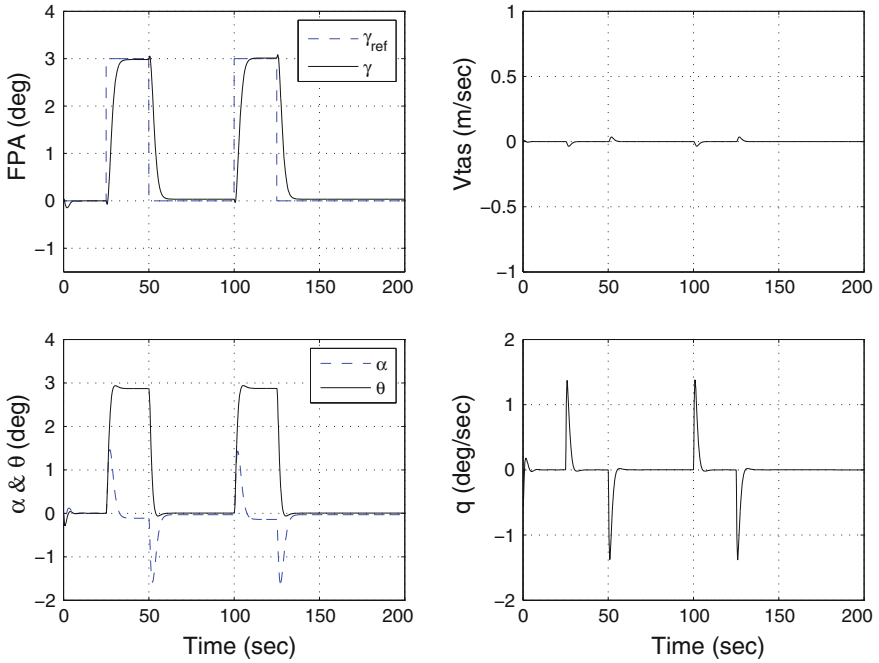

Fig. 5.6 Stabiliser runaway failure states

damage). The system states and the actuator deflections in both cases visually overlap, which shows the robustness of the scheme to parameter variations.

5.3.1.2 Elevator Lock in Place/Jam Failure

In Fig. 5.4 a failure is considered whereby the elevator jams at some offset position. To maintain the performance close to the nominal, the FTC scheme invokes the horizontal stabiliser to counteract the failure, while maintaining the sliding motion throughout the entire system response (Fig. 5.5). There is no performance degradation compared to the nominal situation (Figs. 5.1 and 5.4). In Fig. 5.3, it can be seen that the observer output error quickly converges to zero despite the failure scenario.

5.3.1.3 Horizontal Stabiliser Hardover/Runaway Failure

Figure 5.7 demonstrates the situation when the horizontal stabiliser runs-away to a maximum position limit of 3 deg. Due to the availability of a 'redundant' actuator (the elevator), the scheme can still maintain good tracking performance close to

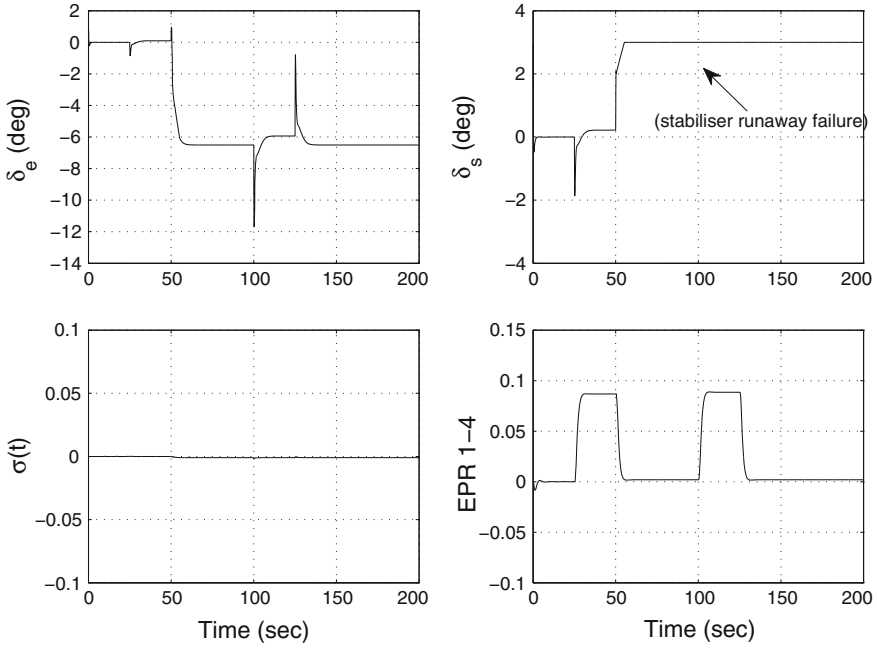

Fig. 5.7 Stabiliser runaway failure surface deflections

nominal as seen in Fig. 5.6. The observer output error is not influenced by the failure and quickly converges to zero.

5.4 Summary

In this chapter, a fault tolerant control scheme was described, which assumes only output information is available, and no information about the actuator faults or failures is known. A linear unknown input observer is employed to estimate the states which are used in the virtual control law. The virtual signals are then translated into physical control signals (associated with the actuators) by using a fixed control allocation scheme which does not require estimates of the actuator effectiveness levels. The closed-loop stability analysis allows for parameter uncertainty in the system matrix in addition to actuator faults or failures. A convex representation of the synthesis problem is established in order to prove closed-loop stability by synthesising appropriate observer and controller gains. The simulation results on a benchmark aircraft model show fast convergence of the observer output error, and demonstrate the excellent FTC features of the scheme.

5.5 Notes and References

In the FTC literature, methods such as $\mathscr{H}_\infty$ control [2] and eigenstructure assignment [3] invariably deal with the output feedback situation and do not require observers per se for estimating the unmeasured states. Other FTC methods such as the Pseudo-Inverse Method [4] use static output feedback to deal with actuator faults and the model-following approach of [5] exploits an adaptive output feedback framework which does not require state estimation. On the other hand papers such as [6, 7] used an integrated FDI/FTC structure and take advantage of the observer (Kalman filter) to provide state estimates to use in the control law. In [8] an ISM controller using output information was used (although not in the framework of FTC) to compensate for matched uncertainties, and a hierarchical sliding mode observer was proposed to estimate the states. In [9] the ISM controller design method was developed into an output feedback framework by introducing a dynamic output dependent sliding surface employing a full order compensator. The unknown input observer considered in Sect. 5.2 is based on the results from [10]. The ISM scheme in this chapter can tolerate the presence of stable invariant zeros associated with the triple (A, B, C) (Assumption 5.3) as compared to [8], where it is assumed that the triple (A, B, C) does not have any invariant zeros.

References

1. Edwards, C., Yan, X., Spurgeon, S.K.: On the solvability of the constrained Lyapunov problem. IEEE Trans. Autom. Control **52**(9), 1975–1981 (2007)
2. Ganguli, S., Marcos, A., Balas, G.J.: Reconfigurable LPV control design for Boeing 747-100/200 longitudinal axis. In: Proceedings of the American Control Conference (2002)
3. Duan, G.: Parametric eigenstructure assignment via output feedback based on singular value decompositions. IEE Control Theory Appl. **150**(1), 93–100 (2003)
4. Konstantopoulos, I., Antsaklis, P.: An optimization approach to control reconfiguration. Dyn. Control **9**(3), 255–270 (1999)
5. Tao, G., Joshi, S.M.: Direct adaptive control of systems with actuator failures: state of the art and continuing challenges. In: Proceedings of the AIAA guidance, navigation and control conference and exhibit, pp. 1–25 (2008)
6. Zhang, Y., Jiang, J.: Integrated design of reconfigurable fault-tolerant control systems. AIAA J. Guid. Control Dyn. **24**(1), 133–136 (2001)
7. Zhang, Y.M., Jiang, J.: Active fault tolerant control system against partial actuator failures. IEE Proc. Control Theory Appl. **149**, 95–104 (2002)
8. Bejarano, F.J., Fridman, L., Poznyak, A.: Output integral sliding mode control based on algebraic hierarchical observer. Int. J. Control **80**(3), 443–453 (2007)
9. Chang, J.: Dynamic output integral sliding-mode control with disturbance attenuation. IEEE Trans. Autom. Control **54**(11), 2653–2658 (2009)
10. Chen, J., Patton, R.: Robust model-based fault diagnosis for dynamical systems. Kluwer Academic Publishers, Berlin (1999)

Chapter 6
An Augmentation Scheme for Fault Tolerant Control Using Integral Sliding Modes

In this chapter a quite different approach is adopted: here an integral sliding mode approach will be retro-fitted to an existing feedback controller. The fault tolerant control allocation scheme in this chapter adopts an a posteri approach, building on an existing state feedback controller designed using only the primary actuators. An integral sliding mode scheme is integrated within the existing controller to introduce fault tolerance. The FTC technique described in this chapter is quite different to the techniques described in Chaps. 3 and 4, which were designed based on the open-loop plant with no cognizance of any existing controller. All the parameters associated with the integral sliding mode schemes in Chaps. 3 and 4 were synthesised simultaneously based on a model of the open-loop plant and specifications for closed-loop performance. In this chapter, for controller design purposes, the actuators are classified as primary and secondary. It is assumed a controller based only on primary actuators has already been designed to provide appropriate closed-loop performance in a fault-free scenario. The idea here is to create an a posteri integral sliding mode design, building on the existing state feedback controller. The idea is to use only the primary actuators in the nominal fault-free scenario, and to engage the secondary actuators only if faults or failures occur. Crucially, in the fault-free case, the closed-loop system behaviour is entirely dependent on the original controller, and the overall scheme behaves exactly as though the ISM scheme is not present. Only in the fault/failure case does the FTC scheme become active. In this way the integral sliding mode FTC scheme described in this chapter can be retro-fitted to almost any existing control scheme to induce fault tolerance. This requires a totally different design philosophy compared to the schemes discussed in Chaps. 3 and 4. The scheme discussed here has an advantage from an industrial perspective, since it can be retro-fitted to an existing control scheme to induce fault tolerance without the need to remove or alter existing control loops. The scheme in this chapter uses measured or estimated actuator effectiveness levels in order to distribute the control signals among the actuators. The effectiveness of the scheme is tested in simulation using the high fidelity nonlinear RECOVER model.

M.T. Hamayun et al., *Fault Tolerant Control Schemes Using Integral Sliding Modes*, Studies in Systems, Decision and Control 61,
DOI 10.1007/978-3-319-32238-4_6

6.1 System Description and Problem Formulation

An LTI system subject to actuator faults or failures can be modelled (as in the previous chapters) as

$$\dot{x}_p(t) = A_p x_p(t) + B_p W(t) u(t) \tag{6.1}$$

where $A_p \in \mathbb{R}^{n\times n}$, $B_p \in \mathbb{R}^{n\times m}$ and $W(t) \in \mathbb{R}^{m\times m}$ is a diagonal semi-positive definite weighting matrix representing the effectiveness of each actuator where the elements $0 \leq w_i(t) \leq 1$ for $i = 1, \ldots, m$. If $w_i(t) = 1$, the corresponding ith actuator has no fault, whereas if $1 > w_i(t) > 0$, an actuator fault is present. In a situation where $w_i(t) = 0$, the actuator has completely failed. Suppose the input distribution matrix can be partitioned as

$$B_p = \begin{bmatrix} B_1 & B_2 \end{bmatrix} \tag{6.2}$$

where $B_1 \in \mathbb{R}^{n\times l}$ and $B_2 \in \mathbb{R}^{n\times(m-l)}$ and $l < m$ and $l < n$. Here B_1 is the input distribution matrix associated with the primary actuators and is assumed to be of rank equal to l, whilst B_2 is associated with the secondary actuators which provide redundancy in the system.

Assumption 6.1 It is assumed that the pair (A_p, B_1) is controllable.

For the primary and secondary actuators, the weighting matrix $W(t)$ is also partitioned as

$$W(t) = \text{diag}(W_1(t), W_2(t)) \tag{6.3}$$

where $W_1(t) = \text{diag}(w_1(t), \ldots, w_l(t))$ and $W_2(t) = \text{diag}(w_{l+1}(t), \ldots, w_m(t))$ are the weighting matrices for the primary and secondary actuators respectively. In this chapter, it is assumed that the matrix $W(t)$ is estimated by some FDI scheme, as given in Sect. 3.3.1 or by using a measurement of the actual actuator deflection compared to the demand. In this chapter, again, the estimated value $\widehat{W}(t)$ will not be a perfect estimate of the real effectiveness matrix $W(t)$.

Assumption 6.2 Assume the estimated matrix

$$\widehat{W}(t) = \text{diag}(\widehat{W}_1(t), \widehat{W}_2(t)) \tag{6.4}$$

satisfies the relationship

$$W(t) = (I - \triangle(t))\widehat{W}(t) \tag{6.5}$$

where $\triangle(t) = \text{diag}(\triangle_1(t), \triangle_2(t))$.

Both the uncertainty blocks $\triangle_1(t)$ and $\triangle_2(t)$ are assumed to be diagonal such that $\triangle_1(t) = \text{diag}(\delta_1(t), \ldots, \delta_l(t))$ and $\triangle_2(t) = \text{diag}(\delta_{l+1}(t), \ldots, \delta_m(t))$, where the diagonal elements $\delta_i(t) \in \mathbb{R}$ satisfy $|\delta_i(t)| < \triangle_{max}$ for some $\triangle_{max} > 0$ where

$$\triangle_{max} = \max(\|\triangle_1(t)\|, \|\triangle_2(t)\|) \tag{6.6}$$

The matrices $\triangle_1(t)$ and $\triangle_2(t)$ model the level of imperfection in the fault estimate, and satisfy

$$W_1(t) = (I_l - \triangle_1(t))\widehat{W}_1(t)$$
$$W_2(t) = (I_{m-l} - \triangle_2(t))\widehat{W}_2(t)$$

Since B_1 is assumed to have full column rank equal to l, there exists an orthogonal matrix $T_p \in \mathbb{R}^{n\times n}$ such that

$$T_p B_1 = \begin{bmatrix} 0 \\ B_{21} \end{bmatrix} \tag{6.7}$$

where $B_{21} \in \mathbb{R}^{l\times l}$ (and B_{21} is nonsingular). By a suitable change of coordinates $x \mapsto T_p x_p$ it can be ensured that the input plant distribution matrix has the form

$$T_p B_p = \begin{bmatrix} 0 & B_{12} \\ B_{21} & B_{22} \end{bmatrix} \tag{6.8}$$

where $B_{22} \in \mathbb{R}^{l\times(m-l)}$. Next scale the last l states to ensure $B_{21}^T B_{21} = B_{21} B_{21}^T = I_l$ (i.e. B_{21} is orthogonal). Consequently it can be assumed without loss of generality that the system in (6.1) can be written as

$$\dot{x}(t) = Ax(t) + BW(t)u(t) \tag{6.9}$$

where

$$B = \left[\begin{array}{c|c} 0 & B_{12} \\ B_{21} & B_{22} \end{array}\right] := \left[\begin{array}{c|c} B_o & B_s \end{array}\right] \tag{6.10}$$

Controllability of (A_p, B_1) implies that the pair (A, B_o) is controllable. Assume that a state feedback control law

$$v_o(t) = Fx(t) \tag{6.11}$$

has been designed a priori to make the system

$$\dot{x}(t) = (A + B_o F)x(t) \tag{6.12}$$

stable. Note that the gain F is the baseline controller specifically designed based on the primary actuators. Now a control allocation scheme will be *retro-fitted* to the control law $v_o(t)$. The physical control law $u(t)$ applied to *all the actuators* is defined as

$$u(t) = N(t)v(t) \tag{6.13}$$

where $v(t) \in \mathbb{R}^l$ is the virtual control effort produced by the actuators, and will be discussed in the next section. The overall control structure is given in Fig. 6.1, where it is clear that the integral sliding mode FTC scheme is retro-fitted to the existing baseline controller $v_o(t)$ (which is designed based on the primary actuators) and will be only active in the case of faults or failures. The control allocation matrix is given by

$$N(t) = \begin{bmatrix} I_l \\ N_2(t)(I_l - \widehat{W}_1(t)) \end{bmatrix} \tag{6.14}$$

where

$$N_2(t) := B_{22}^T B_{21}(B_{21}^T B_{22}\widehat{W}_2(t)B_{22}^T B_{21})^{-1} \tag{6.15}$$

and $\widehat{W}_1(t)$ and $\widehat{W}_2(t)$ are the estimates of the effectiveness levels. Now define

$$\mathscr{W} = \{(\hat{w}_{l+1}, \ldots, \hat{w}_m) \in \underbrace{[0\ 1] \times \cdots \times [0\ 1]}_{m-l \text{ times}} : \det(B_{22}\widehat{W}_2(t)B_{22}^T) \neq 0\} \tag{6.16}$$

Assumption 6.3 Throughout this chapter, it is assumed that $m \geq 2l$.

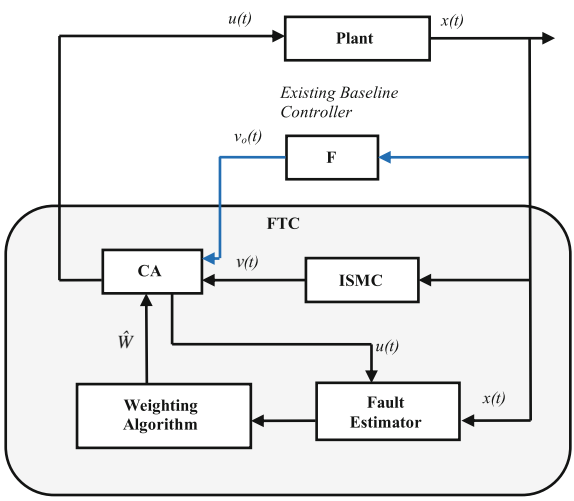

Fig. 6.1 Schematic of the overall control strategy

Remark 6.1 This allows up to $m-2l$ of the entries $\hat{w}_i(t)$ in the matrix $\widehat{W}_2(t)$ to be zero, and yet guarantee $\det(B_{22}\widehat{W}_2(t)B_{22}^T) \neq 0$. The set $\mathscr{W}$ will be shown to constitute the class of faults/failures for which closed-loop stability can be maintained.

Substituting (6.5) and (6.13) into (6.9) yields

$$\dot{x}(t) = Ax(t) + \begin{bmatrix} B_{12}(I_{m-l} - \triangle_2)\widehat{W}_2(t)N_2(t)(I_l - \widehat{W}_1(t)) \\ B_{21}(I_l - \triangle_1)\widehat{W}_1(t) + B_{22}(I_{m-l} - \triangle_2)\widehat{W}_2(t)N_2(t)(I_l - \widehat{W}_1(t)) \end{bmatrix} \nu(t) \tag{6.17}$$

Since B_{21} is orthogonal by construction $B_{21}B_{21}^T = I_l$, then using the definition of $N_2(t)$ in (6.15) it follows that

$$B_{22}\widehat{W}_2(t)N_2(t) = B_{21}B_{21}^T B_{22}\widehat{W}_2(t)N_2(t) \;=\; B_{21} \tag{6.18}$$

Consequently using (6.18), Eq. (6.17) simplifies to

$$\dot{x}(t) = Ax(t) + \begin{bmatrix} B_{12}(I_{m-l} - \triangle_2)\widehat{W}_2N_2(t)(I_l - \widehat{W}_1) \\ B_{21}(I_l - \triangle_1)\widehat{W}_1 + B_{21}(I_l - \widehat{W}_1) - B_{22}\triangle_2\widehat{W}_2N_2(t)(I_l - \widehat{W}_1) \end{bmatrix} \nu(t) \tag{6.19}$$

which can be further simplified to

$$\dot{x}(t) = Ax(t) + \underbrace{\begin{bmatrix} B_{12}(I_{m-l} - \triangle_2)\widehat{W}_2(t)N_2(t)(I_l - \widehat{W}_1(t)) \\ B_{21} - B_{21}\triangle_1\widehat{W}_1(t) - B_{22}\triangle_2\widehat{W}_2(t)N_2(t)(I_l - \widehat{W}_1(t)) \end{bmatrix}}_{\widehat{B}(t)} \nu(t) \tag{6.20}$$

Remark 6.2 In the case of perfect estimation of $\widehat{W}(t)$ (i.e. $\triangle(t) = 0$) and when there is no fault in the primary and secondary actuators (i.e. $W_1(t) = I_l$ and $W_2(t) = I_{m-l}$), the system in (6.20) becomes

$$\dot{x}(t) = Ax(t) + B_o\nu(t) \tag{6.21}$$

and so only the primary control channels will be used.

In a fault/failure scenario, to maintain the closed-loop performance near to nominal, the concept of integral sliding mode control is combined with the control law from (6.13) and (6.14). The nominal fault-free system in (6.21) will be used for the design of the augmentation scheme which will be demonstrated in the sequel.

6.2 Integral Sliding Mode Controller Design

First choose the sliding surface as $\mathscr{S} = \{x \in \mathbb{R}^n : \quad \sigma(t) = 0\}$ where the switching function $\sigma(t)$, based on the nominal system (6.12), is defined as

$$\sigma(t) := Gx(t) - Gx(0) - G\int_0^t (A + B_oF)\,x(\tau)d\tau \tag{6.22}$$

where $G \in \mathbb{R}^{l\times n}$ is the design freedom to be selected. The elimination of the reaching phase, ensures the occurrence of the sliding motion throughout the entire response of the system. In this chapter, the design freedom G is selected as

$$G := B_o^T \tag{6.23}$$

where B_o is defined in (6.10). With this choice of G it follows

$$GB_o = B_{21}^T B_{21} = I_l$$

and so this choice of G serves as a pseudo-inverse of the matrix B_o. Also from (6.20)

$$G\widehat{B}(t) = B_{21}^T\left(B_{21} - B_{21}\triangle_1(t)\widehat{W}_1(t) - B_{22}\triangle_2(t)\widehat{W}_2(t)N_2(t)(I_l - \widehat{W}_1(t))\right) \tag{6.24}$$

which will be used when obtaining an expression for the equivalent control. Taking the time derivative of $\sigma(t)$ defined in (6.22) along the system trajectories yields

$$\dot{\sigma}(t) = G\dot{x}(t) - GAx(t) - GB_oFx(t) \tag{6.25}$$

Substituting (6.20) into (6.25), the expression above simplifies to

$$\dot{\sigma}(t) = G\widehat{B}(t)v(t) - GB_oFx(t) \tag{6.26}$$

Equating $\dot{\sigma}(t) = 0$, and using the fact that $GB_o = I_l$, the expression for the equivalent control is

$$v_{eq}(t) = (G\widehat{B}(t))^{-1}Fx(t) \tag{6.27}$$

The equations of motion governing sliding can be obtained by substituting (6.27) into (6.20) which yields

$$\dot{x}(t) = Ax(t) + \widehat{B}(t)(G\widehat{B}(t))^{-1}Fx(t) \tag{6.28}$$

Adding and subtracting the term $B_oFx(t)$, Eq. (6.28) can be written as

$$\dot{x}(t) = (A + B_oF)x(t) + (\widehat{B}(t)(G\widehat{B}(t))^{-1} - B_o)Fx(t) \tag{6.29}$$

which can be further simplified to

$$\dot{x}(t) = (A + B_oF)x(t) + \begin{bmatrix} B_{12}(I - \triangle_2(t))\widehat{W}_2(t)N_2(t)(I - \widehat{W}_1(t))(G\widehat{B}(t))^{-1} \\ 0_l \end{bmatrix} Fx(t) \tag{6.30}$$

Remark 6.3 Note that in the nominal fault-free case when $W(t) = I$, and in the case of perfect estimation of $\widehat{W}(t)$ matrix, the top row in the second term is zero, and the closed-loop sliding motion is stable. In the case of faults or failures when $\widehat{W}(t) \neq I$, then the second term is not zero and will be treated as unmatched uncertainty.

For the stability analysis which follows, write (6.30) as

$$\dot{x}(t) = (A + B_o F)x(t) + \tilde{B}\tilde{\Phi}(t)Fx(t) \tag{6.31}$$

where

$$\tilde{B} := \begin{bmatrix} B_{12} \\ 0 \end{bmatrix} \tag{6.32}$$

and the time varying uncertain term

$$\tilde{\Phi}(t) := (I_{m-l} - \triangle_2(t))\Psi(t)\left(I_l - \triangle_1(t)\widehat{W}_1(t) - B_{21}^T B_{22}\triangle_2(t)\Psi(t)\right)^{-1} \tag{6.33}$$

where

$$\Psi(t) := \widehat{W}_2(t)N_2(t)(I_l - \widehat{W}_1(t)) \tag{6.34}$$

From (6.18) it is clear that $\widehat{W}_2(t)N_2(t)$ is a right pseudo-inverse for $B_{21}^T B_{22}$. Then by using arguments similar to those given in Chap. 3, it follows $\|\widehat{W}_2(t)N_2(t)\| < \gamma_1$ for some positive scalar γ_1, provided that $\det(B_{22}\widehat{W}_2(t)B_{22}^T) \neq 0$. Since

$$\|\Psi(t)\| \leq \|(I_l - \widehat{W}_1(t))\|\|\widehat{W}_2(t)N_2(t)\| < \|\widehat{W}_2(t)N_2(t)\| < \gamma_1$$

the term $\|\Psi(t)\|$ is bounded. Define γ_1^* as the smallest number (which will be used later in Proposition 6.1) satisfying

$$\|\Psi(t)\| < \gamma_1^* \tag{6.35}$$

In the following subsections the main results of the chapter are presented.

6.2.1 Stability Analysis of the Closed-Loop Sliding Motion

In the case of perfect estimation of the $\widehat{W}(t)$ matrix, (i.e. $\triangle(t) = 0$) and when there are no faults in the system (i.e. $W(t) = I$) the uncertain term $\tilde{\Phi}(t)$ in (6.31) vanishes (i.e. $\tilde{\Phi}(t) = 0$) and the closed-loop sliding motion in (6.31) simplifies to

$$\dot{x}(t) = (A + B_o F)x(t) \tag{6.36}$$

which is stable by choice of the baseline controller F.

In the case of non-perfect estimation of $\widehat{W}(t)$, and in the presence of faults, the stability of (6.31) needs to be proven. To this end, in this most general situation the equation governing the sliding motion in (6.31) can be written as

$$\dot{x}(t) = \underbrace{(A + B_o F)}_{\tilde{A}} x(t) + \tilde{B} \overbrace{\tilde{\Phi}(t) \underbrace{Fx(t)}_{\tilde{y}(t)}}^{\tilde{u}(t)} \tag{6.37}$$

For the subsequent stability analysis, define the $\mathscr{L}_2$ gain between $\tilde{u}$ to $\tilde{y}$ as

$$\gamma_2 = \|\tilde{G}(s)\|_\infty \tag{6.38}$$

where the transfer function matrix

$$\tilde{G}(s) := F(sI - \tilde{A})^{-1}\tilde{B} \tag{6.39}$$

which is stable by design.

Proposition 6.1 *Suppose that the condition*

$$(1 + \gamma_3 \gamma_1^*)\triangle_{max} < 1 \tag{6.40}$$

holds, where γ_1^* and $\triangle_{max}$ are defined in (6.35) and (6.6) and $\gamma_3 = \|B_{22}\|$, then during fault/failure conditions, including the failure of primary actuators, and for any $\hat{w}_{l+1}(t), \ldots, \hat{w}_m(t) \in \mathscr{W}$ where $\mathscr{W}$ is defined in (6.16), the closed-loop system in (6.37) will be stable if:

$$\frac{\gamma_2 \gamma_1^*(1 + \triangle_{max})}{1 - (1 + \gamma_3 \gamma_1^*)\triangle_{max}} < 1 \tag{6.41}$$

where γ_2 is defined in (6.38).

Proof The closed-loop sliding motion in (6.37) can be written as

$$\dot{x}(t) = \tilde{A}x(t) + \tilde{B}\tilde{u}(t) \tag{6.42}$$

$$\tilde{y}(t) = Fx(t) \tag{6.43}$$

where

$$\tilde{u}(t) = \tilde{\Phi}(t)\tilde{y}(t) \tag{6.44}$$

By using the small gain theorem (as discussed in Appendix B.1.2), the feedback interconnection of the known stable matrix $\tilde{G}(s)$ with the bounded uncertain term $\tilde{\Phi}(t)$, and hence Eq. (6.37), will be stable if

$$\|\tilde{G}(s)\|_\infty \|\tilde{\Phi}(t)\| < 1 \tag{6.45}$$

From Eq. (6.33), it is clear that

$$\|\tilde{\Phi}(t)\| \leq \|\big(I_l - \underbrace{\triangle_1(t)\widehat{W}_1(t) - B_{21}^T B_{22}\triangle_2(t)\Psi(t)}_{X(t)}\big)^{-1}\|\|(I_{m-l} - \triangle_2(t))\Psi(t)\| \tag{6.46}$$

Using the fact that $\|\widehat{W}_1(t)\| \leq 1$, and $\|B_{21}^T\| = 1$ (since $B_{21}^T B_{21} = I_l$), from (6.46)

$$\begin{aligned}\|X(t)\| &\leq \|\triangle_1(t)\widehat{W}_1(t)\| + \|B_{21}^T B_{22}\triangle_2(t)\Psi(t)\| \\ &\leq \|\triangle_1(t)\| + \|B_{22}\|\|\triangle_2(t)\|\|\Psi(t)\| \\ &\leq (1 + \gamma_3\gamma_1^*)\triangle_{max} < 1\end{aligned}$$

if the conditions of Proposition 6.1 hold. Hence from (6.46), and using the fact that in general

$$\|(I - X)^{-1}\| \leq (1 - \|X\|)^{-1} \quad \text{if} \quad \|X\| < 1$$

it follows that

$$\|\tilde{\Phi}(t)\| \leq \frac{\gamma_1^*(1 + \triangle_{max})}{1 - (1 + \gamma_3\gamma_1^*)\triangle_{max}} \tag{6.47}$$

From the expression in (6.47) and the fact that $\|\tilde{G}(s)\|_\infty = \gamma_2$, a sufficient condition to ensure the small gain theorem in (6.45) holds, is that

$$\frac{\gamma_2\gamma_1^*(1 + \triangle_{max})}{1 - (1 + \gamma_3\gamma_1^*)\triangle_{max}} < 1$$

This is the condition in (6.41), and the proof of Proposition 6.1 is complete. ■

Remark 6.4 If B_{12} is zero in (6.32) which is the assumption in many CA schemes,[1] then $\widetilde{B} = 0$, and the condition of Proposition 6.1 is trivially satisfied. The scheme in this chapter allows $B_{12} \neq 0$, and consequently considers a more general solution, which helps target a wider range of potential applications.

6.2.2 *Integral Sliding Mode Control Laws*

Now a control law will be designed such that the sliding motion on the sliding surface in (6.22) can be ensured. Define the integral sliding mode control law as

$$\nu(t) = \nu_l(t) + \nu_n(t) \tag{6.48}$$

[1] See for example [1, 2].

where the linear part of the control law (which is known a priori) is

$$\nu_l(t) := Fx(t) \tag{6.49}$$

and the nonlinear part, which induces the sliding motion, is

$$\nu_n(t) := -\rho(t,x)\frac{\sigma(t)}{\|\sigma(t)\|} \qquad \text{for } \sigma(t) \neq 0 \tag{6.50}$$

where $\rho(t,x)$ is the modulation gain whose precise value is given in the statement of Proposition 6.2. Now in the sequel it is demonstrated that the integral sliding mode control law in (6.48)–(6.50) satisfies the reachability condition.

Proposition 6.2 *Assume the conditions of Proposition 6.1 hold. Then if $\rho(t,x)$ is chosen as*

$$\rho(t,x) \geq \frac{(1+\gamma_3\gamma_1^*)\triangle_{max}\|\nu_l(t)\| + \eta}{1-(1+\gamma_3\gamma_1^*)\triangle_{max}} \tag{6.51}$$

where $\eta > 0$ is a small positive scalar, the integral sliding mode control law in (6.48)–(6.50) satisfies the reachability condition and sliding on $\mathscr{S}$ in (6.22) is maintained.

Proof By substituting the control law in (6.48)–(6.50) into (6.26) and by using the fact that $GB_o = I$:

$$\dot{\sigma}(t) = (G\widehat{B}(t))\,(\nu_l(t) + \nu_n(t)) - Fx(t) \tag{6.52}$$

Since by construction $B_{21}^T B_{21} = I_l$, using (6.24) and (6.34), Eq. (6.52) can be written as

$$\begin{aligned}\dot{\sigma}(t) &= (I_l - \triangle_1(t)\widehat{W}_1(t) - B_{21}^T B_{22}\triangle_2(t)\Psi(t))(\nu_l(t)+\nu_n(t)) - Fx(t)\\ &= \nu_n(t) - (\triangle_1(t)\widehat{W}_1(t) + B_{21}^T B_{22}\triangle_2(t)\Psi(t))(\nu_l(t)+\nu_n(t))\end{aligned} \tag{6.53}$$

Now consider the candidate Lyapunov function

$$V(t) = \frac{1}{2}\sigma^T(t)\sigma(t) \tag{6.54}$$

Taking the time derivative of (6.54) and substituting for $\dot{\sigma}(t)$ from (6.53) yields

$$\begin{aligned}\dot{V}(t) &= -\rho(\cdot)\|\sigma\| - \sigma^T(\triangle_1(t)\widehat{W}_1(t) + B_{21}^T B_{22}\triangle_2(t)\Psi(t))(\nu_l(t)+\nu_n(t))\\ &\leq -\rho(\cdot)\|\sigma\| + \|\sigma\|(\triangle_{max} + \gamma_3\triangle_{max}\gamma_1^*)(\|\nu_l\| + \rho(\cdot))\\ &\leq -\rho(\cdot)(1-(\triangle_{max}+\gamma_3\triangle_{max}\gamma_1^*))\|\sigma\| + \|\sigma\|(\triangle_{max}+\gamma_3\triangle_{max}\gamma_1^*)\|\nu_l\|\end{aligned} \tag{6.55}$$

where $\triangle_{max}$ is defined in (6.6). By choosing the value of $\rho(t,x)$ as in (6.51), the expression in (6.55) becomes $\dot{V}(t) \leq -\eta\|\sigma(t)\| = -\eta\sqrt{2V(t)}$, which is the standard

reachability condition, and is sufficient to guarantee that sliding on the surface $\mathscr{S}$ is maintained. ■

Finally in order to obtain the overall physical control law which is used to create the actual control signals sent to all the available control surfaces, substituting (6.48)–(6.50) into (6.13) yields

$$u(t) = \begin{bmatrix} I_l \\ N_2(t)(I_l - \widehat{W}_1(t)) \end{bmatrix} \left(Fx(t) - \rho(t,x)\frac{\sigma(t)}{\|\sigma(t)\|} \right) \tag{6.56}$$

where $N_2(t)$ is defined in (6.15). The efficacy of the scheme is tested in the following section using the high fidelity nonlinear model of the large transport aircraft from Appendix A.

6.3 Case Study: Yaw Damping of a Large Transport Aircraft

The integral sliding mode FTC scheme described in this chapter employs an a posteri approach building on an existing state feedback controller designed using only the primary actuators. In the physical control law given in (6.56), the baseline control law F is assumed to exist a-priori. The technique implemented in the FTC scheme is to use the baseline controller in the nominal fault-free scenario, and activate the fault tolerant features only in the case when faults or failures occur in the actuators. All the simulations that follow are based on the RECOVER benchmark model of a large passenger aircraft (see Appendix A.1).

The objective of the simulations is to damp the lateral dynamics of the aircraft when the initial sideslip $\beta(0)$ is perturbed by 1 deg while the aircraft is flying at a high altitude (12,192 m) at a high speed (236 m/s). The lateral dynamics of the aircraft discussed in Appendix A.1 are used to evaluate the scheme. For yaw damping, the washout filter state:

$$\dot{x}_{wo} = r - 0.333x_{wo} \tag{6.57}$$

is augmented with the lateral dynamics, where r is the yaw rate and x_{wo} is the washout filter state. The nominal state feedback controller F associated with the primary actuators for yaw damping (which is a stability augmentation system for the lateral dynamics of an aircraft) has been taken from the literature[2] and is not part of the design process.

By augmenting the washout filter state given in Eq. (6.57), with the aircraft's lateral dynamics the state-space representation of the model is given as

[2] Specifically the control law is based on eigenstructure assignment [3].

$$A_p = \begin{bmatrix} -0.3330 & 0 & 0 & 1 & 0 \\ 0 & 0 & 0 & 0.0816 & 1 \\ 0 & 0.0413 & -0.0537 & -0.9944 & 0.0823 \\ 0 & -0.0012 & 0.6090 & -0.0869 & -0.0335 \\ 0 & 0.0002 & -2.9236 & 0.3681 & -0.4514 \end{bmatrix}$$

$$B_p = \left[\begin{array}{cc|cccc} 0 & 0 & 0 & 0 & 0 & 0 \\ 0 & 0 & 0 & 0 & 0 & 0 \\ 0.0070 & 0 & 0.0003 & -0.0003 & 0.0002 & -0.0002 \\ -0.4438 & -0.0082 & -0.0046 & 0.0046 & 0.0493 & -0.0493 \\ 0.1451 & -0.1329 & -0.0625 & 0.0625 & 0.0085 & -0.0085 \end{array}\right] \quad (6.58)$$

The states are $(x_{wo}, \phi, \beta, r, p)$, where x_{wo} is the washout filter state (rad) in Eq. (6.57), ϕ is the roll angle (rad), β is the side slip (rad), r is the yaw rate (rad/s) and p is the roll rate (rad/s). The control surfaces which are considered for the design are $\delta_{lat} = (\delta_r, \delta_a, \delta_{sp5}, \delta_{sp8}, Tn_l, Tn_r)$ where δ_r is the rudder deflection (rad), δ_a is the aileron deflection (rad), δ_{sp5} is the left inboard spoiler (rad), δ_{sp8} is the right inboard spoiler (rad) and Tn_l and Tn_r are aggregated engine thrusts (N) (scaled by 10^5) on the left and right wing. It is assumed that the left aileron moves in an anti-symmetrical fashion to the right aileron.[3] In (6.58) the input distribution matrix B_p is divided into primary (δ_r, δ_a) and secondary $(\delta_{sp5}, \delta_{sp8}, Tn_l, Tn_r)$ actuators. A further transformation is required in order to have the structure in (6.10) and to ensure that $B_{21}B_{21}^T = I_2$.

6.3.1 Baseline Controller

Eigenstructure assignment is a method that provides the freedom to allow the appropriate set of eigenvalues and associated eigenvectors to be considered in the design procedure to achieve the desired performance or shape of the closed-loop system response. The feedback gain F, based only on the primary actuator, is assumed to be available a priori and should stabilise the nominal closed-loop system in (6.12). The design of F is based on a set of eigenvalues and the best possible eigenvectors. Based on this available eigenstructure, the feedback gain F can be obtained using the relation

$$(A + B_o F)v_i = \lambda_i v_i \quad i = 1, \ldots, n \quad (6.59)$$

where λ_i is an eigenvalue and v_i is the associated eigenvector.

The ideal closed-loop eigenvalues for the nominal state feedback controller F associated with the primary actuators for yaw damping are

$$\{-0.0051, -0.468, -0.6 \pm 0.628j, -1.106\} \quad (6.60)$$

[3]The outboard ailerons and spoilers ($sp1 - 4$, $sp9 - 12$) are not active at a high speed cruise condition due to structural limit. The spoilers ($sp6$, $sp7$) are ground spoilers and not used in flight.

The motions corresponding to the stable real poles are referred to as the spiral mode (-0.0051), the washout filter (-0.468) and the roll mode (-1.106). The motion corresponding to the complex poles is referred to as the Dutch roll mode. The best possible eigenvectors to ensure decoupling between these modes are

$$\underbrace{\begin{bmatrix} * \\ 0 \\ 1 \\ * \\ * \end{bmatrix}\begin{bmatrix} * \\ 0 \\ 1 \\ * \\ * \end{bmatrix}}_{\text{Dutch roll mode}} \quad \underbrace{\begin{bmatrix} * \\ 1 \\ 0 \\ * \\ * \end{bmatrix}}_{\text{roll mode}} \quad \underbrace{\begin{bmatrix} * \\ 1 \\ 0 \\ * \\ * \end{bmatrix}}_{\text{spiral mode}} \quad \underbrace{\begin{bmatrix} 0 \\ 0 \\ 0 \\ 1 \\ 0 \end{bmatrix}}_{\text{washout filter}} \quad \underbrace{\begin{bmatrix} x_{wo} \\ \phi \\ \beta \\ r \\ p \end{bmatrix}}_{x(t)} \tag{6.61}$$

where $*$ denotes that the value of the element is unimportant. This selection of eigenvectors ensures no coupling of Dutch roll with the roll angle and/roll rate. Furthermore the spiral mode and roll mode are associated with the roll angle only, and should ensure decoupling from the sideslip angle to avoid sideslip in the course of a steady turn. The washout filter which is used for the yaw damping is only associated with the yaw rate. Using the set of eigenvalues and eigenvectors given in (6.60) and (6.61), the ideal baseline control law F for yaw damping (considering only the primary actuators (δ_r, δ_a)), based on eigenstructure assignment is

$$F = \begin{bmatrix} -0.5342 & -0.4817 & 0.0665 & 1.1836 & -0.0133 \\ -21.9319 & -0.5188 & 0.1313 & 1.9001 & 0.6705 \end{bmatrix} \tag{6.62}$$

The state feedback control gain matrix in (6.62) will be taken as the a priori given controller around which the integral sliding mode scheme is created.

6.3.2 Fault Tolerant Control

In the case of faults or failures, the baseline control law in (6.62) cannot be used alone; instead the fault tolerant control law given in (6.56) will be employed to retain performance close to the nominal. In the nominal case, the aileron is the primary control surface for ϕ tracking, and the spoilers are the redundancy; whereas the rudder is the primary control surface for β tracking (i.e. yaw damping), and differential engine thrust is the redundancy. The closed-loop stability condition in (6.41) should be guaranteed in nominal and in fault/failure scenarios. The value of γ_2 for the a priori F using Eq. (6.38) is $\gamma_2 = 0.0424$. Using (6.35) it can be verified using a numerical search that $\gamma_1^* = 7.5920$. Hence to satisfy the stability conditions of Proposition 6.1 in (6.40) and (6.41) where $\gamma_3 = 0.7176$, the maximum value of the error in estimation of the actuator effectiveness levels which can be handled by the physical control law in (6.56) is $\triangle_{max} = 10\,\%$.

6.3.3 Nonlinear Simulation Results

As in previous chapters, the discontinuity in the unit vector has been smoothed using the sigmoidal approximation $\frac{\sigma(t)}{\|\sigma(t)\|+\delta}$ given in Sect. 2.5, where the value of the positive scalar is chosen as $\delta = 0.01$. In the sequel three simulation case studies are investigated: one a fault-free case considering the estimation of the $W(t)$ matrix is perfect; the second considering the same scenario as in case 1, but when the estimation of the $W(t)$ matrix is imperfect; and the third a scenario involving a primary actuator failure with imperfect estimation of $W(t)$.

6.3.3.1 Case 1: Fault-Free Case with Perfect Estimation of $W(t)$

In the case when the estimation of the effectiveness level matrix $W(t)$ is perfect, $\triangle(t) = 0$ and $\triangle_{max} = 0$. Consequently the stability condition in (6.41) reduces to $\gamma_2\gamma_1^* = 0.3217 < 1$. Figures 6.2 and 6.3 demonstrate the nominal fault-free performance. In Fig. 6.2 it can be seen that the roll and yaw modes are decoupled. During the nominal fault-free scenario the secondary actuators are not active (Fig. 6.3) because the integral sliding mode FTC scheme is not active in this case, and only the baseline controller F is employed to achieve the nominal performance.

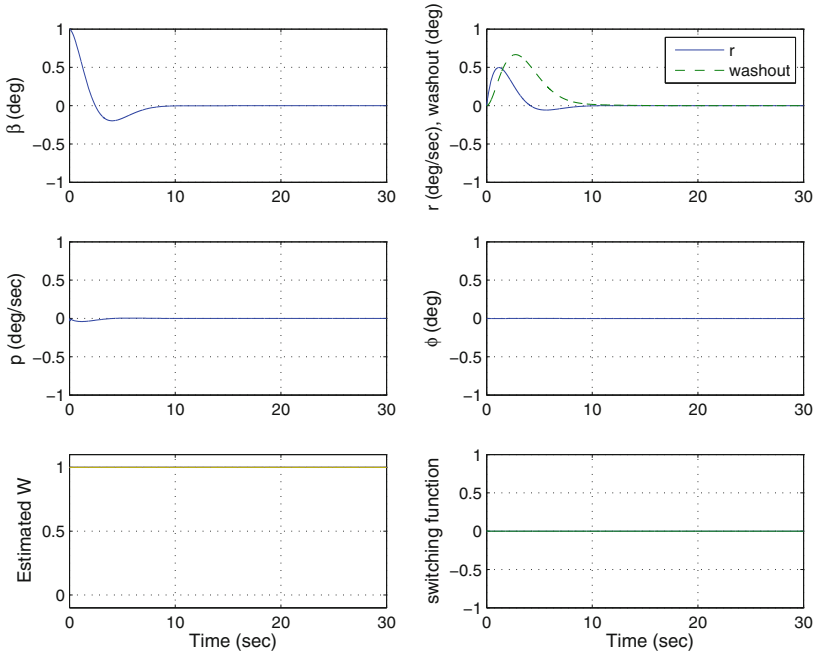

Fig. 6.2 No fault (perfect estimation of $W(t)$): plant states

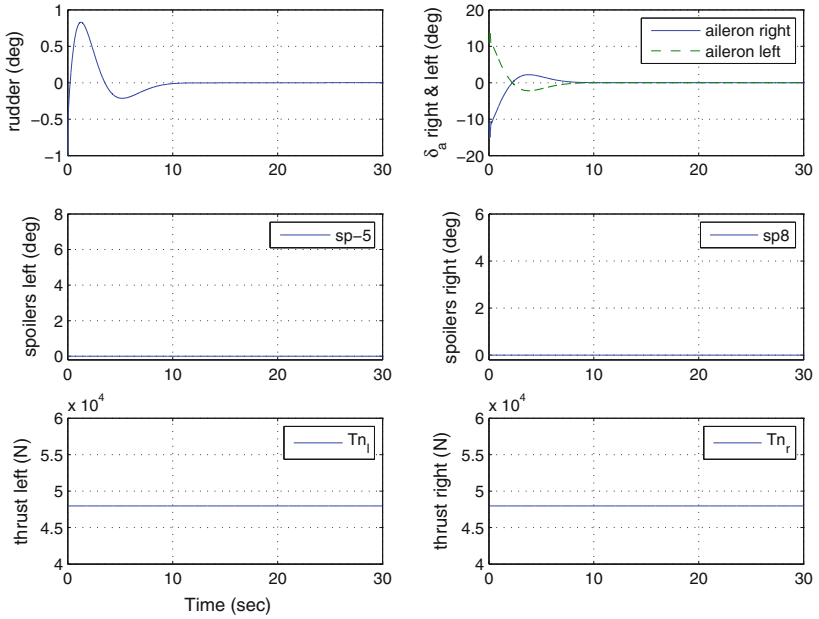

Fig. 6.3 No fault (perfect estimation of $W(t)$): actuators

6.3.3.2 Case 2: Fault-Free Case with Imperfect Estimation of $W(t)$

A second scenario is considered here to demonstrate the efficacy of the scheme when the system is fault-free and the estimation of the $W(t)$ matrix is not perfect. Figure 6.4 shows that due to imprecise information provided by the FDI, the estimate $\widehat{W}(t) \neq I$, (indicating the presence of faults) although in reality there is no fault in the system. In response to this the control allocation scheme engages the secondary actuators (spoilers for ϕ performance and differential engine thrust for β performance) as shown in Fig. 6.5 to maintain closed-loop stability of the system and to retain nominal performance as in Fig. 6.2.

6.3.3.3 Case 3: Primary Failure with Imperfect Estimation of $W(t)$

The third scenario demonstrates the scheme with imperfect estimates $\widehat{W}(t)$ in the case of failures in the primary actuators. Theoretically the maximum percentage error $\triangle_{max}$ the scheme can handle and yet ensure the stability conditions of Proposition 6.1, is 10 %. Figure 6.7, shows the scenario when both the primary actuators (rudder and ailerons) have jammed at offset positions at 6 s, and due to imprecise information provided by the FDI scheme, the effectiveness of the primary actuators is estimated at 10 %, instead of 0 % (Fig. 6.6). Due to this failure, the right wing spoiler *sp*8 is actively engaged by the control allocation scheme, together with the left and right

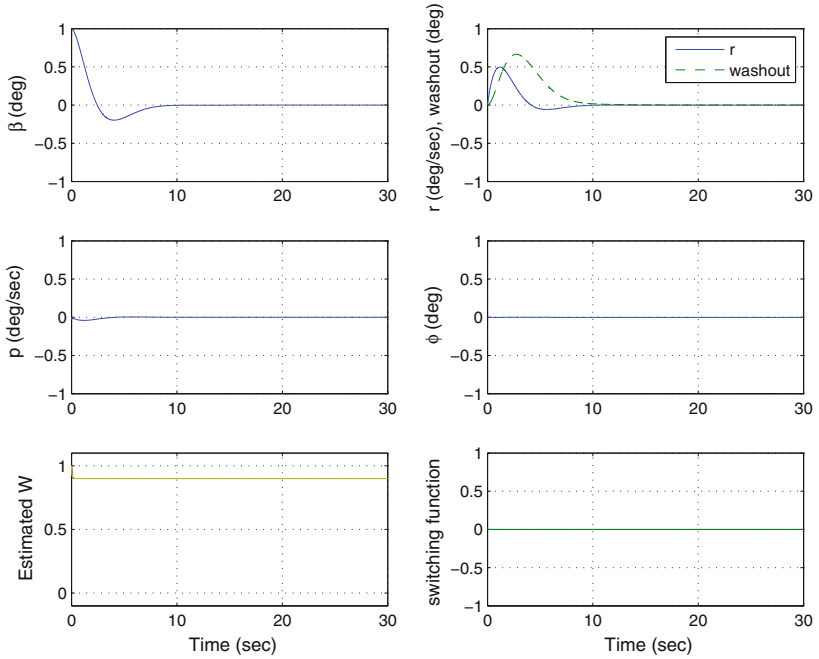

Fig. 6.4 No fault (imperfect estimation of $W(t)$): plant states

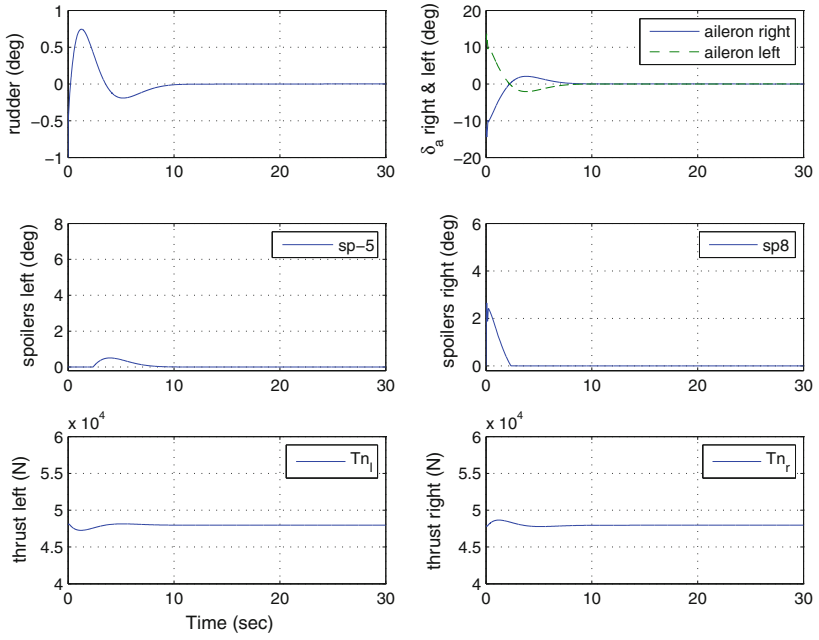

Fig. 6.5 No fault (imperfect estimation of $W(t)$): actuators

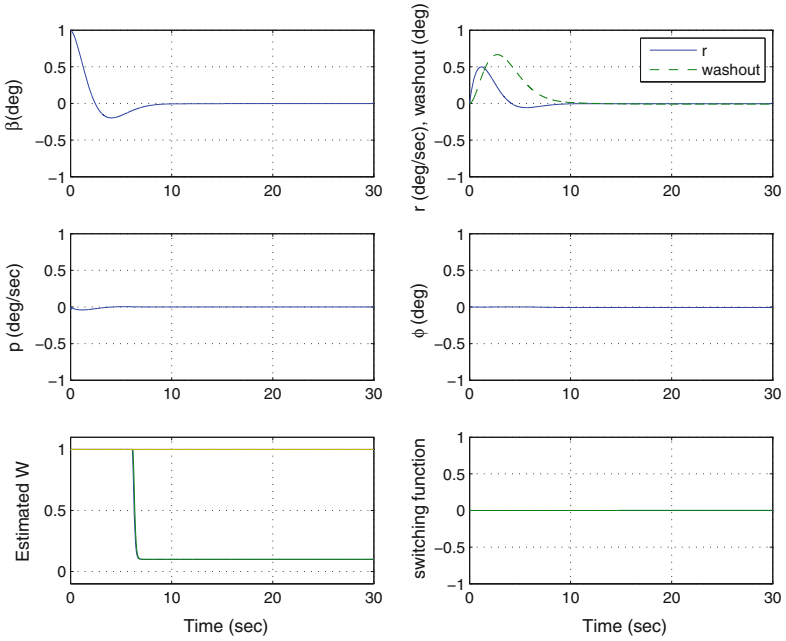

Fig. 6.6 Primary failure (imperfect estimation of $W(t)$): plant states

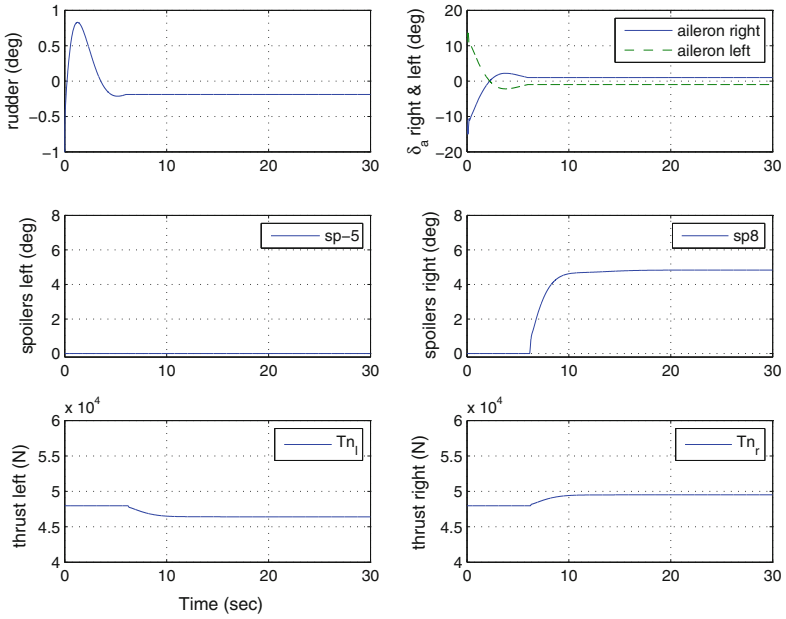

Fig. 6.7 Primary failure (imperfect estimation of $W(t)$): actuators

wing engine thrusts, to cope with this situation, and to maintain performance close to the nominal (Fig. 6.7). The switching function plot in Fig. 6.7 shows that sliding is maintained during the entire system response.

6.4 Summary

This chapter described a fault tolerant control scheme incorporating integral sliding mode and CA, based on an a posteri approach. Here an ISM and CA architecture was incorporated into an existing state feedback controller (designed using only the primary actuators). As in earlier chapters, to distribute the control signals to the functional actuators, the scheme uses the estimated effectiveness levels of the actuators provided by an FDI scheme. The efficacy of the FTC scheme was tested in simulation using the high fidelity nonlinear RECOVER benchmark model.

6.5 Notes and References

Retro-fitting a new component to an existing baseline feedback control scheme to achieve fault tolerance is appealing because it retains the performance of baseline controller nominally. The nominal fault-free performance can be achieved by any design paradigm including $\mathscr{H}_\infty$ control [4], eigenstructure assignment [5], LQR [1], or sliding mode control [6–8]. An early example of retro-fitting adaptive reconfigurable control laws to conventional control laws was explored in [9]. The implementation of retro-fit control laws is possible in a parallel or in an 'in-line' or 'series' approach [10]. In [11], a reconfigurable control effector compensation scheme was proposed, where an adaptive subsystem was implemented in a retro-fit fashion as an add-on signal within the Fast on-Line Actuator Recovery Enhancement (FLARE) system. In [12], a theoretical framework was developed for retro-fitting reconfigurable flight control laws to accommodate severe structural damage and the resulting state dependent disturbances, using prior information about the baseline controller. In [13], a decentralised retro-fitted adaptive FTC scheme was designed for nonlinear models to accommodate loss of effectiveness in flight control actuators. The loss of effectiveness parameters and retro-fit control signals are generated locally to deal with loss of effectiveness in the actuators. In this chapter the baseline yaw damping controller in Sect. 6.3.1 is based on arguments in [14] and the eigenstructure assignment has been performed based on the toolbox associated with [3].

References

1. Härkegård, O., Glad, S.T.: Resolving actuator redundancy—optimal control vs. control allocation. Automatica **41**, 137–144 (2005)
2. Shin, D., Moon, G., Kim, Y.: Design of reconfigurable flight control system using adaptive sliding mode control: actuator fault. Proc. Inst. Mech. Eng. Part G: J. Aerosp. Eng. **219**, 321–328 (2005)
3. Liu, G.P., Patton, R.J.: Eigenstructure Assignment for Control Systems Design. Wiley, Chichester (1998)
4. Ganguli, S., Marcos, A., Balas, G.J.: Reconfigurable LPV control design for Boeing 747-100/200 longitudinal axis. In: Proceedings of the American Control Conference (2002)
5. Duan, G.: Parametric eigenstructure assignment via output feedback based on singular value decompositions. IEE Control Theory Appl. **150**(1), 93–100 (2003)
6. Hess, R.A., Wells, S.R.: Sliding mode control applied to reconfigurable flight control design. J. Guid. Control Dyn. **26**, 452–462 (2003)
7. Shtessel, Y., Buffington, J., Banda, S.: Tailless aircraft flight control using multiple time scale re-configurable sliding modes. IEEE Trans. Control Syst. Technol. **10**, 288–296 (2002)
8. Alwi, H., Edwards, C., Tan, C.P.: Fault Detection and Fault Tolerant Control Using Sliding Modes. Advances in Industrial Control Series. Springer, Berlin (2011)
9. Wohletz, J.M.: Retrofit Systems for Reconfiguration in Civil Aviation. PhD thesis, MIT (2000)
10. Doyle, M.E.: Retrofit reconfigurable flight control system and the F/A-18C. Master's thesis, University of Tennessee - Knoxville (2006)
11. Bošković, J.D., Bergstrom, S.E., Mehra, R.K.: Retrofit reconfigurable flight control in the presence of control effector damage. In: Proceedings of the American Control Conference, pp. 2652–2657 (2005)
12. Bošković, J.D., Prasanth, R., Mehra, R.K.: Retrofit fault-tolerant flight control design under control effector damage. J. Guid. Control Dyn. **30**(3), 703–712 (2007)
13. Bošković, J.D.: A new decentralized retrofit adaptive fault-tolerant flight control design. In: International Journal of Adaptive control and signal Processing (2012)
14. Farineau, J.: Lateral electric flight control laws of a civil aircraft based upon eigenstructure assignment technique. In: American Institute of Aeronautics and Astronautics (1989)

Chapter 7
Nonlinear Integral Sliding Mode

Many of the existing FTC schemes in the literature are based on linear plant representations and are therefore only valid in the vicinity of the designed trim point. Therefore, one of the main challenges for practical implementation, especially for aircraft, is to ensure good performance for a wide range of operating conditions. Some of the linear based designs can be extended to handle variations in operating conditions, but direct nonlinear methods such as nonlinear dynamic inversion (NDI) and backstepping provide equally viable alternatives—with many benefits compared to the extended linear cases. One obvious benefit is the direct exploitation of the well-known aircraft equations of motion, which provides good and consistent performance throughout the flight envelope. This chapter presents a nonlinear fault tolerant scheme for longitudinal control of an aircraft system, comprising an integral sliding mode control allocation scheme and a backstepping structure. In fault-free conditions, the closed-loop system is governed by the backstepping controller and the integral sliding mode control allocation scheme only influences the performance if faults/failures occur in the primary control surfaces. In this situation the allocation scheme redistributes the control signals to the secondary control surfaces and the scheme is able to tolerate total failures in the primary actuator. A backstepping scheme taken from the existing literature is designed for flight path angle tracking (based on the nonlinear equations of motion) and this is used as the underlying baseline controller. The efficacy of the scheme is demonstrated using the RECOVER benchmark model.

7.1 Nonlinear Aircraft Model

In this chapter, the longitudinal motion of a rigid aircraft will be considered. Such a model is typically given by four differential equations

M.T. Hamayun et al., *Fault Tolerant Control Schemes Using Integral Sliding Modes*, Studies in Systems, Decision and Control 61,
DOI 10.1007/978-3-319-32238-4_7

$$\dot{V}_{tas} = \frac{1}{m}\left(-D + T_n \cos(\alpha + \sigma_T) - mg \sin\gamma\right) \tag{7.1}$$

$$\dot{\alpha} = \frac{1}{mV_{tas}}\left(-L - T_n \sin(\alpha + \sigma_T) + mg\cos\gamma\right) + q \tag{7.2}$$

$$\dot{\theta} = q \tag{7.3}$$

$$\dot{q} = \frac{1}{I_y}\left(M + T_n l_{tz} \cos\sigma_T\right) \tag{7.4}$$

where $V_{tas}, \alpha, \theta, q, \gamma$ represent true air speed, angle of attack, pitch angle, pitch rate and flight path angle respectively. The parameters in (7.1)–(7.4) are $m, g, I_y, T_n, l_{tz}, \sigma_T$ which represent mass, gravity, the body axis moment of inertia, total engine thrust, the distance from the engine centre line to the fuselage reference line and the engine inclination angle respectively.

Define the state vector as $x = \text{col}(V_{tas}, \alpha, \theta, q)$, then the drag force, lift force and pitch moments (D, L, M) from (7.1) to (7.4) can be written as:

$$D = \bar{q}SC_D(x, \delta) \tag{7.5}$$

$$L = \bar{q}SC_L(x, \delta) \tag{7.6}$$

$$M = \bar{q}S\bar{c}\left(C_m(x, \delta) + \Delta(x)\right) \tag{7.7}$$

where the dynamic pressure

$$\bar{q} = \frac{1}{2}\rho_{air}V_{tas}^2 \tag{7.8}$$

and $S, \bar{c}, \rho_{air}$ represent the wing area, wing mean aerodynamic chord and air density respectively. The dimensionless drag force, lift force and pitch moment coefficients $C_D(x, \delta)$, $C_L(x, \delta)$ and $C_m(x, \delta)$ are functions of the states and control surface deflections, and are usually obtained through wind tunnel and flight tests. This data is then used to create an aerodynamic database in the form of a lookup table. For the RECOVER model, this data is available. The term $\Delta(x)$ in (7.7) represents unmodelled dynamics which are not considered during the design, but which appear as part of the high fidelity model in RECOVER. This term is explicitly given by

$$\Delta(x) = -\frac{1}{\bar{c}}\left(C_D \sin\alpha + C_L \cos\alpha\right)\bar{x}_{cg} + \frac{\bar{c}\dot{\alpha}}{V_{tas}}\left(C_{m_{\dot{\alpha}}} - \frac{\bar{x}_{cg}}{\bar{c}}C_{L_{\dot{\alpha}}}\cos\alpha\right) \tag{7.9}$$

where $\bar{x}_{cg} = x_{cg_{ref}} - x_{cg}$ represents the difference between the actual and the reference x-axis centre of gravity. In this chapter it is assumed that $\Delta(x)$ is unknown.

7.1.1 Strict Feedback Form

To design the ISM scheme and the baseline backstepping control law, approximations will be made to the longitudinal aircraft dynamics in (7.1)–(7.4) to create a representation in 'strict feedback form'.[1] Here, the following simplifications are introduced.

Assumption 7.1 It is assumed that V_{tas} remains constant: i.e. $\dot{V}_{tas} \approx 0$.

Assumption 7.2 It is assumed that a change to the elevator mainly affects the pitch moment, and the effect on lift and drag can be neglected (i.e. $C_D(\delta) = 0$, $C_L(\delta) = 0$).

Remark 7.1 Assumption 7.1 can be achieved by introducing a separate feedback loop based on the measured speed and the auto throttle.

Remark 7.2 Assumption 7.2 is common in the flight dynamics literature.[2]

Using Assumptions 7.1 and 7.2 together with (7.5)–(7.7), and replacing $\dot{\alpha}$ with $\gamma = \theta - \alpha$ (i.e. flight path angle) to remove the dependency on q, the longitudinal dynamics in (7.1)–(7.4), for controller design purposes, can be rewritten as

$$\dot{\gamma} = \frac{1}{mV_{tas}} \left(\bar{q}SC_L(x) + T_n \sin(\theta - \gamma + \sigma_T) - mg\cos\gamma\right) \tag{7.10}$$

$$\dot{\theta} = q \tag{7.11}$$

$$\dot{q} = \frac{1}{I_y} \left(\bar{q}S\bar{c}\left(C_m(x,\delta) + \Delta(x)\right) + T_n l_{tz}\cos\sigma_T\right) \tag{7.12}$$

In (7.10)–(7.12), the control surface deflection δ only appears in Eq. (7.12) and this allows many nonlinear schemes (e.g. backstepping and nonlinear dynamic inversion) to be used for control law design.

Note that (7.10)–(7.12) are only used for controller design; in the simulations the original Eqs. (7.1)–(7.4), and in fact the more detailed RECOVER benchmark from Appendix A, are used to test the design.

The pitch moment coefficient can be written as a function of the states and control surfaces:

$$C_m(x,\delta) = C_m(x) + \frac{dC_m}{d\delta_e}\delta_e + \frac{dC_m}{d\delta_s}\delta_s \tag{7.13}$$

where δ_e, δ_s are elevator and horizontal stabiliser deflections respectively. Combining Eq. (7.13) with Eqs. (7.10)–(7.12), simplified equations of motion can be written in the form

[1] See for example [1].

[2] See for example [2].

$$\underbrace{\begin{bmatrix}\dot{\gamma}\\ \dot{\theta}\\ \dot{q}\end{bmatrix}}_{\dot{x}(t)} = \underbrace{\begin{bmatrix}\frac{1}{mV_{tas}}\left(\bar{q}SC_L(x) + T_n\sin(\alpha+\sigma_T) - mg\cos\gamma\right)\\ q\\ \frac{1}{I_y}\left(\bar{q}S\bar{c}C_m(x) + T_n l_{tz}\cos\sigma_T\right)\end{bmatrix}}_{f(x)} + \underbrace{\left[\begin{array}{c|c}0 & 0\\ 0 & 0\\ \frac{1}{I_y}\bar{q}S\bar{c}\frac{dC_m}{d\delta_e} & \frac{1}{I_y}\bar{q}S\bar{c}\frac{dC_m}{d\delta_s}\end{array}\right]}_{g(x)} \underbrace{\begin{bmatrix}\delta_e\\ \delta_s\end{bmatrix}}_{u(t)} + \underbrace{\begin{bmatrix}0\\ 0\\ \frac{1}{I_y}\bar{q}S\bar{c}\end{bmatrix}}_{b(x)}\Delta(x) \tag{7.14}$$

The vector $g_e(x)$ is associated with the primary control surface (the elevator). Conversely the vector $g_s(x)$ is the secondary control surface (the stabiliser) which will be used when faults/failures occur on the primary control surface (see Fig. A.2).

Remark 7.3 Note that the term $\frac{dC_m}{d\delta_e}$ is assumed to be available either by online parameter estimation or from a lookup table. In this chapter the information is obtained from a lookup table. However imprecision in the knowledge of $\frac{dC_m}{d\delta_e}$ will appear as matched uncertainty which will be suppressed by the sliding mode terms in the controller. The thrust T_n is also assumed to be available by converting engine pressure ratio (which is the commanded signal from the speed controller) into thrust through a lookup table. (Recall it is assumed speed is controlled by a separate "auto-throttle" control loop.)

To simplify the subsequent analysis, Eq. (7.14) can be written as

$$\begin{bmatrix}\dot{x}_1\\ \dot{x}_2\end{bmatrix} = \begin{bmatrix}f_1(x)\\ f_2(x)\end{bmatrix} + g(x)u(t) + b(x)\Delta(x) \tag{7.15}$$

where the state sub-vector $x_1 = \text{col}(\gamma, \theta)$ and $x_2 = q$. The input distribution vector

$$g(x) = \left[\, g_e(x) \middle| g_s(x) \,\right] = \left[\begin{array}{c|c}0_{2\times 1} & 0_{2\times 1}\\ g_1(x) & g_2(x)\end{array}\right] \tag{7.16}$$

where $g_1(x) = \frac{1}{I_y}\bar{q}S\bar{c}\frac{dC_m}{d\delta_e}$ and $g_2(x) = \frac{1}{I_y}\bar{q}S\bar{c}\frac{dC_m}{d\delta_s}$. The disturbance matrix $b(x)$ in (7.14) can be written as

$$b(x) = \begin{bmatrix}0_{2\times 1}\\ b_1(x)\end{bmatrix} \tag{7.17}$$

where $b_1(x) = \frac{1}{I_y}\bar{q}S\bar{c}$.

7.2 Control Law Development

Consider the effect of faults on each actuator modelled by

$$u_i^e(t) = w_i(t)u_i(t) + \xi(t) \qquad \text{for } i = 1, 2 \tag{7.18}$$

where the scalars $0 \leq w_i(t) \leq 1$, and $\xi(t)$ is an exogenous signal. Here $u_i^e(t)$ represents the effective control signal which influences the aircraft dynamics, taking into account the detrimental impact of the fault. The scalars $w_1(t)$ and $w_2(t)$ are the so-called control surface effectiveness gains associated with the primary (elevator) and secondary (stabiliser) control surfaces respectively. If $w_i(t) = 1$, the corresponding ith control surface is working perfectly, while $w_i(t) = 0$ indicates a total failure. If $0 < w_i(t) < 1$, a partial fault is present in the ith control surface. Ignoring the term $\xi(t)$ which does not affect stability,[3] the system in (7.15) subject to potentially faulty actuators can be written in the form

$$\begin{bmatrix} \dot{x}_1 \\ \dot{x}_2 \end{bmatrix} = \begin{bmatrix} f_1(x) \\ f_2(x) \end{bmatrix} + \begin{bmatrix} 0_{2\times 1} & 0_{2\times 1} \\ g_1(x) & g_2(x) \end{bmatrix} W(t)u(t) + b(x)\Delta(x) \tag{7.19}$$

where the matrix $W(t) = \text{diag}(w_1(t), w_2(t))$.

For simplicity, factorise $g(x)$ so that (7.15) can be written as

$$\begin{bmatrix} \dot{x}_1 \\ \dot{x}_2 \end{bmatrix} = \begin{bmatrix} f_1(x) \\ f_2(x) \end{bmatrix} + g_1(x) \begin{bmatrix} 0_{2\times 1} & 0_{2\times 1} \\ 1 & g_2^s(x) \end{bmatrix} W(t)u(t) + b(x)\Delta(x) \tag{7.20}$$

where

$$g_2^s(x) = \frac{g_2(x)}{g_1(x)} \tag{7.21}$$

For the aircraft example considered here, $g_1(x)$ and $g_2(x)$ are both nonzero since $\frac{dC_m}{d\delta_e} \neq 0$ and $\frac{dC_m}{d\delta_s} \neq 0$ for typical regions in the flight envelope as shown in Fig. 7.1a, b. This guarantees the inverse in (7.21) exists and the system (7.20) is controllable when faults/failures occur on the elevator. (Note that the maximum ceiling is 45,000 ft and maximum level speed is Mach 0.895 at 30,000 ft).

[3] Although of course it has a detrimental impact on performance, since it acts as an external disturbance to the post-fault system.

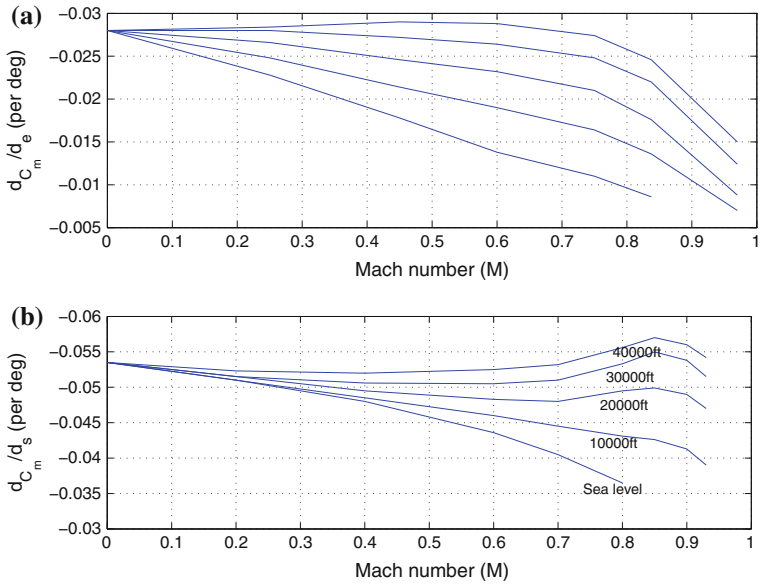

Fig. 7.1 Pitching moment coefficient due to elevator and stabiliser deflections [3, 4]. **a** Elevator. **b** Stabiliser

7.2.1 Nominal Backstepping Control Law

Assume that for the nominal system

$$\dot{x}(t) = f(x) + g_e(x)u_0(t) \tag{7.22}$$

a controller

$$u_0(x) = \mathscr{K}(x) \tag{7.23}$$

has been designed using the primary control surface such that the nominal closed-loop system

$$\dot{x}(t) = f(x) + g_e(x)\mathscr{K}(x) \tag{7.24}$$

is stable. In this chapter, the baseline controller for the elevator is given by a backstepping control scheme

$$u_0(t) = \mathscr{K}(x) = \left(\frac{dC_m}{d\delta_e}\right)^{-1}\left(\frac{I_y\dot{q}_{des} - \bar{q}S\bar{c}C_m(x) - T_n l_{tz}\cos\sigma_T}{\bar{q}S\bar{c}}\right) \tag{7.25}$$

where

$$\dot{q}_{des} = -\begin{bmatrix} \kappa_1\kappa_2\kappa_3 & \kappa_2\kappa_3 & \kappa_3 \end{bmatrix} \begin{bmatrix} \gamma - \gamma_{ref} \\ \theta - \gamma_{ref} - \alpha_0 \\ q \end{bmatrix} \tag{7.26}$$

where α_0 is the angle of attack at a steady state condition. The gains $\kappa_1, \kappa_2, \kappa_3$ must be chosen to satisfy

$$\begin{aligned} \kappa_1 &> -1 \\ \kappa_2 &> 0 \\ \kappa_3 &> \begin{cases} \kappa_2 & \text{if } \kappa_1 \leq 0 \\ \kappa_2(1+k_1) & \text{if } \kappa_1 > 0 \end{cases} \end{aligned} \tag{7.27}$$

7.2.2 Control Allocation

Consider the situation when the actuator effectiveness gains $w_1(t)$ and $w_2(t)$ are not perfectly known. Their estimates $\hat{w}_1(t)$ and $\hat{w}_2(t)$ are assumed to be computed by an FDI scheme (which is required for the approach presented in this chapter). Consequently, as part of the estimation process, and by 'clipping' the estimates arising from the calculations if necessary, it can be assumed that they satisfy $0 \leq \hat{w}_1(t) \leq 1$ and $0 < \hat{w}_2(t) \leq 1$ if they are to represent realistic effectiveness levels. However, these estimates may not be perfect, and so for analysis purposes

Assumption 7.3 It is assumed that $\hat{w}_1(t)$ and $\hat{w}_2(t)$ are related to the real values $w_1(t)$ and $w_2(t)$ according to:

$$\underbrace{\begin{bmatrix} w_1(t) & 0 \\ 0 & w_2(t) \end{bmatrix}}_{W(t)} = \underbrace{\begin{bmatrix} \hat{w}_1(t) & 0 \\ 0 & \hat{w}_2(t) \end{bmatrix}}_{\hat{W}(t)} \begin{bmatrix} 1+\delta_1(t) & 0 \\ 0 & 1+\delta_2(t) \end{bmatrix} \tag{7.28}$$

In (7.28) the scalars $\delta_1(t)$ and $\delta_2(t)$ represent imperfections in the estimates and are assumed to satisfy

$$\delta_{\min} \leq \delta_1(t), \quad \delta_2(t) \leq \delta_{\max} \tag{7.29}$$

where $\delta_{\min}, \delta_{\max}$ are known scalars and $\max\{|\delta_{\min}|, |\delta_{\max}|\} < 1$.

The expressions in (7.28) ensure that the true values of the effectiveness levels

$$w_i(t) \in \left[\hat{w}_i(t) + \delta_{min}\hat{w}_i(t),\ \hat{w}_i(t) + \delta_{max}\hat{w}_i(t) \right] \tag{7.30}$$

and importantly, since $\delta_{min} > -1$, the expression in (7.30) guarantees $w_i(t) \geq 0$. Based on (7.28), Eq. (7.20) can be written as

$$\begin{bmatrix}\dot{x}_1(t)\\ \dot{x}_2(t)\end{bmatrix}=\begin{bmatrix}f_1(x)\\ f_2(x)\end{bmatrix}+g_1(x)\begin{bmatrix}0_{2\times1} & 0_{2\times1}\\ 1 & g_2^s(x)\end{bmatrix}\begin{bmatrix}\hat{w}_1(t)(1+\delta_1) & 0\\ 0 & \hat{w}_2(t)(1+\delta_2)\end{bmatrix}u(t)+b(x)\Delta(x) \tag{7.31}$$

For the potentially faulty system in (7.31), consider as a control law

$$u(t)=N(x)\underbrace{(\mathscr{K}(x)+\nu_n(t))}_{v(t)} \tag{7.32}$$

where the signal $\nu_n(t)$ is associated with the sliding mode component of the control law, and will be defined formally later in the chapter. The 'control allocation matrix' $N(x)$ is given by

$$N(x)=\begin{bmatrix}1\\ \frac{1-\hat{w}_1(t)}{\hat{w}_2(t)g_2^s(x)}\end{bmatrix} \tag{7.33}$$

assuming $\hat{w}_2(t)\neq 0$ (i.e. assuming that the secondary control surface is failure-free) and exploiting the fact that $g_2^s(x)\neq 0$.

Remark 7.4 Note that the control allocation matrix in (7.33) is different to the ones used in the earlier chapters (although it is related to the retro-fit scheme in Chap. 6). Here the control allocation matrix is very bespoke and utilises the specific aircraft equations of motion—especially the strict feedback form in (7.14).

Substituting (7.28) and (7.32)–(7.33) into (7.31) yields (after some straightforward algebra)

$$\underbrace{\begin{bmatrix}\dot{x}_1\\ \dot{x}_2\end{bmatrix}}_{\dot{x}(t)}=\underbrace{\begin{bmatrix}f_1(x)\\ f_2(x)\end{bmatrix}}_{f(x)}+\left(\underbrace{\begin{bmatrix}0_{2\times1}\\ g_1(x)\end{bmatrix}}_{g_e(x)}+\underbrace{\begin{bmatrix}0_{2\times1}\\ g_1(x)\hat{\delta}(t)\end{bmatrix}}_{\hat{g}_e(x)}\right)\underbrace{(\mathscr{K}(x)+\nu_n(t))}_{u(t)}+\underbrace{\begin{bmatrix}0_{2\times1}\\ b_1(x)\end{bmatrix}}_{b(x)}\Delta(x) \tag{7.34}$$

where

$$\hat{\delta}(t):=\big(\hat{w}_1(t)\delta_1(t)+(1-\hat{w}_1(t))\delta_2(t)\big) \tag{7.35}$$

Since by assumption $0\leq\hat{w}_1(t)\leq 1$, it follows that $\hat{\delta}(t)\in\begin{bmatrix}\delta_1(t) & \delta_2(t)\end{bmatrix}$ (i.e. it belongs to the line segment between δ_1 and δ_2), and therefore $\delta_{\min}\leq\hat{\delta}(t)\leq\delta_{\max}$.

Remark 7.5 Notice from Eq. (7.33) that during fault-free conditions and when the actuator effectiveness estimate is perfect, (i.e. when $\widehat{W}(t)=W(t)=I_2$, and therefore $\hat{w}_1(t)=1$) the control signal $u(t)$ becomes

$$u(t)=\begin{bmatrix}\mathscr{K}(x)+\nu_n(t)\\ 0\end{bmatrix} \tag{7.36}$$

Equation (7.36) shows only the primary control surfaces are used. In general if $\widehat{W}(t) \neq I$, then the lower component in (7.33) is nonzero and a control signal is sent to the secondary actuator.

7.2.3 Integral Sliding Mode Design

In this section, an expression for the control law component $\nu_n(t)$ in (7.32) will be developed. In particular this term will add robustness to the control allocation scheme presented in Sect. 7.2.

Define a time-varying sliding surface as

$$\mathscr{S} = \{x \in \mathbb{R}^3 : \quad \sigma(t) = 0\} \tag{7.37}$$

where

$$\sigma(t) := Gx(t) - Gx(0) - G\int_0^t (f(x) + g_e(x)\mathscr{K}(x))d\tau \tag{7.38}$$

and $G \in \mathbb{R}^{1\times 3}$ is the design freedom. In this chapter the gain will be chosen as

$$G := \begin{bmatrix} 0 & 0 & 1 \end{bmatrix} \tag{7.39}$$

First it will be demonstrated that if a sliding motion occurs on $\mathscr{S}$ given in (7.37)–(7.38), then fault tolerance is achieved. Subsequently a control law $v(t)$, to achieve and maintain sliding will be presented.

Proposition 7.1 *If a sliding mode is maintained on $\mathscr{S}$ given by (7.37)–(7.38), then the associated sliding motion is governed by the stable system (7.24)–(7.25).*

Proof From the definition of G in (7.39), it follows that the scalar

$$Gg_e(x) = g_1(x) \neq 0, \quad G\hat{g}_e(x) = g_1(x)\hat{\delta}(t), \quad Gb(x) = b_1(x) \tag{7.40}$$

The fact that $Gg_e(x) \neq 0$ guarantees the existence of an unique equivalent control, and so the sliding mode control problem is well-posed. Taking the derivative of (7.38) along the trajectory of (7.31) and substituting from (7.34) yields

$$\begin{aligned} \dot{\sigma}(t) &= G\dot{x}(t) - G(f(x) + g_e(x)\mathscr{K}(x)) \\ &= Gg_e(x)\nu_n(t) + G\hat{g}_e(x)(\mathscr{K}(x) + \nu_n(t)) + Gb(x)\Delta(x) \\ &= g_1(x)(1 + \hat{\delta}(t))\nu_n(t) + g_1(x)\hat{\delta}(t)\mathscr{K}(x) + b_1(x)\Delta(x) \end{aligned} \tag{7.41}$$

where $\nu_n(t)$ from (7.32) will be defined shortly to ensure a sliding motion on $\mathscr{S}$ can be maintained. During sliding $\dot{\sigma}(t) = \sigma(t) = 0$, and therefore since $g_1(x) \neq 0$ the 'equivalent control' necessary to maintain sliding, is given by equating the left hand

side of (7.41) to zero and solving the resulting algebraic equation to yield

$$v_{eq}(t) = -\left(g_1(x)\left(1+\hat{\delta}(t)\right)\right)^{-1}\left(g_1(x)\hat{\delta}(t)\mathscr{K}(x) + b_1(x)\Delta(x)\right) \tag{7.42}$$

The equations of motion during the sliding mode can be obtained by substituting (7.42) into (7.34) to yield

$$\dot{x}(t) = f(x) + g_e(x)\mathscr{K}(x) \tag{7.43}$$

■

Remark 7.6 Note that Eq. (7.43) is the closed-loop system associated with the baseline controller in (7.23), and that the unknown term $\Delta(x)$ does not appear. This is because $\Delta(x)$ is 'matched' uncertainty and is therefore rejected by the sliding mode controller. Note that the choice of G in (7.39) means that the matrix G is fixed which simplifies the analysis. Furthermore since $(I - g_e(Gg_e)^{-1}G) = \text{diag}(1, 1, 0)$, the contraction properties discussed in Sect. 2.7.4 are still obtained since

$$\|I - g_e(Gg_e)^{-1}G\| = 1$$

(which is the minimum achievable value of the norm over all possible values of G).

The remainder of this section presents a controller to ensure sliding can be achieved and maintained in the presence of faults, and formally demonstrates this is indeed the case.

Here, the sliding mode nonlinear term $v_n(t)$ is defined as

$$v_n(t) = -\rho(t,x)g_1(x)^{-1}\text{sign}\left(\sigma(t)\right) \quad \text{for } \sigma(t) \neq 0 \tag{7.44}$$

where the modulation gain $\rho(t, x)$ is any function satisfying

$$\rho(t,x) > \frac{|g_1(x)|\,\bar{\delta}\,|\mathscr{K}(x)| + |b_1(x)||\Delta(x)| + \eta_0}{(1-\bar{\delta})} \tag{7.45}$$

where $\bar{\delta} = \max\{|\delta_{\min}|, |\delta_{\max}|\} < 1$ and η_0 is small positive scalar. Note: here $\bar{\delta}$ will be used as an user defined parameter employed to select the level of tolerance to the error in estimation of the effectiveness gains that the controller can tolerate.

Proposition 7.2 *The control law given in (7.32), with the allocation matrix in (7.33), and the nonlinear injection term from (7.44) to (7.45), maintains a sliding motion provided* $\bar{\delta} < 1$ *and* $w_2(t) \neq 0$.

Proof Substituting from (7.44) into (7.41) yields

$$\dot{\sigma}(t) = -\rho(t,x)(1+\hat{\delta}(t))\text{sign}\left(\sigma(t)\right) + g_1(x)\hat{\delta}(t)\mathscr{K}(x) + b_1(x)\Delta(x) \tag{7.46}$$

To show that sliding is maintained, consider a positive definite candidate Lyapunov function

$$V(t) = \frac{1}{2}\sigma^2(t) \tag{7.47}$$

It follows from (7.46) to (7.47) that

$$\dot{V}(t) = -\rho(t,x)(1+\hat{\delta}(t))|\sigma(t)| + \sigma(t)g_1(x)\hat{\delta}(t)\mathscr{K}(x) + \sigma(t)b_1(x)\Delta(x) \tag{7.48}$$

Since

$$|\hat{\delta}(t)| < \bar{\delta} < 1 \tag{7.49}$$

using (7.49) and (7.45), Eq. (7.48) becomes

$$\begin{aligned}\dot{V}(t) &\leq |\sigma(t)|\left(-\rho(t,x)(1-|\hat{\delta}(t)|) + |g_1(x)|\,|\hat{\delta}(t)|\,|\mathscr{K}(x)| + |b_1(x)|\,|\Delta(x)|\right)\\ &\leq |\sigma(t)|\left(-\rho(t,x)(1-\bar{\delta}) + |g_1(x)|\,\bar{\delta}\,|\mathscr{K}(x)| + |b_1(x)|\,|\Delta(x)|\right)\\ &\leq -\eta_0|\sigma(t)| = -\eta_0\sqrt{2V(t)}\end{aligned} \tag{7.50}$$

This is sufficient to show that the 'reachability condition' is satisfied and sliding is maintained. ■

The final control signal $u(t)$ which is supplied to all the available control surfaces (primary and secondary) is given by substituting (7.44) into (7.32) to yield

$$u(t) = \underbrace{\begin{bmatrix} 1 \\ \frac{1-\hat{w}_1(t)}{\hat{w}_2(t)g_2^s(x)} \end{bmatrix}}_{N(x)} \underbrace{\left(\mathscr{K}(x) - \rho(t,x)g_1(x)^{-1}\text{sign}\,(\sigma(t))\right)}_{\nu_n(t)} \tag{7.51}$$

Remark 7.7 Note that (7.51) requires the estimates of actuator efficiency $\hat{w}_1(t)$ and $\hat{w}_2(t)$, but does not require knowledge of δ_1, δ_2 or $\Delta(x)$. The errors δ_1, δ_2 are only used in conjunction with $\hat{\delta}$ to prove sliding is maintained.

7.3 Simulations

7.3.1 RECOVER Benchmark Model

All the simulations that follow are based on the RECOVER model at a trim altitude of 2000 m, a mass of 263 tonnes, c.g. at 25 % MAC, a speed of 92.6 m/s and flap settings of 20 deg. The modulation gain $\rho(t,x)$ can be chosen based on worst case estimates of $|g_1(x)|$ and $|b_1(x)|$ in (7.45), obtained from graphs similar to those presented in

Fig. 7.1, together with bounds on $\Delta(t)$ in (7.9) using worst case bounds/estimates of the drag and lift coefficients C_D and C_L, together with the aerodynamic coefficients related to $\dot{\alpha}$. A possible structure for the modulation gain to satisfy (7.45) is

$$\rho(t,x) = \rho_2|\mathscr{K}(x)| + \rho_1\|x\| + \rho_0 \tag{7.52}$$

where the ρ_i are positive constants. Here the gain from (7.44) has been simply chosen as $\rho = 0.65$. This is very easy to implement and is shown to work well in simulation. This is in fact an aggressive choice for $\rho(t,x)$ because the nonlinear term in (7.44) can contribute a signal in the range $\begin{bmatrix} -0.65 & 0.65 \end{bmatrix}$ rad, to the value of the overall virtual control signal because of the signum term. The units of the control signal are radians[4] and so this range represents a significant portion of the available/allowable control signal variation.

Remark 7.8 Although the term $\Delta(x)$ from (7.9) has been excluded from the design process, it appears in the high fidelity full nonlinear model used for simulation. As discussed in Sect. 7.2.3, this will appear as matched uncertainty which will be suppressed by the sliding mode.

Remark 7.9 Note that an estimate of $W(t)$ from (7.15) can be obtained from any FDI scheme of choice. In large passenger aircraft, it is common to measure the actual control surface deflection for monitoring purposes. Consequently, in this chapter, it is assumed that $W(t)$ is estimated by comparing the measured control surface deflection and the command from the flight control system.[5] In particular since any mismatch resulting from errors in the estimate of $W(t)$ used in the controller appears as matched uncertainty, the controller is able to compensate.

7.3.2 Outer-Loop Control

In order to maintain V_{tas} at a setpoint during the simulations, a PD based auto-throttle has been implemented as a separate loop. The corresponding proportional and derivative gains have been chosen as $K_{p_{V_{tas}}} = 1$ and $K_{d_{V_{tas}}} = 0.5$. An outer-loop altitude control loop is also implemented as shown in Fig. 7.2, to provide a flight path reference signal to the inner-loop sliding mode-backstepping controller. This is based on a PID structure with gains $K_{p_{he}} = 0.001$, $K_{i_{he}} = 4 \times 10^{-5}$ and $K_{d_{he}} = 0.02$. Finally an Instrument Landing System (ILS) glide slope intercept and tracking facility is also included to create an automatic landing mode for the aircraft. This takes the form of a simple scalar feedback loop with proportional gain $K_{P_{GS}} = 7$.

[4] Although in all the plots they have been scaled and presented in terms of degrees because these units are more intuitive to most readers.

[5] As shown in [5], this is not an unrealistic assumption in aircraft systems. Using the same idea as in [6] (i.e. 'least squares' method), information provided by the actual actuator deflection is compared with the signals from the controller to provide estimates of the effectiveness of the actuators.

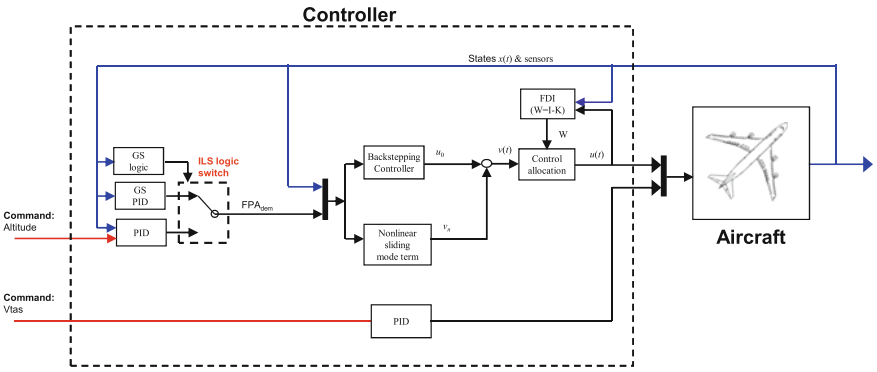

Fig. 7.2 Controller interconnection

In this chapter, since only the longitudinal axis is considered, the Instrument Landing System (ILS) switches between an altitude/FPA command and glide slope[6] (GS) tracking (as shown in Fig. 7.2). Specifically it changes the outer-loop control from being pilot commanded (i.e. altitude demand tracking), to an automated landing mode using the GS signal. When the aircraft is inside the GS coverage zone, the GS controller will become active and provides the inner-loop FPA command to the core longitudinal ISM controller, and no pilot input is required. This configuration can be found in all current large commercial aircraft in service (although the specific details of the outer-loop and inner-loop controller may differ[7]).

7.3.3 Results

The fault/failure cases and manoeuvres that are considered here are associated with the GARTEUR FM-AG16 benchmark scenarios: specifically concerning the elevator. The simulation begins at a low speed and a low altitude (92.6 m/s and 2000 m). The aircraft starts to descend to 900 m at 50 s and maintains altitude to intercept the ILS glide slope signal. Once the glide slope is intercepted, the aircraft descends at a commanded flight path angle of −3 deg towards the runway. The flare (the last manoeuvre before touchdown) is not implemented in RECOVER and therefore the aircraft altitude is held at 50 m above the runway. For consistency and for comparison, the actuator failures are set to occur at 100 s.

[6]The glide slope in the ILS provides vertical guidance to the aircraft during descent to the runway in order to provide an automated landing [6, 7]. The standard glide slope path demand is 3 deg. The glide slope signal is emitted by an antenna, located near the end of the runway and the glide slope provides the precise altitude required leading to the touchdown zone of the runway [7].

[7]For details see Sects. 11.8–11.10 in [8].

For the simulations which follow, the gains in the backstepping control law have been chosen as $\kappa_1 = 1$, $\kappa_2 = 0.6$ and $\kappa_3 = 3$. The control law (7.51) requires the estimates of actuator efficiency $\hat{w}_1(t)$ and $\hat{w}_2(t)$ which can be provided by a FDI scheme, or, more specifically by a fault estimation scheme. In this chapter, it will be assumed that a measurement of the actual actuator deflection is available.

7.3.3.1 Fault-Free

Figure 7.3a shows good flight path tracking while the outer-loop PID controller maintains tight control of speed. Figure 7.3b shows good altitude and glide slope tracking performance. Figure 7.3b shows the first demanded change of altitude to 900 m at 50 s. The second change in altitude is due to the tracking of the ILS glide slope—which is activated when the aircraft is within the range and altitude of the ILS signal. This activation is shown in Fig. 7.3b as a boolean signal; where 1 indicates GS capture. Once the ILS glide slope is activated at 448 s, the outer-loop ILS controller provides a flight path command (of about -3 deg in Fig. 7.3a) and forces the glide slope deviation error to zero as shown in Fig. 7.3b. Figure 7.3d shows that since there are no faults present, there is no control signal command to the stabiliser as shown in Fig. 7.3c.

7.3.3.2 Elevator Loss of Effectiveness

Figure 7.4 shows the results when a fault occurs which renders the elevator only 50 % effective. The same manoeuvre as in the previous fault-free test is considered. The fault is set to occur at 100 s. Figure 7.4a, b show no degradation of flight path angle, altitude and glide slope tracking in comparison to the fault-free case. Figure 7.4d confirms the decrease in the elevator effectiveness to 50 %. Figure 7.4d also shows that sliding is still maintained despite the uncertainty and the faults in the system. Figure 7.4c shows the effect of loss of effectiveness on elevator deflection. Now, the stabiliser has become active as the control signal is partially redistributed to compensate for the reduction of elevator effectiveness.

7.3.3.3 Elevator Float

Figure 7.5 shows the effect of an elevator float failure in which the control surface is unable to produce any moment, and moves freely in the direction of the airflow. This can occur due to the loss of hydraulics for example. Once the failure occurs at 100 s, as shown in Fig. 7.5c, the surface deflection becomes equal to the angle of attack of the aircraft as shown in Fig. 7.5a. After the failure, the stabiliser becomes active and tries to compensate for the failed elevator. Figure 7.5a, b show that no degradation in the flight path angle, altitude and glide slope tracking performance occurs despite the failure of the primary control surface. Finally Fig. 7.5d shows

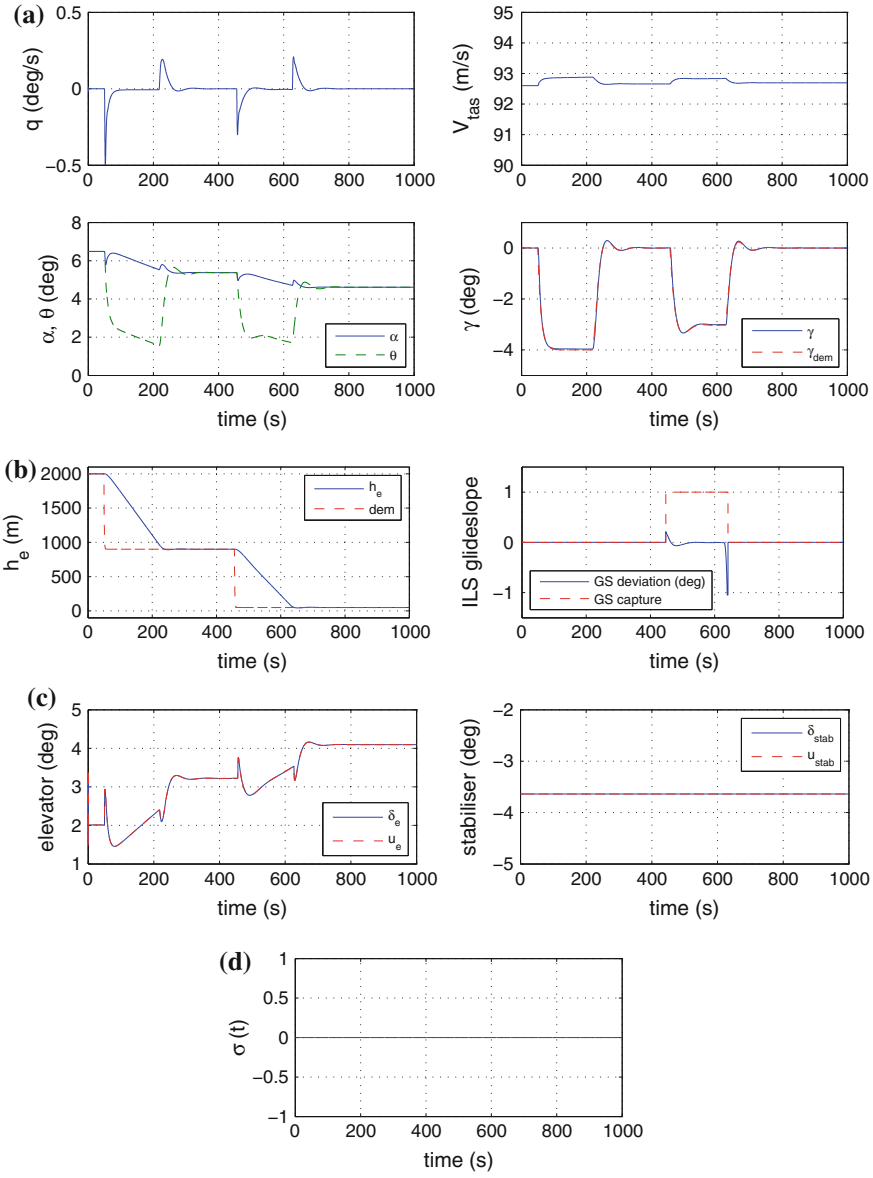

Fig. 7.3 Fault-free performances. **a** States. **b** Altitude and ILS glide slope deviation. **c** Control surface deflections. **d** Switching function $\sigma(t)$

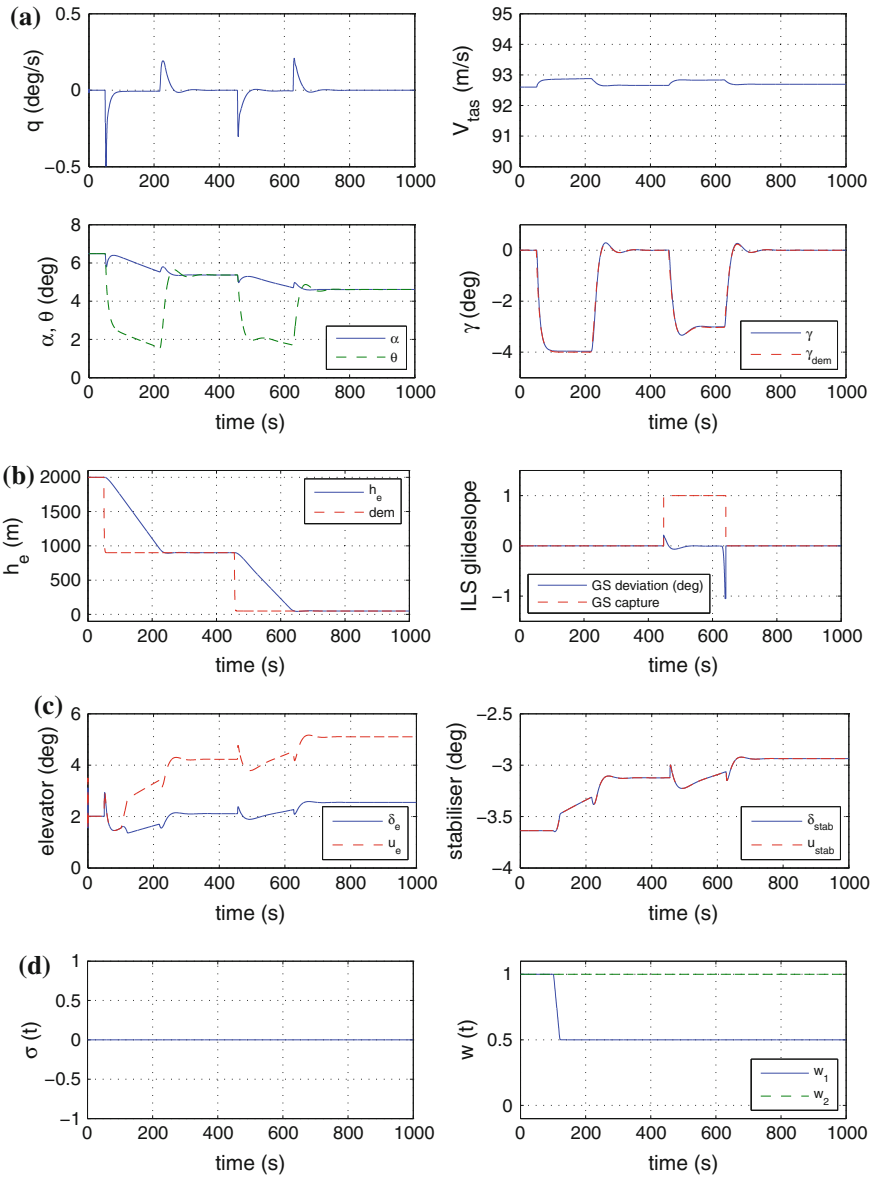

Fig. 7.4 Elevator loss of effectiveness performances. **a** States. **b** Altitude and ILS slope deviation. **c** Control surface deflections. **d** Switching function $\sigma(t)$ and actuator effectiveness $W(t)$

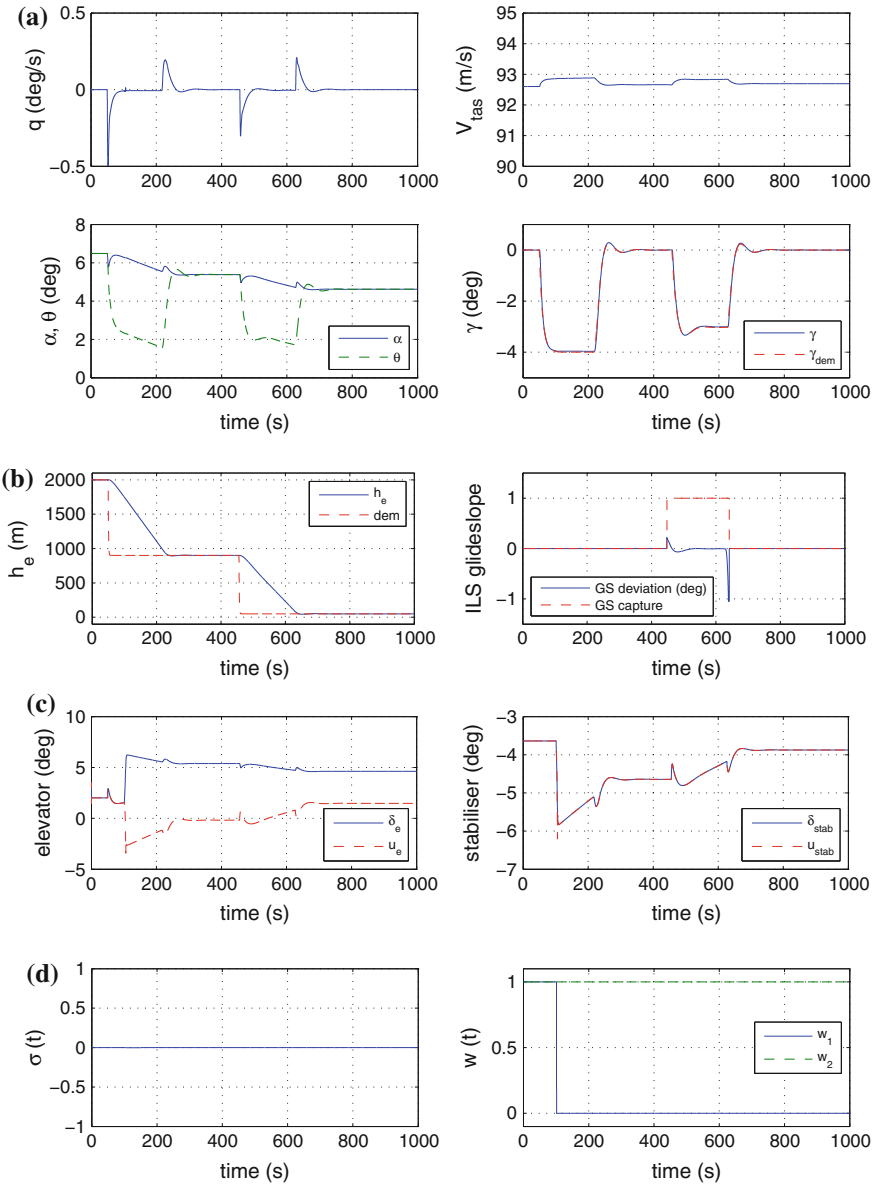

Fig. 7.5 Elevator float performances. **a** States. **b** Altitude and ILS slope deviation. **c** Control surface deflections. **d** Switching function $\sigma(t)$ and actuator effectiveness $W(t)$

the actuator effectiveness level and also shows no degradation in the sliding mode performance.

7.3.3.4 Elevator Float–Imperfect $\widehat{W}(t)$

Figure 7.6 shows a comparison between the fault-free and the case when the elevator suffers a *float failure* with imperfect estimation of the actuator effectiveness level $\widehat{W}(t)$. A float failure corresponds to the control surface 'floating' about its zero moment position, thus becoming ineffective. In the simulation, an elevator float is simulated by replacing the control signal by the angle of attack of the aircraft. In terms of Eq. (7.18), this can be modelled as

$$u_1^e(t) = 0 + \alpha(t) \tag{7.53}$$

which in terms of (7.18) equates to $w_1(t) = 0$ and $\xi(t) = \alpha(t)$. As a consequence the effective control signal $u_1^e(t)$ is completely disconnected from the command signal $u_1(t)$ generated by the control law. Figure 7.6a, b show that no degradation in the flight path angle, altitude and glide slope tracking performance occurs (all lines overlap) compared to the fault-free case, despite the failure of the primary control surface and imperfect estimation of the actuator effectiveness level $\widehat{W}(t)$. Figure 7.6b shows an altitude change command of 900 m at 50 s. A further altitude change to initiate tracking of the ILS glide slope is activated when the aircraft is within range of the ILS signal. Figure 7.6b shows the glide-slope-capture boolean signal equals 1 to indicate GS capture. Once the ILS glide slope is activated at 448 s, the outer-loop ILS controller provides the flight path command (of about -3 deg in Fig. 7.6a) forcing the glide slope deviation error to zero (Fig. 7.6b). Figure 7.6c indicates the effect of an elevator float failure in which the control surface is unable to produce any pitching moment, and moves freely in the direction of the airflow. This can occur due to the loss of hydraulics for example. Once the failure occurs at 100 s, as shown in Fig. 7.6c, the surface deflection becomes equal to the angle of attack of the aircraft as shown in Fig. 7.6a. After the failure, the stabiliser becomes active and tries to compensate for the failed elevator. The effect of imperfect estimation can be seen in Fig. 7.6d, where even though the elevator has totally failed, the elevator effectiveness estimation $\hat{w}_1(t)$ wrongly shows 50 % effectiveness. Note that in the fault-free case $w_1(t) = w_2(t) = 1$, but for simplicity, the lines are not labelled in Fig. 7.6d. Finally, Fig. 7.6d also shows no visible degradation in the sliding mode performance when compared to the fault-free case.

7.3.3.5 Elevator Lock in Place

Figure 7.7 shows the results of an elevator jammed in a non-trim position at 100 s. The non-trim jam position creates an extra moment which needs to be compensated for. As before, Fig. 7.7a, b show no visible degradation of flight path angle, altitude

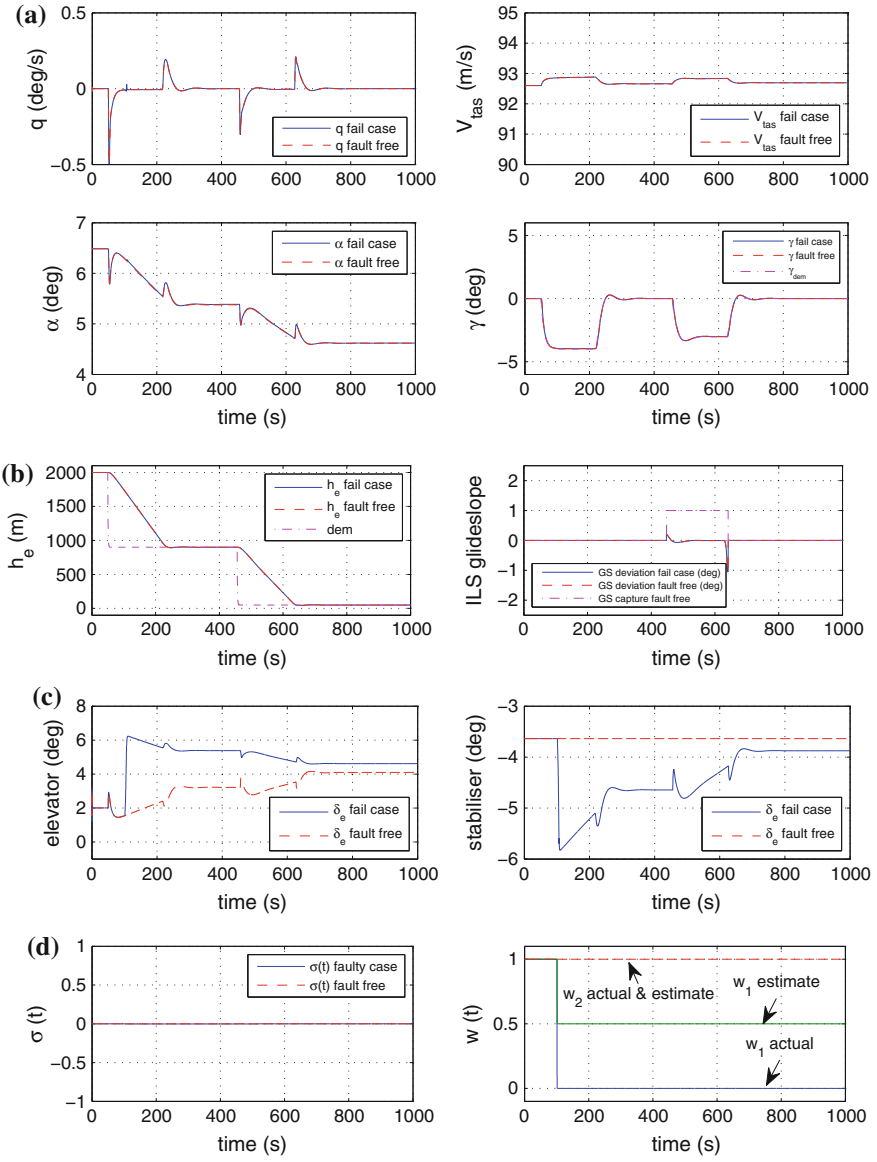

Fig. 7.6 Elevator float performances—imperfect $\widehat{W}(t)$. **a** States. **b** Altitude and ILS slope deviation. **c** Control surface deflections. **d** Switching function $\sigma(t)$ and actuator effectiveness $W(t)$

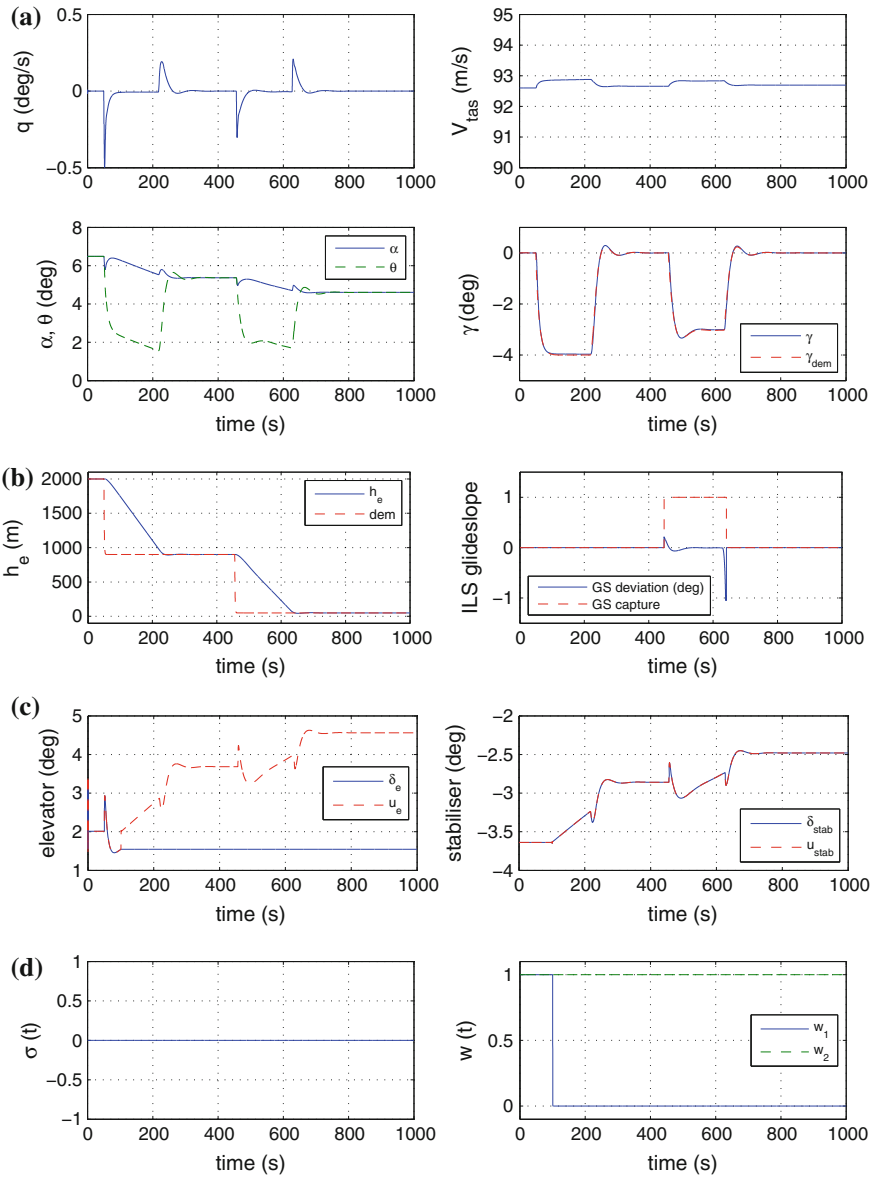

Fig. 7.7 Elevator lock in place performances. **a** States. **b** Altitude and ILS slope deviation. **c** Control surface deflections. **d** Switching function $\sigma(t)$ and actuator effectiveness $W(t)$

or glide slope tracking. Figure 7.7c shows that once the elevator jams at 100 s, the stabiliser becomes active as the control signal is reallocated.

7.3.3.6 Elevator Lock in Place—Imperfect $\widehat{W}(t)$

Figure 7.8 shows the comparison between fault-free and the case when an elevator jams at a non-trim position (at 100 s), and in the presence of imperfect actuator effectiveness estimation $\widehat{W}(t)$. The non-trim jam position creates an extra moment which needs to be compensated for. Note that the elevator jam is represented by

$$u_1^e(t) = 0 + u_1(t_f) \tag{7.54}$$

which in terms of (7.18) is associated with $w_1(t) = 0$ for all $t \geq t_f$ and $\xi(t) = u_1(t_f)$, where t_f is the time when the elevator failure occurs. Again this means for all $t \geq t_f$ the effective control signal $u_1^e(t)$ is decoupled from the command $u_1(t)$ determined by the control law. Figure 7.8c shows that once the elevator jams at 100 s, the stabiliser becomes active as the control signal is reallocated. The effect of the imperfect estimation can be seen in Fig. 7.8d. Here, although the elevator has totally failed due to the lock in place failure, the elevator effectiveness estimation $\hat{w}_1(t)$ wrongly shows 50 % effectiveness. Again, as in Fig. 7.6, despite the elevator jamming at a non-trim position, and imperfect estimation associated with $\hat{w}_1(t)$, Fig. 7.6a, b show no degradation in terms of all the tracking performance measures, compared to the fault-free case.

7.3.3.7 Elevator Float: Backstepping control only—Imperfect $\widehat{W}(t)$

Figure 7.9 shows a comparison between the fault-free case and when the elevator floats, using *only the baseline backstepping controller*, in the presence of imperfect actuator effectiveness estimation $\widehat{W}(t)$. The same control allocation scheme as in Figs. 7.6, 7.7 and 7.8 has been considered to redistribute the control signal to the stabiliser. In comparison to the fault-free condition, Fig. 7.9a shows that the unmodelled term $\Delta(x)$ from (7.9) causes imperfect tracking of the flight path angle. When compared with the fault-free condition, Fig. 7.9b shows a small difference in terms of altitude tracking as the imperfect flight path angle tracking has been compensated by the outer-loop altitude control. Whereas in Fig. 7.6a, b, the effect of the elevator failure and uncertainty has been totally compensated by the sliding mode, thus maintaining the same tracking performance as in the fault-free case.

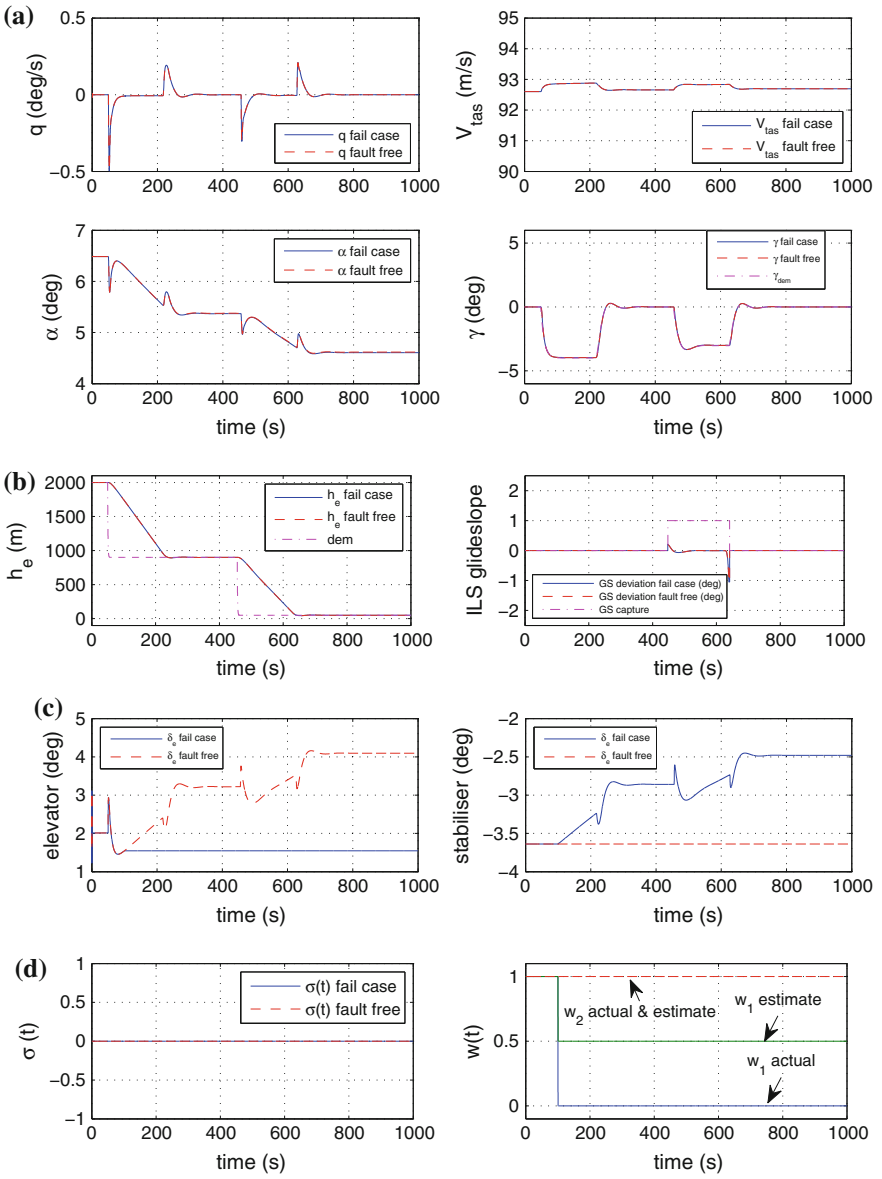

Fig. 7.8 Elevator lock in place performances—imperfect $\widehat{W}(t)$. **a** States. **b** Altitude and ILS slope deviation. **c** Control surface deflections. **d** Switching function $\sigma(t)$ and actuator effectiveness $W(t)$

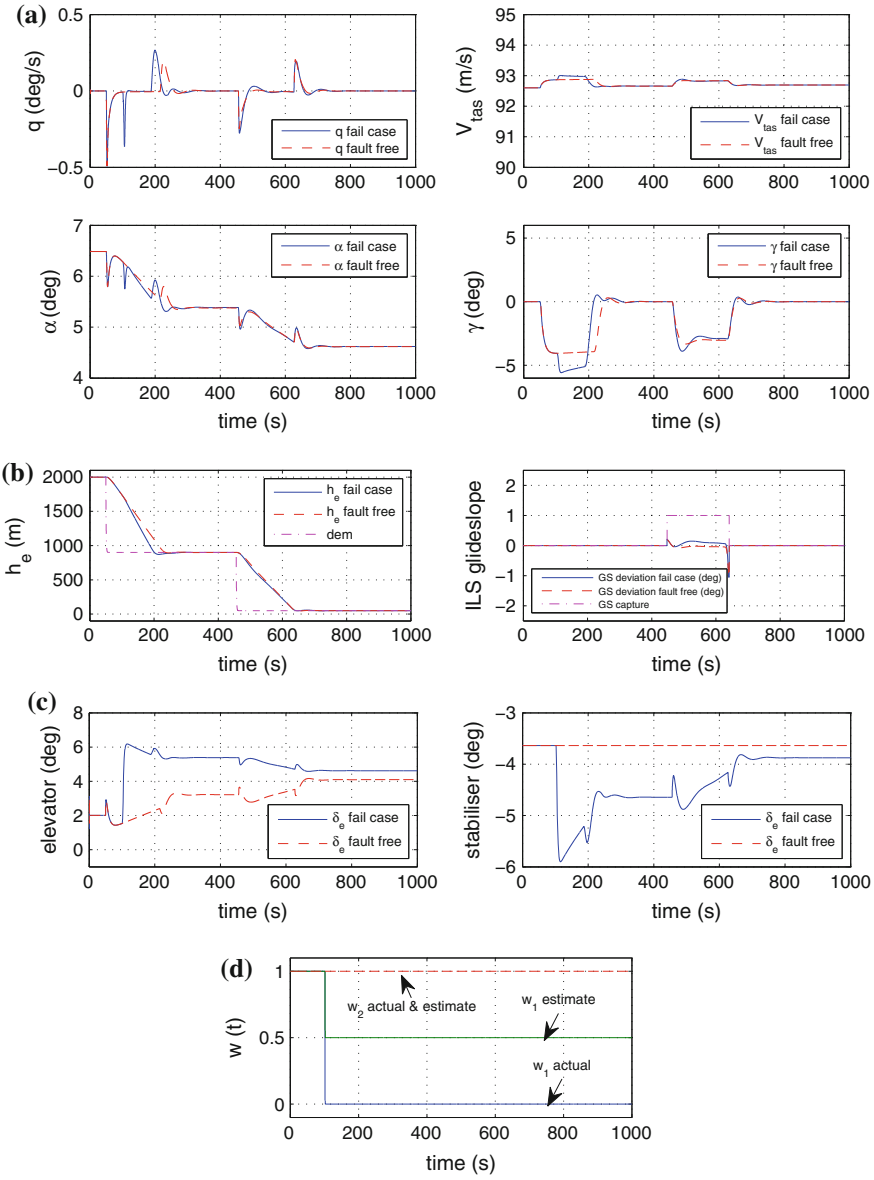

Fig. 7.9 Backstepping control only: elevator float performances—imperfect $\widehat{W}(t)$. **a** States. **b** Altitude and ILS slope deviation. **c** Control surface deflections. **d** Actuator effectiveness $W(t)$

7.4 Summary

This chapter has presented a nonlinear fault tolerant scheme for longitudinal aircraft control. The scheme is designed directly from the nonlinear longitudinal equations of motion and incorporates an integral sliding mode control allocation scheme together with a baseline backstepping control law for flight path angle tracking. In fault-free conditions only the primary control surface (the elevator) is used. However, when faults/failures occur, the integral sliding mode control allocation scheme is able to automatically provide robustness, and the control signals are redistributed to the redundant secondary control surface (the horizontal stabiliser). The control law has been tested on the RECOVER benchmark model. The simulations show that even in the presence of unmodelled dynamics (which have not been considered during the design process) excellent results are obtained for both nominal fault-free and fault/failure scenarios. Although the scheme in this chapter is described specifically in terms of the longitudinal equations of motion of an aircraft, in principle, the underlying methodology can be applied to other systems controlled by a backstepping structure, provided redundancy in the controls exists.

7.5 Notes and References

A number of authors have applied sliding mode techniques to the design of flight control laws: see for example [9–12]. However many of these papers do not consider fault tolerant control aspects and focus instead on the robustness properties introduced by the sliding modes. Some notable exceptions are [13, 14]; however these schemes (including [14]) can only deal with partial actuator faults and cannot cope with the problem of total actuator failure. Recent work on aircraft FTC using sliding modes (for example [6, 15, 16]) used a passive type of FTC control where the same controller is used for both the nominal fault-free case and in the event of faults/failures occurring. Despite the potential of these controllers, they are still based on linearisations of the plant dynamics about a specific operating condition [16, 17]. The combination of the backstepping ISM structure with control allocation presented in this chapter, allows the same controller to be used in both nominal fault-free and faulty situations, and distinguishes the ideas in this chapter from existing backstepping based SMC/ISM schemes for nonlinear systems (see for example [18–20]). Note that the choice of allocation matrix in Sect. 7.2.2 is different compared to the one in [16, 17], and takes into account the structure of the aircraft equations of motion considered in this chapter. For further details about the backstepping controller described in Sect. 7.2.1, see [1, 21]. Compared with the existing schemes designed from linear models, the underlying nonlinear backstepping controller has guaranteed levels of stability and performance for a wide range of flight conditions. Furthermore, the backstepping design from [1, 21] has a simple structure and does not require exact knowledge of the aircraft dynamics (e.g. the coefficient of forces and

moments). Some of the aerodynamic arguments used to justify the simplifications in the nonlinear equations of motion described in Sect. 7.1.1 are taken from [2].

References

1. Härkegård, O.: Backstepping and control allocation with applications to flight control. Ph.D. thesis, Division of Automatic Control, Department of Electrical Engineering Linköping University, Sweden (2003)
2. Etkin, B., Reid, L.D.: Dynamics of Flight: Stability and Control. Wiley, New York (1996)
3. Edwards, C., Lombaerts, T., Smaili, H.: Fault Tolerant Flight Control: A Benchmark Challenge, vol. 399. Springer, Berlin (2010)
4. Hanke, C., Nordwall, D.: The simulation of a jumbo jet transport aircraft. Volume II: Modelling data. Technical Report CR-114494/D6-30643-VOL2, NASA and The Boeing Company (1970)
5. Brière, D., Traverse, P.: Airbus A320/A330/A340 electrical flight controls: A family of fault-tolerant systems. In: Digest of Papers FTCS-23 The Twenty-Third International Symposium on Fault-Tolerant Computing, pp. 616–623 (1993)
6. Alwi, H., Edwards, C., Stroosma, O., Mulder, J.A.: Fault tolerant sliding mode control design with piloted simulator evaluation. AIAA J. Guid. Control Dyn. **31**(5), 1186–1201 (2008)
7. Alwi, H., Edwards, C., Tan, C.P.: Fault Detection and Fault Tolerant Control Using Sliding Modes. Advances in Industrial Control Series. Springer, Berlin (2011)
8. Mclean, D.: Automatic Flight Control Systems. Prentice-Hall, New York (1990)
9. Nonaka, K., Sugizaki, H.: Integral sliding mode altitude control for a small model helicopter with ground effect compensation. In: Proceedings of the American Control Conference (2011)
10. Wang, J., Zong, Q., Tian, B., Wang, F.: Flight control for hypersonic vehicle based on quasi-continuous integral high-order sliding mode. In: 24th Chinese Control and Decision Conference (CCDC) (2012)
11. Zhang, R., Sun, C., Zhang, J., Zhou, Y.: Second-order terminal sliding mode control for hypersonic vehicle in cruising flight with sliding mode disturbance observer. J. Control Theory Appl. **11**(2), 299–305 (2013)
12. Hu, Q., Xiao, B.: Adaptive fault tolerant control using integral sliding mode strategy with application to flexible spacecraft. J. Control Theory Appl. **44**(12), 2273–2286 (2013)
13. Hu, Q., Zhang, Y., Huo Xinga, X., Xiao, B.: Adaptive integral-type sliding mode control for spacecraft attitude maneuvering under actuator stuck failures
14. Peng, L., Jian-jun, M., Wen-qiang, L., Zhi-qiang, Z.: Adaptive conditional integral sliding mode control for fault tolerant flight control system. In: 7th International Conference on System Simulation and Scientific Computing (2008)
15. Alwi, H., Edwards, C., Stroosma, O., Mulder, J.A.: Evaluation of a sliding mode fault-tolerant controller for the EL AL incident. AIAA J. Guid. Control Dyn. **33**(3), 677–694 (2010)
16. Hamayun, M.T., Edwards, C., Alwi, H.: Design and analysis of an integral sliding mode fault tolerant control scheme. IEEE Trans. Autom. Control **57**(7), 1783–1789 (2012)
17. Alwi, H., Edwards, C.: Fault tolerant control using sliding modes with on-line control allocation. Automatica **44**, 1859–1866 (2008)
18. Rubagotti, M., Estrada, A., Castanos, F., Ferrara, A., Fridman, L.: Integral sliding mode control for nonlinear systems with matched and unmatched perturbations. IEEE Trans. Autom. Control **56**(11), 2699–2704 (2011)
19. Koshkouei, A.J., Zinober, A.S.I., Burnham, K.J.: Adaptive sliding mode backstepping control of nonlinear systems with unmatched uncertainty. Asian J. Control **6**(4), 447–453 (2004)
20. Davila, J.: Robust backstepping controller for aircraft dynamics. In: 18th IFAC World Congress (2011)
21. Härkegård, O., Glad, S.T.: A backstepping design for flight path angle control. In: Proceedings of the 39th IEEE Conference on Decision and Control, CDC, pp. 3570–3575 (2000)

Chapter 8
Linear Parameter Varying FTC Scheme Using Integral Sliding Modes

This chapter describes *an extension* of the FTC scheme described in Chap. 3 and considers Linear Parameter Varying (LPV) systems rather than LTI systems. LPV systems can be considered as an extension or generalisation of LTI systems. They represent a certain class of finite dimensional linear systems, in which the entries of the state-space matrices continuously depend on a time varying parameter vector which belongs to a bounded compact set. The objective is to synthesise an FTC scheme which will work over a wider range of operating conditions. To design the virtual control law, the varying input distribution matrix is factorised into a fixed and a varying matrix. As discussed earlier in the text, the virtual control law, designed using the ISM technique, is translated into the actual actuator commands using a CA scheme. In this way the controller is automatically 'scheduled' and closed-loop stability is established throughout the entire operating envelope. The FTC scheme can maintain closed-loop stability even in the presence of total failures of certain actuators, provided that redundancy is available in the system. The FTC scheme takes into account imperfect estimation of the actuator effectiveness levels and also considers an adaptive scheme for the nonlinear modulation gains to account for this estimation error. The efficacy of the FTC scheme is tested in simulation by applying it to an LPV model of a benchmark transport aircraft, previously used in the literature.

8.1 Problem Formulation

LPV methods are appealing for nonlinear plants which can be modelled as time varying systems with state dependent parameters which are measurable online. An LPV system can be defined in state-space representation form as

$$\dot{x}(t) = A(\rho)x(t) + B(\rho)u(t) \tag{8.1}$$

$$y(t) = C(\rho)x(t) + D(\rho)u(t) \tag{8.2}$$

M.T. Hamayun et al., *Fault Tolerant Control Schemes Using Integral Sliding Modes*, Studies in Systems, Decision and Control 61,
DOI 10.1007/978-3-319-32238-4_8

where the matrices are of appropriate dimensions and the time varying parameter vector $\rho(t)$ lies in a specified bounded compact set. In (8.1) and (8.2), the matrix entries change according to the parameter vector $\rho(t)$. If all the system states are available, then a suitable state feedback controller $u(t) = -Fx(t)$ can be designed in order to achieve the desired performance (and closed-loop stability) of the system

$$\dot{x}(t) = (A(\rho) - B(\rho)F)x(t)$$

for all the admissible values of $\rho(t)$ in a compact set. To account for actuator faults or failures, the linear parameter varying plant in (8.1) can be represented as

$$\dot{x}(t) = A(\rho)x(t) + B(\rho)W(t)u(t) \tag{8.3}$$

where $A(\rho) \in \mathbb{R}^{n\times n}$, $B(\rho) \in \mathbb{R}^{n\times m}$ and $W(t) \in \mathbb{R}^{m\times m}$ is a diagonal semi-positive definite weighting matrix whose diagonal entries $w_1(t), \ldots, w_m(t)$ model the efficiency level of the actuators. As throughout the text, if $w_i(t) = 1$ it means that the ith actuator is working perfectly and is fault-free, whereas if $1 > w_i(t) > 0$ some level of fault is present (and that particular actuator works at reduced efficiency). If $w_i(t) = 0$ it means the ith actuator has completely failed and the actuator does not respond to the control signal $u_i(t)$.

Assumption 8.1 The time varying parameter vector $\rho(t)$ is assumed to lie in a specified bounded compact set $\Omega \subset \mathbb{R}^r$ and is assumed to be available for the controller design.

Assumption 8.2 Further assume that the varying plant matrices $A(\rho)$ and $B(\rho)$ depend affinely on the parameter $\rho(t)$, that is

$$A(\rho) = A_0 + \sum_{i=1}^{r} \rho_i A_i, \quad B(\rho) = B_0 + \sum_{i=1}^{r} \rho_i B_i$$

Assumption 8.3 To design the virtual control law, which is explained in the sequel, assume that the parameter varying matrix $B(\rho)$ can be factorised as

$$B(\rho) = B_f E(\rho) \tag{8.4}$$

where $B_f \in \mathbb{R}^{n\times m}$ is a fixed matrix and $E(\rho) \in \mathbb{R}^{m\times m}$ is a matrix with varying components and is assumed to be invertible for all $\rho(t) \in \Omega$. This of course is a restriction on the class of systems for which the results in this chapter are applicable, but for example many aircraft systems fall into this category.

As discussed in Chap. 3, to resolve actuator redundancy, assume that by permuting the states, the matrix B_f can be partitioned as

$$B_f = \begin{bmatrix} B_1 \\ B_2 \end{bmatrix} \tag{8.5}$$

where $B_1 \in \mathbb{R}^{(n-l)\times m}$, and $B_2 \in \mathbb{R}^{l\times m}$ is of rank $l < m$.

Assumption 8.4 It is assumed that $\|B_2\| \gg \|B_1\|$ so that B_2 provides the dominant contribution of the control action within the system as compared to B_1.

Furthermore scale the last l states to ensure that $B_2 B_2^T = I_l$. This can be done without loss of generality.
Using (8.4) and (8.5), the system in (8.3) can be written as

$$\dot{x}(t) = A(\rho)x(t) + \begin{bmatrix} B_1 E(\rho)W(t) \\ B_2 E(\rho)W(t) \end{bmatrix} u(t) \tag{8.6}$$

The design of the virtual control will be based on the fault-free system i.e. when $W(t) = I$. Define the virtual control input signal as:

$$\nu(t) := B_2 E(\rho)u(t) \tag{8.7}$$

where $\nu(t) \in \mathbb{R}^l$ is the total control effort produced by the actuators. Using the fact $B_2 B_2^T = I_l$, one particular choice for the physical control law $u(t) \in \mathbb{R}^m$ which is used to distribute the control effort among the actuators is

$$u(t) := (E(\rho))^{-1} B_2^T \nu(t) \tag{8.8}$$

Note the expression in (8.8) satisfies (8.7) since $(E(\rho))^{-1}B_2^T$ is a right pseudo-inverse of $B_2 E(\rho)$.

Remark 8.1 The control structure in (8.8) is different from Chaps. 3 and 4, since it involves the varying matrix $E(\rho)$.

Substituting (8.8) into (8.6) yields the state-space representation

$$\dot{x}(t) = A(\rho)x(t) + \underbrace{\begin{bmatrix} B_1 E(\rho)W(t)(E(\rho))^{-1}B_2^T \\ B_2 E(\rho)W(t)(E(\rho))^{-1}B_2^T \end{bmatrix}}_{B_w(\rho)} \nu(t) \tag{8.9}$$

in terms of the virtual control $\nu(t)$. In the nominal case, when there is no fault in the system, i.e. when $W(t) = I$, Eq. (8.9) simplifies to

$$\dot{x}(t) = A(\rho)x(t) + \underbrace{\begin{bmatrix} B_1 B_2^T \\ I_l \end{bmatrix}}_{B_\nu} \nu(t) \tag{8.10}$$

exploiting the fact that $B_2 B_2^T = I_l$.

Assumption 8.5 The pair $(A(\rho), B_\nu)$ is controllable for all values of $\rho(t) \in \Omega$.

In this chapter all the states are assumed to be available for the controller design, therefore a state feedback law $v(t) = -Fx(t)$ can be designed in order to stabilise the nominal system

$$\dot{x}(t) = (A(\rho) - B_v F)x(t)$$

for all values of $\rho(t) \in \Omega$, as well as to achieve the desired closed-loop performance.[1] The nominal fault-free system in (8.10) is used in the next section to design the virtual control law.

8.2 Integral Sliding Mode Controller Design

This section focuses initially on the design of the sliding surface and then subsequently the control law, so that the sliding motion on the sliding surface can be sustained for all time.

8.2.1 Design of Integral Switching Function

Here the switching function suggested in Eq. (3.21) from Sect. 3.2.1 is extended to LPV plants. Choose the sliding surface as

$$\mathscr{S} = \{x \in \mathbb{R}^n : \quad \sigma(t) = 0\}$$

where

$$\sigma(t) := Gx(t) - Gx(0) - G\int_0^t (A(\rho) - B_v F)\, x(\tau)d\tau \tag{8.11}$$

and $G \in \mathbb{R}^{l\times n}$ represents design freedom. Here

$$G := B_2 \left(B_f^T B_f\right)^{-1} B_f^T \tag{8.12}$$

is suggested where B_f is defined in (8.4). With this choice of G, and using the special properties of matrix B_2 (i.e. $B_2 B_2^T = I_l$), it is easy to verify that

$$GB_v = B_2 \left(B_f^T B_f\right)^{-1} B_f^T B_f B_2^T = I_l \tag{8.13}$$

[1] This may be viewed from a controllability viewpoint, and in the literature, the concept of parameter varying invariant subspaces [1] has been proposed to compute the controllable subspaces for LPV systems with affine parameter dependence.

which means that nominally when there are no faults in the system and $W = I_m$, the special choice of G in (8.12) serves as a left pseudo-inverse of the matrix B_v. Also from Eq. (8.9)

$$\begin{aligned} GB_w(\rho) &= B_2 \left(B_f^T B_f\right)^{-1} B_f^T B_f E(\rho) W(t) (E(\rho))^{-1} B_2^T \\ &= B_2 E(\rho) W(t) (E(\rho))^{-1} B_2^T \end{aligned} \tag{8.14}$$

which will be used in the sequel when defining the control law.
Taking the time derivative of the switching function $\sigma(t)$ along the trajectories of (8.9) yields

$$\dot{\sigma}(t) = G\dot{x}(t) - GA(\rho)x(t) + GB_v Fx(t) \tag{8.15}$$

and after substituting from (8.9)

$$\dot{\sigma}(t) = GB_w(\rho)v(t) + \underbrace{GB_v}_{I_l} Fx(t) \tag{8.16}$$

Therefore the expression for the equivalent control (associated with $\dot{\sigma}(t) = 0$) can be written as

$$v_{eq}(t) = -\left(B_2 E(\rho) W(t) (E(\rho))^{-1} B_2^T\right)^{-1} Fx(t) \tag{8.17}$$

provided the matrix $W(t)$ is such that $\det(B_2 E(\rho) W(t) (E(\rho))^{-1} B_2^T) \neq 0$. Substituting (8.17) into (8.9) yields the expression for the sliding motion as

$$\dot{x}(t) = A(\rho)x(t) - B_w(\rho)\left(B_2 E(\rho) W(t) (E(\rho))^{-1} B_2^T\right)^{-1} Fx(t) \tag{8.18}$$

By adding and subtracting the term $B_v Fx(t)$ to the right hand side of Eq. (8.18) yields

$$\dot{x}(t) = (A(\rho) - B_v F)\, x(t) + \begin{bmatrix} \tilde{\Phi}(t, \rho) \\ 0_l \end{bmatrix} Fx(t) \tag{8.19}$$

where the term which models the uncertainty is

$$\tilde{\Phi}(t, \rho) := B_1 B_2^T - B_1 E(\rho) W(t) (E(\rho))^{-1} B_2^T \left(B_2 E(\rho) W(t) (E(\rho))^{-1} B_2^T\right)^{-1} \tag{8.20}$$

Remark 8.2 From Eq. (8.20) it is clear that when there are no actuator faults in the system (i.e. $W(t) = I_m$), then $\tilde{\Phi}(t, \rho) \equiv 0$. However in the case of faults or failures (i.e. when $W(t) \neq I_m$), then $\tilde{\Phi}(t, \rho) \neq 0$ which will be treated as unmatched uncertainty while sliding.

The closed-loop stability of the motion while sliding must be ensured in the presence of 'uncertainty' $\tilde{\Phi}(t, \rho)$. To facilitate the closed-loop stability analysis, notice Eq. (8.19) can be written as

$$\dot{x}(t) = (A(\rho) - B_v F)\, x(t) + \widetilde{B}\tilde{\Phi}(t, \rho) F x(t) \tag{8.21}$$

where

$$\widetilde{B} := \begin{bmatrix} I_{n-l} \\ 0 \end{bmatrix} \tag{8.22}$$

Now in order to define the class of faults or failures which the FTC scheme in this chapter can mitigate, let the diagonal entries of $W(t)$ belong to the set

$$\mathscr{W}_\varepsilon = \{(w_1, \ldots, w_m) \in \underbrace{\begin{bmatrix} 0 & 1 \end{bmatrix} \times \cdots \times \begin{bmatrix} 0 & 1 \end{bmatrix}}_{m \text{ times}} : (GB_w(\rho))^T (GB_w(\rho)) > \varepsilon I\} \tag{8.23}$$

where ε is a small positive scalar satisfying $0 < \varepsilon \ll 1$. Note when $W(t) = I_m$, $(GB_w(\rho))^T (GB_w(\rho)) = I > \varepsilon I$ and therefore $\mathscr{W}_\varepsilon \neq \emptyset$. If the actuator effectiveness matrix $W(t) = \text{diag}(w_1(t), \ldots, w_m(t)) \in \mathscr{W}_\varepsilon$ then by construction

$$\|(GB_w(\rho))^{-1}\| = \| \left(B_2 E(\rho) W(t) (E(\rho))^{-1} B_2^T\right)^{-1} \| < \frac{1}{\sqrt{\varepsilon}}$$

The set $\mathscr{W}_\varepsilon$ will be shown to constitute the class of faults/failures for which closed-loop stability can be maintained. From (8.20) note that for any $W(t) \in \mathscr{W}_\varepsilon$

$$\|\tilde{\Phi}(t, \rho)\| \leq \gamma_1 \left(1 + \frac{c}{\sqrt{\varepsilon}}\right) \tag{8.24}$$

where $c = \max_{\rho \in \Omega} \|E(\rho)\| \|(E(\rho))^{-1}\|$ (i.e. the worst case condition number associated with $E(\rho)$); and $\gamma_1 = \|B_1\|$, which is small by hypothesis. Proving the stability of the closed-loop sliding motion in (8.21) (in the nominal as well as in the fault/failure scenarios) is one of the important parts of the design process which is demonstrated in the following subsection.

Remark 8.3 The conditions in this chapter are subtly different to those in Chaps. 3 and 4. In (8.23) the norm of $(GB_w(\rho))^{-1}$ must be guaranteed to be bounded by limiting $W(t) \in \mathscr{W}_\varepsilon$ thus introducing an explicit ε to bound $\|GB_w(\rho)\|$ away from zero. This is not necessary in Chaps. 3 and 4 and so the 'price' for facilitating a wider operating envelope is a slightly more restricted set of possible failures.

8.2.2 Closed-Loop Stability Analysis

In the nominal fault-free scenario when $W(t) = I_m$, it is easy to verify $\tilde{\Phi}(t, \rho) = 0$, and Eq. (8.21) simplifies to

$$\dot{x}(t) = (A(\rho) - B_v F)\, x(t) \tag{8.25}$$

which is stable by design of F. However in fault/failure scenarios, closed-loop stability needs to be proven. To this end, Eq. (8.21) can also be represented by

$$\dot{x}(t) = \underbrace{(A(\rho) - B_v F)}_{\widetilde{A}(\rho)} x(t) + \widetilde{B} \overbrace{\tilde{\Phi}(t, \rho) \underbrace{F x(t)}_{\widetilde{y}(t)}}^{\widetilde{u}(t)} \tag{8.26}$$

Define γ_2 to be the $\mathscr{L}_2$ gain associated with the operator

$$\widetilde{G}(s) := F(sI - \widetilde{A}(\rho))^{-1}\widetilde{B} \tag{8.27}$$

Proposition 8.1 *For any possible combination of faults or failures belonging to the set $\mathscr{W}_\varepsilon$, the closed-loop sliding motion in (8.26) will be stable if*

$$\gamma_2 \gamma_1 \left(1 + \frac{c}{\sqrt{\varepsilon}}\right) < 1 \tag{8.28}$$

Proof The specially written structure in (8.26) can be thought of as a feedback interconnection of an LPV plant and a time varying feedback gain associated with

$$\dot{x}(t) = \widetilde{A}(\rho)x(t) + \widetilde{B}\widetilde{u}(t) \tag{8.29}$$

$$\widetilde{y}(t) = Fx(t) \tag{8.30}$$

where

$$\widetilde{u}(t) = \tilde{\Phi}(t, \rho)\widetilde{y}(t) \tag{8.31}$$

If (8.28) is satisfied then according to the small gain theorem (Appendix B.1.2), if

$$\|\widetilde{G}(s)\|\|\tilde{\Phi}(t, \rho)\| < 1 \tag{8.32}$$

the closed-loop system in (8.26) will be stable. ■

In the next subsection the ideas of integral sliding modes are used to design the virtual control law $v(t)$ in order to produce the virtual control effort.

8.2.3 ISM Control Laws

Consider the (integral sliding mode) control law

$$v(t) = (GB_{\hat{w}}(\rho))^{-1}(v_l(t) + v_n(t)) \tag{8.33}$$

where

$$GB_{\hat{w}}(\rho) = B_2 E(\rho)\widehat{W}(t)(E(\rho))^{-1}B_2^T \tag{8.34}$$

and $\widehat{W}(t)$ is an estimate of $W(t)$. The linear part of the control law $v_l(t)$ in (8.33) is defined as

$$v_l(t) := -Fx(t) \tag{8.35}$$

and the nonlinear discontinuous part, which enforces sliding and provides robustness against fault/failure scenarios is given by

$$v_n(t) := -\kappa(t, x)\frac{\sigma(t)}{\|\sigma(t)\|} \quad \text{for } \sigma(t) \neq 0 \tag{8.36}$$

where $\kappa(t, x) > 0$ is an adaptive modulation function given by

$$\kappa(t, x) = \|F\|\|x(t)\|\bar{\kappa}(t, x) + \eta \tag{8.37}$$

where η is a positive scalar. The positive adaptation gain $\bar{\kappa}(t, x)$ evolves according to

$$\dot{\bar{\kappa}}(t, x) = -\varsigma_1\bar{\kappa}(t, x) + \varsigma_2\varepsilon_0\|F\|\|x(t)\|\|\sigma(t)\| \tag{8.38}$$

where ς_1, ς_2 and ε_0 are positive (design) scalar gains.

Assumption 8.6 In the analysis which follows, it is assumed the actuator efficiency level $W(t)$ is not perfectly known but that the estimate $\widehat{W}(t)$ satisfies

$$W(t) = \widehat{W}(t)(I + \Delta(t)) \tag{8.39}$$

where the diagonal matrix $\Delta(t)$ represents imperfections in the estimation of $W(t)$.

Substituting (8.39) into (8.14) yields

$$GB_w(\rho) = B_2 E(\rho)\widehat{W}(t)(E(\rho))^{-1}B_2^T + B_2 E(\rho)\widehat{W}(t)\Delta(t)(E(\rho))^{-1}B_2^T \tag{8.40}$$

Using (8.33), Eq. (8.16) becomes

$$\dot{\sigma}(t) = GB_w(\rho)(GB_{\hat{w}}(\rho))^{-1}(v_l(t) + v_n(t)) + Fx(t)$$

Substituting for (8.40) and for ν_l from (8.35) yields

$$\begin{aligned}\dot{\sigma}(t) &= (I + \widehat{\Delta}(t))(\nu_l(t) + \nu_n(t)) + Fx(t)\\ &= (I + \widehat{\Delta}(t))\nu_n(t) - \widehat{\Delta}(t)Fx(t)\end{aligned} \tag{8.41}$$

where

$$\widehat{\Delta}(t) = (B_2 E(\rho)\widehat{W}^{\frac{1}{2}}(t)\Delta(t)\widehat{W}^{\frac{1}{2}}(t)\left(E(\rho)\right)^{-1}B_2^T)\,(B_2 E(\rho)\widehat{W}(t)\left(E(\rho)\right)^{-1}B_2^T)^{-1} \tag{8.42}$$

Define

$$\mathscr{D}_{\varepsilon_0} = \left\{\Delta(t) \text{ from (8.39)} \;:\; \|\widehat{\Delta}(t)\| < \sqrt{1-2\varepsilon_0}\right\} \tag{8.43}$$

for some scalar $0 < \varepsilon_0 \ll 1/2$. Clearly the set $\mathscr{D}_{\varepsilon_0}$ is not empty since $\Delta(t) = 0 \in \mathscr{D}_{\varepsilon_0}$. It is easy to show that if

$$\|\widehat{\Delta}(t)\| < \sqrt{1-2\varepsilon_0} \tag{8.44}$$

then

$$2I_l + \widehat{\Delta}(t) + \widehat{\Delta}^T(t) > 2\varepsilon_0 I_l \tag{8.45}$$

Consider the positive definite candidate Lyapunov function

$$V(t) = \underbrace{\sigma^T(t)\sigma(t)}_{V_1(t)} + \underbrace{\frac{1}{\varsigma_2}e^2(t)}_{V_2(t)} \tag{8.46}$$

where

$$e(t) = \bar{\kappa}(t,x) - \frac{1}{\varepsilon_0} \tag{8.47}$$

Since $\|\widehat{\Delta}(t)\| < \sqrt{1-2\varepsilon_0}$, taking the derivative of $V_1(t)$ from (8.46), and then substituting from (8.41), yields

$$\begin{aligned}\dot{V}_1(t) &= -\kappa(t,x)\|\sigma(t)\|(2I_l + \widehat{\Delta}(t) + \widehat{\Delta}^T(t)) - 2\sigma^T(t)\widehat{\Delta}(t)Fx(t)\\ &\le -2\kappa(t,x)\varepsilon_0\|\sigma(t)\| + 2\|\sigma(t)\|\|\widehat{\Delta}(t)\|\|Fx(t)\|\\ &\le -2\kappa(t,x)\varepsilon_0\|\sigma(t)\| + 2\|\sigma(t)\|\sqrt{1-2\varepsilon_0}\,\|F\|\,\|x(t)\|\end{aligned} \tag{8.48}$$

From (8.47) it follows that $\bar{\kappa}(t,x) = e(t) + \frac{1}{\varepsilon_0}$. Then using the fact that $\sqrt{1-2\varepsilon_0} < 1$ and substituting (8.37) into (8.48), it follows

$$\dot{V}_1(t) \le -2\varepsilon_0\|F\|\|x(t)\|\|\sigma(t)\|e(t) - 2\eta\varepsilon_0\|\sigma(t)\| \tag{8.49}$$

Taking the derivative of $V_2(t)$ from (8.46), using the fact that $\dot{e}(t) = \dot{\bar{\kappa}}(t,x)$ from (8.47) and substituting from (8.38) gives

$$\begin{aligned}\dot{V}_2(t) &= \frac{2}{\varsigma_2} e(t)\dot{e}(t) = \frac{2}{\varsigma_2} e(t)\dot{\bar{\kappa}}(t,x) \\ &= -\frac{2\varsigma_1}{\varsigma_2} e(t)\bar{\kappa}(t,x) + 2\varepsilon_0 e(t)\|F\|\|x(t)\|\|\sigma(t)\| \end{aligned} \tag{8.50}$$

Therefore, from (8.49) and (8.50) and substituting for $\bar{\kappa}(t,x)$ from (8.47) yields

$$\begin{aligned}\dot{V}(t) &= \dot{V}_1(t) + \dot{V}_2(t) \\ &\leq -\frac{2\varsigma_1}{\varsigma_2} e(t)\bar{\kappa}(t,x) - 2\eta\varepsilon_0\|\sigma(t)\| \\ &= -\frac{2\varsigma_1}{\varsigma_2\varepsilon_0} e(t) - \frac{2\varsigma_1}{\varsigma_2} e^2(t) - 2\eta\varepsilon_0\|\sigma(t)\| \end{aligned} \tag{8.51}$$

It is easy to show that

$$-\frac{2\varsigma_1}{\varsigma_2\varepsilon_0} e(t) - \frac{2\varsigma_1}{\varsigma_2} e^2(t) \leq \frac{\varsigma_1}{2\varsigma_2\varepsilon_0^2}$$

for all values of $e(t)$ and therefore from (8.51) it follows that

$$\dot{V}(t) \leq \frac{\varsigma_1}{2\varsigma_2\varepsilon_0^2} - 2\eta\varepsilon_0\|\sigma(t)\| \tag{8.52}$$

which implies that $\sigma(t)$ moves into a boundary layer about $\sigma(t) = 0$ of size $\frac{\varsigma_1}{4\varsigma_2\varepsilon_0^3\eta}$.

Remark 8.4 The adaptation scheme in (8.37) and (8.38) makes the approach in this chapter quite different from Chaps. 3 and 4. Adaptation is required here because of the complex relationship between $\Delta(t)$ and $\widehat{\Delta}(t)$ in (8.42) and the limitations associated with (8.43).

Remark 8.5 The fact that a traditional sliding mode scheme involving a unit vector structure has been selected as the basis for the control law, has facilitated the inclusion of an adaptive scheme. An adaptive gain is highly desirable in FTC schemes to compensate for sudden significant changes to the plant.

Finally the physical control law, which is used to distribute the control effort among the available actuators is obtained by substituting (8.33)–(8.36) into (8.8) which yields

$$u(t) = -(E(\rho))^{-1}B_2^T\left(B_2E(\rho)\widehat{W}(t)(E(\rho))^{-1}B_2^T\right)^{-1}\left(Fx(t) + \kappa(\cdot)\frac{\sigma(t)}{\|\sigma(t)\|}\right) \tag{8.53}$$

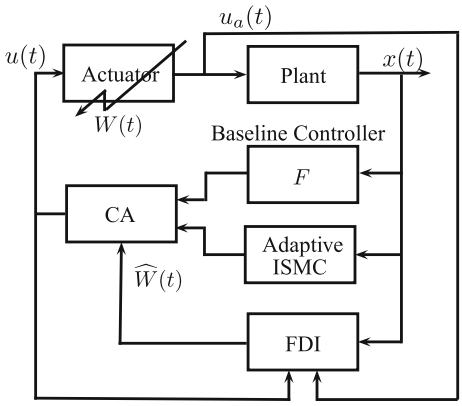

Fig. 8.1 Overall FTC scheme

Remark 8.6 Note the physical control law in (8.53) requires an estimate of the effectiveness level of the actuators $\widehat{W}(t)$ (see Fig. 8.1 for details). In this chapter, it is assumed that this estimate is provided by an FDI scheme (see for example Sect. 3.3.1). This information can also be obtained by directly comparing the controller signals with the actual actuator deflection, as measured by control surface sensors, which are available in many aircraft systems.

8.2.4 Design of the State Feedback Gain

In this section, using the nominal system (8.10), the state feedback gain F will be designed. In designing F two objectives must be met: the first is equivalent to achieving pre-specified nominal performance for all admissible values of $\rho(t)$, and the second one is to satisfy the closed-loop stability condition in (8.28) via the small gain theorem. Nominal performance will be incorporated by the use of a LQR type cost function

$$J = \int_0^\infty (x^T Q x + u^T R u) dt$$

where Q and R are s.p.d. matrices. The LPV system matrices $(\widetilde{A}(\rho), \widetilde{B}, F)$ which depend affinely on the parameter vector $\rho(t)$ in (8.29) and (8.30) can be represented by the polytopic system $(\widetilde{A}(\omega_i), \widetilde{B}, F)$ where the vertices $\omega_1, \omega_2, \ldots, \omega_{n_\omega}$ for $\omega_{n_w} = 2^r$ correspond to the extremes of the allowable range of $\rho(t) \in \Omega$. Consequently

$$\widetilde{A}(\rho) = \sum_{i=1}^{2^r} \widetilde{A}_i \delta_i, \quad \sum_{i=1}^{2^r} \delta_i = 1, \quad \delta_i \geq 0$$

The LQR performance criteria can then be posed as an optimisation problem:
Minimise trace (X^{-1}) subject to

$$\begin{bmatrix} A(\omega_i)X + XA^T(\omega_i) - B_v Y - Y^T B_v^T & (Q_1 X - R_1 Y)^T \\ Q_1 X - R_1 Y & -I \end{bmatrix} < 0 \quad (8.54)$$

$$X > 0 \quad (8.55)$$

where

$$Q_1 = \begin{bmatrix} Q^{\frac{1}{2}} \\ 0_{l\times n} \end{bmatrix}, \quad R_1 = \begin{bmatrix} 0_{n\times l} \\ R^{\frac{1}{2}} \end{bmatrix}^T \quad (8.56)$$

and $Y := FX$ and $X^{-1} \in \mathbb{R}^{n\times n}$ is the Lyapunov matrix.
To satisfy the closed-loop stability condition in (8.28), it is sufficient to apply the Bounded Real Lemma at each vertex of the polytope and ensure that

$$\begin{bmatrix} A(\omega_i)X + XA^T(\omega_i) - B_v Y - Y^T B_v^T & \tilde{B} & Y^T \\ \tilde{B}^T & -\gamma^2 I & 0 \\ Y & 0 & -I \end{bmatrix} < 0 \quad (8.57)$$

for $i = 1 \ldots 2^r$. Since the objective is to seek a common Lyapunov matrix for the LMI formulations at each vertex, this can be achieved by introducing the slack variable $Z \in \mathbb{R}^{n\times n}$ and posing the problem as:

Minimise trace(Z) subject to (8.54), (8.55) and (8.57) and

$$\begin{bmatrix} -Z & I_n \\ I_n & -X \end{bmatrix} < 0 \quad (8.58)$$

The decision variables are X and Y. The matrix Z satisfies trace$(Z) \geq$ trace(X^{-1}). Therefore the LMIs in (8.54)–(8.58) can be solved for all the vertices of the polytopic system. The state feedback matrix is obtained from the expression $F = YX^{-1}$.

8.3 Simulations

The simulations in this chapter are based on the RECOVER benchmark model. For the controller design the LPV model of RECOVER given in Appendix A.1.1 is used. The aerodynamic coefficients are polynomial functions of velocity V_{tas} and angle of attack α in the range of $\left[\,150,\ 250\,\right]$ m/s and $\left[\,-2,\ 8\,\right]$ deg respectively, and at an altitude of 7000 m. The states of the LPV plant are $(\bar{\alpha}, \bar{q}, \bar{V}_{tas}, \bar{\theta}, \bar{h}_e)$ which represent *deviation* of the angle of attack, pitch rate, true air speed, pitch angle and altitude from their trim values. The inputs of the LPV plant are $(\bar{\delta}_e, \bar{\delta}_s, \bar{T}_n)$, which represent

deviation of elevator deflection, horizontal stabiliser deflection and total engine thrust from their trim values respectively. The trim values of the states are

$$(\alpha_{trim}, q_{trim}, V_{tas_{trim}}, \theta_{trim}, h_{e_{trim}}) = (1.05\,\text{deg},\ 0\,\text{deg/s},\ 227.02\,\text{m/s},\ 1.05\,\text{deg},\ 7000\,\text{m})$$

and the trim values of the LPV plant inputs are

$$(\delta_{e_{trim}}, \delta_{s_{trim}}, T_{n_{trim}}) = (0.163\ \text{deg},\ 0.590\ \text{deg},\ 42291\ \text{N})$$

For the controller design, the state $\bar{h}_e$ is removed and the states of the LPV plant have been reordered as $(\bar{\theta}, \bar{\alpha}, \bar{V}_{tas}, \bar{q})$. The LPV system matrices are given by

$$A(\rho) = A_0 + \sum_{i=1}^{7} A_i \rho_i \quad \text{and} \quad B(\rho) = B_0 + \sum_{i=1}^{7} B_i \rho_i \tag{8.59}$$

where

$$(\rho_1, \ldots, \rho_7) := \left(\bar{\alpha}, \bar{V}_{tas}, \bar{V}_{tas}\bar{\alpha}, \bar{V}_{tas}^2, \bar{V}_{tas}^2\bar{\alpha}, \bar{V}_{tas}^3, \bar{V}_{tas}^4\right) \tag{8.60}$$

where $\bar{\alpha} = \alpha - \alpha_{trim}$ and $\bar{V}_{tas} = V_{tas} - V_{tas_{trim}}$. For full details of the LPV plant see the Appendix A.1.1. The input distribution matrix $B(\rho)$ has been factorised into fixed and varying matrices:

$$B(\rho) = \underbrace{\left[\begin{array}{ccc} 0 & 0 & 0 \\ 0.01 & 0 & 0 \\ \hline 0 & 1 & 0 \\ 0 & 0 & 1 \end{array}\right]}_{B_f} \underbrace{\left[\begin{array}{ccc} 100b_{31}(\rho) & 100b_{32}(\rho) & 100b_{33}(\rho) \\ 0 & 0 & b_{23}(\rho) \\ b_{41}(\rho) & b_{42}(\rho) & b_{43}(\rho) \end{array}\right]}_{E(\rho)} \tag{8.61}$$

Note that the top portion of B_f corresponds to the B_1 term in (8.5) which has been made small compared to the B_2 term. In order to introduce a tracking facility, the plant states are augmented with the integral action states given by

$$\dot{x}_r(t) = r(t) - C_c \bar{x}(t) \tag{8.62}$$

where $r(t)$ is the command to be tracked, and C_c is the controlled output distribution matrix. The controlled outputs have been chosen as flight path angle (FPA) and $\bar{V}_{tas}$, where FPA $= \bar{\theta} - \bar{\alpha}$. By defining new states as

$$x_a(t) = \text{col}(x_r(t), \bar{x}(t))$$

the augmented system from (8.10) becomes

$$\dot{x}_a(t) = A_a(\rho)x_a(t) + B_{v_a}v(t) + B_r r(t) \tag{8.63}$$

where

$$A_a(\rho) := \begin{bmatrix} 0 & -C_c \\ 0 & A(\rho) \end{bmatrix}, \quad B_{v_a} := \begin{bmatrix} 0 \\ B_v \end{bmatrix}, \quad B_r = \begin{bmatrix} I_l \\ 0 \end{bmatrix} \tag{8.64}$$

which is used as the basis for the control law design. In the augmented system, the choice of G in (8.12) becomes $G_a := B_2(B_{f_a}^T B_{f_a})^{-1}B_{f_a}^T$ where

$$B_{f_a} = \begin{bmatrix} 0 \\ B_f \end{bmatrix} \tag{8.65}$$

8.3.1 Control Design Objectives

The tracking requirements for FPA and true air speed V_{tas} are decoupled responses, with settling times of 20 and 45 s respectively in the fault-free scenario. In the case of an elevator or horizontal stabiliser failure, the tracking requirement for V_{tas} remains unchanged (because speed is controlled by thrust) but for the FPA response, a settling time of 30 s is considered. In this example, a fixed gain matrix F is valid for the entire range of the LPV model. Note that designing a fixed matrix F, allows the MATLAB state-feedback synthesis code 'msfsyn' to be used to solve the LMIs (8.54)–(8.58). For designing the state feedback gain F, the Q and R matrices in (8.54) have been chosen as

$$Q = \text{diag}(1.1, 0.04, 1, 1, 0.03, 5) \quad \text{and} \quad R = \text{diag}(0.007, 1.1)$$

where the first two states in the Q matrix are integral action states. The state feedback gain resulting from the optimisation is given by

$$F = \begin{bmatrix} -1.1161 & -2.3532 & -10.3807 & 3.8107 & 3.7409 & -1.3623 \\ -0.9891 & 0.0177 & 9.6902 & -4.9097 & -0.0222 & 3.3779 \end{bmatrix} \tag{8.66}$$

In the nominal case, the engines are considered to be fault-free. The positive scalar from (8.23) has been chosen as $\varepsilon = 0.28$. It can then be shown (using a numerical search algorithm) that the maximum value of $\|\tilde{\Phi}(t, \rho)\|$ from Eq. (8.24) is 0.0673. To satisfy the closed-loop stability condition in (8.28), the value of γ_2 associated with the operator in (8.27) should satisfy $\gamma_2 < \frac{\sqrt{\varepsilon}}{\gamma_1(\sqrt{\varepsilon}+c)} = 14.8588$. The value associated with F in (8.66) is $\gamma_2 = 11.0000$, and hence the stability condition in (8.28) is satisfied. During the simulations, the discontinuity associated with the nonlinear control term in (8.36) has been smoothed by using a sigmoidal approximation $\frac{\sigma_a(t)}{\|\sigma_a(t)\|+\delta}$, where δ

is a small positive scalar. This ensures a smooth and realistic control signal is sent to the actuators and allows extra design freedom especially when faults/failures occur. Here δ has been chosen as $\delta = 0.01$. The adaptive gain parameters from (8.37) and (8.38) used in the simulation are: $\eta = 1$, $\varsigma_1 = 1$, $\varsigma_2 = 0.01$ and $\varepsilon_0 = 0.01$. The control law in (8.53) requires information about the actuator effectiveness level matrix $W(t)$, which can be estimated by some FDI scheme, as given in Sect. 3.3.1. As in the GARTEUR FM-AG16 project, in this chapter, it is assumed that a measurement of the actual actuator deflection is available, which is not an unrealistic assumption in modern aircraft systems. Information provided by the actual actuator deflection can be compared with the signals from the controller to indicate the effectiveness of the actuator.

8.3.2 Simulation Results

The manoeuvre considered in this chapter represents a change of altitude and speed using a series of -3 deg FPA and -10 m/s V_{tas} commands. This covers a wide range of the flight envelope highlighting the efficacy of the FTC scheme when dealing with faults and failures. In this chapter two failure scenarios will be considered, one is an elevator jam and the other is a stabiliser runaway. For consistency, all the actuator failures are set to occur at 300 s.

Remark 8.7 Note that even though the controller is designed based on the LPV model from Appendix A.1.1, it is tested on the *full high fidelity nonlinear aircraft model* used as a FTC benchmark in GARTEUR FM-AG16 project.

8.3.2.1 Elevator Jam

Figure 8.2 shows a comparison between the fault-free case and a scenario in which the elevator jams at 300 s. Despite the elevator jam, there is no visible difference in terms of the FPA and speed V_{tas} tracking performance. There is also no visible difference in terms of the altitude change between the failure and the fault-free case. It can be seen that immediately after the failure at 300 s, the estimate of the elevator effectiveness level drops to 10 %. This indicates non-perfect estimation (it should be zero). Despite this imperfection, there is no difference in terms of tracking performance. The plot of the norm of the switching function $\|\sigma(t)\|$ also shows no visible difference between the fault-free and the failure case. Finally, a plot of the adaptive gain shows the variation of $\kappa(t, x)$ defined in (8.37). Again, there is no visible difference in terms of the adaptive gain between the fault-free and failure case. Note that in the fault-free case, the variation of the adaptive gain is due to a combination of variations in $\|\sigma(t)\|$ and the states $\|x(t)\|$, as described in the formula in (8.38).

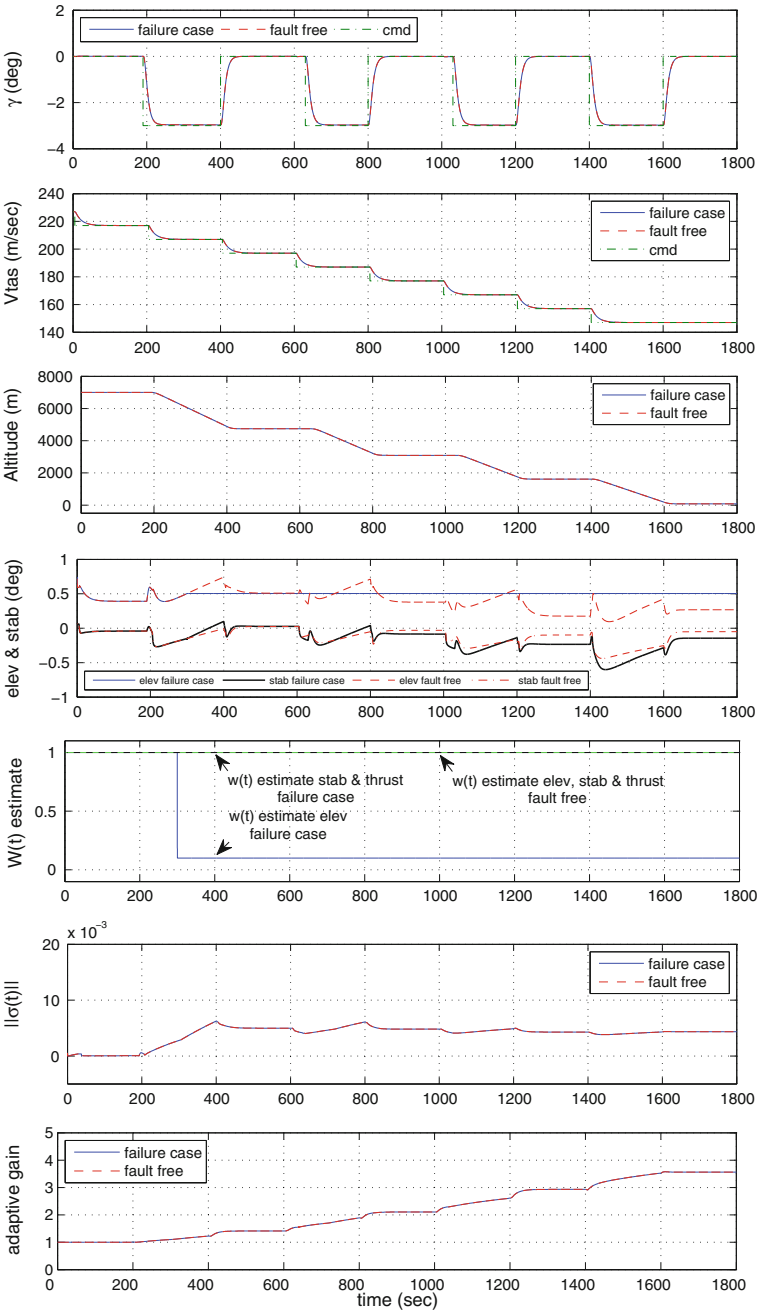

Fig. 8.2 Elevator jam

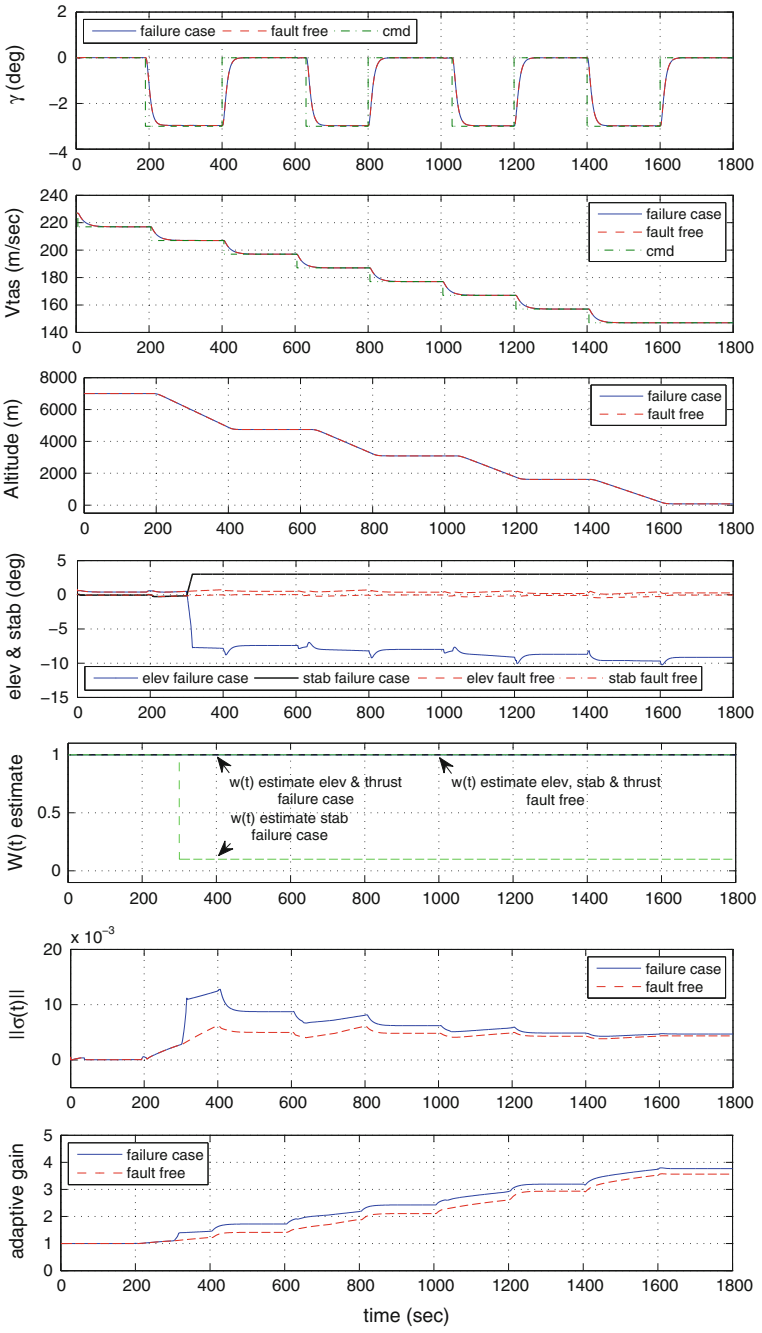

Fig. 8.3 Stabiliser runaway

8.3.2.2 Stabiliser Runaway

Figure 8.3 shows the results for the case when a stabiliser runaway occurs. The effect of the stabiliser runaway can be seen in the control surface plot where the stabiliser moves at a maximum rate to the maximum position of 3 deg. The effect of the control relocation can be seen in the plot of the elevator which moves to 7 deg immediately after the failure occurs at 300 s. Despite the stabiliser runaway and the imperfect estimation of the stabiliser effectiveness, there is no visible difference in terms of tracking performance between the fault-free and the failure case. (The estimated stabiliser effectiveness level is shown as 10 % whereas the actual value should be zero.) The plot of the norm of the switching function $\|\sigma(t)\|$ shows the difference between the fault-free and the failure case. Here it can be seen that the norm for the failure case is slightly higher than the fault-free case immediately after the failure at 300 s, but is still relatively small. Finally, the plot of the adaptive gain shows there is a slight difference between the fault-free and the failure case.

8.4 Summary

This chapter described a FTC scheme for linear parameter varying systems. Integral sliding mode control in conjunction with CA was used to maintain nominal performance and robustness in the face of actuator faults or failures. The virtual control signal, generated by the integral sliding mode control law was translated into the physical actuator commands by using the control allocation scheme. The closed-loop stability of the system throughout the entire flight envelope was guaranteed—even in the event of total failure of a certain class of actuators (provided appropriate redundancy is available in the system). The scheme also takes into account imperfect estimation of actuator effectiveness levels and considers an adaptive gain for the nonlinear component of the control law. The FTC scheme has been tested on a full nonlinear aircraft benchmark model to highlight the efficacy of the scheme.

8.5 Notes and References

LPV methods have attracted much attention in recent years—especially for aircraft systems [2]. Using LPV techniques, guaranteed performance can be ensured over a wide range of operating regimes [3]. For LPV systems, several controller synthesis methods have been proposed in recent years in the framework of FTC: the advantages and capabilities of LPV controller synthesis (based on a single quadratic Lyapunov function approach) over gain-scheduling controller designs (based on $\mathscr{H}_\infty$ controller synthesis) are discussed and compared in [4] by implementing the two techniques on a high fidelity atmospheric re-entry vehicle model. In [5], an output feedback synthesis method using LMIs is presented in order to preserve closed-loop stability in the case

of multiple actuator faults. The authors in [6] have explored the combined use of fault estimation and fault compensation for LPV systems. Recently in [7] an active FTC technique was proposed for LPV systems to deal with actuator faults, in which the faults are identified by using an UIO technique, and a state feedback controller is realised by approximating the LPV system in a polytopic form. There is almost no literature on the use of sliding mode controllers for LPV systems with the exception of [8–11]. The work in [8, 9] has proposed SMC schemes for LPV systems—although not in the context of fault tolerant control. In [12] the nonlinear longitudinal model of the RECOVER transport aircraft was approximated by polynomially fitting the aerodynamics coefficients obtained from [13], to create an LPV representation using the function substitution method. In this chapter, the LPV plant matrices are taken from [12]. In [2] the same system is considered but only elevator failures (lock and float) are considered, whereas the FTC scheme described in this chapter is also tested by considering a stabiliser failure (as well as elevator failure scenarios).

References

1. Balas, G., Bokor, J., Szabo, Z.: Invariant subspaces for LPV systems and their applications. IEEE Trans. Autom. Control **48**(11), 2065–2069 (2003)
2. Ganguli, S., Marcos, A., Balas, G.J.: Reconfigurable LPV control design for Boeing 747-100/200 longitudinal axis. In: Proceedings of the American Control Conference (2002)
3. Balas, G.J.: Linear parameter-varying control and its application to a turbofan engine. Int. J. Robust Nonlinear Control **12**, 763–796 (2002)
4. Marcos, A., Veenman, J., Scherer, C., Zaiacomo, G., Mostaza, D., Kerr, M., Koroglu, H., Bennani, S.: Application of LPV modeling, design and analysis methods to a re-entry vehicle. In: Proceedings of the AIAA GNC/AFM/MST/ASC/ASE Conference, pp. 1–18 (2010)
5. Theilliol, D., Aberkane, S., Sauter, D.: Fault tolerant control design for polytopic LPV systems. Int. J. Appl. Math. Comput. Sci. **17**(1), 27–37 (2007)
6. Patton, R.J., Klinkhieo, S.: LPV fault estimation and FTC of a two link manipulator. In: Proceedings of the American control Conference, pp. 4647–4652. Baltimore, MD (2010)
7. Montes, S., Puig, V., Witczak, M., Dziekan, L.: Fault tolerant strategy for actuator faults using LPV techniques: application to a two degree of freedom helicopter. J. Appl. Math. Comput. Sci. **22**(1), 161–171 (2012)
8. Sivrioglu, S., Nonami, K.: Sliding mode control with time-varying hyperplane for AMB systems. IEEE/ASME Trans. Mechatron. **3**(1), 51–59 (1998)
9. Nonami, K., Sivrioglu, S.: Sliding mode control with gain scheduled hyperplane for LPV plant. Variable Structure Systems, Sliding Mode and Nonlinear Control, vol. 247, pp. 263–279. Springer, London (1999)
10. Alwi, H., Edwards, C.: Robust fault reconstruction for linear parameter varying systems using sliding mode observers. Int. J. Robust Nonlinear Control **24**(14), 1947–1968 (2013)
11. Alwi, H., Edwards, C.: Fault tolerant control of an octorotor using LPV based sliding mode control allocation. In: Proceedings of the American Control Conference, pp. 6505–6510 (2013)
12. Khong, T.H., Shin, J.: Robustness analysis of integrated LPV-FDI filters and LTI-FTC system for a transport aircraft. In: Proceedings of the AIAA Guidance, Navigation, and Control Conference and Exhibit, AIAA-2007-6771 (2007)
13. Marcos, A., Balas, G.: Linear parameter varying modeling of the Boeing 747-100/200 longitudinal motion. In: Proceedings of the AIAA Guidance, Navigation and Control Conference, AIAA-01-4347, pp. 1–11 (2001)

Chapter 9
Real-Time Implementation of an ISM Fault Tolerant Control Scheme on the SIMONA Flight Simulator

This chapter describes the results of implementing the LPV integral sliding mode FTC controller from Chap. 8 on the 6-DOF SIMONA motion flight simulator at Delft University of Technology. This demonstrates proof of concept in a realistic operational environment, and shows the applicability of the integral sliding mode FTC scheme. The LPV FTC scheme has been evaluated with a pilot-in-the-loop to give insight into real-time performance issues, and to assess the effect on the handling of the aircraft in nominal and in fault/failure scenarios.

9.1 SIMONA Research Simulator (SRS)

The SIMONA (SImulation, MOtion and NAvigation) research simulator (SRS) (Fig. 9.1) is a realistic 6 degree-of-freedom pilot-in-the-loop flight simulator located at Delft University of Technology. The SRS has a typical commercial aircraft cockpit with two side-by-side pilot seats, and typical pilot controls (a hydraulically activated control column, electrically actuated side stick, a rudder pedal (from an actual B777 aircraft), control wheel, thrust lever, flap and landing gear lever). At the centre of the cockpit is a mode control panel (MCP) from a B737 (Fig. 9.2), to allow auto-pilot commands and configuration selection, as well as an electronic flight control display (which can be configured to represent any aircraft display) to provide pilots with typical flight information such as control surface deflections and the aircraft trajectory. The SRS has an outside virtual world projection which can be set to any location. The SRS 180 $\times$ 40 deg outside visual field of view is supplied by three LCD projectors and provides the pilot with an immense sense of motion and the attitude of the aircraft. The motion of the SRS is provided by 6 large hydraulic hexapods and the SRS motion cueing algorithm, allowing any aircraft dynamics and manoeuvres to be implemented. The SRS is operated by a network of modular computers, each with a different function and task (visual cuing, motion control, running the aircraft model, data logging, control load feel, and the flight control computer).

M.T. Hamayun et al., *Fault Tolerant Control Schemes Using Integral Sliding Modes*, Studies in Systems, Decision and Control 61,
DOI 10.1007/978-3-319-32238-4_9

Fig. 9.1 SIMONA research simulator (picture courtesy of Delft University of Technology)

Communication and synchronisation between the different computers in the network are provided by high speed fibre optic cables. The custom-built motion and visualisation system, and its modular structure allow the SRS to be configured to represent any aircraft and has the capability of implementing any existing or 'experimental' flight control scheme. In this chapter, the SRS has been configured to represent the RECOVER B747-100/200 aircraft[1] with an outside virtual world representation of the area around Amsterdam-Schiphol airport. This SRS configuration is programmed using DUECA (Delft University Environment for Communication and Activation). The DUECA software architecture also handles the real-time scheduling, and ensures that each of the computers are synchronised.

[1] For details of the RECOVER benchmark model see the Appendix A.1.

Fig. 9.2 Mode Control Panel (MCP)

9.2 Design and SRS Implementation

This chapter considers the design of the adaptive ISM controller given in Chap. 8 and its implementation on the SRS. It is assumed that a measurement of the actual actuator deflections are available. Furthermore, the monitoring channels are separate from the control channels, and so faults in the actuators do not affect the fidelity of the control surface monitoring signals. In these experiments the diagonal elements $\hat{w}_i(t)$ of $\widehat{W}(t)$ in (8.53) have been estimated based on a least squares approach using information provided by the actual actuator deflections and the command signals from the controller.

9.2.1 SRS Implementation

The LPV design discussed in Sect. 8.3 is only associated with the longitudinal axis, although a lateral axis controller[2] must also be incorporated for the purpose of testing and evaluation. However the description of the SRS implementation will only focus on the longitudinal controller. In this chapter, the controller has been initially developed and tuned using MATLAB V2006b (the original version supported by the RECOVER model) using an ODE4 fixed time step solver with a step size of 0.01 s. For the implementation, the SIMULINK model of the designed ISM controller (which has the GARTEUR FM-AG16 standardised inputs–outputs in order to fit with the SRS implementation) has been converted to C code using the MATLAB Real-Time Workshop(R) utility. The C coded controller is then implemented on a PC with an Intel(R) Xeon(R) 3.07 GHz processor which has been used as the flight control computer. However the computational load measured as the time needed for a single integration step on the flight computer was found to be 0.15 msec. Figure 9.3 shows the overall controller configuration and the interface to the SRS, where it is clear that the inner-loop longitudinal controller provides flight path and speed tracking, which the pilot can command directly using the MCP dials at the centre of the cockpit. The outer-loop longitudinal controller provides altitude control using a simple PID scheme to provide a flight path angle command to the inner-loop ISM controller. In the results which follow $K_{p_{FPA}} = 0.1$, $K_{i_{FPA}} = 0.07$ and $K_{d_{FPA}} = 0.1$.

[2] See [1] for details of the lateral controller.

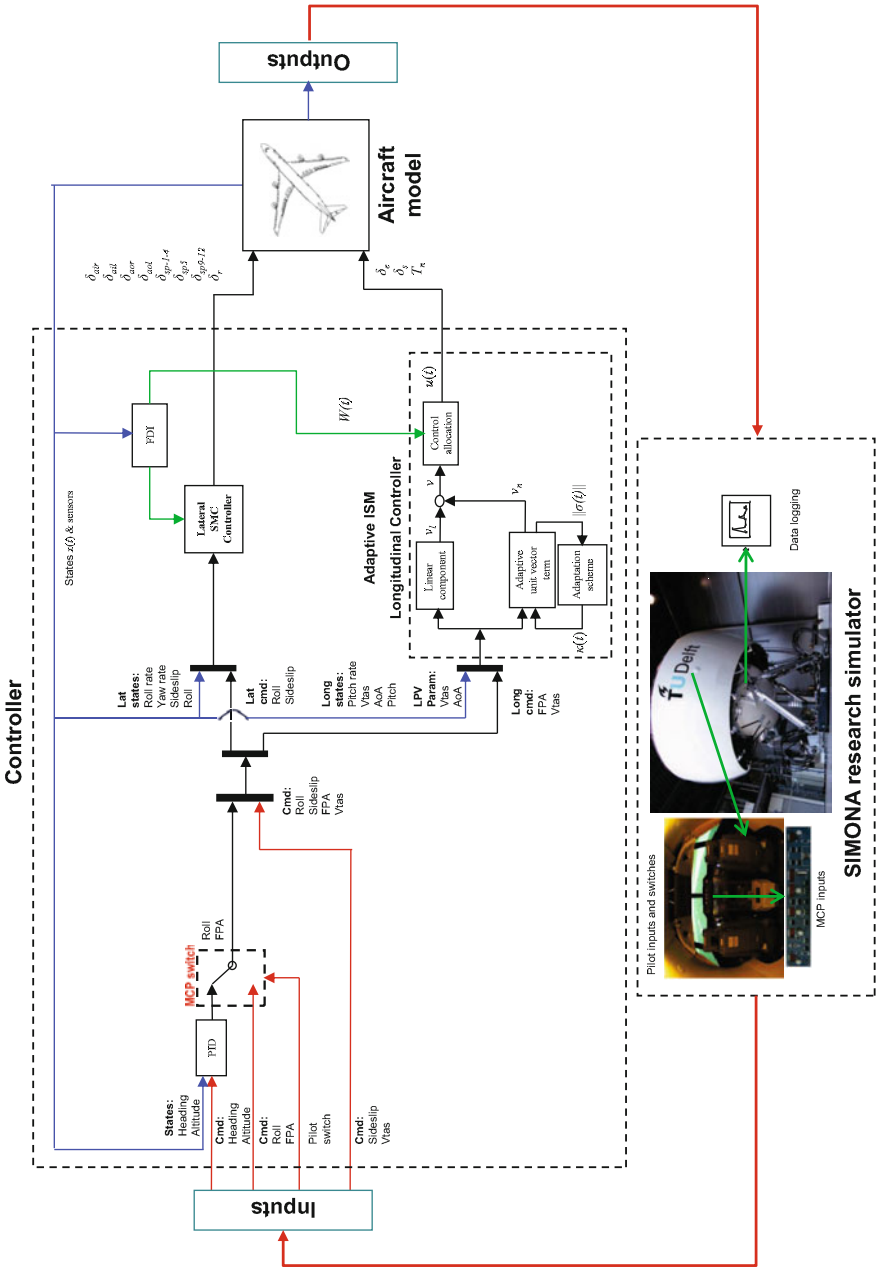

Fig. 9.3 Controller interconnection

9.3 SRS Piloted Evaluation Results

The results in this section represent evaluation tests by an experienced commercial pilot. Figure 9.4 shows the overall manoeuvres for three different tests: fault-free, elevator jam and stabiliser runaway. The following describes the sequence of manoeuvres conducted during the pilot evaluation:

1. Straight and level flight at 250 kts (128.6 m/s), 2000 ft (609.6 m) heading North.
2. Insert failure (for failure cases).
3. Right turn 90 deg (East).
4. Left turn back to 0 deg (North).
5. Altitude change to 4000 ft (1219.2 m).
6. Altitude change back to 2000 ft (609.6 m).
7. Acceleration to 300 kts (154.3 m/s) (indicated air speed).
8. Deceleration to 250 kts (128.6 m/s) (indicated air speed).
9. Deceleration to 228 kts (117.3 m/s) (indicated air speed).

Note that each manoeuvre was allowed to reach steady state before the next sequence was tested.

The controller has been tested at the trim condition

$$(5.53\ \text{deg},\ 0.0017\ \text{deg/s},\ 133.8\,\text{m/s},\ 5.53\ \text{deg},\ 600\,\text{m})$$

with an input trim (2 deg, -1.59 deg, 45568 N) with an initial mass of 317,000 kg and with the flaps fully retracted. This represents one of the trim conditions used

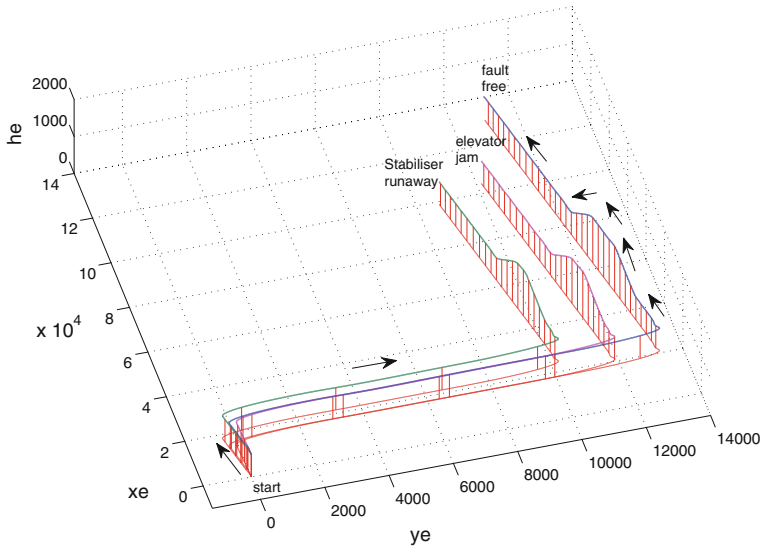

Fig. 9.4 Pilot evaluation: Trajectory

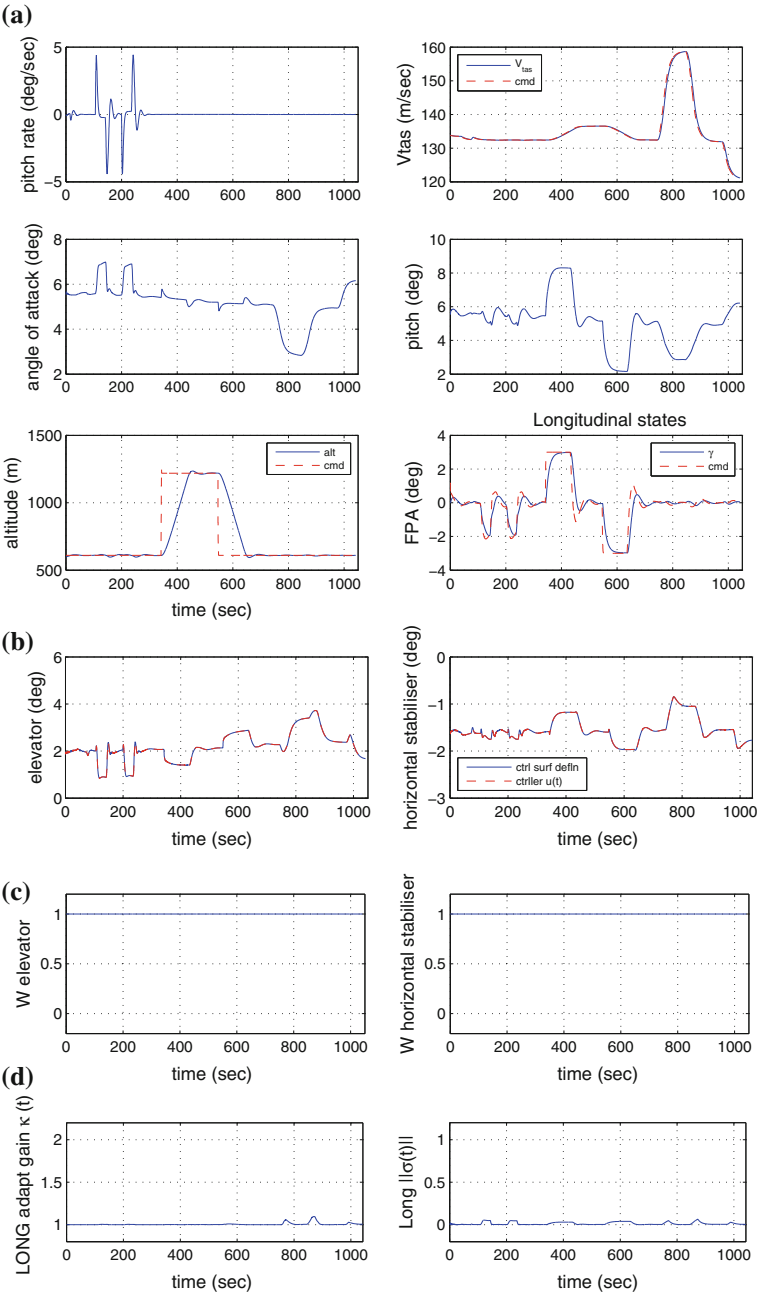

Fig. 9.5 Pilot evaluation—fault-free longitudinal performance. **a** Longitudinal states, **b** Longitudinal control surfaces, **c** control surface effectiveness estimation, **d** switching function and adaptive gain

for the GARTEUR FM-AG16 benchmark problem and it is different to the trim conditions of the LPV model in Appendix A.1.1. Using different flight conditions for the evaluation highlights the capability of the designed controller to operate in regions away from the design point.

Remark 9.1 Note that the aircraft trajectories for the three different tests in Fig. 9.4 are not identical. This is due to the fact that the manoeuvres were 'manually' flown by the pilot using the mode control panel. Although the magnitudes of the heading, altitude and speed commands are the same, the times at which each manoeuvre is executed are different.

9.3.1 Fault-Free

Figure 9.5 shows longitudinal fault-free performance. The longitudinal states and the tracking performance is shown in Fig. 9.5a. Figure 9.5b shows the control surface deflections during nominal fault-free conditions. Figure 9.5c shows that no fault/failure is present in the elevator or stabiliser (the actuator effectiveness is $W(t) = 1$ for both surfaces). Finally Fig. 9.5d shows the nominal variation in the switching function and the adaptive gain due to changes in the operating conditions.

9.3.2 Elevator Jam

Figure 9.6 shows the pilot evaluation for the case of an elevator jam. Figure 9.6c shows the elevator failure occurred at approximately 63 s when the effectiveness level drops to zero. The effect of the elevator jam can be seen in Fig. 9.6b. After this point in time, the stabiliser becomes more active in order to compensate for the jammed elevator. Despite the presence of a failure, Fig. 9.6a shows similar state tracking performance as the fault-free case. Finally Fig. 9.6e shows the switching function is still close to zero indicating sliding is still maintained. Figure 9.6d shows a magnified portion of the estimate of the elevator effectiveness levels in the case of the elevator fault in Fig. 9.6c. Figure 9.6d shows that the estimation provided by the FDI scheme considered in this chapter[3] is not perfect, and includes detection delays (arising from the moving window of information and the filters employed to ensure a usable estimate of the actuator effectiveness levels).

[3] See page 265 of [2].

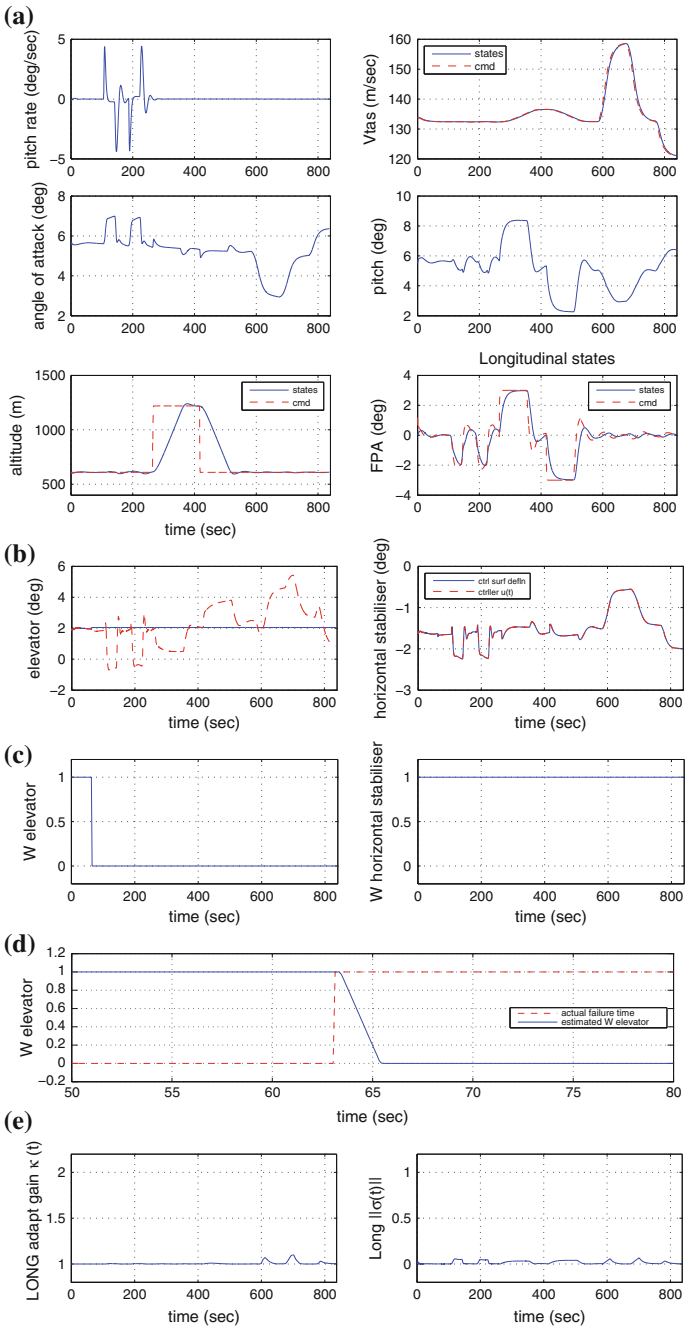

Fig. 9.6 Pilot evaluation—Elevator jam. **a** states, **b** control surfaces, **c** control surface effectiveness estimation, **d** zoomed in elevator estimated effectiveness level estimation

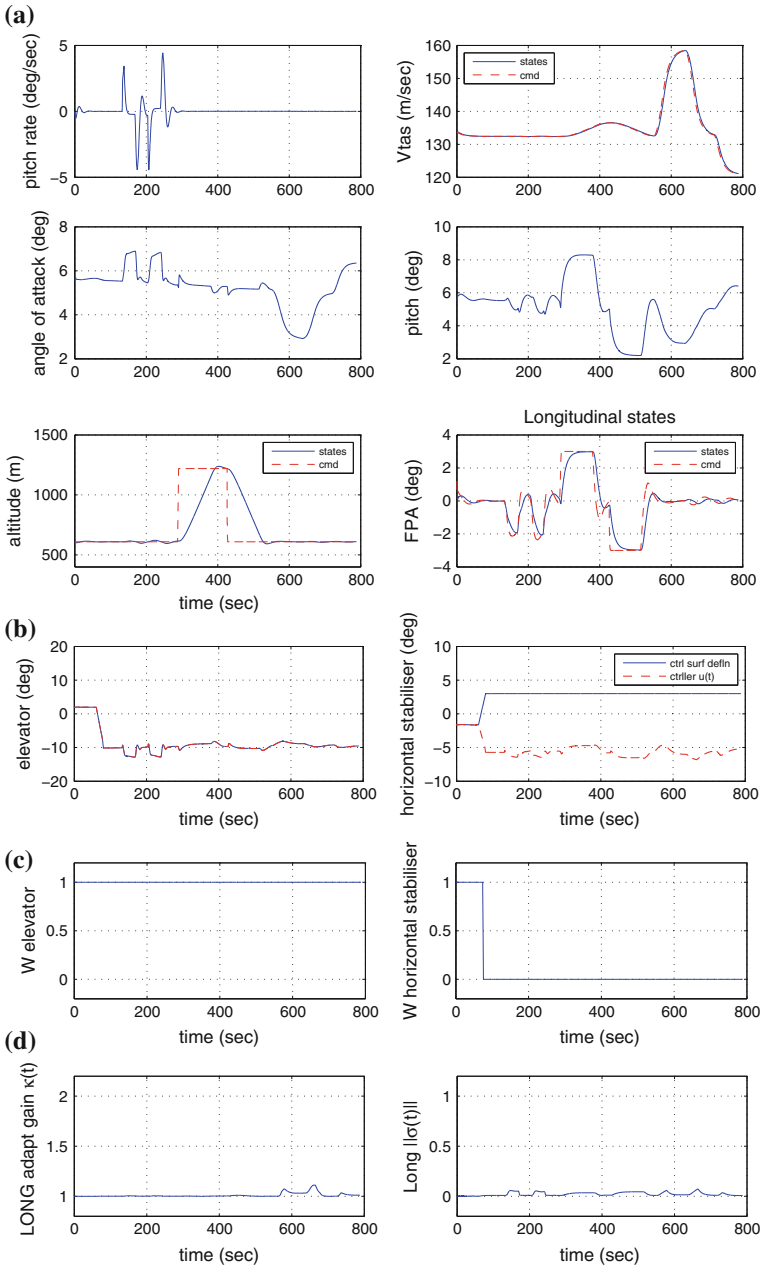

Fig. 9.7 Pilot evaluation: Stabiliser runaway. **a** states, **b** control surfaces, **c** control surface effectiveness estimation, **d** switching function and adaptive gain

9.3.3 Stabiliser Runaway

Figure 9.7 shows the evaluation results for the more challenging case of a stabiliser runaway at approximately 74 s (see Fig. 9.7c). The effect of the stabiliser runaway can be seen in Fig. 9.7b, where the stabiliser runs-away at its maximum rate to the maximum physical limits of 3 deg. Figure 9.7b also shows the deflection of the elevator to approximately −10 deg immediately after the stabiliser saturates in order to compensate for the stabiliser runaway. Despite the presence of this critical failure, Fig. 9.7a shows hardly any noticeable difference in terms of state tracking performance as compared to the fault-free case. Figure 9.7d shows that sliding is still being maintained, and the adaptive gain remains low.

9.3.4 Pilot Feedback

The following observations and discussions represent feedback from the pilot and the SRS researcher conducting the evaluation for all the three scenarios. Generally, the feedback from the pilot and the SRS researcher indicates that all three tests (nominal, the elevator jam and the stabiliser runaway) showed very similar performance and the pilot was unable to discern a meaningful difference, without looking at the surface deflections. The pilot reported that no transients were observed at the time of the failures. (In fact the SRS researcher had to double check that failures had actually occurred).

Some specific comments from the pilot and SRS researcher on the performance of the longitudinal controller are:

- Speed capturing was satisfactory, with some creep towards the set speed at the end.
- Altitude change capturing resulted in a rather careful 1400 feet (426.7 m) per minute rate for a 2000 ft (609.6 m) change. A rule of thumb is 2000 ft per minute (609.6 m per minute) for a 2000 ft change. A small overshoot of 60 ft (18.3 m) was observed on both climb and descent, which though not excessive, would not be acceptable in practice. The altitude set point was passed at around 600 ft (182.8 m) per minute. The subsequent undershoot of 20 ft (6.1 m) is also not desirable. A first-order response with no over or undershoot is desirable, rather than the current damped second order response.
- Speed tracking was acceptable during the manoeuvres (1 or 2 kts (0.51 or 1.03 m/s) deviations were observed, which is acceptable).
- Altitude tracking was generally good, apart from the small 40 ft (12.2 m) drop during heading capture.

9.4 Summary

This chapter has presented the results from real-time implementation and testing of the LPV based adaptive FTC scheme described in Chap. 8, on the SIMONA research simulator. The integral sliding mode approach ensures ideal sliding throughout the closed-loop system response, and maintains near to nominal performance in the face of actuator faults/failures. The scheme also takes into account imperfect estimation of the actuator effectiveness levels and considers an adaptive gain in the nonlinear component of the control law, to account for the imperfect estimation of the actuator effectiveness levels. The FTC scheme has been implemented and evaluated in a realistic operational environment with a pilot-in-the-loop. Evaluation results from the SIMONA research simulator show good tracking performance even in the event of faults/failures.

9.5 Notes and References

The SIMONA research simulator is a powerful tool and serves as a proof of concept test-bed in various research areas, for example: research into human-machine interaction [3], human motion perception [4–6], air traffic control [7], flight procedures [8, 9], aircraft handling qualities [10, 11], fly-by-wire control algorithms and flight deck displays [12, 13]. The SRS has been used to evaluate the real-time performance of different fault tolerant control algorithms in a pilot-in-the-loop configuration, considering the real EL AL flight 1862 accident scenario [14, 15]. A re-enactment of this incident was considered and implemented on the SIMONA research simulator in [16, 17]. In [16], a sliding mode FTC scheme using a fixed control allocation structure was tested whereas in [17], an adaptive nonlinear dynamic inversion approach was used for manual fly-by-wire control. Adaptive sliding mode FTC schemes were proposed in [18] where both fixed and online control allocation structures were compared by implementing them both in a piloted simulator environment. Recently in [19], propulsion-control tests were conducted on SIMONA, considering the failure of all control surfaces. The proposed fault tolerant sliding mode control allocation scheme in [19] was shown to be capable of dealing with the loss of all control surfaces and was able to achieve a safe emergency landing using only the engines.

References

1. Alwi, H., Edwards, C., Stroosma, O., Mulder, J.A.: Evaluation of a sliding mode fault-tolerant controller for the EL AL incident. AIAA j. Guid. Control Dyn. **33**(3), 677–694 (2010)
2. Alwi, H., Edwards, C., Tan, C.P.: Fault Detection and Fault Tolerant Control Using Sliding Modes. Advances in Industrial Control Series. Springer, London (2011)

3. Stroosma, O., Paassen, R.V., Mulder, M.: Using the SIMONA research simulator for human-machine interaction research. In: AIAA Modeling and Simulation Technologies Conference (2003)
4. Heerspink, H.M., Berkouwer, W.R., Stroosma, O., Paassen, R.V., Mulder, M., Mulder, J.: Evaluation of vestibular thresholds for motion detection in the SIMONA research simulator. In: AIAA Modeling and Simulation Technologies Conference (2005)
5. Valente Pais, A.R., Mulder, M., Paassen, R.V., Wentink, M., Groen, E.L.: Modeling human perceptual thresholds in self–motion perception. In: AIAA Modeling and Simulation Technologies Conference (2006)
6. Zaal, P.M.T., Nieuwenhuizen, F.M., Mulder, M., Paassen, R.V.: Perception of visual and motion cues during control of self–motion in optic flow environments. In: AIAA Modeling and Simulation Technologies Conference (2006)
7. Vormer, F.J., Mulder, M., Paassen, R.V., Mulder, J.: Optimization of flexible approach trajectories using a genetic algorithm. J. Aircr. **43**, 941–952 (2006)
8. De Gaay, W.F., Paassen, R.V., Mulder, M., In't Veld, A.C., Clarke, J.P.: Implementing time-based spacing for decelerating approaches. J. Aircr. **44**(1), 106–118 (2007)
9. De Prins, J.L., Schippers, F.K.M., Mulder, M., Paassen, R.V., In't Veld, A.C., Clarke, J.P.: Enhanced self-spacing algorithm for three-degree decelerating approaches. J. Guid. Control Dyn. **30**, 576–590 (2007)
10. Gouverneur, B., Mulder, J., Paassen, R.V., Stroosma, O.: Optimization of the SIMONA research simulator's motion filter settings for handling qualities experiments. In: AIAA Modeling and Simulation Technologies Conference (2003)
11. Field, E.J., Pinney, T.R., Paassen, R.V., Stroosma, O., Rivers, R.A.: Effects of implementation variations on the results of piloted simulator handling qualities evaluations. In: AIAA Modeling and Simulation Technologies Conference (2004)
12. Lam, T.M., Mulder, M., Paassen, R.V., Mulder, J.: Comparison of control and display augmentation for perspective flight-path displays. J. Guid. Control Dyn. **29**, 564–578 (2006)
13. Mulder, M., Veldhuijzen, A.R., Paassen, R.V., Mulder, J.: Integrating Fly-by-Wire controls with perspective flight-path displays. J. Guid. Control Dyn. **28**, 1263–1274 (2005)
14. Stroosma, O., Smaili, H., Lombaerts, T., Mulder, B.: Piloted simulator evaluation of new fault-tolerant flight control algorithms for reconstructed accident scenarios. In: AIAA Modeling and Simulation Technologies Conference (2008)
15. Stroosma, O., Lombaerts, T., Smaili, H., Mulder, M.: Real-time assessment and piloted evaluation of fault tolerant flight control designs in the SIMONA research flight simulator. In: Edwards, C., Lombaerts, T., Smaili, H. (eds.), Fault Tolerant Flight Control of LNCIS, vol. 399, pp. 451–475. Springer, Heidelberg (2010)
16. Alwi, H., Edwards, C., Stroosma, O., Mulder, J.: Piloted sliding mode FTC simulator evaluation for the ELAL Flight 1862 incident. In: AIAA Guidance, Navigation and Control Conference and Exhibit (2008)
17. Lombaerts, T., Smaili, H., Stroosma, O., Chu, Q.P., Mulder, J., Joosten, D.A.: Piloted simulator evaluation results of new fault-tolerant flight control algorithm. J. Guid. Control Dyn. **32**(6), 1747–1765 (2009)
18. Alwi, H., Edwards, C., Stroosma, O., Mulder, J.: Fault tolerant sliding mode control design with Piloted Simulator Evaluation. J. Guid. Control Dyn. **31**(5), 1186–1201 (2008)
19. Alwi, H., Edwards, C., Stroosma, O., Mulder, J.: Sliding-mode propulsion-control tests on a motion flight simulator. J. Guid. Control Dyn. **38**(4), 671–684 (2014)

Appendix A
Benchmark Model of Large Transport Aircraft

A.1 RECOVER Benchmark Model

The RECOVER (REconfigurable COntrol for Vehicle Emergency Return) benchmark model [1], which runs in the MATLAB/SIMULINK environment has been used in the Group for Aeronautical Research and Technology in Europe Flight Mechanics Action Group (GARTEUR FM-AG16). The purpose of the FM-AG16 project [1] was to conduct research in Europe to develop advanced FTC schemes for aerospace applications to cope with realistic malfunctions in actuators, sensors and control surfaces. The RECOVER model consists of 77 states and includes four engines and 25 other control surfaces (four elevators, one stabiliser, four ailerons, 12 spoilers and flaps). The RECOVER aircraft model includes realistic sensor and actuator models with realistic limits and aerodynamic effects (such as blowdown). The RECOVER software has the ability to test actuator fault/failure scenarios (elevator jam, stabiliser runaway, aileron jam and rudder runaway) and also includes the EL AL flight 1862 failure case. This software is an upgraded version of Delft University's Aircraft Simulation and Analysis Tool, DASMAT, and Flight lab 747 FTLAB747 [2]. In the upgraded version [3], the mechanically linked control surfaces (inherited from the original B747-100/200 aircraft) have been removed and replaced by individually controlled surfaces similar to more modern aircraft which use fly-by-wire systems. The removal of the mechanical link allows more flexibility in terms of fault tolerant control by creating a highly redundant system which is suitable to test state-of-the-art FTC schemes. The RECOVER software [2–4], used in this book has been used by many researchers [5–9] and is a validated benchmark platform for research in the fields of FTC and FDI.

The rigid body states of the B747-100/200 aircraft for the longitudinal, lateral and directional axis are

$$x(t) = (p, q, r, V_{tas}, \alpha, \beta, \phi, \theta, \psi, h_e, x_e, y_e) \tag{A.1}$$

M.T. Hamayun et al., *Fault Tolerant Control Schemes Using Integral Sliding Modes*, Studies in Systems, Decision and Control 61,
DOI 10.1007/978-3-319-32238-4

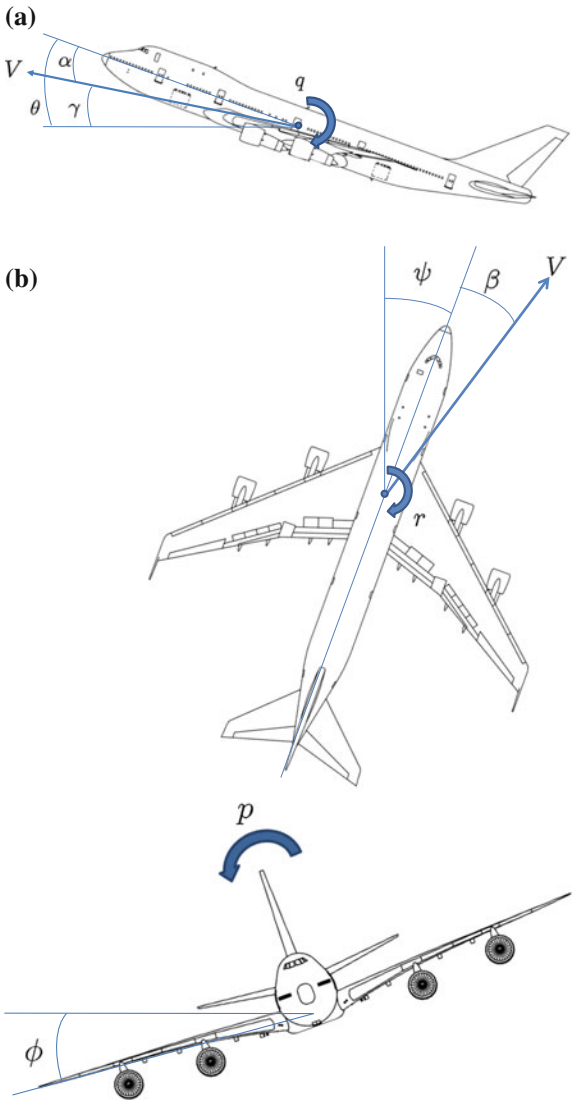

Fig. A.1 Aircraft attitudes (adapted from [1]). **a** Longitudinal. **b** Lateral and directional

which are determined from the 6-DOF equations. In Eq. A.1 the states for the longitudinal axis (Fig. A.1a) are $x_{long} = (q, V_{tas}, \alpha, \theta, h_e)$, which represent pitch rate q (rad/s), true air speed V_{tas} (m/s), angle of attack α (rad), pitch angle θ (rad) and altitude h_e (m). On the other hand the states for the lateral and directional axis (Fig. A.1b) are $x_{lat} = (p, r, \beta, \phi, \psi)$, which represent roll rate p (rad/s), yaw rate r (rad/s), sideslip β (rad), roll angle ϕ (rad) and yaw angle ψ (rad). In Eq. (A.1), the states (h_e, x_e, y_e) represent geometric earth position, along the z-axis, x-axis and y-axis respectively. The typical control surfaces for the longitudinal and lateral axis control

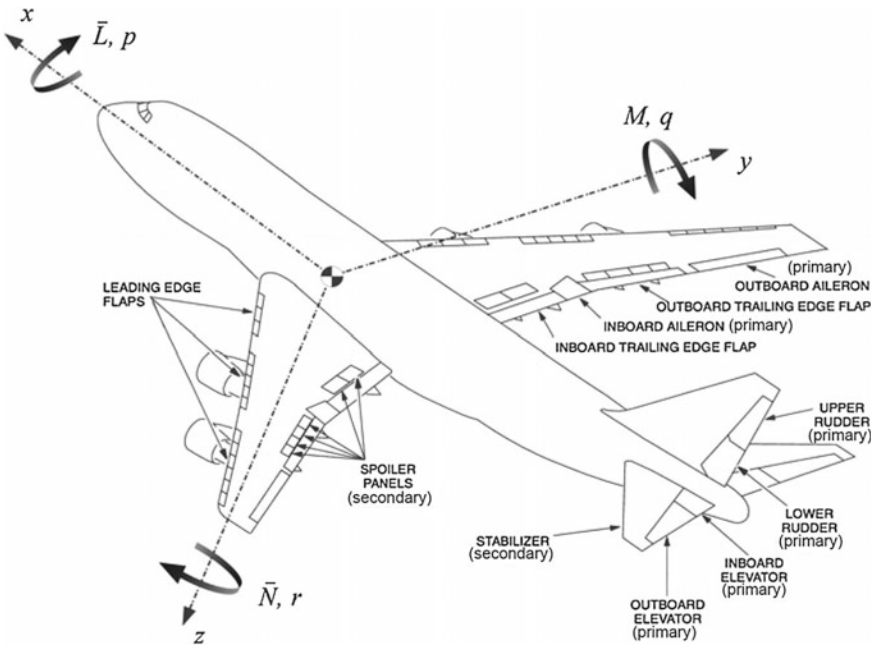

Fig. A.2 Boeing 747 flight control surface arrangements and body axes and moment definitions (L = rolling moment, M = pitching moment, N = yawing moment, p = roll rate, q = pitch rate, r = yaw rate) (Figure adapted from [1])

are shown in Fig. A.2. The control surfaces which are typically used for longitudinal axis control comprise 4 elevators (inboard and outboard), a horizontal stabiliser, 4 engines thrusts (two on each wing), which can be controlled through the Engine Pressure Ratio (EPR). For lateral axis control, 4 ailerons (inboard and outboard on each wing), 12 spoilers (2 inboard and 4 outboard spoilers on each wing), 2 rudders (upper and lower), and 4 engines thrusts (controlled through EPR) are used. A linear state-space model of the RECOVER benchmark can be obtained at a given trim point. At the trim point, the aircraft is in steady state for example straight and level flight. In this book the longitudinal and lateral axis of the benchmark model, at different trim conditions, is considered as the basis for designing the FTC schemes. For example in Chaps. 3 and 5, the simulations are based around an operating condition of straight and level flight at 263,000 kg, 92.6 m/s true airspeed, and at an altitude of 600 m based on 25.6 % of maximum thrust and at a 20 deg flap position. The result is a 12th order linear model, which can be divided into two six order models for longitudinal and lateral axis control. The first four states $x_{long} = (q, V_{tas}, \alpha, \theta)$ and $x_{lat} = (p, r, \beta, \phi)$ are used for the controller design. At this trim condition the state-space matrices are:

$$A_{long} = \begin{bmatrix} -0.5137 & 0.0004 & -0.5831 & 0 \\ 0 & -0.0166 & 1.7171 & -9.8046 \\ 1.0064 & -0.0021 & -0.6284 & 0 \\ 1.0000 & 0 & 0 & 0 \end{bmatrix} \tag{A.2}$$

$$B_{long} = \begin{bmatrix} -0.6228 & -1.3578 & 0.0082 & 0.0218 & 0.0218 & 0.0082 \\ 0 & -0.1756 & 1.4268 & 1.4268 & 1.4268 & 1.4268 \\ 0.0352 & -0.0819 & 0.0021 & -0.0021 & -0.0021 & -0.0021 \\ 0 & 0 & 0 & 0 & 0 & 0 \end{bmatrix} \tag{A.3}$$

$$A_{lat} = \begin{bmatrix} -1.0579 & 0.1718 & -1.6478 & 0.0004 \\ 0.1186 & -0.2066 & 0.2767 & -0.0019 \\ 0.1014 & -0.9887 & -0.0999 & 0.1055 \\ 1.0000 & 0.0893 & 0 & 0 \end{bmatrix} \tag{A.4}$$

$$B_{lat} = \begin{bmatrix} -0.0832 & 0.0832 & -0.2285 & 0.2285 & -0.2625 & -0.0678 & 0.0678 \\ -0.0154 & 0.0154 & -0.0123 & 0.0123 & -0.0180 & -0.0052 & 0.0052 \\ 0 & 0 & 0 & 0 & 0.0017 & 0.0006 & -0.0006 \\ 0 & 0 & 0 & 0 & 0 & 0 & 0 \\ 0.2625 & 0.1187 & 0.0246 & 0.0140 & -0.0140 & -0.0246 & \\ 0.0180 & -0.2478 & 0.1269 & 0.0724 & -0.0724 & -0.1269 & \\ -0.0017 & 0.0174 & 0.0005 & 0.0005 & -0.0005 & -0.0005 & \\ 0 & 0 & 0 & 0 & 0 & 0 & \end{bmatrix} \tag{A.5}$$

where the control surfaces for the longitudinal axis are

$$\delta_{long} = (\delta_e, \delta_s, e1_{long}, e2_{long}, e3_{long}, e4_{long}) \tag{A.6}$$

which represent elevator deflection (rad) (4 elevators are aggregated to produce one control input), horizontal stabiliser deflection (rad) and four longitudinal engines pressure ratios. For lateral axis control the control surfaces comprise

$$\delta_{lat} = (\delta_{air}, \delta_{ail}, \delta_{aor}, \delta_{aol}, sp_{1-4}, sp_5, sp_8, sp_{9-12}, \delta_r, e1_{lat}, e2_{lat}, e3_{lat}, e4_{lat}) \tag{A.7}$$

which represent aileron inboard (right and left) deflection (rad), aileron outboard (right and left) deflection (rad), left wing spoiler deflections (rad) ($sp_1 - sp_4$, sp_5), right wing spoiler deflections (rad) (sp_8, $sp_9 - sp_{12}$), rudder deflection (rad) (the upper and lower rudders are aggregated to produce one control input) and four lateral engine pressure ratios. The spoilers sp_6 and sp_7 are ground spoilers and are not used in flight. Further details of the RECOVER model can be found in [1, 2] and the references therein.

A.1.1 LPV Plant of a RECOVER Benchmark Model

The LPV plant representation of the RECOVER model used for longitudinal controller design is obtained from [10], where the LPV model is approximated by polynomially fitting the aerodynamic coefficients obtained from [11] to create an LPV representation using the function substitution method. The aerodynamic coefficients are polynomial functions of velocity V_{tas} and angle of attack α in the range of $\left[\,150,\ 250\,\right]$ m/s and $\left[\,-2,\ 8\,\right]$ deg respectively and at the altitude of 7000 m. The states of the LPV plant are $(\bar{\alpha}, \bar{q}, \bar{V}_{tas}, \bar{\theta}, \bar{h}_e)$ which represent *deviation* of the angle of attack, pitch rate, true air speed, pitch angle and altitude from their trim values. The inputs of the LPV plant are $(\bar{\delta_e}, \bar{\delta_s}, \bar{T_n})$, which represent deviation of elevator deflection, horizontal stabiliser deflection and total engine thrust from their trim values respectively. The trim values of the states are

$$(\alpha_{trim}, q_{trim}, V_{tas_{trim}}, \theta_{trim}, h_{e_{trim}}) = (1.05\,\text{deg}, 0\,\text{deg/s}, 227.02\,\text{m/s}, 1.05\,\text{deg}, 7000\,\text{m})$$

and the trim values of the LPV plant inputs are

$$(\delta_{e_{trim}}, \delta_{s_{trim}}, T_{n_{trim}}) = (0.163\,\text{deg}, 0.590\,\text{deg}, 42291\,\text{N})$$

The LPV system matrices are given by

$$A(\rho) = A_0 + \sum_{i=1}^{7} \rho_i A_i \quad \text{and} \quad B(\rho) = B_0 + \sum_{i=1}^{7} \rho_i B_i \tag{A.8}$$

where

$$(\rho_1, \ldots, \rho_7) := (\bar{\alpha}, \bar{V}_{tas}, \bar{V}_{tas}\bar{\alpha}, \bar{V}_{tas}^2, \bar{V}_{tas}^2\bar{\alpha}, \bar{V}_{tas}^3, \bar{V}_{tas}^4)$$

where $\bar{\alpha} = \alpha - \alpha_{trim}$ and $\bar{V}_{tas} = V_{tas} - V_{tas_{trim}}$. After reordering, the LPV plant states for the control law design become $(\bar{\theta}, \bar{\alpha}, \bar{V}_{tas}, \bar{q})$. The LPV system matrix is given by

$$A(\rho) = \begin{bmatrix} 0 & 0 & 0 & a_{14}(\rho) \\ 0 & a_{33}(\rho) & a_{32}(\rho) & a_{34}(\rho) \\ a_{21}(\rho) & a_{23}(\rho) & a_{22}(\rho) & 0 \\ 0 & a_{43}(\rho) & a_{42}(\rho) & a_{44}(\rho) \end{bmatrix} \tag{A.9}$$

where

$$\begin{aligned} a_{14}(\rho) &= 1 \\ a_{33}(\rho) &= -0.5935 - 2.5923 \times 10^{-3}\rho_2 \\ a_{32}(\rho) &= -5.2124 \times 10^{-4} - 6.2678 \times 10^{-7}\rho_2 + 1.1121 \times 10^{-11}\rho_4 \\ a_{34}(\rho) &= 0.9914 \end{aligned}$$

$$
\begin{aligned}
a_{21}(\rho) &= -9.7851 \\
a_{23}(\rho) &= 5.7733 - 84.5625\rho_1 - 3.5127 \times 10^{-2}\rho_2 - 0.7450\rho_3 - 0.7736 \times 10^{-4}\rho_4 \\
&\quad -1.6408 \times 10^{-3}\rho_5 \\
a_{22}(\rho) &= -6.1168 \times 10^{-3} - 2.1091 \times 10^{-5}\rho_2 - 2.2374 \times 10^{-8}\rho_4 \\
a_{43}(\rho) &= -1.9626 + 3.4170\rho_1 - 0.01729\rho_2 + 0.0301\rho_3 - 0.38081 \times 10^{-4}\rho_4 \\
&\quad +6.630 \times 10^{-5}\rho_5 \\
a_{42}(\rho) &= -4.9579 \times 10^{-4} - 3.8893 \times 10^{-6}\rho_2 - 7.6201 \times 10^{-9}\rho_4 \\
&\quad +0.19644 \times 10^{-11}\rho_6 \\
a_{44}(\rho) &= -0.46087 - 0.00203\rho_2
\end{aligned}
$$

and the LPV input distribution matrix is

$$
B(\rho) = \begin{bmatrix} 0 & 0 & 0 \\ b_{31}(\rho) & b_{32}(\rho) & b_{33}(\rho) \\ 0 & 0 & b_{23}(\rho) \\ b_{41}(\rho) & b_{42}(\rho) & b_{43}(\rho) \end{bmatrix} \tag{A.10}
$$

where

$$
\begin{aligned}
b_{31}(\rho) &= -0.0358 - 1.1877 \times 10^{-5}\rho_2 + 1.5311 \times 10^{-6}\rho_4 + 3.9135 \times 10^{-9}\rho_6 \\
b_{32}(\rho) &= -0.0716 \\
b_{33}(\rho) &= -3.6326 \times 10^{-4} - 5.8732 \times 10^{-3}\rho_1 + 1.6002 \times 10^{-6}\rho_2 \\
&\quad +0.25871 \times 10^{-4}\rho_3 \\
b_{23}(\rho) &= 1.3323 - 0.058133\rho_1 \\
b_{41}(\rho) &= -1.7696 - 0.0089\rho_2 + 0.5985 \times 10^{-4}\rho_4 + 0.4428 \times 10^{-6}\rho_6 \\
&\quad +0.6912 \times 10^{-9}\rho_7 \\
b_{42}(\rho) &= -3.9993 - 0.035233\rho_2 - 0.776 \times 10^{-4}\rho_4 \\
b_{43}(\rho) &= 0.015328.
\end{aligned}
$$

References

1. Edwards, C., Lombaerts, T., Smaili, H.: Fault Tolerant Flight Control: A Benchmark Challenge. Springer, Berlin (2010)
2. Marcos, A., Balas, G.J.: A Boeing 747-100/200 aircraft fault tolerant and diagnostic benchmark. Technical Report AEM–UoM–2003–1, Department of Aerospace and Engineering Mechanics, University of Minnesota (2003)
3. Smaili, M., Breeman, J., Lombaerts, T., Joosten, D.: A simulation benchmark for integrated fault tolerant flight control evaluation. In: AIAA Modeling and Simulation Technologies Conference and Exhibit (2006)
4. van der Linden C.M.: DASMAT Delft University Aircraft Simulation Model and Analysis Tool. Technical Report LR-781, Delft University of Technology, Delft, The Netherlands (1996)

5. Alwi, H., Edwards, C., Tan, C.P.: Fault Detection and Fault Tolerant Control Using Sliding Modes. Advances in Industrial Control Series. Springer, Berlin (2011)
6. Wang, T., Xiey, W., Zhang, Y.: Adaptive sliding mode fault tolerant control of civil aircraft with separated uncertainties. In: 48th AIAA Aerospace Sciences Meeting Including the New Horizons Forum and Aerospace Exposition, pp. 1–9 (2010)
7. Ganguli, S., Marcos, A., Balas, G.J.: Reconfigurable LPV control design for Boeing 747-100/200 longitudinal axis. In: Proceedings of the American Control Conference (2002)
8. Alwi, H., Edwards, C.: Robust actuator fault reconstruction for LPV systems using sliding mode observers. In: Proceedings of the 49th IEEE Conference on Decision and Control, pp. 84–89 (2010)
9. Henning, A., Balas, G.J.: MPC supervisory flight controller: a case study to flight EL AL 1862. In: AIAA Guidance, Navigation and Control Conference and Exhibit, pp. 1–17 (2008)
10. Khong, T.H., Shin, J.: Robustness analysis of integrated LPV-FDI filters and LTI-FTC system for a transport aircraft. In: AIAA Guidance, Navigation, and Control Conference and Exhibit, AIAA-2007-6771 (2007)
11. Marcos, A., Balas, G.J.: Development of linear-parameter-varying models for aircraft. AIAA J. Guid. Control Dyn. **27**(2), 218–228 (2004)

Appendix B
Closed-Loop Stability and Feedback Gain Synthesis

B.1 $\mathscr{L}_2$ Gain and Small Gain Theorem

B.1.1 $\mathscr{L}_2$ Gain

In the case of LTI systems the $\mathscr{L}_2$ gain can be calculated accurately [1]. Consider a LTI system

$$\dot{x}(t) = Ax(t) + Bu(t)$$
$$y(t) = Cx(t) + Du(t)$$

where it is assumed that the system matrix A is *Hurwitz*. The system above can be written as $G(s) = C(sI - A)^{-1}B + D$, then according to Theorem 6.4 in [2], the $\mathscr{L}_2$ gain of the system $G(s)$ is $\sup_{\omega \in \mathbf{R}} \|G(\, j\omega)\|_2$, which is the induced 2-norm of the system $G(j\omega)$. The $\mathscr{L}_2$ gain of the system in the time domain is equal to the $\mathscr{H}_\infty$ norm in the frequency domain [2], which means if $Y(j\omega) = G(j\omega)U(j\omega)$, then from Theorem 6.4 [2] it is shown that

$$\|y\|_{\mathscr{L}_2}^2 \leq (\sup_{\omega \in \mathbf{R}} \|G(j\omega)\|_2)^2 \|u\|_{\mathscr{L}_2}^2 \tag{B.1}$$

where $\|u\|_{\mathscr{L}_2}^2 = \int_0^\infty u^T(t)u(t)dt$.

B.1.2 Small Gain Theorem

The small gain theorem is a systematic approach to investigate the input-output stability of interconnected dynamical systems [2]. Consider the feedback interconnection in Fig. B.1. Suppose that e_1 is the input to system H_1 and y_1 is the output,

M.T. Hamayun et al., *Fault Tolerant Control Schemes Using Integral Sliding Modes*, Studies in Systems, Decision and Control 61,
DOI 10.1007/978-3-319-32238-4

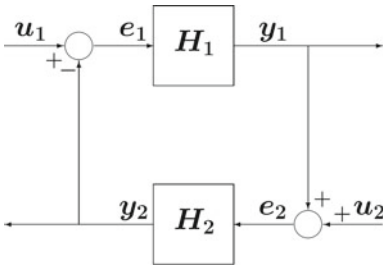

Fig. B.1 Feedback interconnection of two systems (adapted from [2])

then the system H_1 is finite gain $\mathscr{L}_2$ stable if $\|y_1\|_{\mathscr{L}_2} \leq \gamma_1 \|e_1\|_{\mathscr{L}_2}$. Now consider the interconnection of two systems as shown in Fig. B.1, then according to the small gain theorem [2], with the assumption that the two systems H_1 and H_2 are finite gain $\mathscr{L}_2$ stable, with $\mathscr{L}_2$ gains γ_1 and γ_2 respectively, then the feedback connection will be finite gain $\mathscr{L}_2$ stable if

$$\gamma_2 \gamma_1 < 1 \tag{B.2}$$

The proof can be found in [2].

B.2 LMI Equivalence of Closed-Loop Stability Analysis

To satisfy the stability condition of Theorem 3.1 in Chap. 3, a closed-loop analysis is carried out in an LMI framework, in order to find a feedback gain F such that the $\mathscr{H}_\infty$ norm of the transfer function $\tilde{G}(s) = F(sI - \tilde{A})^{-1}\tilde{B}$ is less than some predefined scalar γ i.e. $\|\tilde{G}(s)\|_\infty < \gamma$. Two constraints are imposed on the design of the feedback gain F which need to be satisfied simultaneously. Firstly to achieve (nominal) performance, an LQR formulation is used; and secondly, to ensure the design of an F to satisfy the stability condition of Theorem 3.1, a Bounded Real Lemma (BRL) formulation is used.

B.2.1 LMI Formulation of the LQR problem

In Sect. 3.2.4 the design of the feedback gain F is based on the nominal system in (3.18). For the LMI formulation of the LQR problem, consider the LTI system

$$\dot{x}(t) = Ax(t) + B_v v(t) \tag{B.3}$$

$$z(t) = Q_1 x(t) + R_1 v(t) \tag{B.4}$$

where v represents the (virtual) control input and Q_1 and R_1 are symmetric positive definite matrices where $Q_1^T R_1 = 0$. The LQR problem involves determining the

control law $v(t) = -Fx(t)$ such that $J = \int_0^\infty z^T z$ is minimised. Consider the Lyapunov function $V(x) = x^T Px$ where $P > 0$ and assume the inequality

$$\dot{V} + z^T z \leq 0 \qquad \text{holds for all } x \text{ and } z \tag{B.5}$$

Integrating (B.5) yield the expression

$$J = \int_0^\infty z^T z \leq V(0) - V(\infty)$$

Since a stabilising gain F is required, $x(t) \to 0$ as $t \to \infty$ and $V(\infty) = 0$. Therefore

$$J \leq x^T(0)Px(0)$$

Clearly the cost J depends on the specific initial condition $x(0)$. If $x(0)$ is treated as a random variable with zero mean, then[1]

$$\begin{aligned} \mathbb{E}(J) &\leq \mathbb{E}\left(\text{trace}\left(x^T(0)Px(0)\right)\right) \\ &= \text{trace}\left(\mathbb{E}\left(x^T(0)Px(0)\right)\right) \\ &= \text{trace}(P)\text{Var}\left(x(0)\right) \end{aligned} \tag{B.6}$$

where $\text{Var}(\cdot)$ represents the variance of a random variable. From (B.6) minimising $\text{trace}(P)$ subject to (B.5) is an appropriate approach.

Taking the time derivative of $V(x)$ and substituting from (B.3) yields

$$\dot{V} = x^T(PA + A^T P)x + x^T PB_v v + v^T B_v^T Px$$

Substituting the value of $\dot{V}$ above and (B.4) into (B.5), implies the inequality in (B.5) is equivalent to

$$PA + A^T P + Q_1^T Q_1 - PB_v F - F^T B_v^T P - Q_1^T R_1 F - F^T R_1^T Q_1 + F^T R_1^T R_1 F < 0 \tag{B.7}$$

Inequality (B.7), is clearly not convex [1], and cannot be written as an LMI representation. Define $X = P^{-1}$ then by pre and post multiplying the inequality in (B.7) by X together with the change of variable $Y = FX$, implies inequality (B.7) can be written as

$$AX + XA^T + X^T Q_1^T Q_1 X - B_v Y - Y^T B_v^T - X^T Q_1^T R_1 Y - Y^T R_1^T Q_1 X + Y^T R_1^T R_1 Y < 0 \tag{B.8}$$

[1] Here $\mathbb{E}(\cdot)$ is the mathematical expectation operator, and in establishing (B.6) the fact that the linear operators $\mathbb{E}(\cdot)$ and $\text{trace}(\cdot)$ commute is exploited [3].

Finally using the Schur complement [1], inequality (B.8) can be written as

$$\begin{bmatrix} AX + XA^T - B_v Y - Y^T B_v^T & (Q_1 X - R_1 Y)^T \\ (Q_1 X - R_1 Y) & -I \end{bmatrix} < 0 \tag{B.9}$$

where the matrices X and Y are the decision variables. The requirement now is to minimise trace(X^{-1}). From the definition of $X = P^{-1}$, using the Schur complement [1], the inequality

$$\begin{bmatrix} -Z & I \\ I & -X \end{bmatrix} < 0 \tag{B.10}$$

implies $X^{-1} < Z$ and therefore

$$\text{trace}(Z) > \text{trace}(X^{-1}) \tag{B.11}$$

The overall problem then becomes:

Minimise trace(Z) subject to (B.10) and (B.9).

Once X and Y are synthesised, the feedback gain F can be recovered as $F = YX^{-1}$.

B.2.2 LMI Formulation of the BRL

In Sect. 3.2.2, the closed-loop stability of the sliding motion is governed by

$$\dot{x}(t) = \underbrace{(A - B_v F)}_{\tilde{A}} x(t) + \tilde{B}\vartheta(t) \tag{B.12}$$

$$z(t) = Fx(t) \tag{B.13}$$

where $\vartheta(t) = \Phi(t)z(t)$. The $\mathscr{L}_2$ gain from ϑ to z (which in this LTI situation is the $\mathscr{H}_\infty$ norm of $\tilde{G}(s) = F\left(sI - \tilde{A}\right)^{-1}\tilde{B}$) is less than γ if there exists a Lyapunov function $V(x) = x^T P x$ where $P > 0$ such that

$$\int_0^\infty (\dot{V}(\tau) + z^T z - \gamma^2 \vartheta^T \vartheta) d\tau < 0 \qquad \text{for all } x \text{ and } \vartheta \tag{B.14}$$

holds, since rearranging the inequality in (B.14) and assuming $x(0) = 0$ yields

$$\int_0^\infty z^T z < \gamma^2 \int_0^\infty \vartheta^T \vartheta - V(\infty) \leq \gamma^2 \int_0^\infty \vartheta^T \vartheta$$

To guarantee (B.14) holds, the inequality

$$\dot{V} + z^T z - \gamma^2 \vartheta^T \vartheta < 0 \tag{B.15}$$

for all x and ϑ will be enforced.[2] Taking the time derivative of the function $V(x)$ and substituting from (B.12) yields

$$\dot{V} = x^T (P(A - B_v F) + (A - B_v F)^T P)x + \vartheta^T \tilde{B}^T P x + x^T P \tilde{B} \vartheta$$

Substituting $\dot{V}$ and (B.13) into (B.15) means (B.15) is equivalent to

$$x^T (P(A - B_v F) + (A - B_v F)^T P)x + \vartheta^T \tilde{B}^T P x + x^T P \tilde{B} \vartheta + x^T F^T F x - \gamma^2 \vartheta^T \vartheta < 0$$

which can be written as

$$\begin{bmatrix} x \\ \vartheta \end{bmatrix}^T \begin{bmatrix} P(A - B_v F) + (A - B_v F)^T P + F^T F & P\tilde{B} \\ \tilde{B}^T P & -\gamma^2 I \end{bmatrix} \begin{bmatrix} x \\ \vartheta \end{bmatrix} < 0 \tag{B.16}$$

or in other words

$$\begin{bmatrix} P(A - B_v F) + (A - B_v F)^T P + F^T F & P\tilde{B} \\ \tilde{B}^T P & -\gamma^2 I \end{bmatrix} < 0 \tag{B.17}$$

Inequality (B.17) can be written as

$$\begin{bmatrix} P(A - B_v F) + (A - B_v F)^T P & P\tilde{B} \\ \tilde{B}^T P & -\gamma^2 I \end{bmatrix} + \begin{bmatrix} F^T \\ 0 \end{bmatrix} \begin{bmatrix} F & 0 \end{bmatrix} < 0 \tag{B.18}$$

which from the Schur complement [1], is equivalent to

$$\begin{bmatrix} P(A - B_v F) + (A - B_v F)^T P & P\tilde{B} & F^T \\ \tilde{B}^T P & -\gamma^2 I & 0 \\ F & 0 & -I \end{bmatrix} < 0 \tag{B.19}$$

[2] See page 122 of [1].

From Eq. (B.19) it is clear that the expression in the top left position is not convex and cannot be written as an LMI representation. However multiplying both sides of (B.19) by $\text{diag}(P^{-1}, I, I)$ means (B.19) is equivalent to

$$\begin{bmatrix} (A - B_v F)P^{-1} + P^{-1}(A - B_v F)^T P & \tilde{B} & P^{-1}F^T \\ \tilde{B}^T & -\gamma^2 I & 0 \\ FP^{-1} & 0 & -I \end{bmatrix} < 0 \tag{B.20}$$

Letting $P^{-1} = X$, the inequality in (B.20) is equivalent to

$$\begin{bmatrix} (A - B_v F)X + X(A - B_v F)^T P & \tilde{B} & XF^T \\ \tilde{B}^T & -\gamma^2 I & 0 \\ FX & 0 & -I \end{bmatrix} < 0 \tag{B.21}$$

Finally with the change of variable $Y = FX$, inequality (B.21) can be written as

$$\begin{bmatrix} AX + XA - B_v Y - Y^T B_v^T & \tilde{B} & Y^T \\ \tilde{B}^T & -\gamma^2 I & 0 \\ Y & 0 & -I \end{bmatrix} < 0 \tag{B.22}$$

where the matrices X and Y represent the decision variables. Inequality (B.22) is convex and available LMI tools can be used to find a feasible solution. The gain matrix F can be recovered using the relation $F = YX^{-1}$.

References

1. Boyd, S.P., Ghaoui, L., Feron, E., Balakrishnan, V.: Linear Matrix Inequalities in System and Control Theory. Society for Industrial and Applied Mathematics, Philadelphia (1994)
2. Khalil, H.K.: Nonlinear Systems. Prentice Hall, Upper Saddle River (1992)
3. Byrne, C.L.: Signal Processing: A Mathematical Approach, 2nd Edition. CRC Press, Boca Raton (2014)

Index

M.T. Hamayun et al., *Fault Tolerant Control Schemes Using Integral Sliding Modes*, Studies in Systems, Decision and Control 61,
DOI 10.1007/978-3-319-32238-4